EXPLORING THE EFFECTS OF VOID DECKS ON URBAN VENTILATION IN SINGAPORE

A Computational Design & Simulation Approach for Wind Microclimate-Informed Urban Planning

by
AVIVA OPSOMER

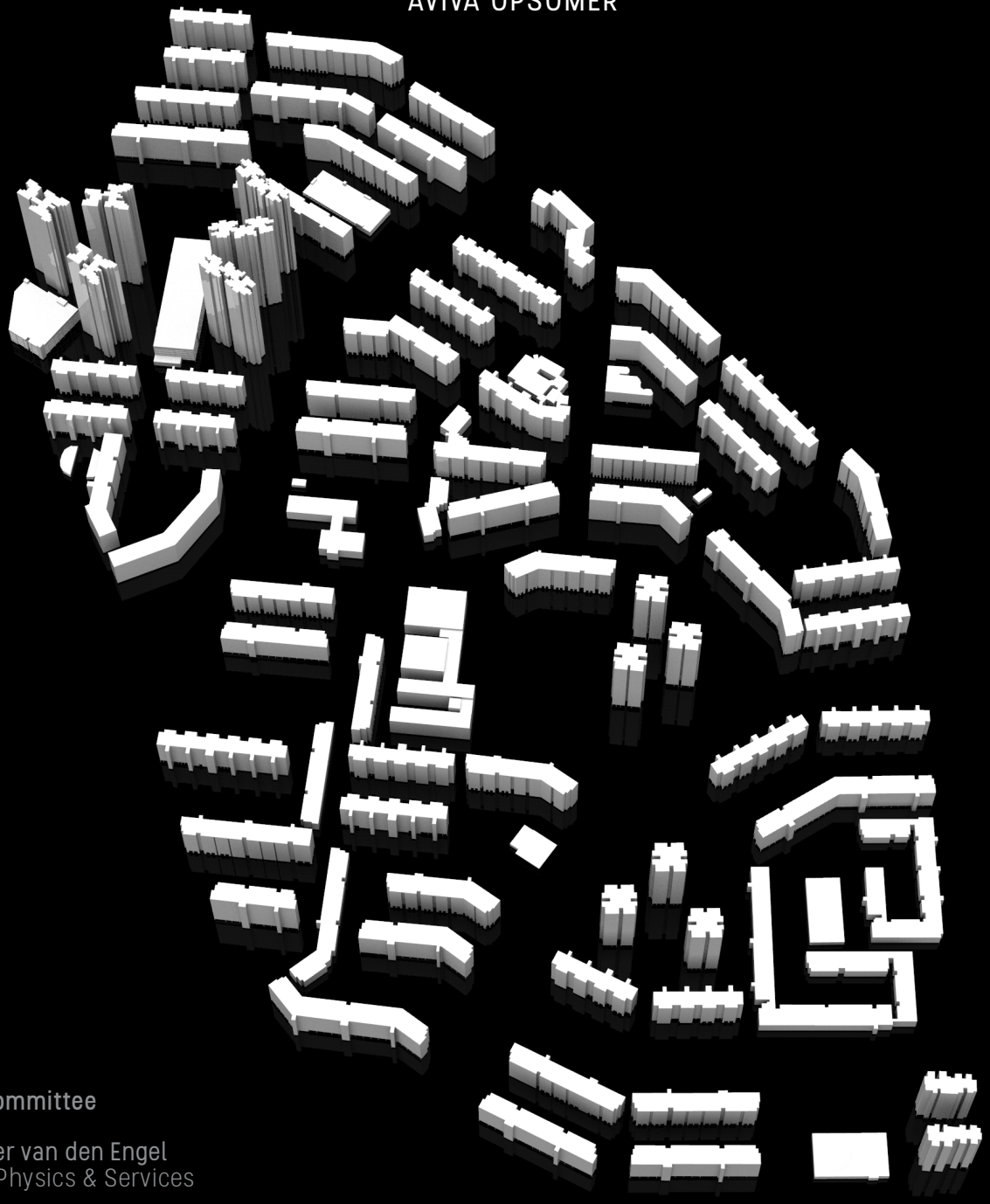

Thesis Committee

Dr.ir. Peter van den Engel
Building Physics & Services

Dr. Clara García-Sánchez
3D GeoInformation

Dr.ir. Martin Tenpierik
Building Physics & Services

Dr.ir. Esther Gramsbergen
Delegate Board of Examiners

TU Delft

EXPLORING THE EFFECTS OF VOID DECKS ON URBAN VENTILATION IN SINGAPORE

A COMPUTATIONAL DESIGN & SIMULATION APPROACH FOR WIND MICROCLIMATE-INFORMED URBAN PLANNING

by
AVIVA OPSOMER

in partial fulfilment of the requirements for the degree of

Master of Science
Master Track: Building Technology

TU Delft
Faculty of Architecture and the Built Environment
to be defended publicly on Friday, 10 July 2020

Thesis Committee

Dr.ir. Peter van den Engel
Building Physics & Services

Dr. Clara García-Sánchez
3D GeoInformation

Dr.ir. Martin Tenpierik
Building Physics & Services

Dr.ir. Esther Gramsbergen
Delegate Board of Examiners

TU Delft Delft University of Technology

Preface

This thesis is written in partial fulfilment of the requirements for the Master of Science specialisation track in Building Technology at the Faculty of Architecture and the Built Environment at TU Delft.

The research presents a workflow based on the use of computational fluid dynamics and parametric design tools to explore the effect of various building void deck geometries on the urban wind microclimate in Singapore.

Acknowledgements

I would like to express my gratitude to my supervisors, Dr. Clara García-Sánchez, Dr.ir. Peter van den Engel and Dr.ir. Martin Tenpierik, and external examiner, Dr.ir. Esther Gramsbergen, for all their guidance and advice during this research.
Clara has supported me in so many ways during the entire process; from all her help in overcoming OpenFOAM's steep learning curve and setting up the computer clusters to the weekly progress meetings with feedback on the research approach and how to proceed. Her continuous drive and enthusiasm about the project really motivated me to push it to the best I could. Thank you for introducing me to the world of urban CFD and for inspiring me to continue my learning process in this field.
Peter overlooked the research from a broader perspective and helped reminding me not to get indulged in the technical aspects only, but to always look at the bigger context and reflect on topics such as adaptive comfort and how to translate the conclusions of my research into guidelines that can be used by architects and urban planners. Thank you for this advice; it has resulted in a multidisciplinary work which combines various aspects.
Martin also showed interest in this project and backed me up with additional feedback at the intermediate progress meetings, which was truly appreciated. Your willingness to help students, both in the thesis research and other courses, is incredible; thank you.
I would like to thank the 3D GeoInformation research group at BK in particular for giving me access to their computational resources to be able to carry out this urban microclimate research.

Furthermore, I would like to thank Dr. Filip Biljecki from the NUS Urban Analytics Lab for the collaboration in the early stages of this Singapore-focused project. Besides, the ATHENS crash course in aerodynamics, taught by Prof. Dr. ir. Bert Blocken and Dr. Alessio Ricci was really helpful at the starting phase of my thesis.

On a personal note, I would like to thank my parents for all the opportunities they have given me and for always motivating me to give the best of myself to work towards my dreams. I would also like to dedicate a short note to my dad, who was the one who accompanied me to Delft the very first time when I had to choose my study path at the age of seventeen. Like no other, he taught us what perseverance is, which I believe has been indispensable to me during this thesis. I hope to have made you proud today.

Not to forget, a last big thanks goes out to my siblings and my friends in Delft and around the world for their support and all the good times we have shared.

AVIVA OPSOMER,
Delft, July 2020

CONTENTS

Abstract

Rising temperatures due to climate change and the increased Urban Heat Island (UHI) effect both have a major impact on Singapore's outdoor comfort. Research has reported an average UHI in Singapore of 4°C, which can even exceed 7°C at some times of the day. (Acero & Ruefenacht, 2017) Increasing convective surface heat transfer from the human body by means of induced wind speeds is an important strategy to improve outdoor thermal comfort. However, the combination of its high urban density, leading to a considerable number of obstructions for urban wind flows, and the generally low wind speeds due to its geographical proximity to the equator makes urban ventilation in Singapore challenging. (Acero & Ruefenacht, 2017) Since the 1970s, void decks, open spaces at the ground floor of buildings, have become a typical characteristic of public housing flats in Singapore. These have been shown to potentially increase wind speeds by more than twofold. (Chew & Norford, 2019) However, the effect of void deck geometries on the imbalance between outdoor thermal and pedestrian wind comfort in a realistic urban setting has not been addressed before.

Hence, the main research question of this thesis was formulated as follows:

How can the geometry design of void decks be optimized to enhance urban ventilation for outdoor thermal comfort in Singapore while ensuring good pedestrian comfort?

A strong mismatch between pedestrian wind comfort and outdoor thermal comfort was observed in the study area with the simulated monsoon wind conditions. This marks the importance to perform wind microclimate analyses in a tropical environment as Singapore, focusing on both aspects. This work demonstrates a design methodology that combines parametric design tools with CFD (computational fluid dynamics) simulations with the aim to make better wind-informed design decisions for an urban context.

Using a parametric building model, ten void deck geometry variants were generated and compared. The implications of the observed flow pattern in terms of urban planning were clarified. For example, while a horizontally converging void deck geometry was found to be effective at directing the urban ventilation towards a target location due to the funnel-shaped induced wind speed region downstream, horizontally diverging void decks led to a more evenly spread region of accelerated flow along the void length. The highest amplification factors inside the void deck were obtained for a vertically diverging geometry. This geometry was subsequently applied to all the buildings facing the prevailing wind directions in the study area, Clementi, using a parametric urban model. This model allows the user to apply various void deck geometries to different building groups independently from each other based on their orientation. A comparison of the wind speed and air temperature distributions after the urban-scale intervention to the current situation showed a wind speed increase and temperature decrease in almost all the void decks. While the amplified wind speed region extended downstream of some void decks, other areas in between the buildings showed a slowed down wind flow. The temperature effects were more extreme at the more closely-packed areas with a smaller distance in between the buildings. Overall, it was concluded that the void deck modifications did not only affect the local wind microclimate inside the void decks, but also altered the wind conditions in between the buildings. Ideally, these wind speed-amplifying void decks should be used in combination with other urban cooling strategies.

The proposed workflow was demonstrated for the geometry design of void decks, but is also applicable in the optimization process of other building features which may affect the urban wind microclimate, such as canopies and building podia.

01

INTRODUCTION

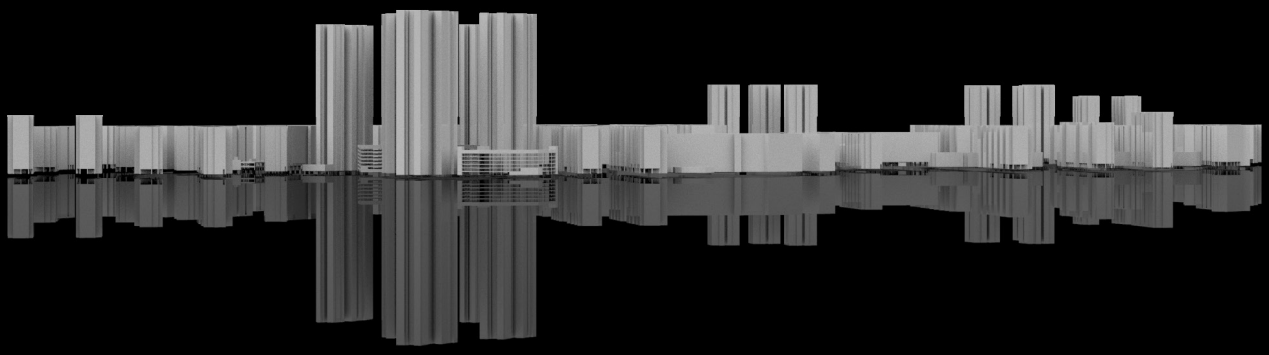

Rising temperatures due to climate change and the increased Urban Heat Island (UHI) effect both have a major impact on cities, and these effects can be expected to be even more apparent in tropical climates like Singapore's. Research has reported an average UHI in Singapore of 4°C, which can even exceed 7°C at some times of the day. (Acero & Ruefenacht, 2017) This is an issue in terms of outdoor comfort that may limit the intensity of usage of outdoor spaces.

The combination of overhead sun (due to Singapore's proximity to the Equator) and a relatively low density (with a distance of approximately 30m in between the buildings) in Clementi, the focus area of this research, further complicates this as self-shading (by buildings casting shade on each other and the surrounding outdoor spaces) is very limited.

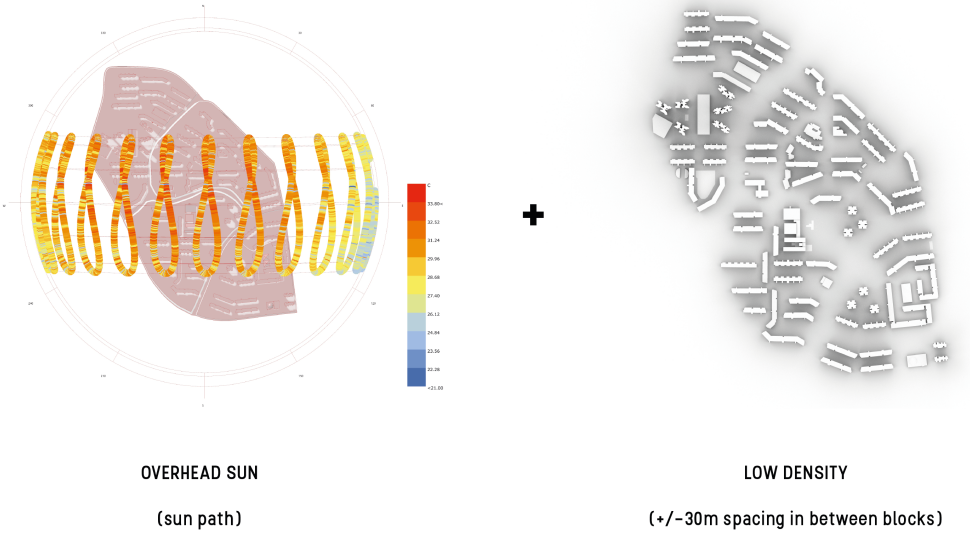

Figure 1.1: sun path implications in study area

Void decks, open spaces at the ground floor of – mostly residential – buildings, can be a good solution to overcome this by serving as providers of a locally enhanced outdoor climate. Thus, by moving the outdoor interactional spaces from the streets toward these void decks, outdoor activities can still be performed under pleasant climatic conditions.

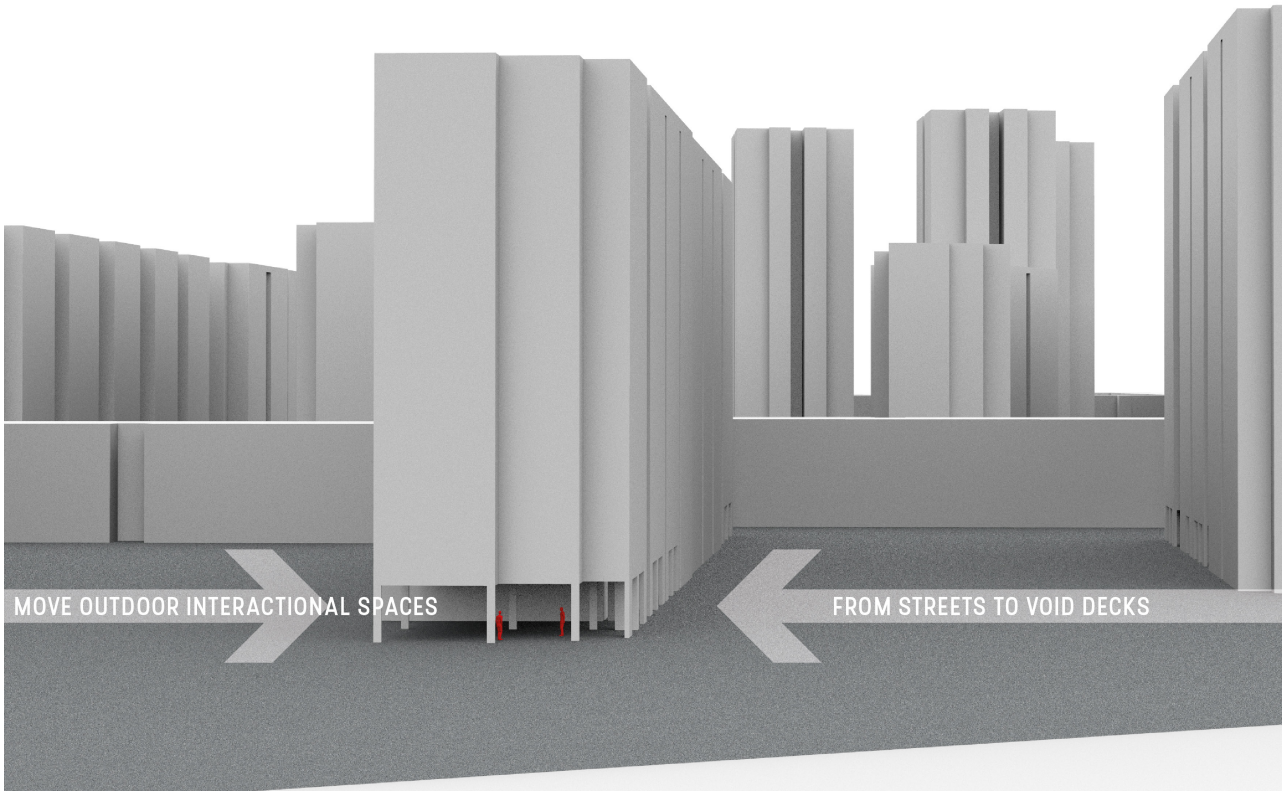

Figure 1.2: void deck as outdoor interactional space

The purpose of void decks in terms of urban microclimates is threefold:

1) Provision of shading: by 'lifting up' the buildings, an open space is created on the ground floor. This space is largely shaded by the building itself and therefore helps in limiting one's radiant heat gain.

2) Increase of wind speeds: void decks may help to increase pedestrian-level wind speeds, which, in turn, aids in increasing the convective heat loss from the body.

3) Provision of shelter from the rain: as precipitation is abundant in Singapore's tropical climate, void decks are also useful in providing shelter during showers.

Besides these climatic benefits, void decks also contribute to social interaction and an expansion of the pedestrian route network leading to increased connectivity, amongst others. The main focus in this thesis lies on the effect of void decks on the enhancement of the urban wind microclimate. This work demonstrates a design methodology that combines computational design and fluid dynamics simulations which can help architects, engineers and urban planners in optimizing the geometry of these building elements with the goal of enhancing the pedestrian-level wind conditions at an urban-district scale.

A common approach in urban planning to analyse the challenges and potentials for the future development of an area is to break it down into several thematic 'layers' stacked on top of each other, as visualized in the axonometric diagram below (*figure 1.3, left*). These include, for example, a radiation, air quality, biodiversity, noise and traffic layer. However, *wind* is an often-disregarded aspect in this layer approach.

> *"Urban planners can use different design tools, adapted to different phases of projects design, to assess qualitatively and quantitatively solar radiation in urban areas. But, wind is a microclimatic parameter generally neglected by urban planners. However, wind speed at pedestrian level is one of the most important environmental parameters determining user satisfaction in urban open spaces."*
>
> *(Reiter, 2010)*

This demonstrates the relevance of this research topic. An integral approach is required to ensure the establishment of a pleasant and comfortable outdoor climate in the built environment. This 'missing layer', the local wind microclimate, should therefore be mapped onto the study area as well.

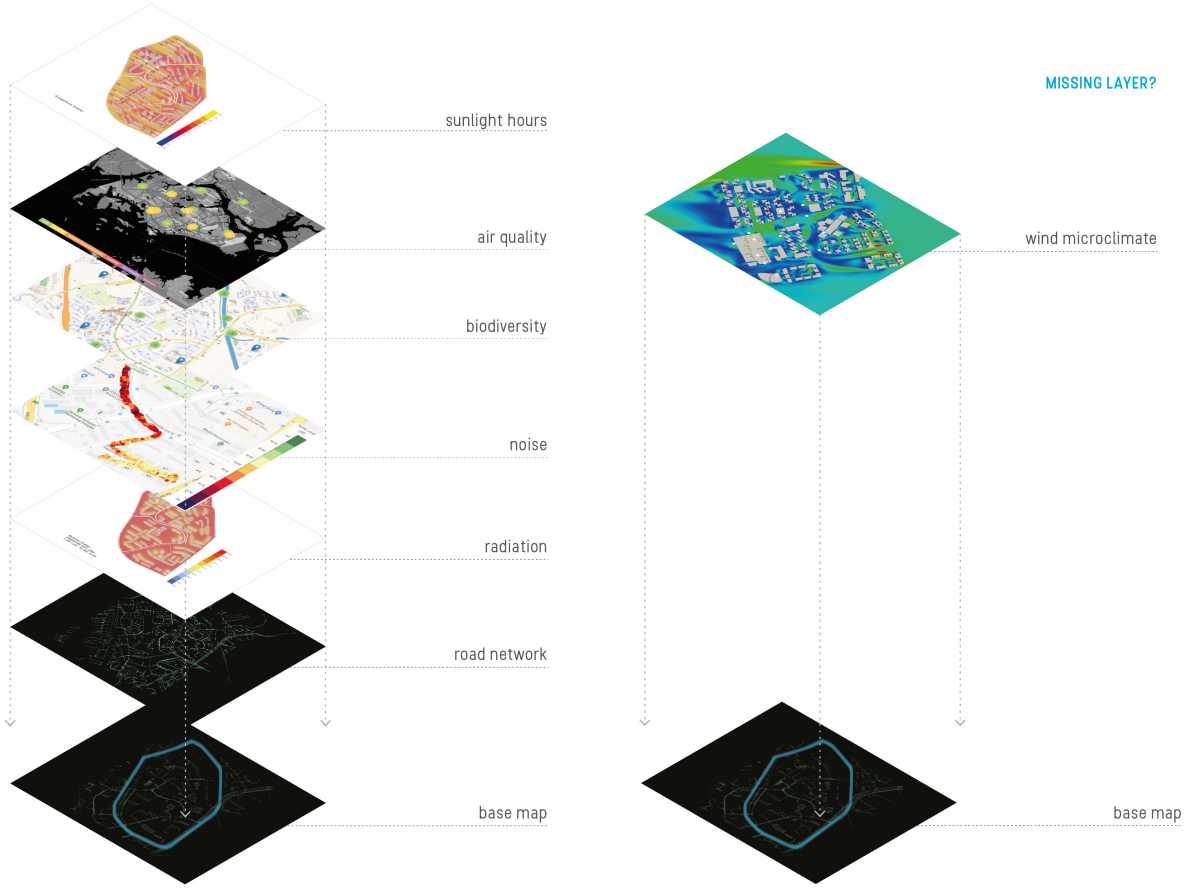

Figure 1.3: layer approach; wind as the 'missing layer' in urban planning

This can be done according to two different scenarios. In the first one, one starts with a pre-determined activity pattern, i.e. by first determining which types of functions / activities will be planned at specific locations and mapping the wind microclimate on top of that layer, after which the void deck geometries need to be adjusted in order to meet the comfort requirements for the pre-set activity level in each location. In the second scenario, the order in which the activity pattern and the wind microclimate are mapped onto the base map of the study area are reversed. In other words, one first examines the wind microclimate in the area and then determines an appropriate activity pattern which suits the wind con-

ditions at the various locations. In that case, less drastic adjustments of the void deck geometries are required in order to meet the outdoor comfort requirements. Although it cannot be guaranteed that the required comfort level will be achieved in the entire area in any of the two scenarios, the second approach, which we may call “wind microclimate-informed urban planning”, clearly has a higher chance of succeeding at most locations. Thus, by considering the urban wind microclimate in the early stages of the design process, better design decisions can be made to ensure a good outdoor comfort for the planned functions in the area.

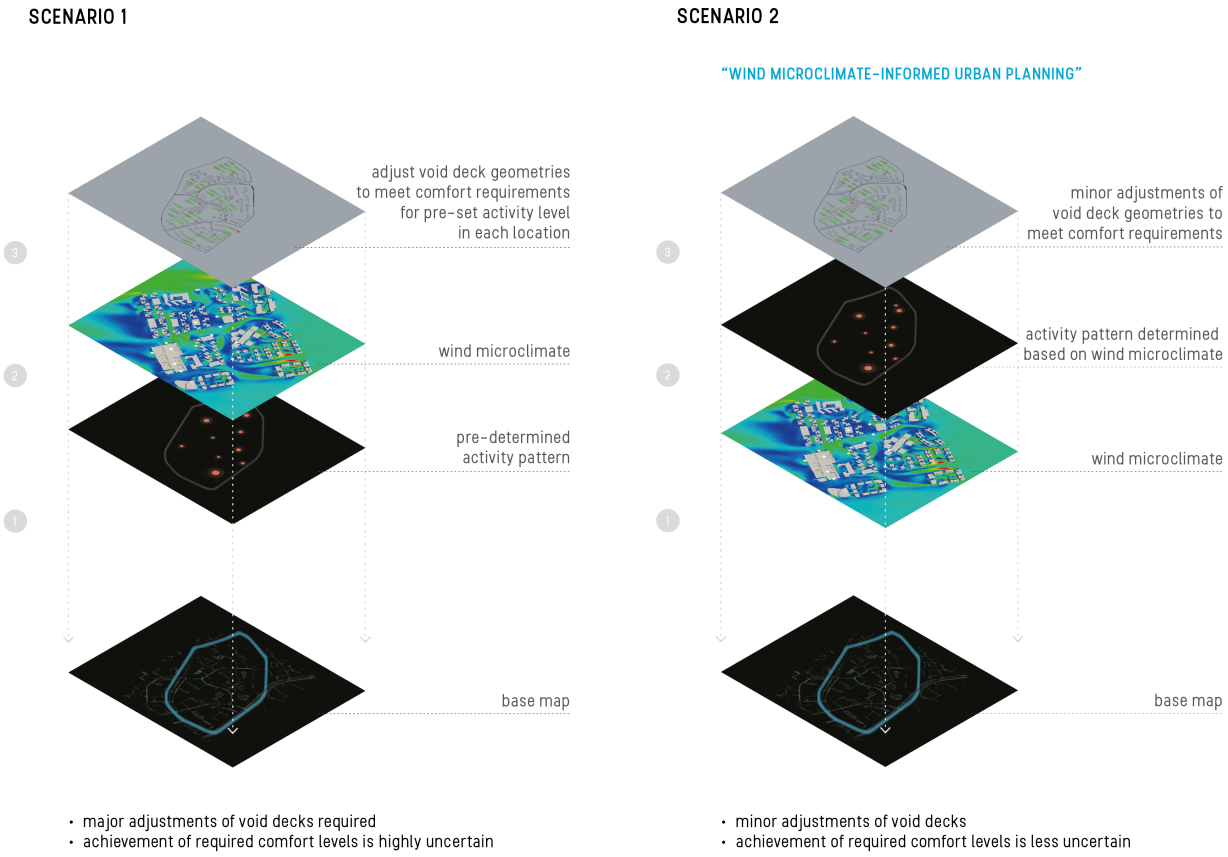

Figure 1.4: wind microclimate-informed urban planning

02

RESEARCH FRAMEWORK

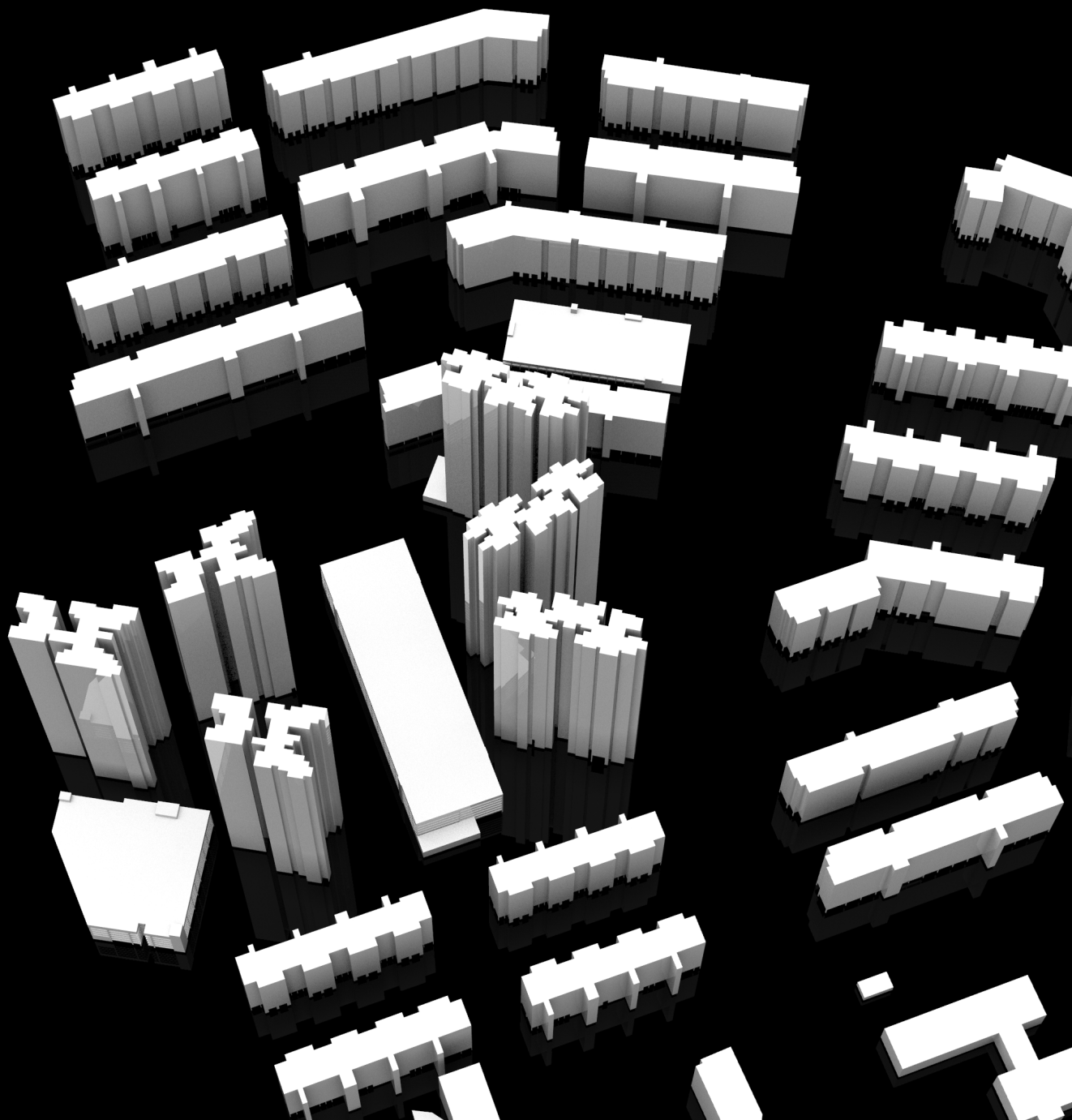

2.1 Background

Rising temperatures due to climate change and the increased Urban Heat Island (UHI) effect both have a major impact on Singapore's outdoor comfort. Research has reported an average UHI in Singapore of 4°C (*figure 2.1*), which can even exceed 7°C at some times of the day. (Acero & Ruefenacht, 2017) The urban heat island is also partially exacerbated by the tropical city state's high reliance on air conditioning systems, which release waste heat into the surrounding environment. (Hicks, 2018)

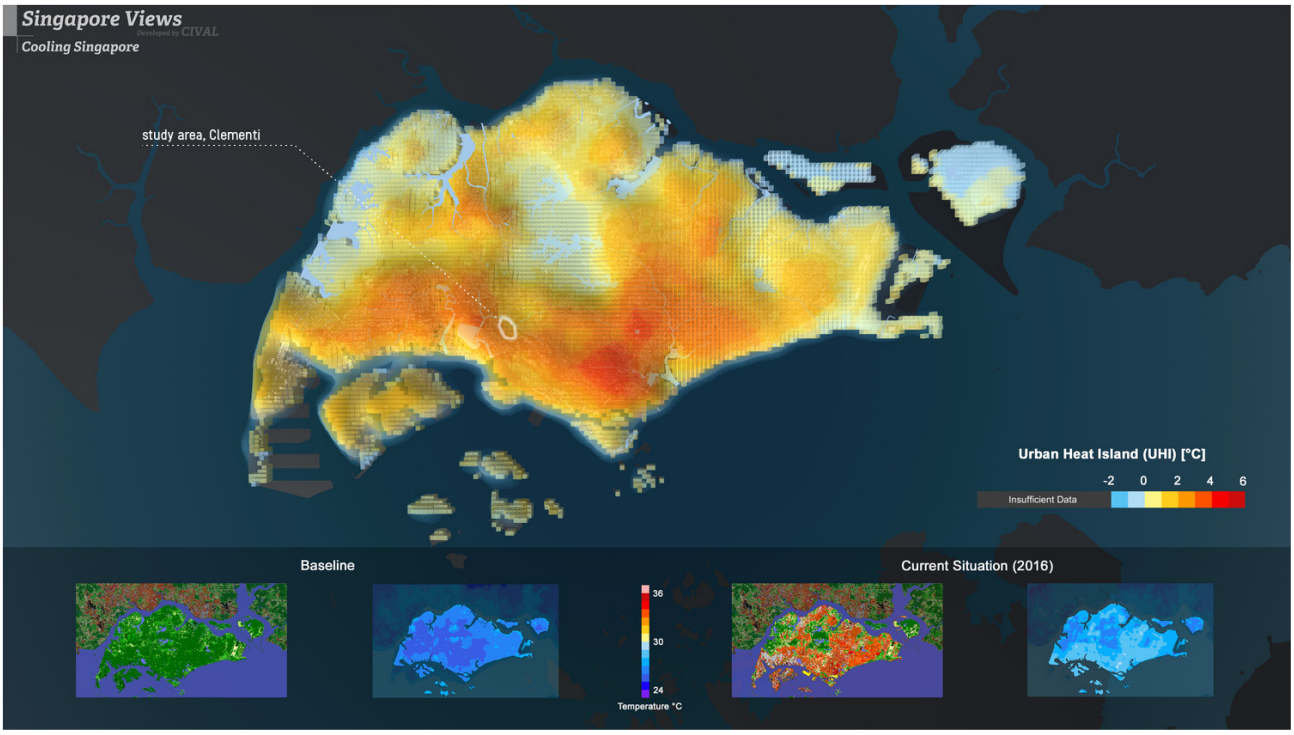

Figure 2.1: Urban Heat Island Singapore. Adapted from "Cooling Singapore & CIVAL," by M.O. Mughal & S. Zhong, 2018 (https://www.coolingsingapore.sg/urban-heat-island)

Increasing convective surface heat transfer from the human body by means of induced wind speeds is an important strategy to improve outdoor thermal comfort. The combination of its high urban density, leading to a considerable number of obstructions for urban wind flows, and the generally low wind speeds due to its geographical proximity to the equator makes urban ventilation in Singapore a challenging task. (Acero & Ruefenacht, 2017) The introduction of void decks in buildings can provide a good solution to tackle this. A recent study by Chew & Norford (2019) has shown a significant potential increase in wind velocities by more than twofold through the implementation of void decks. However, while this may positively affect the outdoor thermal comfort and air quality, it should be noted that the increased velocities might lead to a reduced pedestrian wind comfort. An extensive study on walkability showed that the average walking distance in Singapore is 259m, which is considerably short compared to other cities stated in this research. (Axhausen, Erath, Ordóñez, & van Eggermond, 2015) In order to improve the walkability in the city, the parameters of outdoor thermal comfort and wind velocities should therefore be studied in parallel.

Furthermore, it is important to address urban ventilation in conjunction with ventilation at the building scale. As stated in the 3rd Green Building Masterplan, the city-state aims for 80% of all its buildings to be certified by Green Mark, Singapore's green building benchmarking scheme, by 2030. (BCA, 2017) Various strategies thus need to be put in place to increase the energy efficiency of buildings, including natural ventilation. Therefore, natural building ventilation needs to be addressed at an urban level as it requires a good outdoor air quality and acceptable wind speeds.

Hence, effective urban ventilation strategies in tropical areas like Singapore can help to improve outdoor comfort and thus need to be taken into consideration when designing buildings and cities. The challenge lies in the creation of urban wind conditions within an optimal range for the combination of outdoor thermal comfort and pedestrian wind comfort.

2.2 Problem Statement

While void decks may enhance urban ventilation by increasing wind speeds in tropical dense places like Singapore, a good balance needs to be found between thermal comfort on the one hand and pedestrian comfort on the other.

2.3 Objective

The objective of the research is to investigate wind flow patterns around various existing void decks in Singapore, and to demonstrate how changes in void deck geometries may impact the outdoor thermal and pedestrian wind comfort at an urban scale.

Wind analyses will be carried out for a particular part of the city, located in the Clementi area, and these results will be assessed against outdoor comfort criteria. Different void deck geometries will be generated and tested with a single-building model before being implemented in an urban-scale void deck intervention. The design assignment will thus consider a location-specific intervention, although the conclusions may, to a certain extent, be extrapolated to buildings with similar orientations in the country.

The final product will consist of an improved void deck geometry proposal for the study area, as well as a general workflow demonstration of how architects, engineers and urban planners can make use of parametric design and computational fluid dynamics tools to enhance urban ventilation in a tropical climate.

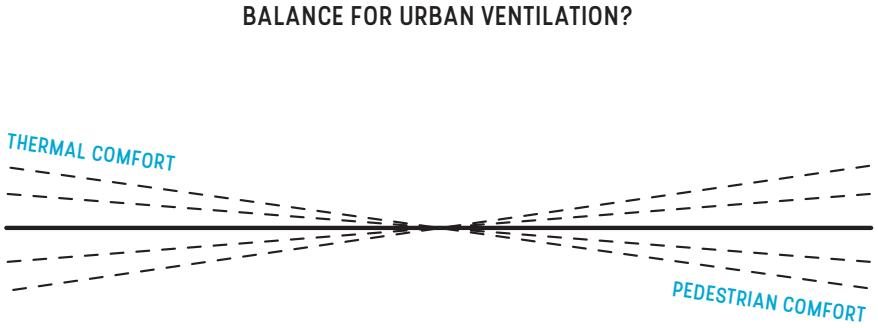

Figure 2.2: the challenge - balance between increased wind speeds for urban ventilation (outdoor thermal comfort) and maintaining good pedestrian wind comfort

2.4 Research Questions

The main research question of this thesis has been formulated as follows:

How can the geometry design of void decks be optimized to enhance urban ventilation for outdoor thermal comfort in Singapore while ensuring good pedestrian comfort?

In order to answer the main research question, the following sub-questions will be addressed:

- Which void deck geometries and configurations have been applied to existing buildings in Singapore?
- How do current void deck designs affect wind flow patterns for urban ventilation in Singapore with regard to thermal comfort?
- What are the effects of current void deck designs on pedestrian wind comfort?
- Where do significant mismatches between urban ventilation and pedestrian comfort occur?
- Which design strategies can be adopted to enhance Singapore's urban ventilation for outdoor thermal comfort while ensuring good pedestrian comfort?

2.5 Approach & Methodology

A research structure linking the research questions to various research / report parts is shown on the next pages, followed by the step-by-step approach which indicates how the research is planned to be carried out.

The research will be conducted by means of a series of computational fluid dynamics (CFD) simulations within the open-source OpenFOAM libraries in combination with the post-processing tools ParaView and PyVista for Python to analyse the current wind flows around void decks in Singapore. The impact of the void decks on the wind flow pattern will be investigated with a particular focus on thermal comfort and pedestrian wind comfort. Based on these results, problematic locations showing a strong mismatch between these two will be identified. Thereafter, an optimization study of the building void deck volumes will be done to improve the urban ventilation in the study area. Tools that may be used include, but are not limited to, Rhino and Grasshopper for parametric design optimizations. The wind flows around the proposed void deck geometry in the urban context will then be simulated to assess the effectiveness of the solution. This evaluative loop serves as a reflection on the proposed design. The research will conclude with a recommended workflow for architects, engineers and urban planners regarding the use of a combined computational design and simulation approach for urban ventilation enhancement through the use of void decks.

The following measures will strengthen the **scientific rigour** of the research:

– The CFD simulations will be performed for the prevailing Northeast and Southwest (December to March and June to September resp.) monsoon wind directions. This will ensure reliable results for the most probable wind conditions.

– While most previous studies on void decks have performed wind simulations on single or rows of generic building shapes with variations in parameters such as the building height and canyon width, this study will be carried out on a realistic 3D city model that includes surrounding buildings. Therefore, the study will realistically optimize according to the state of the flow disturbed by the other buildings present.

– Various existing void deck geometries and configurations in Singapore will be studied in their context. This provides a better base for comparison to draw conclusions on the effectiveness of void decks for urban ventilation.

– The appropriate set of approximated Navier-Stokes equations is to be chosen in accordance with the aim of the CFD simulation to predict the flows. In this case, the study entails an urban wind flow analysis, which will be performed with Reynolds-averaged Navier-Stokes (RANS) simulations.

– Proper attention will be paid to the computational mesh generation for the CFD analyses. The mesh generation is generally a time-consuming, yet essential, part of CFD-simulations. A higher grid resolution needs to be set in those areas where large flow gradients occur. (Blocken, 2015) In this case, the mesh will need to be refined at the locations of the void decks, as these are the main areas of interest for the flow patterns. A CFD analysis of downtown Oklahoma City by García-Sánchez, Gorlé & Philips (2014) illustrated that the influence of grid refinement is especially apparent at dense building sites. As this research focuses on Singapore, which is characterized by a high urban density, thorough attention must thus be paid to the mesh generation.

– The boundary conditions to be set in the simulation will be based on measurements reported by the Meteorological Service Singapore.

– The domain extension will be designed so that the boundaries do not affect the flow inside the region of interest. This implies that a sufficiently large distance needs to be reserved between the non-physical boundaries (i.e. top and side faces) of the computational domain and the urban model. (Blocken, 2015) Guidelines for the computational domain based on the model dimensions and blockage ratio are summa-

rized by Blocken (2015) and will be applied in combination with the COST Action 732 (2007) Best Practice Guideline for the CFD Simulation of Flows in the Urban Environment.

The **limitations** of the research scope are summarized below:

– Although various urban ventilation strategies exist, this research focuses on building void decks in particular.

– Due to time and computational cost constraints, a wind study of the entire city falls beyond the scope of this project. Instead, Clementi will serve as the focus area to carry out the analyses. The study area was chosen for its variation in building heights and shapes.

– The study will be carried out for Clementi, Singapore, and is thus context-specific. The flow simulations will be performed on a 3D-model of the study area and design improvements for the void decks will be proposed based on the CFD results. As such, the proposed design solution will be location-specific to similar-oriented buildings in Singapore, and thus not externally valid in other contexts.

– Although Large Eddy Simulations (LES) of urban flows generally involve smaller turbulence model-form uncertainties compared to Reynolds Averaged Navier-Stokes (RANS) simulations, which only solve the mean flow while approximating the turbulence, they involve higher computational costs and uncertainties in the input variables. (García-Sánchez et al., 2014) RANS simulations are thus deemed more suitable for the purpose of this project.

2.6 Planning & Organization

The research team comprises the following members:

- Research executor: Aviva Opsomer
- Supervisor Chair of Building Physics & Services (Architectural Engineering + Technology Department): Dr.ir. Peter van den Engel
- Additional adviser Chair of Building Physics & Services: Dr.ir. Martin Tenpierik
- Supervisor Chair of 3D GeoInformation (Urbanism Department, Section Environmental Modelling): Dr. Clara García-Sánchez
- External collaborator NUS Urban Analytics Lab: Dr. Filip Biljecki
- Delegate Board of Examiners: Dr.ir. Esther Gramsbergen

This thesis has a Climate and Computational Design focus. The *Climate Design* focus lies in the theme of urban ventilation, while the *Computational Design* aspect involves the use of parametric design and advanced CFD-tools (OpenFOAM) to analyse and improve the air flows in the urban environment. Dr.ir. Peter van den Engel is appointed as the supervisor from the chair of Building Physics & Services for the climate design aspects while Dr. Clara García-Sánchez from the the 3D GeoInformation research group will provide guidance on the computational flow analyses and the overall urban-scale approach.
Furthermore, Dr. Filip Biljecki from the NUS Urban Analytics Lab will serve as the main contact in Singapore to help with the acquisition of local data when necessary.

The time span for this thesis research is three academic quarters, starting in Q2 up to the end of Q4 of the academic year 2019-2020. A planning in terms of presentations, deliverables and steps is given on the next page.

LINK RESEARCH QUESTIONS – RESEARCH STRUCTURE

RESEARCH QUESTIONS	RESEARCH PARTS	OUTPUT
Q1: Which void deck geometries and configurations have been applied to existing buildings in Singapore?	Climate Analysis Singapore Urban Ventilation Strategies for Tropical Climates Characteristics of Existing Void Decks in Singapore	Overview of void deck characteristics in Singapore Mapped existing void deck types
Q2: How do current void deck designs affect wind flow patterns for urban ventilation in Singapore with respect to thermal comfort?	Study Area Urban Atmospheric Boundary Layer Simulation Set-Up • CFD Simulation Method & Governing Eq. • Turbulence Model • Computational Model Outdoor Thermal Comfort • Parameters Defining Thermal Comfort • Thermal Comfort Guidelines • Discussion of Results: Thermal Comfort	Urban 3D model CFD simulation results of existing void decks & outdoor thermal comfort assessment
Q3: What are the effects of current void deck designs on pedestrian wind comfort?	Pedestrian Wind Comfort • Parameters Defining Pedestrian Comfort • Pedestrian Comfort Guidelines/ Standards • Discussion of Results: Pedestrian Comfort	CFD simulation results of existing void decks & pedestrian wind comfort assessment
Q4: Where do significant mismatches between urban ventilation and pedestrian comfort occur?	Mismatch Urban Ventilation & Pedestrian Wind Comfort Void Deck Characteristics at Mismatch / Discomfort Locations	Identification of mismatch / discomfort locations in study area Mapped mismatch / discomfort locations
Q5: Which design strategies can be adopted to enhance Singapore's urban ventilation for outdoor thermal comfort while ensuring good pedestrian comfort?	Void Geometry Design Variants Design Intervention • Grouping of Void Decks for Design Intervention • Grouped Void Deck Settings in Urban Parametric Model Post-intervention comfort assessment	Parametric void deck model (building scale & urban scale) Void deck geometry variants CFD simulation results of design variants Proposed urban-scale void deck intervention Post-intervention outdoor thermal & pedestrian wind comfort assessment Conclusions on combined parametric design & CFD workflow for void deck geometry optimizations & wind microclimate enhancement

STEP-BY-STEP APPROACH

1. Define location to conduct wind study
2. Classify and map existing void decks in Singapore

→ ANSWER RESEARCH SUB-QUESTION Q1

3. Prepare urban 3D-model with void decks
4. Set up CFD simulation model
5. Perform simulation of urban model with existing void decks for one common wind direction
6. Repeat simulation for several other most common wind directions
7. Analyze and assess thermal comfort around void decks based on simulation results & literature

→ ANSWER RESEARCH SUB-QUESTION Q2

8. Analyze and assess pedestrian wind comfort around void decks based on simulation results & literature

→ ANSWER RESEARCH SUB-QUESTION Q3

9. Identify mismatch locations of urban ventilation & pedestrian comfort
10. Analyze void deck characteristics of mismatch locations

→ ANSWER RESEARCH SUB-QUESTION Q4

11. Build parametric void deck model (building & urban scale)
12. Create void deck design variants
13. Perform CFD simulation for each design variant to assess effectiveness and compare results
14. Propose urban-scale void deck geometry intervention to achieve good balance between outdoor thermal & pedestrian wind comfort
15. Compose guidelines for computational design & simulation approach for wind-microclimate enhancement

→ ANSWER RESEARCH SUB-QUESTION Q5

→ FORMULATE CONCLUSION TO MAIN RESEARCH QUESTION

TIMELINE

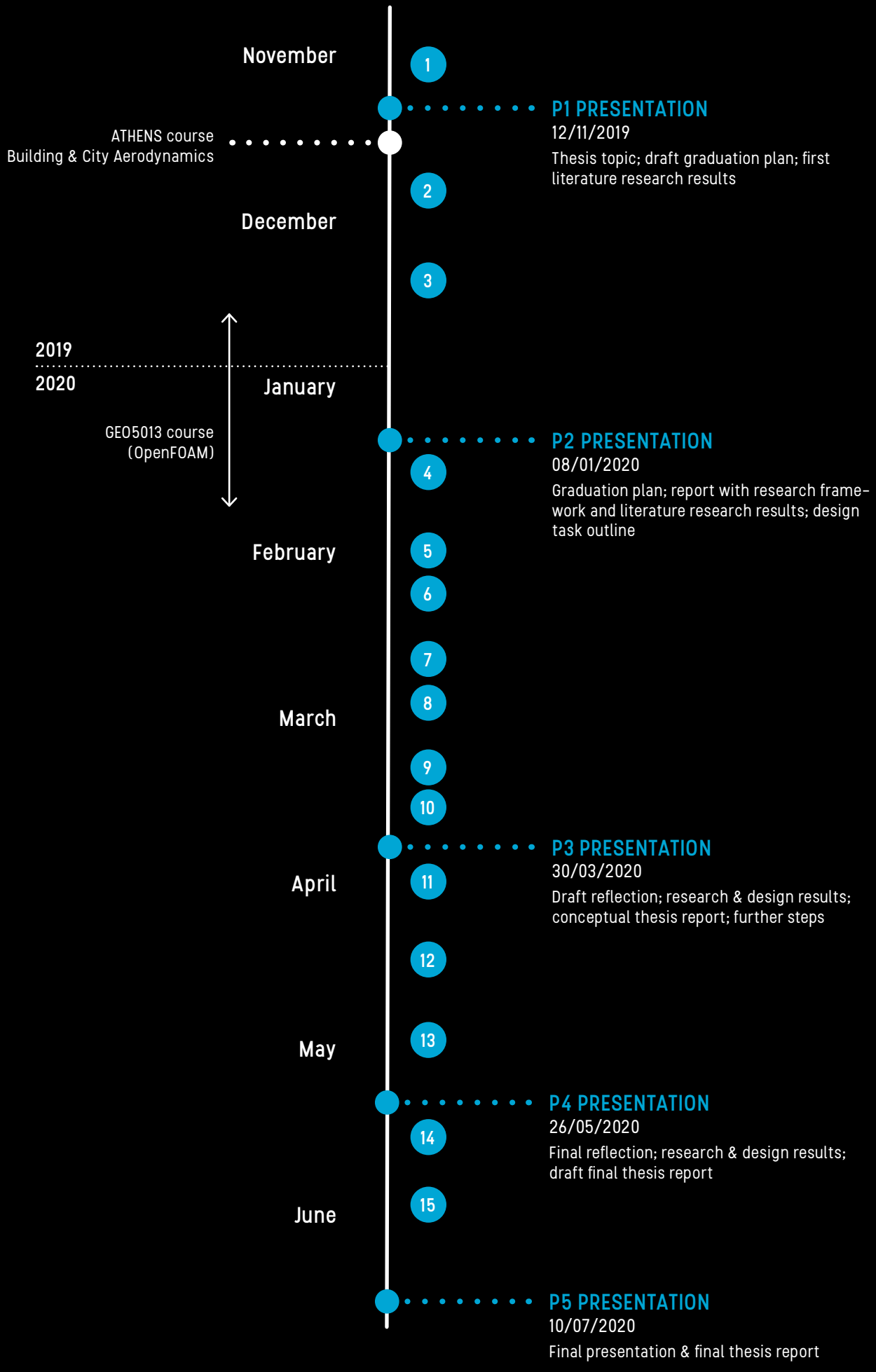
November
1
P1 PRESENTATION
12/11/2019
Thesis topic; draft graduation plan; first literature research results
ATHENS course
Building & City Aerodynamics
2
December
3
2019
2020
January
GEO5013 course
(OpenFOAM)
P2 PRESENTATION
08/01/2020
4
Graduation plan; report with research framework and literature research results; design task outline
February
5
6
7
8
March
9
10
P3 PRESENTATION
30/03/2020
April
11
Draft reflection; research & design results; conceptual thesis report; further steps
12
May
13
P4 PRESENTATION
26/05/2020
14
Final reflection; research & design results; draft final thesis report
June
15
P5 PRESENTATION
10/07/2020
Final presentation & final thesis report
S
STEPS

2.7 Relevance

Relation with Master Track

This thesis topic cannot be classified as one topic of Building Technology, but rather lies at the intersection of Building/Urban Physics, Climate Design and Design Informatics. The key characteristic of the Building Technology Master Track is that it bridges design and engineering aspects, promoting a multidisciplinary approach to solve problems. Within this thesis, both technical and design aspects are involved; the former focusing on computational fluid dynamics to analyze wind flows in urban environments and the latter using computational design to create different design variants and narrowing down the solution space by comparing their performances. Both a research-through-design and design-through-research approach are used; the former focusing on the use of parametric design to generate different void deck geometries and analyzing the effect of these on the flow pattern; and the latter by using the conclusions of this analysis to propose a final urban-scale design intervention. This thesis touches upon different scales of the built environment as the effect of a building element – the void decks – on the flow pattern and the outdoor comfort is studied both directly around the building itself and at the neighbourhood scale. A building technologist should be able to understand how modifications of a particular building element – in this case the void decks – may influence the environment surrounding a building at a much larger, urban, scale.

Societal relevance

According to the World Health Organization (2019), 91% of people worldwide are exposed to excessive ambient air pollution, causing 4.2 million deaths every year. Next to that, cities around the world cope with trapped heat due to urban heat islands. In dense tropical urban environments, these effects are even more apparent, rendering the need for effective urban ventilation strategies essential. This thesis explores one of such strategies, which is commonly applied in Singapore, and aims to optimize void deck geometries to enhance urban ventilation while maintaining a comfortable pedestrian comfort. The latter will become more important in the future, when mobility in cities will be less reliant on cars and more focused on walkability. Moreover, buildings will need to become more energy-efficient to achieve national-level targets, such as Singapore's aim to green at least 80% of its building stock by 2030. (BCA, 2017) Natural ventilation strategies will thus be necessary to reduce the reliance on HVAC-systems, but these can only be implemented if the outdoor conditions (air quality and wind speeds) are within an acceptable range. Therefore, wind flows need to be studied at an urban level to formulate efficient natural building ventilation strategies.

Scientific relevance

The publication of some recent papers on the effectiveness of void decks for urban ventilation marks the relevance of the topic and the quest of cities for simple methods to improve outdoor comfort and, subsequently, walkability. While previous studies have performed wind simulations on generic building shapes with variations in parameters such as the building height and canyon width, this study aims to take the research on void decks a step further by performing CFD simulations in a realistic urban setting. To the best of our knowledge, no study has addressed before how various void deck geometry designs affect wind and thermal comfort at an urban scale.
Besides, while many guidelines and standards have been developed for indoor ventilation, guidelines to establish a good urban wind climate are still scarce. Further research on the topics of outdoor thermal comfort and pedestrian comfort is needed to develop these guidelines for various climates.

03

LITERATURE REVIEW

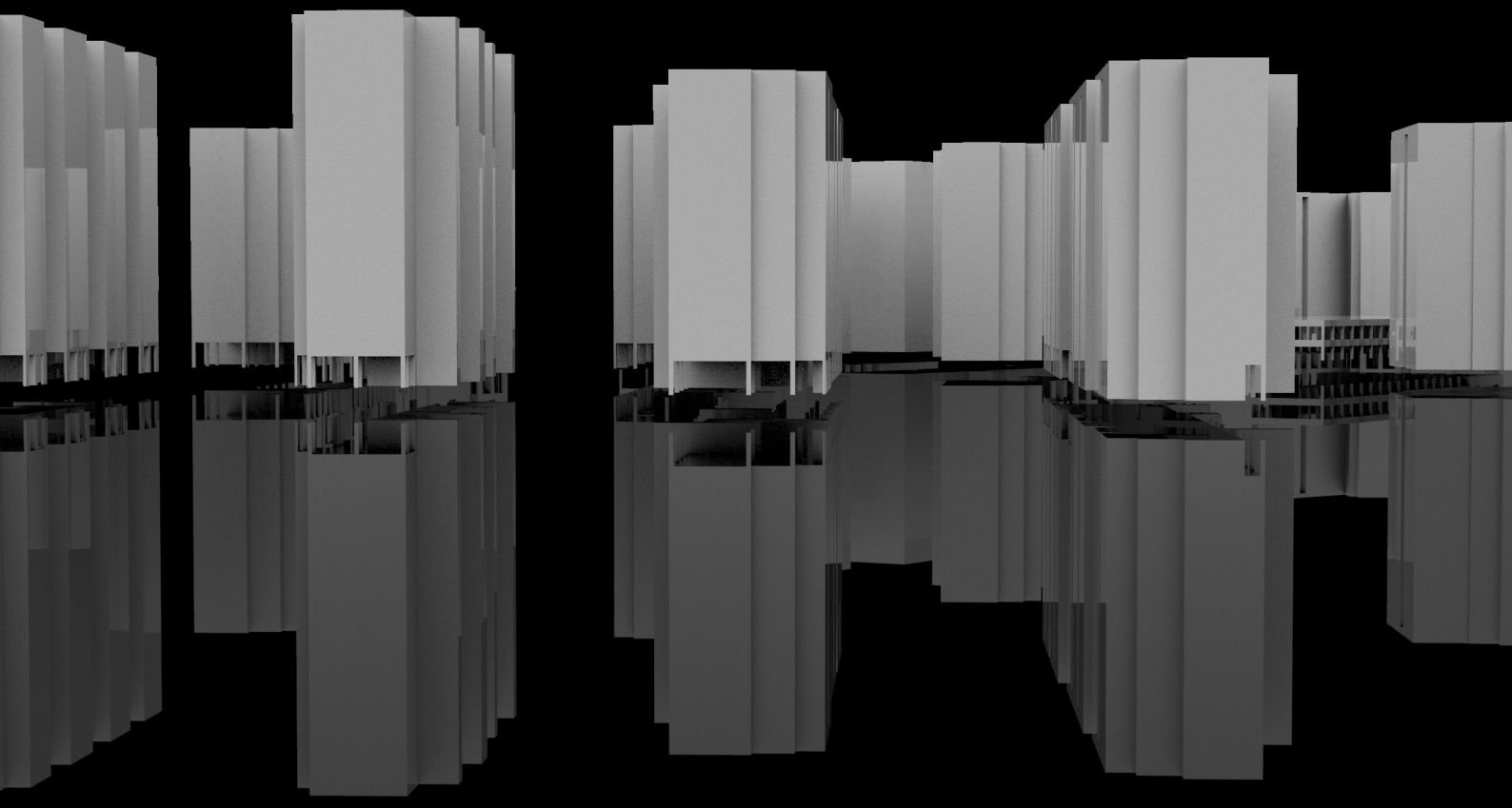

3.1 Climate Analysis Singapore

Wind

As can be seen from the annual wind rose below, there are three prevailing wind directions in Singapore, namely north, north-northeast and south winds; the former two thus being more or less opposite to the latter. These opposing wind directions reflect the dominant influence of the monsoons on Singapore's annual wind flow behaviour.

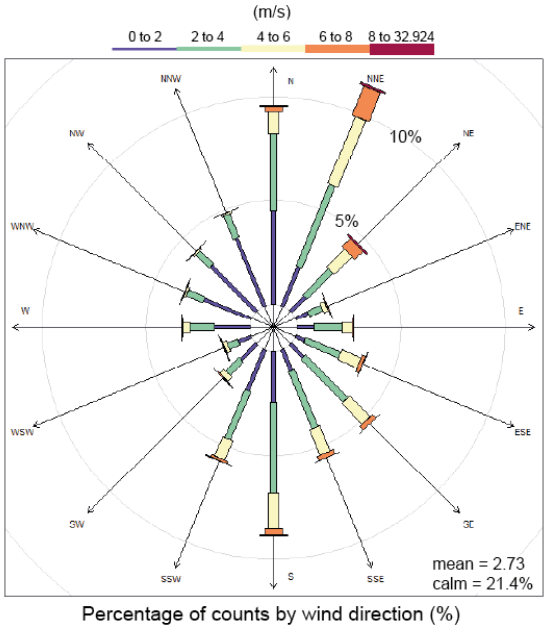

Figure 3.1: annual wind rose 1981-2010, Changi Climate Station. From "Meteorological Service Singapore", 2019 (http://www.weather.gov.sg/climate-climate-of-singapore/)

The Northeast Monsoon occurs from December to March and the Southwest Monsoon between June and September, which means that there are two inter-monsoon periods; April – May and October – November. To illustrate how these monsoons define the yearly wind pattern, the wind roses from December to March and from June to September, respectively, were plotted based on the available weather data (EnergyPlus epw-format) from the EPWMap for Ladybug (*figure 3.2*).

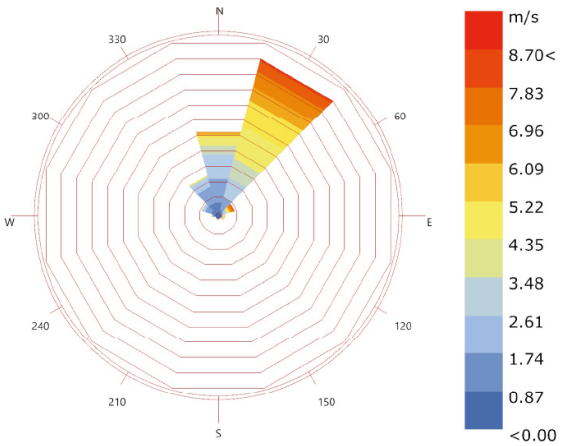

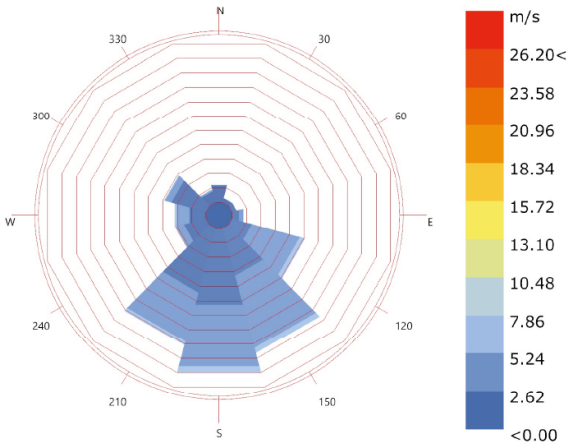

Figure 3.2: wind rose Northeast Monsoon (December – March) (left) & Southwest Monsoon (June – September) (right). (Plots based on data obtained from: https://www.ladybug.tools/epwmap/)

When comparing these two monsoon wind roses to the annual one, a clear similarity can be observed. The wind speed range shows that the Northeast Monsoon is stronger than the Southwest Monsoon. While these two monsoon periods are quite pronounced, the inter-monsoon months (April, May, October and November) have a larger variation in wind directions and much lower wind speeds. (Meteorological Service Singapore, 2019)

The graph below (*figure 3.3*) shows the monthly and hourly variation in surface wind speeds and directions, whereby every arrow represents the average hourly wind. The variable character of the wind during the inter-monsoons is apparent from the various different arrow directions in the plot, especially for the months April and October.

Apart from the seasonally changing wind pattern due to the monsoons, the diurnal variation in wind speeds, shown by the colour bar legend on the right, is notable as well. The graph clearly shows that higher wind speeds occur during the day as compared to the night.

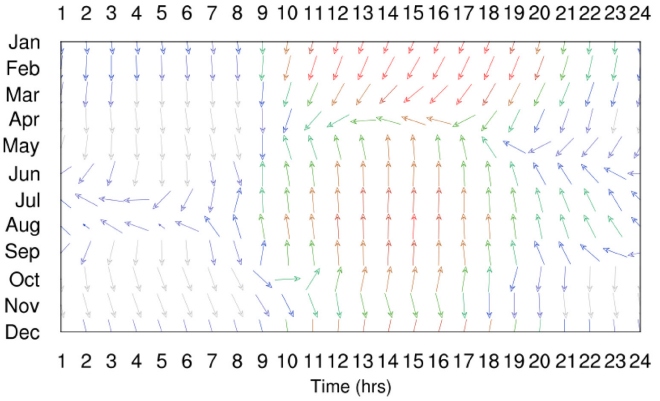

Figure 3.3: monthly and hourly variation in surface wind speeds and directions 1981-2010, Changi Climate Station. From "Meteorological Service Singapore", 2019 (http://www.weather.gov.sg/climate-climate-of-singapore/)

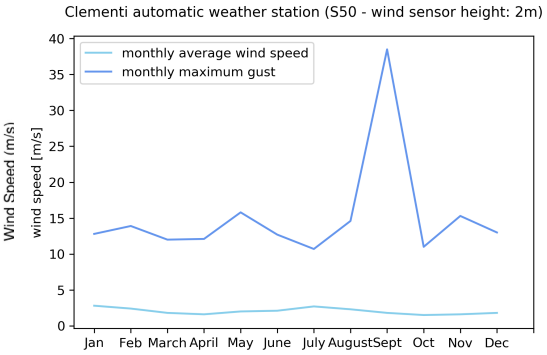

Figure 3.4: plot created based on 2017 monthly average wind speed & 2017 monthly maximum gust measurement data (Clementi weather Station, from "Annual Climatological Report 2017" by Meteorological Institute Singapore, 2017)

Wind speeds in Singapore are generally rather low due to the city state's proximity to the equator. (Acero & Ruefenacht, 2017) This, along with the high urban density, makes urban ventilation, and thus the establishment of a good outdoor thermal comfort, rather challenging. The mean surface wind speed is generally lower than 2.5 m/s; that is, except in case of a surge during the Northeast Monsoon or a surface wind gust due to thunderstorms during the Southwest Monsoon, which can temporarily yield a much higher value. (Meteorological Service Singapore, 2019) As an example, the monthly average reported wind speeds of 2017 were compared to the monthly maximum gust for the meteorological station closest to the study area (station ID S50; wind sensor at 2m height) by plotting the data from the Annual Climatological Report 2017 by the Meteorological Institute Singapore, as shown in *figure 3.4*.

As can be seen from the graph, the maximum gust wind speed reported every month is considerably higher than the average wind speed. An interesting observation in this case is that the maximum gust wind speed that occurred in September 2017 was much higher than those of the other months. While the difference between the maximum gust and the average wind speed was 36.7 m/s in September, the mean difference of the other months was 11.0 m/s. This may be attributed to a Southwest Monsoon Sumatra squall, causing gusty surface winds.

Being surrounded by water, the sea breeze effect, which causes a cool sea breeze to be blown inland underneath the rising warm urban air during the day and, reversely, the cool air over land to be drawn in underneath the rising warm air over sea at night, is another common phenomenon in Singapore. (Meteorological Service Singapore, 2019)

Temperature

Overall, the temperature in Singapore is quite consistent throughout the year. As can be seen from *figure 3.5*, there are no large temperature fluctuations. In fact, the maximum difference in the average monthly temperature is only 1.8 °C. In comparison, the highest monthly average temperature measured at the Clementi weather station in 2017 was 28.5°C and therefore exceeds the highest average monthly temperature over the entire period of 1981–2010. ("Annual Climatological Report 2017" by Meteorological Institute Singapore, 2017) Referring back to the 1981–2010 graphs, the highest mean daily maximum temperature over one month is 32.4 °C (April), while the lowest daily minimum temperature averaged over a single month is 23.9°C (January). Looking at the extremes, the highest reported temperature (at a specific time) over the period 1981–2010 is 36°C, while the lowest one is 20.1°C.

The water surrounding the islands has a larger heat capacity than the land, which means that a larger amount of heat is required to cause an increase in sea temperature. (MSS – Meteorological Service Singapore, 2019) As mentioned previously, the cooler sea breezes thus have a moderating influence on the land climate.

The average yearly temperature in Singapore has been increasing by 0.25°C per decade due to the effects of climate change. (National Environment Agency, 2009) In fact, as the MSS (2019) reports, eight out of the ten hottest years measured in Singapore occurred in this century. These observations of global warming, in combination with an average reported Urban Heat Island (UHI) of 4°C in Singapore (Acero & Ruefenacht, 2017), lead to a further increase of outdoor temperatures in the city state.

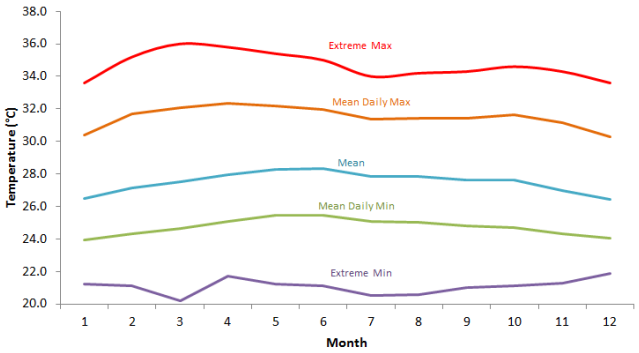

Figure 3.5: mean monthly temperature variation 1981–2010, Changi Climate Station. From "Meteorological Service Singapore", 2019 (http://www.weather.gov.sg/climate-climate-of-singapore/)

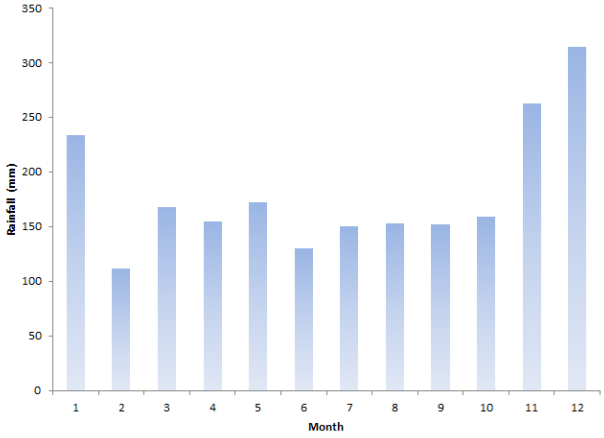

Figure 3.6: monthly rainfall 1981–2010, Changi Climate Station. From "Meteorological Service Singapore", 2019 (http://www.weather.gov.sg/climate-climate-of-singapore/)

Precipitation

With an average number of rainy days (≥ 2mm rainfall) of 167 per year, rainfall is abundant in Singapore. (Meteorological Service Singapore, 2019) In contrast to the small temperature fluctuations, the precipitation shows more variation throughout the year. This can be seen from the chart in *figure 3.6*, depicting the average precipitation [mm] per month measured over the period 1981–2010. As can be seen from the graph, the months with the highest precipitation are November, December and January, whereas the month with the lowest precipitation is February.

Relative Humidity

Apart from its high temperatures, Singapore's climate also has a high relative humidity. The average yearly relative humidity is 83.9 %, with no significant variation between the months. (Meteorological Service Singapore, 2019) Interestingly, when looking at the change in relative humidity over the course of the day there is more variation though.

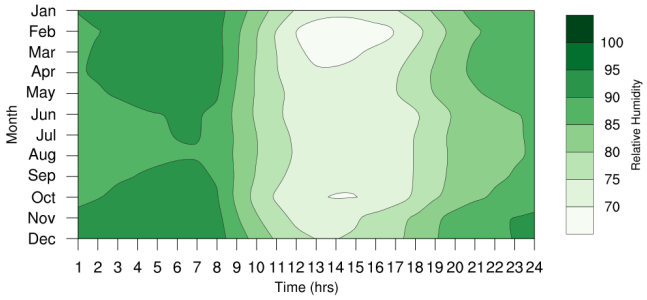

Figure 3.7: monthly and hourly variation in relative humidity 1981-2010, Changi Climate Station. From "Meteorological Service Singapore", 2019 (http://www.weather.gov.sg/climate-climate-of-singapore/)

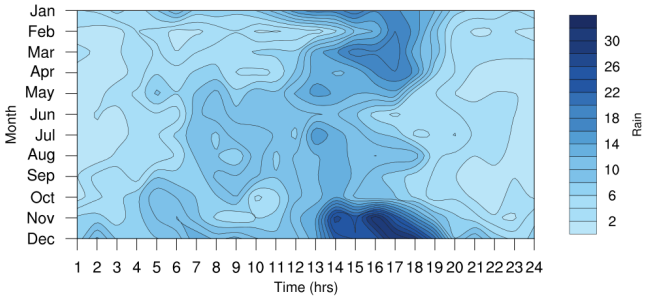

Figure 3.8: hourly variation of rainfall per month 1981-2010, Changi Climate Station. From "Meteorological Service Singapore", 2019 (http://www.weather.gov.sg/climate-climate-of-singapore/)

As can be observed from the left plot (*figure 3.7*), the relative humidity ranges between 85% and 95% in the early morning, but gradually decreases to a value below 75% (or even lower in some cases) in the early afternoon and then gradually increases back to values above 85% in the late afternoon and evening. This may be due to afternoon / early evening showers, as there seems to be a relation with the rainfall pattern (*figure 3.8*). As can be seen from the graph, these heavy afternoon / evening showers are most common from October to mid-April. These are the months in which relative humidity values of 85% start earlier in the evening, with a further increase in the early hours of the next morning.

Sunshine & Cloud Cover

Given its proximity (1.3° North – Google Earth Pro, 2019) to the Equator, Singapore experiences overhead sun throughout the entire year. This can be seen from the sun path projected over the study area using the Ladybug tool for Grasshopper *(figure 3.9)*.

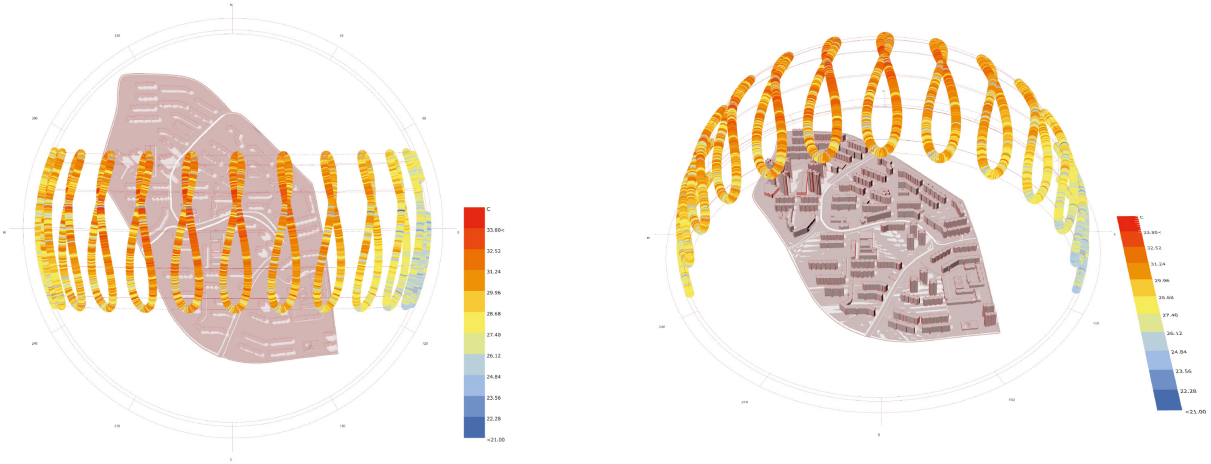

Figure 3.9: sun path diagram with dry bulb temperature (yearly data). (Created using Ladybug tools for Grasshopper.)

As a result, the amount of sunshine received in Singapore is relatively constant throughout the year, with an average number of sunshine hours per day of four to five during the driest and eight to nine during the wettest months. (Meteorological Service Singapore, 2019) A substantial part of its potential amount of sunshine is blocked by Singapore's extensive cloud cover, resulting in an often overcast sky. The average monthly hours of sun are displayed in the graph below *(figure 3.10)*. As can be observed, the highest number of sunshine hours occur at the end of the Northeast Monsoon (February and March), while the most overcast conditions apply around the beginning of this monsoon period (November and December).

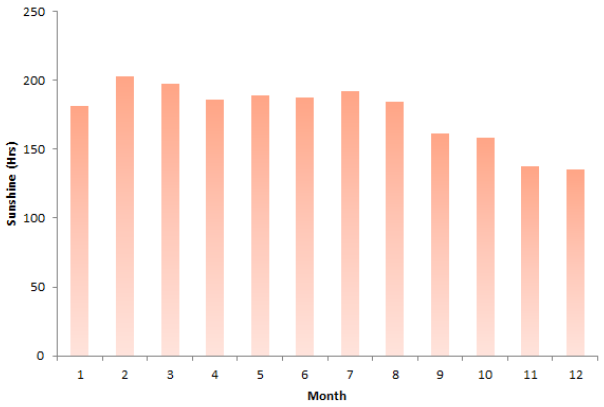

Figure 3.10: average monthly sunshine hours, Changi Climate Station.
From "Meteorological Service Singapore", 2019 (http://www.weather.gov.sg/climate-climate-of-singapore/)

3.2 Urban Atmospheric Boundary Layer

The lowest part of the atmosphere, ranging from 100m to 3000m, is influenced by the earth's surface and the transport processes taking place in this layer. Defined by Stull (1988, p. 2) as "that part of the troposphere that is directly influenced by the presence of the earth's surface, and responds to surface forcings with a timescale of about an hour or less", the atmospheric boundary layer (ABL) is profoundly different from the free atmosphere on top of it. The main differences between the ABL and the free atmosphere, which together constitute the troposphere, are listed below.

	atmospheric boundary layer (ABL)	free atmosphere
depth	Variable depth between 100m and 3000m in time and space with diurnal variations over land	Less variable depth (8-18km) and slow time variations
mean wind speed	Near logarithmic wind speed in surface layer	Nearly geostrophic
turbulence	Present over entire depth	Mostly laminar; low/sporadic turbulence
vertical transport	Turbulence-dominated	Mean wind flow-dominated (slow vertical transport)
dispersion	Rapid turbulent mixing in 3D (horizontally & vertically)	Molecular diffusion; rapid horizontal transport by mean wind
energy dissipation	Strong drag (earth's surface) and large energy dissipation	Small viscous dissipation

Table 3.1: characteristics of ABL & free atmosphere. Based on Blocken (Basic Aspects of Fluid Flow. In Sports, Building and City Aerodynamics (ATHENS course KUL27 November 2019), by B. Blocken, 2019, Leuven, Belgium: KU Leuven.) and Stull (An Introduction to Boundary Layer Meteorology (1st ed. reprint, p. 612), by R.B. Stull, 1988, Dordrecht, The Netherlands: Kluwer Academic Publishers.)

Looking at urban environments in particular, a few sub-layers, as displayed in *figure 3.11*, can be distinguished. Firstly, the layer stretching from the ground level up to the roof level of the buildings in the urban area is commonly referred to as the *urban canopy layer*. As the name suggests, the *wake layer* on top of this is characterized by the wakes and internal boundary layers (IBLs) formed as a result of the individual buildings and changes in surfaces. In the third layer, the *surface layer*, the individual effects of those wakes are not recognizable anymore, although there is still a significant overall influence by the urban character of the area. Lastly, the top-most layer of the urban ABL is called the *mixed layer*.

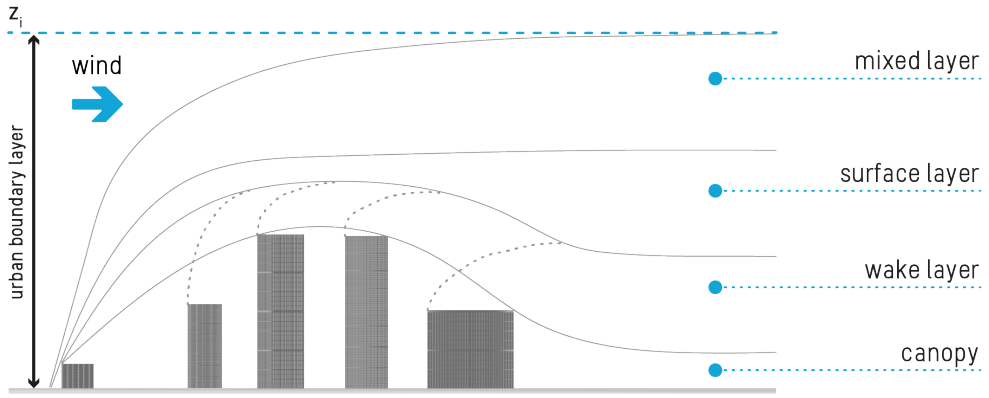

Figure 3.11: urban ABL structure

The mean horizontal wind speeds in the ABL increase with height according to a logarithmic profile described by the log law for flow over a uniform terrain:

$$U(z) = \frac{u^*_{ABL}}{\kappa} * \ln\left(\frac{z + z_0}{z_0}\right) \qquad (3.1)$$

with

$U(z)$ = mean wind speed [m/s] at height z[m];
u^*_{ABL} = friction velocity [m/s];
κ = von Kármán constant ≈ 0.41;
z_0 = aerodynamic roughness length of terrain [m] (see *section 6.1.3.1.*)

The influence of the aerodynamic roughness length z_0 on the logarithmic wind speed profile in the ABL is shown in *figure 3.12* (note, the aerodynamic roughness length is denoted as y_0 in the plot). The gradient of the wind speed (i.e. the change in U with z) gets smaller with increasing height above the surface. (Blocken, 2009) By comparing the drawn log-profiles for different aerodynamic roughness lengths, it becomes clear that a higher y_0-value (or z_0) results in a reduced steepness of the curve.

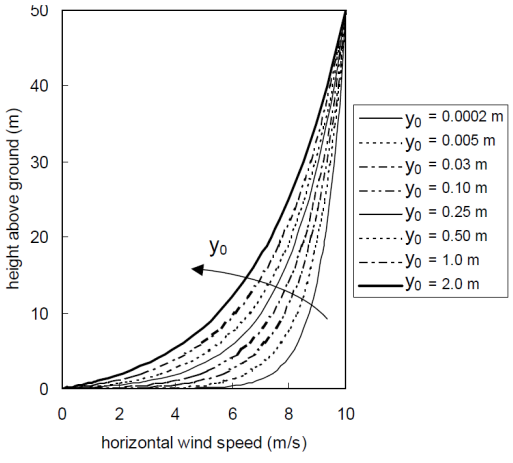

Figure 3.12: logarithmic law plotted for different roughness lengths (wind speed of 10m/s at reference height 50m). From CFD in Building Engineering Course Book: fundamentals and applications in urban physics and wind engineering (Eindhoven University of Technology, Unit Building Physics and Systems – 7S892), by Blocken, 2009. (https://www.academia.edu/3984861/CFD_in_Building_Engneering_Course_Book)

3.3 Urban Geometry Ventilation Strategies for Tropical Climates

Various urban ventilation measures can be taken to enhance outdoor comfort in tropical climates. The focus of this thesis lies on the design of urban geometry in such a way that it facilitates ventilation in the city. Urban geometry strategies to improve outdoor comfort in tropical climates can generally be divided into three groups (Acero & Ruefenacht, Cooling Singapore, 2017):

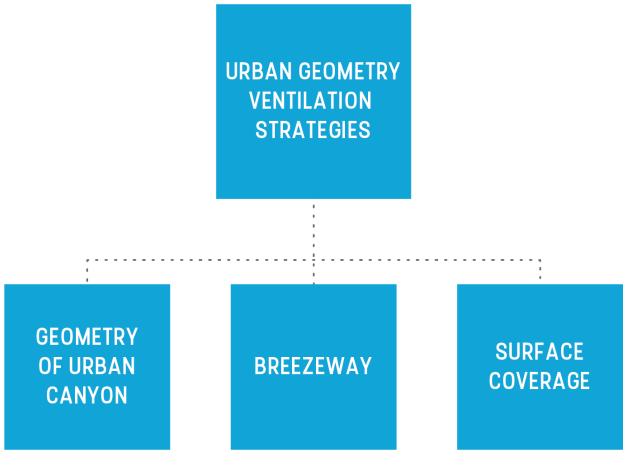

Figure 3.13: urban geometry strategies to improve outdoor comfort

Firstly, some design strategies with regard to the geometry of urban canyons can be implemented. This mainly entails the selection of appropriate dimensions for the street canyons to increase the shaded area in the streets whilst allowing wind flows to pass through. Important considerations here are for example the sky view factor and the canyon aspect ratio. The sky view factor (SVF) represents the ratio between the radiation received on a planar surface and the total radiation that is emitted by the hemisphere, so a low SVF is beneficial during the day to reduce the solar heat gain, although this also implies that outgoing radiation at night will be more 'trapped' than in case of a high SVF. (Acero & Ruefenacht, Cooling Singapore, 2017) Similarly, a good balance is to be sought between a low canyon aspect ratio (canyon height H divided by the canyon width W), which would improve the 'entrance' of wind flows through the streets and thus lead to a higher removal of heat and pollutants, and a high one, which would imply more shading from the sun. (Acero & Ruefenacht, Cooling Singapore, 2017) However, instead of planning a uniform city layout based on these ratios, it is better to create more variation in building heights. By arranging buildings according to ascending heights, a larger portion of the incoming wind flow is able to reach the buildings at the rear. (Acero & Ruefenacht, Cooling Singapore, 2017) Moreover, the staggering of building heights and void decks can help to increase wind speeds. (Acero & Ruefenacht, Cooling Singapore, 2017) Besides, the taller buildings in this arrangement may increase ventilation in the streets due to downdraught, although it should be noted that this could have a negative impact on the pedestrian wind comfort. Also, these tall buildings impact the terrain roughness. In terms of the canyon width, increasing the dimension would allow for a larger air movement, which would improve the release of accumulated heat. (Acero & Ruefenacht, Cooling Singapore, 2017) These canyons could also help in bringing more sea breezes into the city centre. However, in case of space constraints other measures exist. For example, by increasing the building permeability through the integration of void decks at the ground level and elevated voids at higher levels, wind flows through the city centre will be blocked less, as explained by Acero and Ruefenacht (2017). They emphasize that voids at the ground level will have a larger effect on the removal of pollutants and heat generated at the ground level. However, they do mention that mid-level voids also play an important role in case of very tall buildings or deep canyons. Since the main circulation in people's daily routes takes place at the ground level, it makes sense to prioritize the focus on voids at this level in this research.

Related to the aspects mentioned above, the second set of strategies for urban ventilation focuses on breezeways. In addition to determining the appropriate dimensions of streets, proper attention should be paid to how these streets are oriented and linked together in the grid plan. Open spaces should be provided along the seashore to enable sea breezes to penetrate into the city, and these should be linked effectively with other open spaces, such as at road junctions. (Acero & Ruefenacht, Cooling Singapore,

2017) Moreover, additional urban elements can be used to guide the wind flows along the desired path. This can be done by implementing void decks at the ground level of buildings and/or wing walls. (Acero & Ruefenacht, Cooling Singapore, 2017) Of course, in order to achieve the desired wind flow pattern in the city, this requires a detailed analysis of the void decks, wing walls, building setbacks and other urban elements that could influence the wind flows during the design phase of new developments.

Thirdly, Acero and Ruefenacht (2017) mention the impact of surface coverage on outdoor comfort. They explain that the combination of the terrain elevation and the added urban layer influence the type of microclimate that will establish on a particular location. In this sense, it is important to realize that the terrain should always be included when analysing wind flows in urban environments and that void decks, and any other urban elements aimed at improving ventilation, should not be treated as an isolated object while designing these.

An overview of all the urban geometry strategies that can be applied to enhance urban ventilation is shown in *figure 3.14*. As highlighted, this research on void decks focuses on building porosity and guiding wind flows with urban elements, which fall under the "breezeway" ventilation strategy.

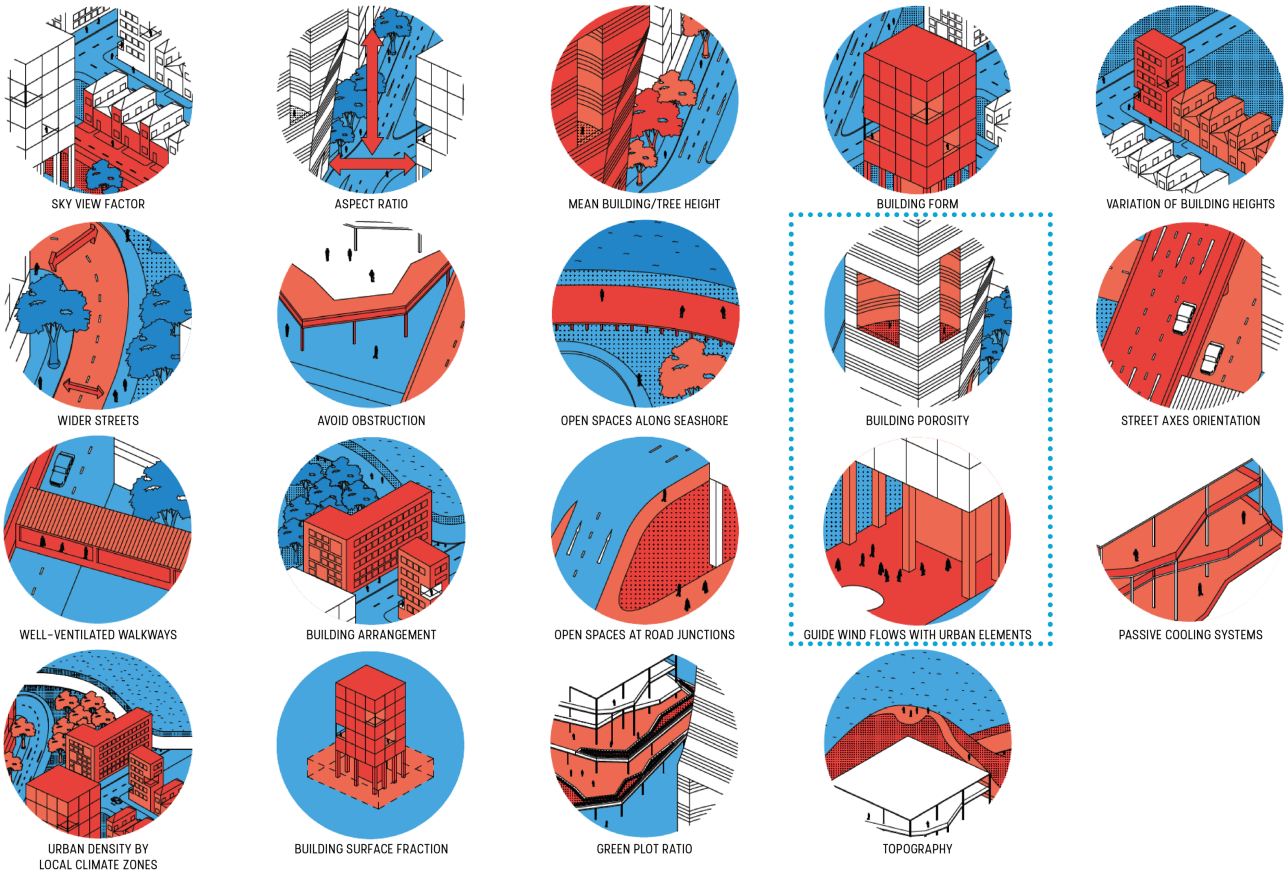

Figure 3.14: urban geometry strategies to enhance urban ventilation. Adapted from "Strategies for Cooling Singapore: a catalogue of 80+ strategies to mitigate urban heat island and improve outdoor thermal comfort" by J.A. Acero & L.A. Ruefenacht, Cooling Singapore, 2017. (https://www.coolingsingapore.sg/catalogue-of-strategies)

3.4 Characteristics of Void Decks in Singapore

Although Singapore and Hong Kong both have a similar tropical climate, their building planning, and thus also their urban ventilation, is very different. While Hong Kong's typical building typology includes a podium underneath the towers, thus blocking most of the urban wind flows, Singapore has introduced the shaded void deck as a strategy to increase urban ventilation by perforating buildings at the ground level. (Ng, 2016)

According to Giok Ling and Tan (1992), there are three main factors that make these void decks popular amongst residents in Singapore:

- Wide user relevance, as the void decks can be used by anyone and for a large range of activities
- Void decks provide favourable environmental conditions (shade and shelter)
- Convenient location (at the bottom of each block)

In this section, the main characteristics of void decks in Singapore are briefly summarized with respect to the following aspects: construction period, orientation, amenities and defining elements inside and enclosing the void decks, location and adjacencies, size and spatial layout. For a further elaboration on void decks, please refer to *Appendix A (Void Decks Elaboration)*.

Void decks are a common characteristic of Singapore's public housing buildings, which are managed by the Housing and Development Board (HDB) and accommodate more than 80% of its total population. (Housing and Development Board, 2019) These HDB blocks are organized in 23 – and a 24th one currently in planning phase – residential neighbourhoods, also known as New Towns, spread over the mainland as shown in *figure 3.15*.

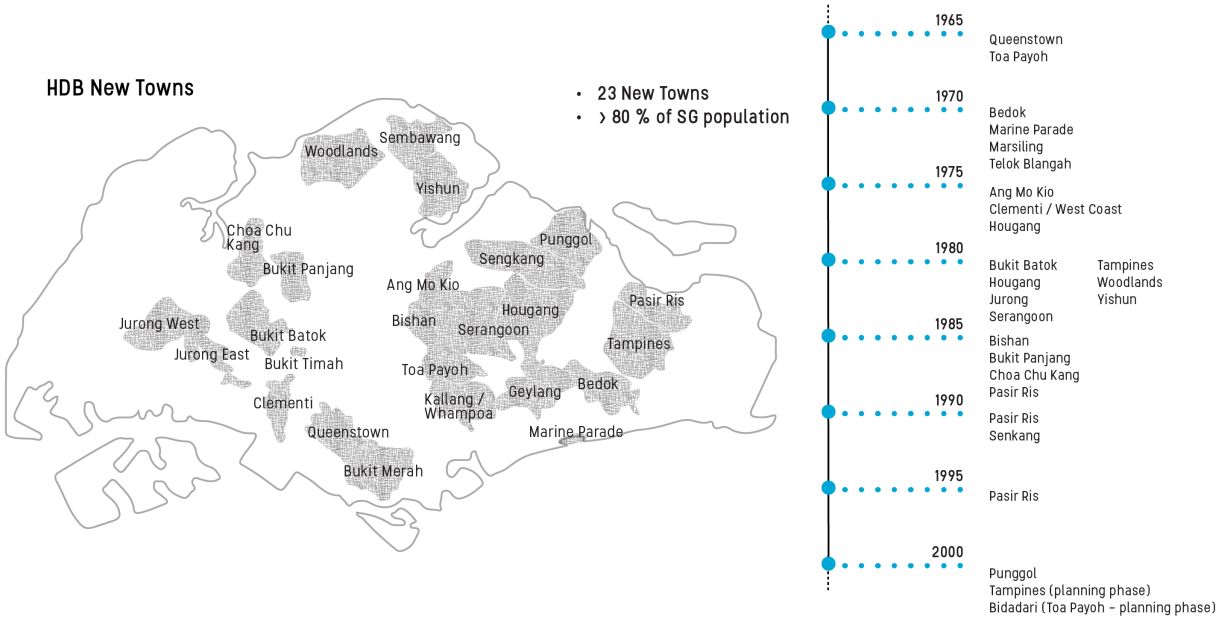

Figure 3.15: overview of HDB New Towns in Singapore

The HDB building typologies underwent changes as these New Towns developed in different stages. Throughout the past decades, different bio-climatic design strategies have been applied to New Town developments in Singapore, which has resulted in a variety of different block arrangements and orientations (Roesler & Vihervaara, 2015), as shown in *figure 3.16*.

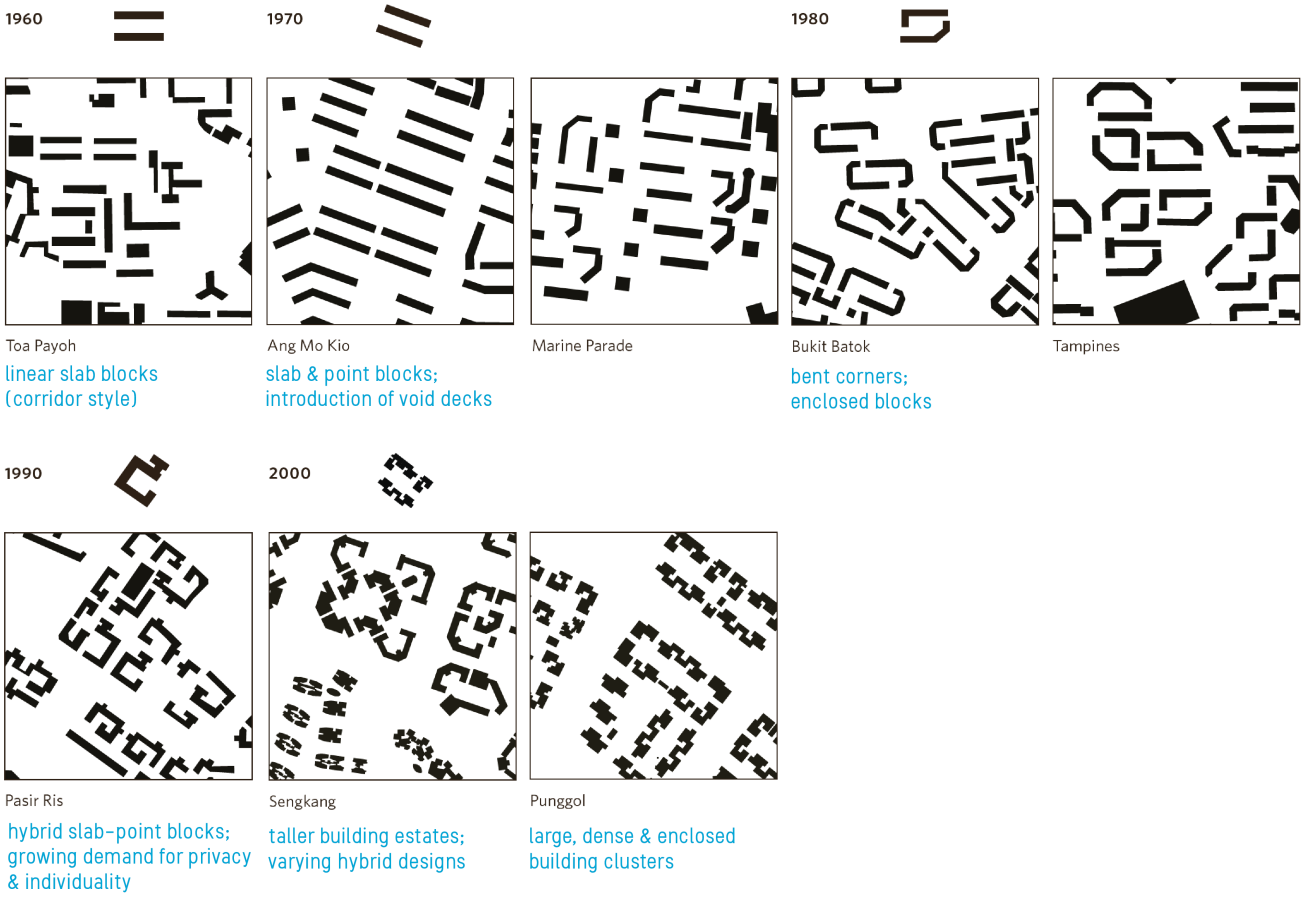

Figure 3.16: evolution of HDB block configurations. Adapted from "Evolution of New Towns – New domestic landscapes of HDB and popular cultures of natural ventilation" by S. Roesler & A. Vihervaara, Future Cities Laboratory, 2015. (http://e-collection.library.ethz.ch/eserv/eth:49661/eth-49661-01.pdf)

Ground-floor void decks emerged in the 1970s, the first one supposedly originating from 1963 in Tiong Bahru (Yeo, 2016), and have remained a characteristic of HDB flats in Singapore up until today. Void decks are known for their openness, which is only obstructed by the load-bearing walls, structural columns, lifts and stairwells, gutters, benches and a few recreational elements in some cases. Their simplicity allows for a large range of activities and functions (e.g. covered play area, outdoor gym, public art gallery, bicycle storage), which can be adapted to meet the changing needs of the residents. As such, void decks are often seen as "an extension to the home". (Cairns, Jacobs, Yingying, Padawangi, Siddique, & Tan, 2014)

New developments have shown a reintroduction of ground-floor apartment units to accommodate disabled and elderly people. To compensate for this reduced communal space on the ground floor, elevated void decks and sky gardens, as well as separate communal precinct pavilions, have become common features in newer estates. This evolution is shown in *figure 3.17*.

Secondly, it was found that the void decks in the older, long slab-block, HDB buildings were mostly aligned with the prevailing North and South wind directions. However, later residential buildings became more enclosed (*see figure 3.18*) due to an increased demand for privacy, which resulted in an increased variation in building – and therefore void deck – orientations.

CONSTRUCTION PERIOD

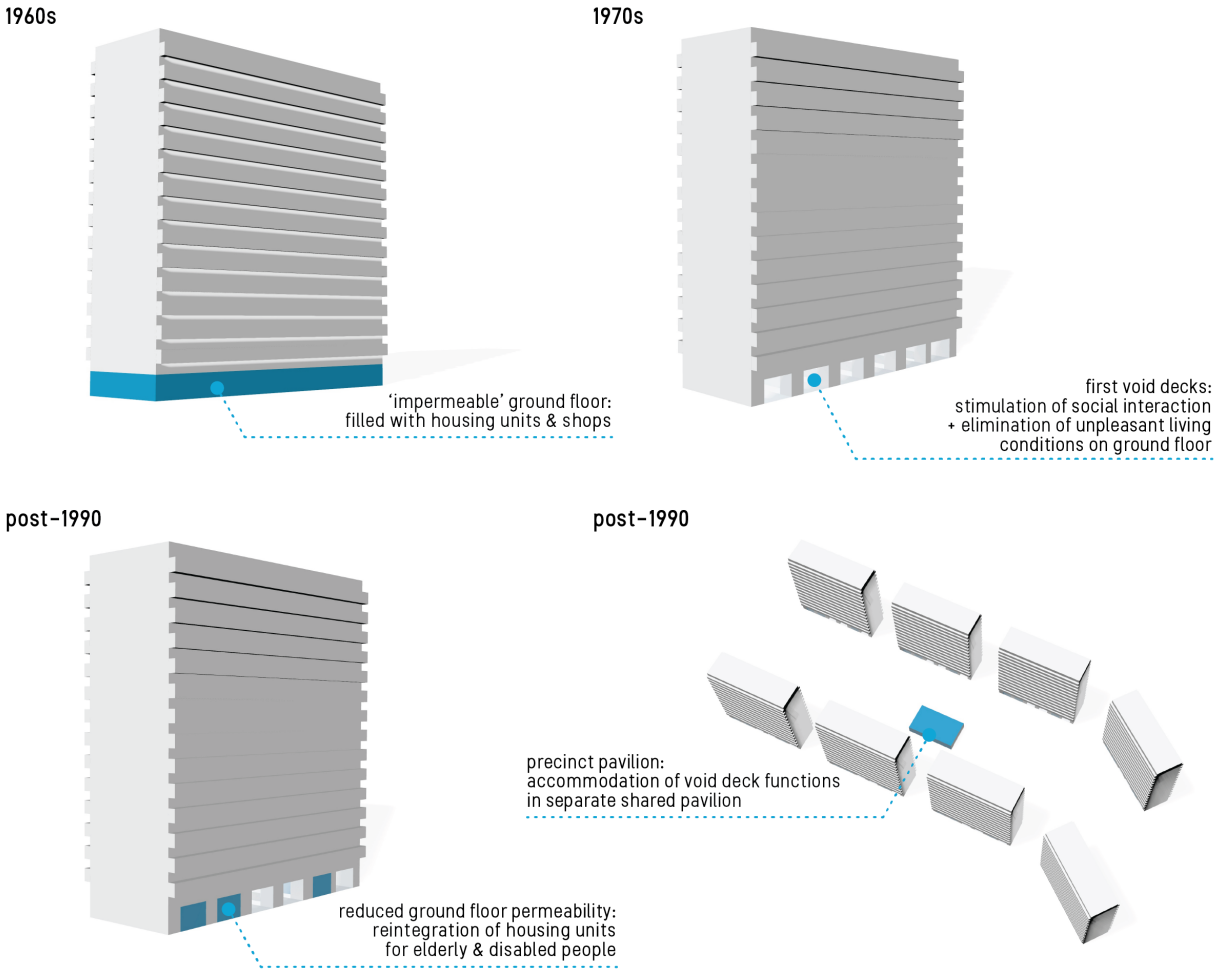

Figure 3.17: void deck characteristics – construction period

ORIENTATION OF OPENING

1960s – 1980s

HDB blocks aligned with E-W axis to prevent excessive solar heat gains on façades

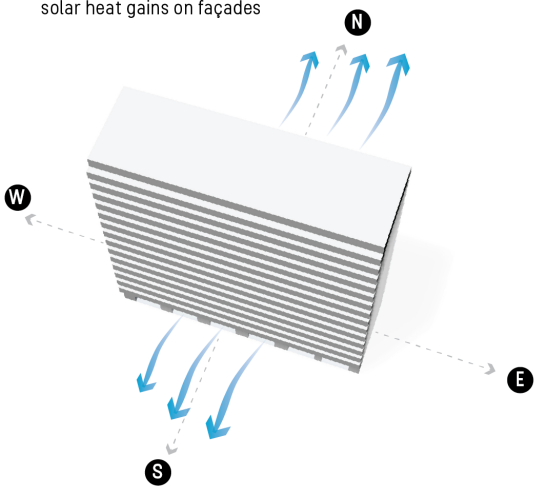

=› void deck openings facing N & S
(coinciding with prevailing wind directions)

later estates

new building typologies & more enclosed building clusters due to increased demand for privacy

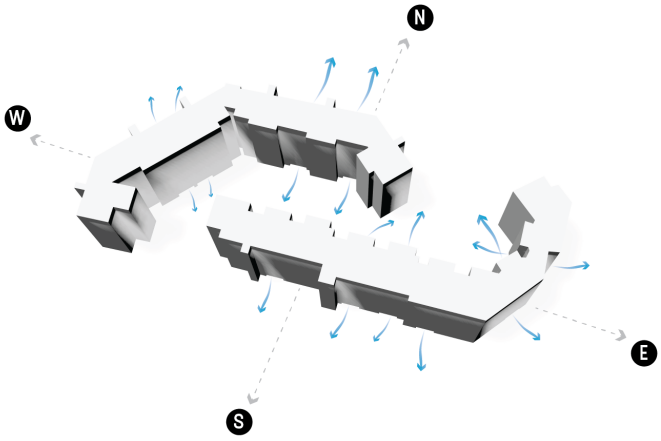

=› more variation in building & void deck orientation

Figure 3.18: void deck characteristics – orientation of opening

Besides the evolution in building – and thus void deck – orientations, there has also been a change in size. As buildings grew taller in height over time, the former long slab blocks were replaced by taller blocks with a reduced area per floor. This resulted in a significant reduction in void deck sizes. Moreover, their initially simple rectangular shape became more complex due to the earlier mentioned increased variation in orientations and building shapes.

The intensity of usage of void decks does not only depend on the provided amenities, but also to a great extent on the location. The most-used void decks have been found to be those at the breeziest locations, those which are most visible for passersby, and the ones which are located near shophouses or simply have a higher probability of encounters with neighbours along the route to e.g. the market. (Giok Ling & Tan, 1992) This marks the importance of a good wind microclimate and a strategic location of the void decks to be successful as places of interaction. To stimulate this, void decks have been linked with play-grounds since 1982; forming semi-enclosed clusters of HDB blocks with the playground acting as a focal point. (Giok Ling & Tan, 1992) This planning reasoning resulted in the formation of self-sustaining 2 to 4 ha-clusters (e.g. 200m by 200m), as determined based on the distance which people are willing to walk in a tropical climate (around 350m), with amenities all within a close, walkable, range.

3.5 Outdoor Thermal comfort

3.5.1 Parameters Defining Thermal Comfort

The factors which define a thermal environment and the comfort level and human response to it are (Parsons, 2014):

- Air temperature
- Radiant temperature
- Humidity
- Air velocity
- Activity level (metabolic rate)
- Clothing level

The latter two factors relate to the adaptive comfort principle; the tendency to restore one's thermal comfort through adaptive measures, which leads to an 'active interaction' with our environment. (Nicol, Humphreys & Roaf, 2012) Besides the aforementioned factors, it should be noted that thermal comfort is time-dependent, meaning that thermal perception also depends on the duration of exposure to a certain temperature. As pointed out by Nicol, Humphreys and Roaf (2012), not all adaptive comfort strategies which are typically applied in indoor environments are also applicable to outdoor settings. Important adaptive outdoor comfort strategies include the provision of shading, shielding from the wind and clothing adaptation. (Nicol, Humphreys & Roaf, 2012) This adaptive behaviour plays an important role amongst Singaporeans to increase outdoor thermal comfort. This is for example apparent from the low average clothing value in Singapore as compared to that in other warm climates, as shown in *table 3.2*.

city, country	I_{cl} [clo]	climate type	source
Taichung City, Taiwan (summer)	0.6	warm-humid	Lin (2009)
Singapore	0.3	warm-humid	Yang et al. (2013)
Guayaquil, Ecuador	0.5	warm-humid	Johansson and Yahia (2011)
Hong Kong (summer)	0.45	warm-humid	Cheng et al. (2012)
Lisbon, Portugal (summer)	0.4	Mediterranean	Andrade et al. (2011)
Damascus, Syria (summer)	0.6	hot-dry	Yahia and Johansson (2013)

Table 3.2: average clothing values in warm climates. From Urban Climate Challenges in the Tropics – Rethinking Planning and Design Opportunities (1st Ed., p. 175), by Emmanuel, R., 2016, UK: Imperial College Press. Copyright 2016 by Imperial College Press.

Although clothing adaptation is thus a very common strategy in Singapore, moving to shaded areas was found to be the foremost preferred thermal adaptation method. (Baruti, Johansson and Åstrand, 2019) In this regard, void decks in Singapore provide excellent options for people to adapt their thermal comfort state whenever they feel it is necessary. Moreover, Pijpers-van Esch (2015) states that people tend to be more tolerant towards the thermal environment if they reside in a space of their own free will, as opposed to if they are required to be there (e.g. waiting; work-related). She therefore promotes the development of outdoor spaces with a variety of micro-climates for people with different comfort perception levels so that they have more options to stay in a place that is comfortable to them.

A second remark to be made is that the comfort parameters are always related to each other. As such, different models, known as thermal indices, have been developed to assess the thermal comfort of an environment based on the combination of these parameters. While rational thermal indices are based on theory (usually the body's heat balance), empirical ones are based on the statistic relationship between different thermal parameters (derived based on a combination of measurements and subjective thermal comfort perception from e.g. questionnaires). (Johansson, 2016) The following section summarizes the most common thermal indices that can be used to assess outdoor thermal comfort and provides some guidelines for the comfort range.

3.5.2 Thermal Comfort Guidelines

The overview below (*table 3.3*) includes the most common rational and empirical thermal indices to assess outdoor thermal comfort and summarizes their main characteristics as well as their applicability to Singapore.

RATIONAL THERMAL INDICES				
thermal index	**description**	**parameters**	**comfort range**	**applicability**
Perceived Temperature (PT)	adaptation of PMV to outdoor contexts [°C scale]	N/A	0°C < PT < 20°C corresponds to state 0 (no thermal stress; comfortable)	not applicable to Singapore (assumed clothing level too high)
Physiological Equivalent Temperature (PET)	index expressing the air temperature at which energy balance for typical indoor conditions is balanced with same skin temperature and sweat rate as calculated for complex outdoor conditions [°C scale]	T_a [°C], MRT [°C], v[m/s]	18°C < PET < 23°C corresponds to no thermal stress; comfortable	not all parameters available (MRT)
Universal Thermal Climate Index (UTCI)	outdoor index developed to be valid in all climate types and all seasons [°C scale]	T_a [°C], MRT [°C], v[m/s], p_{vapour} [Pa]	18°C < UTCI < 26°C	overestimation of UTCI (assumed walking speed too high for Singapore; assumed clothing values based on Europe)
Skin Wettedness (w)	thermal acceptability based on skin wettedness [/]	M, R_e [Pa*m^2/W], p_{atm} [Pa]	threshold 1: w < 0.0012*M + 0.15 threshold 2: w < 0.3	thermal acceptability threshold 2 only applicable for metabolic rate M = 125 W/m2; threshold 1 is preferred
EMPIRICAL THERMAL INDICES				
thermal index	**description**	**parameters**	**comfort range**	**applicability**
Temperature of Equivalent Perception (TEP)	outdoor thermal comfort index for subtropics, based on questionnaire survey in São Paulo [°C scale]	T_a [°C], MRT [°C], v[m/s], RH	19.6°C < TEP < 27.2°C corresponds to neutrality	not all parameters available (MRT)
Wet-Bulb Globe Temperature (WBGT)	index of heat stress experienced by a person in both indoor and outdoor environments [°C scale]	T_{nw} [°C], T_g [°C], T_a [°C]	recommended value dependent on metabolic rate & state of acclimatisation	no available on-site measurements of wet-bulb and globe temperature
Temperature-Humidity Index (THI)	index to assess discomfort specifically in warm-humid regions [°C scale]	T_a [°C], RH	21°C ≤ THI ≤ 24°C => 100% of subjects feel comfortable; 24°C < THI ≤ 26°C => 50% of subjects feel comfortable; THI > 26°C => 100% of subjects feel uncomfortably hot; *Remark: calibration to local climate conditions Singapore => discomfort threshold to be raised to 31°C	specifically developed for warm-humid regions; data available
Heat Index (HI)	apparent temperature; thermal index applicable to situations with T_a > 20°C [°C scale]	T_a [°C], RH	HI ≥ 27°C => caution / danger	applicable to Singapore (T_a > 20°C); data available

Table 3.3: overview of thermal indices for outdoor thermal comfort assessment

The indices which cannot be applied to assess the outdoor thermal comfort in the study area of this research due to e.g. unavailability of some of the required parameters or invalid assumptions for the adaptive aspects of thermal comfort (e.g. clothing value, metabolic rate) for the case of Singapore are filtered out. A description of those indices can be found in *Appendix B (Thermal Indices)*.

The outdoor thermal comfort indices which are applicable to Singapore with the data that is available in this research project are the Temperature-Humidity Index (THI) and the Heat Index (HI). Both can be determined based on the air temperature T_a (°C) and relative humidity RH. The **Temperature-Humidity Index**

(THI) was developed specifically to assess discomfort in warm-humid regions. (McIntyre, 1980; as cited in Johansson, 2016) It is therefore a relevant thermal index for this research, although the results should be interpreted with caution due to the exclusion of several other important thermal comfort parameters such as radiant temperatures and metabolic rate.

$$THI = 0.8 * T_a + \frac{RH * T_a}{500} \quad [°C] \qquad (3.2)$$

with
T_a = air temperature [°C]
RH = relative humidity [%]

The corresponding thermal comfort range based on this index can be described according to the three comfort classes shown in *table 3.4* (Emmanuel, 2005; as cited in Johansson, 2016):

THI range	perceived comfort
21˚C ≤ THI ≤ 24˚C	100% of assessed persons feel comfortable
24˚C < THI ≤ 26˚C	50% of assessed persons feel comfortable
THI > 26˚C	100% of assessed persons feel uncomfortably hot

Table 3.4: original THI comfort limits (uncalibrated to Singapore's local context)

However, as mentioned by Emmanuel (2005), a wider tolerance range for elevated temperatures can be expected in tropical regions as compared to mid-latitude areas due to the combination of acclimatization and adaptive behaviour (e.g. adjusted clothing and food habits). As these effects should not be neglected, he emphasizes the importance of calibrating thermal index comfort ranges to local or similar climate conditions. A thermal acceptability analysis of 13 outdoor urban spaces in Singapore found an acceptable operative temperature range between 26.3 °C and 31.7 °C. (Jusuf et al., 2013) It was concluded that people are more likely to expect higher temperatures outside than inside and, as a consequence, their tolerance towards swingeing outdoor temperatures is often higher than towards those indoors. In this regard, the THI discomfort threshold for Singapore's tropical climate should be raised to 31°C. (Lee, Ponraj, Ossen, Iwao, & Chelliapan, 2014; as cited in Heng & Chow, 2019)

The **Heat Index (HI)**, also referred to as "apparent temperature", represents the temperature sensation of the body due to exposure to the combination of heat and humidity and can be determined using the following formula (Blazejczyk, Jendritski, Staiger et al., 2012; as cited in Johansson, 2016):

$$HI = -8.784695 + 1.61139411 * T_a + 2.338549 * RH - 0.14611605 * T_a * RH - 1.2308094 * 10^{-2} * T_a^2 - 1.6424828 * 10^{-2} * RH^2 + 2.211732 * 10^{-3} * T_a^2 * RH + 7.2546 * 10^{-4} * T_a * RH^2 - 3.582 * 10^{-6} * T_a^2 * RH^2 \quad [°C] \qquad (3.3)$$

with
T_a = air temperature [°C]
RH = relative humidity [%]

This thermal index is only applicable in situations with temperatures above 20°C (Johansson, 2016) and can thus be used for the case of Singapore. The corresponding assessment scale is shown in *table 3.5* below.

HI range	category
27˚C ≤ HI < 32˚C	caution
32˚C ≤ HI < 41˚C	extreme caution
41˚C ≤ HI < 54˚C	danger
HI ≥ 54 ˚C	extreme danger

Table 3.5: HI assessment scale. From Urban Climate Challenges in the Tropics – Rethinking Planning and Design Opportunities (1st Ed., p. 188), by Emmanuel, R., 2016, UK: Imperial College Press. Copyright 2016 by Imperial College Press.

Since this index focuses merely on the thermally unacceptable or dangerous range, the Temperature-Humidity Index for warm-humid climates is more suitable in this project to assess the outdoor thermal comfort in Singapore.

Furthermore, it is interesting to elaborate a little on the influence of air speed on thermal comfort since a major part of this research focuses on wind velocities. The cooling effect of wind speed is dependent on the relative humidity in the environment. (Johansson, 2016) This is shown in the graph (*figure 3.19*) below, which illustrates the temperature offset as a function of wind speed for different values of relative humidity. Firstly, the chart shows that, for the same relative humidity, a higher temperature offset – or cooling effect – is reached in case of a higher wind speed and, as a consequence, a higher temperature can be tolerated. By increasing the wind speed, a person can thus still feel thermally comfortable even at a high temperature. However, since the slope of the graph is steeper at lower wind speeds, the relative thermal effect will be larger at low wind speeds as compared to high wind speeds. Secondly, the cooling effect, represented by the temperature offset, reduces with increasing relative humidity. Although an increased wind speed generally has a positive effect on thermal comfort – due to increased convective heat losses – in warm climates, the cooling effect can thus be expected to be limited for very humid climates (and higher for warm, dry, climates). Since Singapore has a warm climate with a high average yearly relative humidity of 83.9 % (Meteorological Service Singapore, 2019; *see section 3.1 Climate Analysis Singapore*), the cooling effect might thus be limited. This is one of the main subjects that will be studied in this research project.

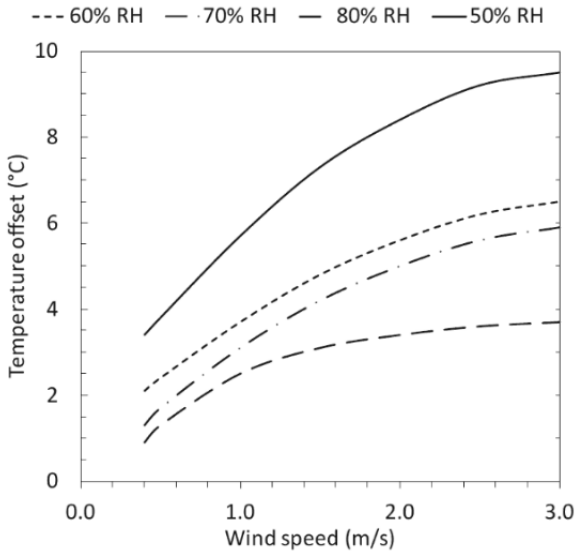

Figure 3.19: cooling effect of wind at different levels of relative humidity. From Urban Climate Challenges in the Tropics - Rethinking Planning and Design Opportunities (1st Ed., p. 172), by Emmanuel, R., 2016, UK: Imperial College Press. Copyright 2016 by Imperial College Press.

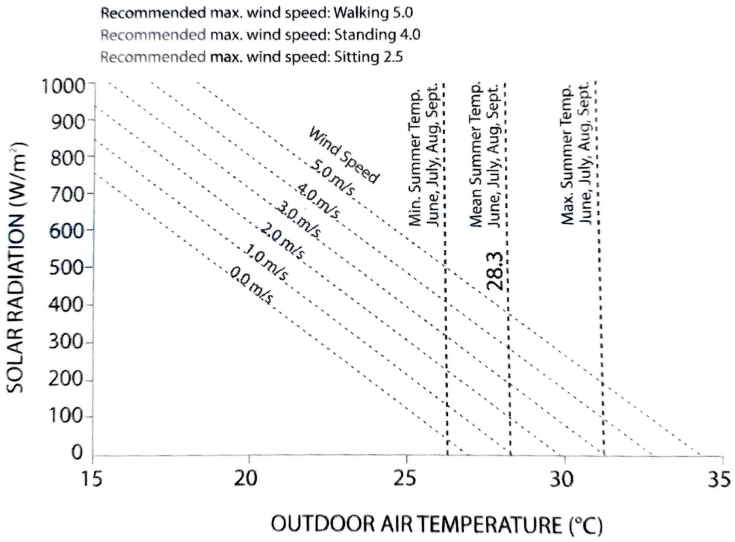

Figure 3.20: simplified comfort outdoor temperature chart for Hong Kong. From Urban Climate Challenges in the Tropics - Rethinking Planning and Design Opportunities (1st Ed., p. 83), by Emmanuel, R., 2016, UK: Imperial College Press. Copyright 2016 by Imperial College Press.

A simplified comfort outdoor temperature chart developed for tropical places such as Hong Kong may serve as a useful reference to assess the thermal comfort in Singapore. This chart (*figure 3.20*) combines many of the described parameters, such as the outdoor air temperature, wind speed, activity level and solar radiation, and relates these to each other to graphically define how much urban ventilation would be needed in order for a person to feel comfortable under the given conditions. The point of intersection of the amount of solar radiation received by a person - estimated at 100-150 W/m² in case this person is standing in shade, e.g. surrounded by tall buildings, and 700-900 W/m² in case of direct sun on the person (Ng, 2016, p.83) - and the outdoor air temperature with the diagonal air speed lines shows the approxi-

mated required urban air speed under those conditions. For example, for an average yearly air temperature of 27.7ÅC as measured in 2017 (Changi Climate Station, Meteorological Institute Singapore, 2017), a person in the shade would need an air speed of approximately 2.0 m/s to be thermally comfortable, while a person in plain sun would require much higher wind speeds, which from a pedestrian (mechanical) wind comfort point of view would be unpleasant. This highlights the importance in urban planning to provide shade in the first place, with additional wind-inducing measures to achieve a good balance between thermal and pedestrian wind comfort.

A last note to be made is that the neutral temperature – the index temperature corresponding to thermal perception vote 0 (not cool nor warm), so for 50% of the votes being 'lower than neutral' and 50% 'higher than neutral' (de Dear & Spagnolo, 2003) – is not necessarily equal to the preferred temperature. (Johansson, 2016) In other words, one may perceive the thermal environment at a certain moment as 'slightly warm' or 'slightly cool', but this does not directly imply that one wants the temperature in the space to be adjusted. However, for the case of warm-humid climates, such as Singapore, various studies have indicated a preferred temperature lower than the neutral one. (Lin, 2009; Lin, de Dear, & Hwang, 2011; Jusuf, Wong, & Yang, 2013; as cited in Johansson, 2016) According to a study by Hwang and Lin (2007), the preferred outdoor temperature is 1.2°C lower than the neutral one. This may be attributed to thermal alliesthesia, a concept which describes the effect of environmental stimuli on one's thermoregulation. (de Dear & Parkinson, 2015) Positive thermal alliesthesia concerns a positive effect on one's current thermophysiological state, while the opposite holds for negative thermal alliesthesia. (de Dear, 2011) In warm climates, this implies that if someone feels hot, anything that would cool him/her down will feel pleasant, even if it would lead to a sense of cold after a while. (Johansson, 2016) In the context of this thesis, the use of void decks as an urban ventilation strategy to amplify wind speeds, and thus increase heat loss from the human body to improve thermal comfort, can be considered as positive thermal alliesthesia. In conclusion, the concept of thermal alliesthesia was established to make a distinction between a thermal environment which is found 'acceptable' and one which would be perceived as 'pleasant'. While thermal comfort studies often focus on thermal acceptability, it is important to make this distinction and to aim for the creation of thermally pleasant environments. Of course, this is not always straightforward, considering the large spread in thermal perceptions of different people.

3.6 Pedestrian Wind Comfort

3.6.1 Parameters Defining Pedestrian Comfort

The parameters that determine whether wind discomfort occurs are (Beranek, 1979):

- person's physical condition
- person's psychological condition
- temperature
- activity level
- person's habituation to the climate

An extended Land Beaufort scale, which identifies the effects of different wind conditions (with wind speeds determined at pedestrian level) on people, was developed by Lawson and Penwarden (1975) as shown below.

Beaufort	description	wind speed at 1.75m height [m/s]	effect
0	calm	0.0 - 0.1	
1	light air	0.2 - 1.0	no noticeable wind
2	light breeze	1.1 - 2.3	wind felt on face
3	gentle breeze	2.4 - 3.8	hair disturbed; clothing flaps; newspaper difficult to read
4	moderate breeze	3.9 - 5.5	raises dust and loose paper; hair disarranged
5	fresh breeze	5.6 - 7.5	wind force felt on body; danger of stumbling when entering a windy zone
6	strong breeze	7.6 - 9.7	umbrellas used with difficulty; hair blown straight; difficult to walk steadily; sideways wind force ~ forwards walking force; unpleasant wind noise on ears
7	near gale	9.8 - 12.0	inconvenience felt when walking
8	gale	12.1 - 14.5	generally impedes progress; great difficulty with balance in gusts
9	strong gale	14.6 - 17.1	people blown over

Table 3.6: extended Land Beaufort Scale with wind effects on. From The Effects of Wind on People in the Vicinity of Buildings, by Lawson & Penwarden, 1975 (as cited in Blocken & Carmeliet, 2003).

Important to note here is that the wind speeds at pedestrian level were determined for an open terrain with an aerodynamic roughness length z_0 of 0.03m. (Blocken & Carmeliet, 2004) From Davenport and Wieringa's (1992, refer to *figure 6.4*) roughness classification we know that this terrain type is characterized by its flatness, with only some low vegetation and very isolated objects. Given the highly urbanized context of the study area in this research, the above scale will not properly reflect the wind effects experienced by pedestrians at void decks in Singapore. Some municipalities have thus established their own wind comfort guidelines or standards to assess wind effects in the urban context, which is elaborated on in the next section.

A further distinction in wind effects can be made between constant winds and wind gusts (sudden increased wind speeds of short duration). When comparing results from Deguchi, Murakami and Uehara (1980) for constant wind to reported effects of wind gusts by Bottema (1993) as shown in the table below, it becomes clear that a sudden increase in wind speed can lead to the same effects as those due to constant wind of higher velocities. This demonstrates that not only the wind speed at a specific moment is of importance; the time scale also has an influence on how wind is experienced by pedestrians.

CONSTANT WIND EFFECTS (Deguchi, Murakami, & Uehara, 1980)		WIND GUST EFFECTS (Bottema, 1993)	
wind speed	effect	wind speed	effect
5 m/s	minor disturbance of hair and clothes; wind felt on face	4 m/s during 5 s	disturbance of hair; flapping clothes
10 m/s	hair disturbed; fluttering clothes	7 m/s during 5 s	hair disarranged
25-33 m/s	people blow away	23 m/s	people blow away

Table 3.7: constant wind effects vs. wind gust effects.
Based on Duguchi, Murakami, & Uehara (1980) and Bottema (1993).

3.6.2 Pedestrian Comfort Guidelines / Standards

For building and urban planning projects, it is interesting to translate the effects of winds on humans into clear guidelines for architects, engineers and urban planners. Despite the lack of standards or guidelines for the thermal effects of wind, some recommendations with respect to pedestrian wind comfort (i.e. to prevent excessive wind forces on pedestrians) have been developed. (Pijpers-van Esch, 2015) In fact, the development of new high-rise structures nowadays often requires wind comfort studies to be performed before a building permit can be granted. These wind comfort guidelines make a distinction between wind discomfort (often specified for different outdoor activities) and wind danger around buildings. For both cases a threshold wind speed can be formulated as well as the related maximum allowed exceedance probability (P_{max}) of this wind speed.

Unlike outdoor thermal comfort assessments, which are highly dependent on local factors and therefore require an adaptation of the comfort classes to the climate being researched, pedestrian wind comfort assessments deal with the actual wind forces being exerted on people and how these may affect us, and are thus more widely applicable. Wind safety risks should be mitigated as much as possible, regardless of the location. A comparison of different criteria to prevent wind discomfort and danger was provided by Blocken, Janssen and van Hooff (2013) based on four activity categories: sitting long, sitting short, strolling and walking fast. This comparison was extended and adapted to include the recently developed comfort criteria by the City of London and RWDI and to provide some more insight in the specifications and applicability of each, leading to the following overview *(table 3.8)*.

PEDESTRIAN WIND COMFORT CRITERIA							
pedestrian comfort guideline / standard	parameters	wind discomfort threshold				wind danger threshold	specifications & applicability
		sitting long	sitting short	strolling	walking fast		
Isyumov & Davenport	mean wind speed U	U > 3.6 m/s (3 Bft) ; P_{max} = 1.5%	U > 5.3 m/s (4 Bft) ; P_{max} = 1.5%	U > 7.6 m/s (5 Bft) ; P_{max} = 1.5%	U > 9.8 m/s (6 Bft) ; P_{max} = 1.5%	U > 15.1 m/s (8 Bft) ; P_{min} = 0.01%	Wind speed threshold based on Beaufort, so actually a range
Lawson	mean wind speed U	U > 1.8 m/s (3 Bft) ; P_{max} = 2%	U > 3.6 m/s (3 Bft) ; P_{max} = 2%	U > 5.3 m/s (4 Bft) ; P_{max} = 2%	U > 7.6 m/s (5 Bft) ; P_{max} = 2%	-	Wind speed threshold based on Beaufort, so actually a range
Melbourne	mean wind speed U & standard deviation of turbulent fluctuations σ_u	U + 3.5 * σ_u > 10 m/s ; P_{max} = 0.022%	U + 3.5 * σ_u > 13 m/s ; P_{max} = 0.022%	U + 3.5 * σ_u > 16 m/s ; P_{max} = 0.022%	-	U + 3.5 * σ_u > 23 m/s ; P_{min} = 0.022%	Impact of gustiness on wind comfort taken into account; occasional gusty surface winds occur during monsoon surges and thunderstorms in Singapore
NEN 8100	mean wind speed U	U > 5 m/s ; P_{max} = 2.5%	U > 5 m/s ; P_{max} = 5%	U > 5 m/s ; P_{max} = 10%	U > 5 m/s ; P_{max} = 20%	U > 15 m/s ; P_{min} = 0.05%	More stringent wind speed criteria (but higher P_{max}) except for static activities
City of London	mean & GEM wind speed U	U > 2.5 m/s ; P_{max} = 5%	U > 4 m/s ; P_{max} = 5%	U > 8 m/s ; P_{max} = 5%	Lawson business walking conditions lead to complaints London => category re-named as 'uncomfortable'	U > 15 m/s ; P_{min} = 0.022%	Most recently developed (2019); elaborate distinction between different types of outdoor activities

Table 3.8: overview of guidelines and criteria for pedestrian wind comfort assessment. Adapted from Pedestrian wind comfort around buildings: Comparison of wind comfort criteria based on whole-flow field data for a complex case study (Building and Environment 59(2013), 547-562), by Blocken, Janssen, & van Hooff, 2013.

As the Isyumov & Davenport and Lawson criteria are based on the Beaufort scale, which specifies wind speed ranges, they do not impose a clear threshold value for the comfort assessment. This makes them less convenient for this research.

Moreover, one can observe that the Dutch NEN 8100 standard poses more stringent wind speed criteria – though with a higher maximum exceedance probability – than the other guidelines, except for static activities (activity A, sitting long; and B, sitting short). Since the average wind speeds in Singapore were shown to be very low, it makes more sense to choose a wind comfort guideline with lower wind speed classes. Also, static activities can be expected to be more commonly practised in a hot-humid climate than very active activities, which are often performed indoors.

Furthermore, the table shows that Melbourne's guideline specifies the comfort criterion both in terms of a mean wind speed and the standard deviation of turbulent fluctuations. (Blocken et al., 2013) Referring back to *table 3.7*, which showed the impact of gustiness on wind comfort, it would be good to include this effect in wind comfort guidelines for Singapore as well, as it was explained in the climate analysis (*section 3.1*) that temporary high wind speeds may occur due to surges during the Northeast Monsoon and thunderstorms during the Southwest Monsoon respectively. Especially in the wake of buildings, turbulent gust speeds can be expected to increase, despite the reduced average wind speeds in this area. (Cao & Chitty, 2014) However, more research is needed to determine how Melbourne's wind comfort guideline could be adapted to Singapore's wind conditions to create a useful assessment scale.

The recently developed comfort criteria by the City of London (in collaboration with wind engineering consultancy RWDI) are found to be most suitable for the wind comfort assessment of the urban case as these provide an elaborate distinction between very specific types of outdoor activities (e.g. specific types of walking, such as 'business walking', and 'frequent sitting'). The table below shows the main wind comfort categories that were developed for the city.

category	mean & GEM wind speed	max. exceedance probability	description of (dis)comfort category
frequent sitting	2.5 m/s	5%	acceptable for frequent outdoor sitting use, e.g. restaurant, café
occasional sitting	4 m/s	5%	acceptable for occasional outdoor seating, e.g. general public outdoor spaces, balconies and terraces intended for occasional use
standing	6 m/s	5%	acceptable for entrances, bus stops, covered walkways or passageways beneath buildings
walking	8 m/s	5%	acceptable for external pavements, walkways
uncomfortable	> 8 m/s	5%	not comfortable for regular pedestrian access
unsafe	15 m/s	0.022%	unsafe wind conditions for both pedestrians and cyclists

Table 3.9: City of London wind comfort criteria to be used in the urban case assessment. Adapted from Wind microclimate guidelines for developments in the city of London, by City of London Corporation, 2019.

Note that wind conditions below the stated threshold are considered acceptable for the corresponding mentioned activity, while those exceeding the threshold are unacceptable for that particular activity. For example, a mean wind speed of 3 m/s implies acceptable wind conditions for occasional outdoor seating, standing and walking, but discomfort for frequent outdoor sitting as this value exceeds the threshold of 2.5 m/s. The safety limit for both pedestrians and cyclists is set at 15 m/s (mean and Global Environmental Multiscale – GEM – wind speed from any direction) with a maximum exceedance probability of 0.022%. (City of London Corporation, 2019) However, the guidelines state that the city aims for even more stringent comfort criteria for cyclists as they observed a recent increase in the number of cyclists in London.

Lastly, it is worth mentioning that, although no specific urban wind comfort standards or guidelines have been developed by governmental institutions in Singapore, there are some mentions of wind aspects in the BCA Green Mark schemes. For example, the *Green Mark for Residential Buildings: 2016 Criteria* (Green Mark Department, Building and Construction Authority, 2017) does not merely focus on indoor ventilation of dwelling units, e.g. by setting specific criteria on window openings, but also stimulates passive building design strategies that may have an influence on ventilation at urban level (in part 5.01a Passive Design Strategies), such as staggering of building blocks, the provision of void decks at the ground level or other void spaces in between buildings, and carrying out macro ventilation simulations to improve the block layout. These are thus more practical design considerations, rather than wind speed criteria as the ones described for The Netherlands and the city of London. Since Singapore's Building and Construction Authority (2017) has proclaimed its dedication to greening 80% of all its buildings by 2030, this is a relevant fact as these certification schemes can be expected to be followed in the planning process of many new as well as the retrofitting process of many existing buildings.

3.7 Computational Fluid Dynamics for the Built Environment

Computational fluid dynamics (CFD) is used in many applications to numerically solve flow problems in the built environment, ranging from urban microclimate modelling for outdoor thermal and pedestrian wind comfort as well as wind-driven rain, indoor ventilation and outdoor pollutant dispersion. (Blocken, 2009) The three most common CFD approaches are Direct Numerical Simulation (DNS), Large Eddy Simulation (LES) and Reynolds Averaged Navier Stokes (RANS). The differences between these methods are outlined in *table 3.10* below.

	DNS	LES	RANS
solved	all eddies (exact Navier-Stokes equations are solved completely)	large eddies ("filtered" Navier-Stokes equations are solved => not exact)	mean flow (averaged Navier-Stokes equations are solved => not exact)
modelled (approximated)	nothing	small eddies	all eddies
computational resources	huge computational resources required; very time-consuming	less computationally demanding than DNS; more computationally demanding than RANS	much less computationally expensive than DNS and LES

Table 3.10: DNS, LES and RANS CFD approaches. Based on Computational Fluid Dynamics. In Sports, Building and City Aerodynamics (ATHENS course KUL27 November 2019) , by B. Blocken, 2019, Leuven, Belgium: KU Leuven.

Since LES and RANS include modelling, they both require the use of a turbulence model. These are the two main CFD approaches used for outdoor simulations in the built environment. Although LES tends to be more accurate than RANS in the prediction of turbulence, it requires the specification of inlet conditions that vary both spatially and temporally (Cao & Chitty, 2014), which makes it prone to high uncertainty. Besides, the increased computational cost as compared to RANS should be considered. These factors often render RANS to be a more feasible approach for simulations in the built environment.

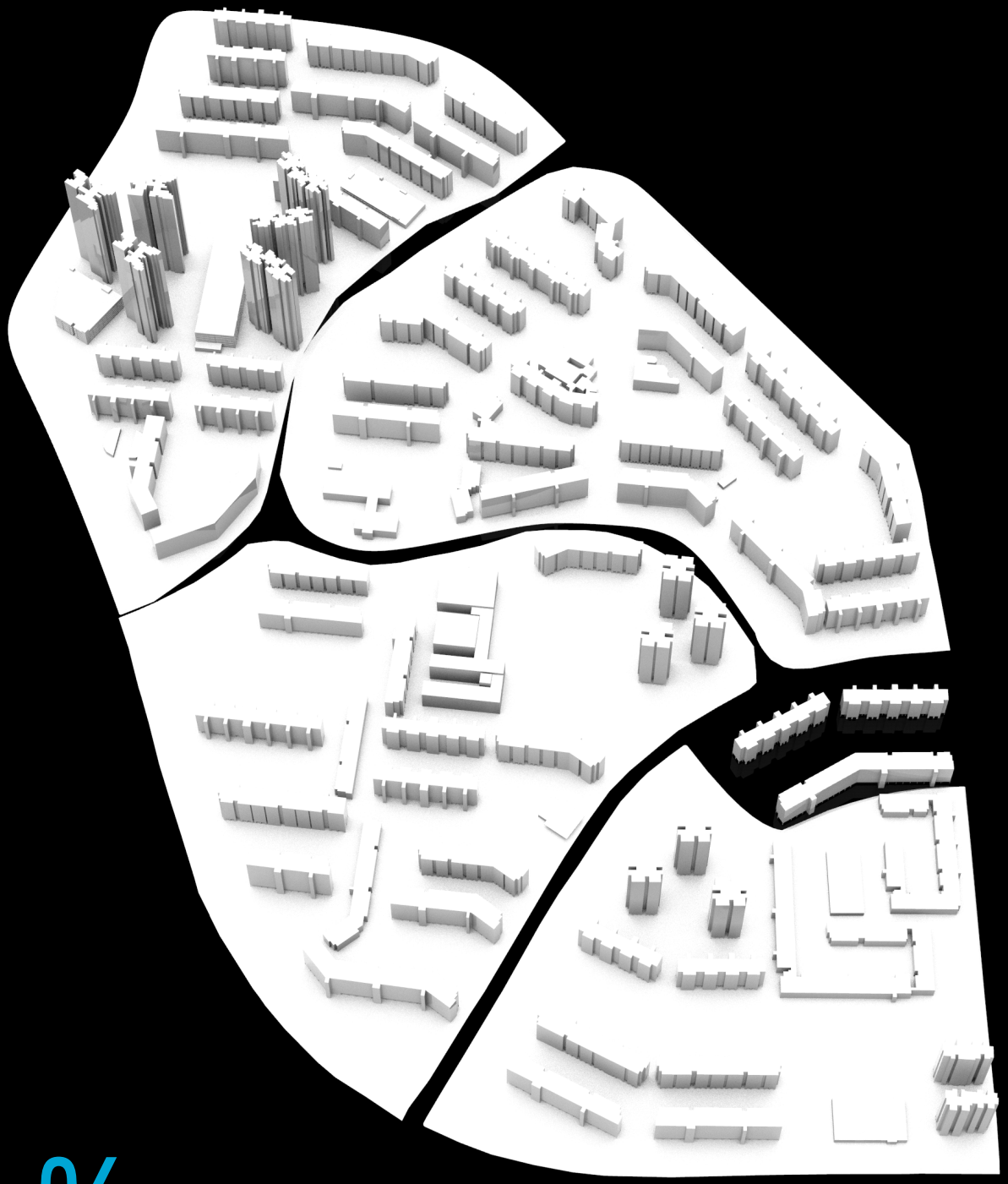

04

STUDY AREA

The study area of this urban ventilation research is located in Clementi, Singapore. This New Town was constructed between 1975 and 1980, with new buildings added at later periods. The building area included in the model (contained in between Commonwealth Avenue West on the south/southwest, Clementi Avenue 6 on the west, Clementi Road on the east and the Ulu Pandan Park Connector on the northern edge) for the simulations is marked in *figure 4.1*. Although this is not one of the densest areas – with a minimum distance of 30m between façades, which is more than 1960 and (post-)1980 estates (Roesler & Vihervaara, 2015) – in Singapore, it was considered for the wind flow study because of its variety in building types as well as building heights, representative for the various HDB buildings across Singapore, including long slab blocks of 12, 13 and 16 storeys and (hybrid slab-) point blocks of 20, 25 and even up to 40 storeys. While the former are characterized by their simple rectangular layout, the latter shrank in footprint while growing taller in height and more complex in shape. In addition, most of the buildings in this area have void decks incorporated at the ground floor level. These characteristics made the area interesting for the topic of this research.

Figure 4.1: study area

Since void decks only started to emerge in the 1970s, the majority of the void decks in the study area are one of the earliest found in Singapore; characterized by a simple rectangular layout and covering almost the entire ground floor area of the blocks. However, the buildings that were constructed in Clementi at later periods have smaller void decks, which are not necessarily rectangular in shape.

Regarding the orientation of the void decks in the study area, most of them correspond to the orientation that was defined by HDB as optimal to prevent excessive solar heat gains on the façades while allowing the prevailing winds from north, north-northeast and south to pass through the void decks (*see part 3.4*). As can be seen from the buildings in the study area (*figure 4.1*), the majority thus have their long axis

perpendicular to either the north and south, or northeast. This alignment of the void deck openings with the prevailing monsoon wind directions is also common at some other New Towns, such as the long slab blocks in Ang Mo Kio, Tampines, Yishun and Bukit Panjang. To some extent, the conclusions from the study of Clementi may thus be extrapolated to buildings with similar void deck orientations at these estates.

After defining the location and extent of the study area, an urban 3D-model was prepared to simulate wind flow distributions around the building structures. The modelling process consisted of the following steps. First, an OSM-data file for the selected area was downloaded from OpenStreetMap and imported into Grasshopper using the Elk plugin. Using the OSM Data component, the required data of the buildings could be extracted. Next, the building outlines were created and these were then extruded to create the 3D geometry. As no building height data was available for the area, the height of the buildings had to be estimated based on the extracted data of the number of floors of the buildings. The extrusion height could be determined based on the typical floor-to-floor heights in Singapore, as stated in the HDB Precast Pictorial Guide 2014 (Housing and Development Board, 2014):

- Typical floor-to-floor height: 2.8 m
- GF floor-to-floor height: 3.6 m
- Topmost floor-to-floor height: 2.8 m

Although this method will not result in a completely accurate model, using the number of storeys as a height predictor in case of a lack of elevation measurements from remote sensing techniques has been shown to result in fairly well-approximated 3D city models useful for spatial analyses both within and beyond GIS applications. (Biljecki, Ledoux, & Stoter, 2017) The Grasshopper script that was used to create the model using the described steps is shown below.

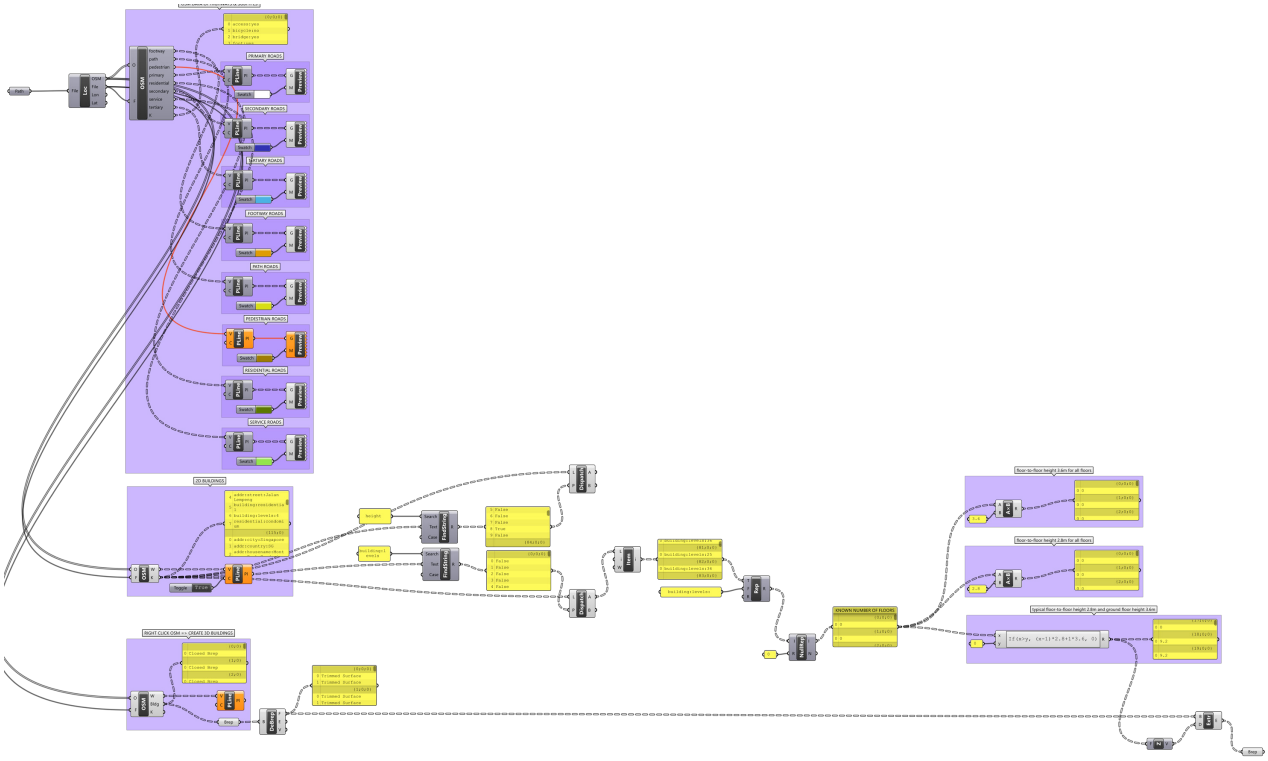

Figure 4.2: from OSM data to urban 3D model (Grasshopper script)

As can be seen from the generated 3D geometry in the image below, this height (number of floors) data was not available for all the buildings. The buildings that were lacking this data (red non-extruded building plots) were mostly non-residential or recent developments.

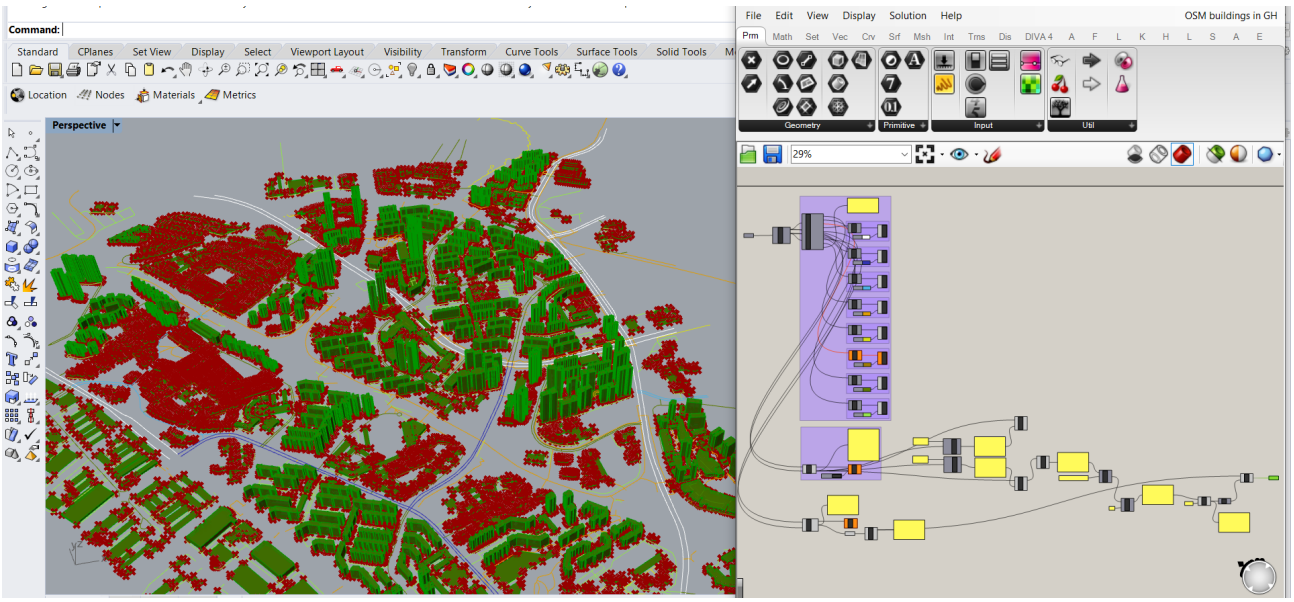

Figure 4.3: 3D-modelling process of urban area for simulation model (Rhino & Grasshopper)

In order to include those buildings in the model as well, the "3D path measurement" tool in Google Earth Pro was used to define the heights of the missing buildings. Most of these buildings had a more complex geometry (e.g. no flat roofs and consisting of several connected parts) and therefore could not simply be extruded. These buildings were thus modelled separately in Rhino.

Next, the void deck were modelled. Since the entire research is focused on these building parts, they were modelled as accurately as possible with the limited information available. Since the large obstructions (such as structural cores with stairwells and elevator shafts, and entirely enclosed rooms on the ground floor for e.g. mechanical equipment) and the obstructions at the edges of the building perimeter can be assumed to have the largest effect on the wind flow pattern around the buildings, these were the most important elements to be included in the 3D model. The void decks were modelled in Rhino based on observations in Google Street View (whenever this option was available) in combination with simple measurements in Google Earth Pro.

Lastly, the large-scale terrain characteristics were modelled implicitly. As the vast majority of the buildings in the study area are elevated from the surrounding roads, these elevation differences were taken into consideration – though in simplified form due to the lack of terrain elevation measurements – in the urban flow simulations. The elevated position of the buildings plays a role in terms of the shift in the logarithmic wind speed profile, but apart from that, the terrain relief also impacts the urban flows. Edge fillets were applied to the terrain edges wherever possible to ensure a smooth transition of the terrain, and therefore to prevent sudden flow acceleration due to sharp edges.

An image of the final 3D model of the study area, including the buildings with void decks and terrain, is shown below.

Figure 4.4: 3D-model of study area (including void decks and terrain) for urban flow simulations

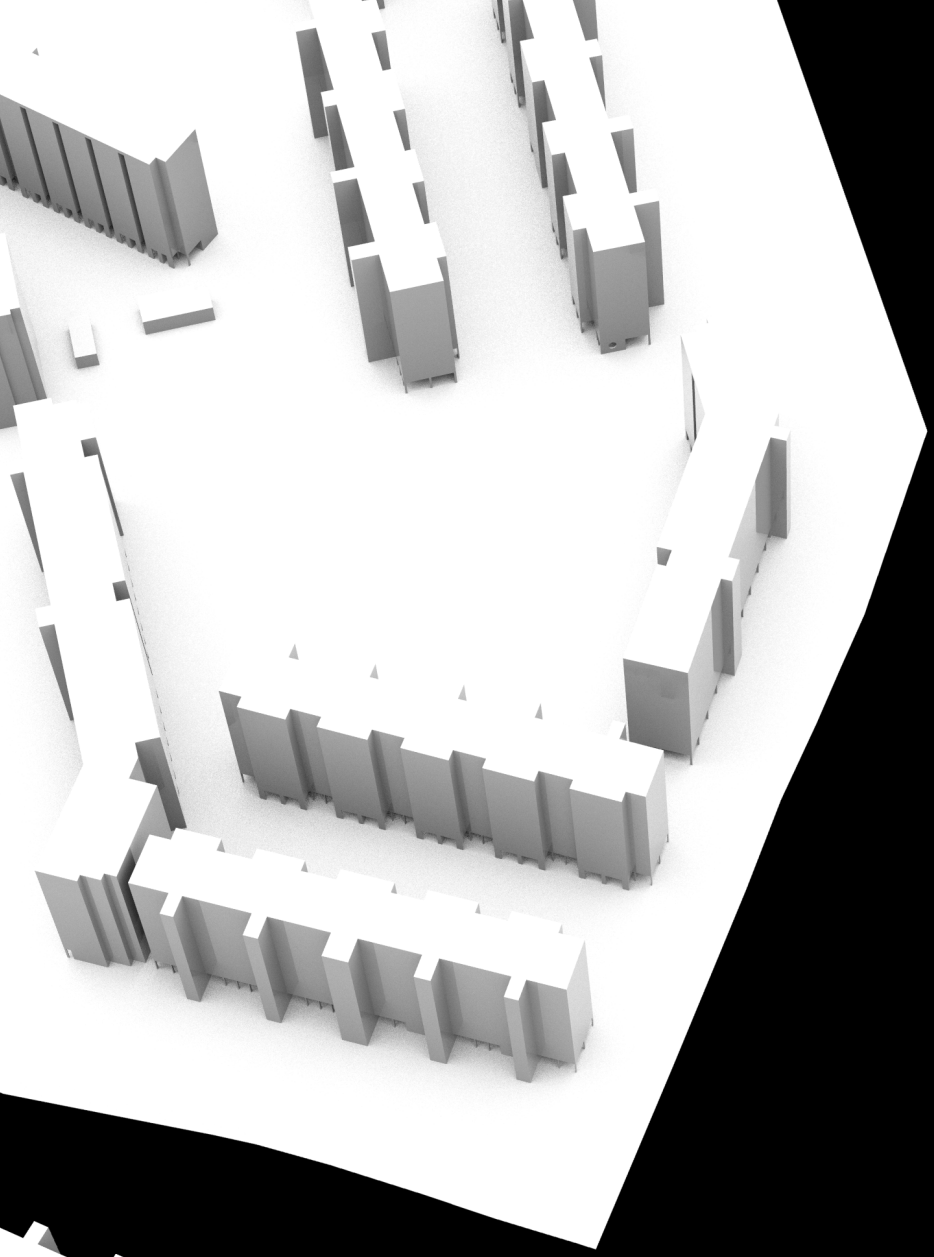

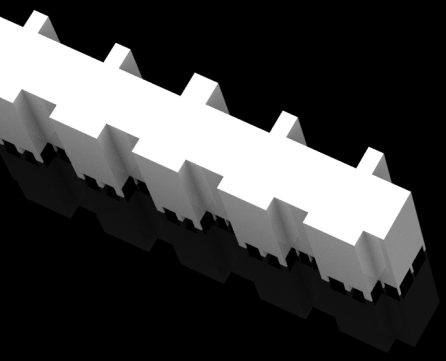

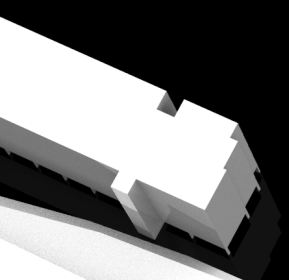

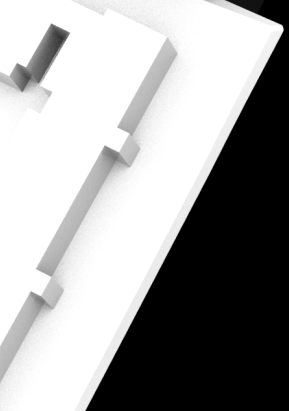

05

PARAMETRIC DESIGN

The design task entails a parametric void deck geometry design for building void decks in Singapore with the aim to optimize the wind flows tailored for outdoor thermal comfort and pedestrian wind comfort. The three key design intervention principles that are focused on in this parametric study are shown below (*figure 5.1*).

HOW CAN THE DESIGN DIVERT / MAGNIFY / REDUCE OCCURRING AIR FLOWS AT SPECIFIC AREAS?

HOW CAN THE DESIGN ADAPT TO SEASONALLY CHANGING WIND FLOW PATTERNS?

HOW CAN THE BUILDING VOID DECKS 'WORK TOGETHER' ON NEIGHBOURHOOD SCALE?

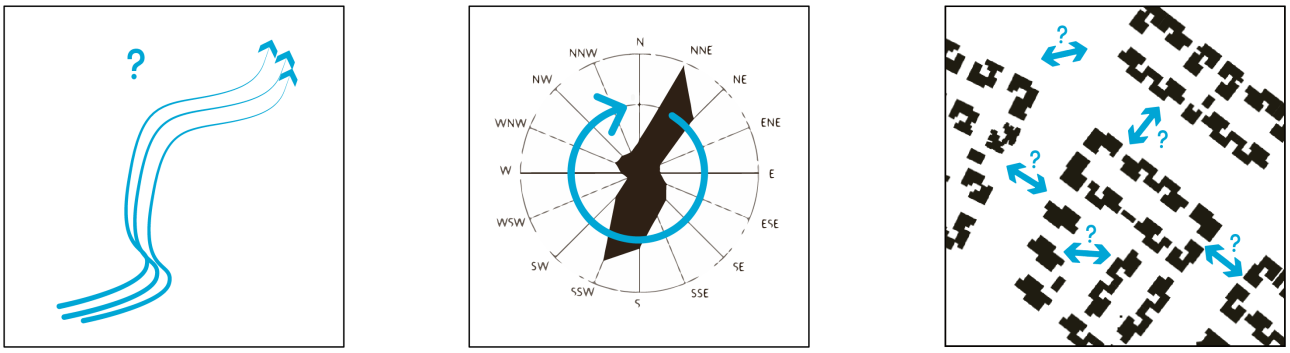

Figure 5.1: design intervention principles

Since the goal is to improve the wind flow pattern, and thus the outdoor comfort conditions at the neighbourhood scale as a whole, there is no one-size-fits-all solution. A particular void deck geometry might thus be very appropriate in one location, while it could lead to a reduced comfort state around a building at a different location. It is therefore important to establish a parametric workflow which enables one to group buildings according to certain similarities and to create an optimal void deck geometry for each of those groups.

In order to facilitate a combined parametric design and simulation approach, three models were created; one 3D model of the study area in its current situation (represented in *figure 4.4*) and two parametric models (one of a single building and one with all the buildings in the study area) in which the geometry of the void decks can be modified. These all fit their own purpose, as shown in *figure 5.2* below. The combination of these three, linked with the open source OpenFOAM CFD toolbox, enables designers, urban planners and engineers to quickly analyse, modify and test different void deck geometries for any building in the area. In this way, the impact of a specific void deck geometry modification on the surrounding flow pattern can be tested both at the building and urban scale. The next sections describe the set-up and components of the parametric models.

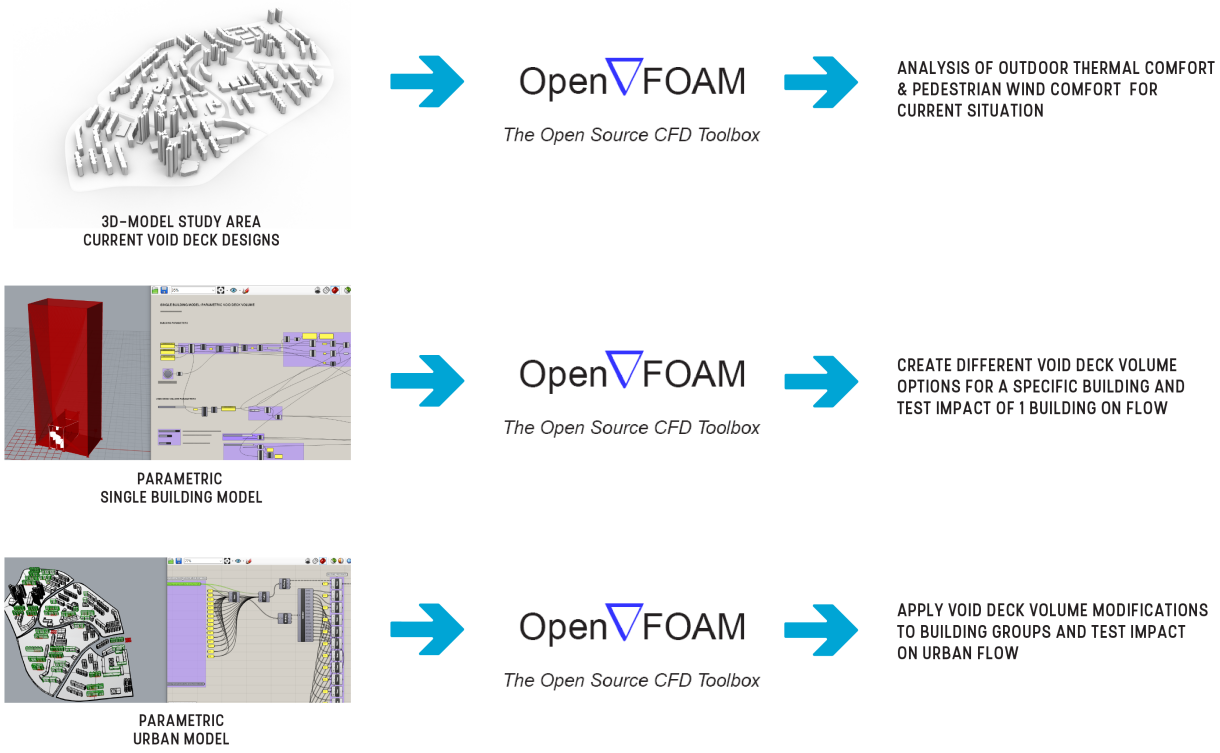

Figure 5.2: computational design & simulation approach

5.1 Parametric Building Model

The aim of the parametric Grasshopper model for a single building is to create different void deck volume variants for any specific building and to quickly test the impact of one building with a particular void deck geometry on the flow pattern. The number of void deck geometry input parameters was limited to 7 as a lot of design variations could already be generated with these.

The building input parameters are:

- building length
- building width
- building height
- building orientation

The void deck geometry parameters included in the Grasshopper model are:

- void length (expressed as percentage of building length)
- position of void deck on ground floor (allows the designer to move the void deck along the building length)
- void width at horizontal contraction (expressed as percentage of void width at inflow) with option for straight or curved taper
- void width at horizontal expansion (expressed as percentage of void width at inflow) with option for straight or curved taper
- void height
- void height decrease at vertical contraction (decrease with respect to void height set at inflow)
- void height increase at vertical expansion (increase with respect to void height set at inflow)

The single building Grasshopper script for the parametric void deck geometry is shown in *figure 5.3*, with a break-down of all the elements in the subsequent images.

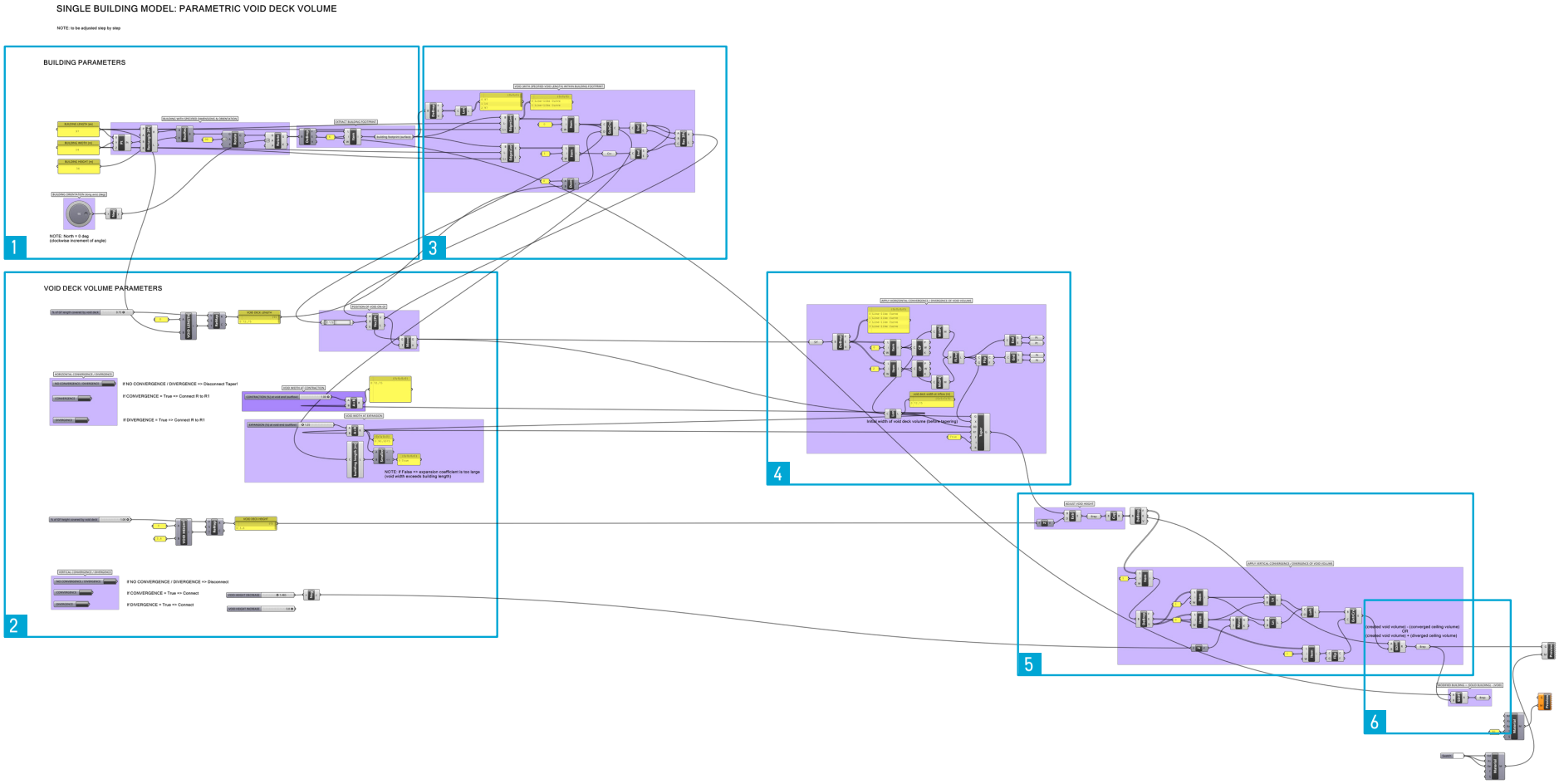

Figure 5.3: parametric building model – Grasshopper script

1 BUILDING PARAMETER INPUT

2 VOID DECK GEOMETRY PARAMETER INPUT

3 VOID DECK BASE GEOMETRY CREATION (SPECIFIED VOID LENGTH)

4 VOID GEOMETRY MODIFICATIONS: HORIZONTAL CONVERGENCE / DIVERGENCE

5 VOID GEOMETRY MODIFICATIONS: VOID HEIGHT & VERTICAL CONVERGENCE / DIVERGENCE

6 SUBTRACTION OF BUILDING VOLUME WITH CREATED VOID DECK VOLUME

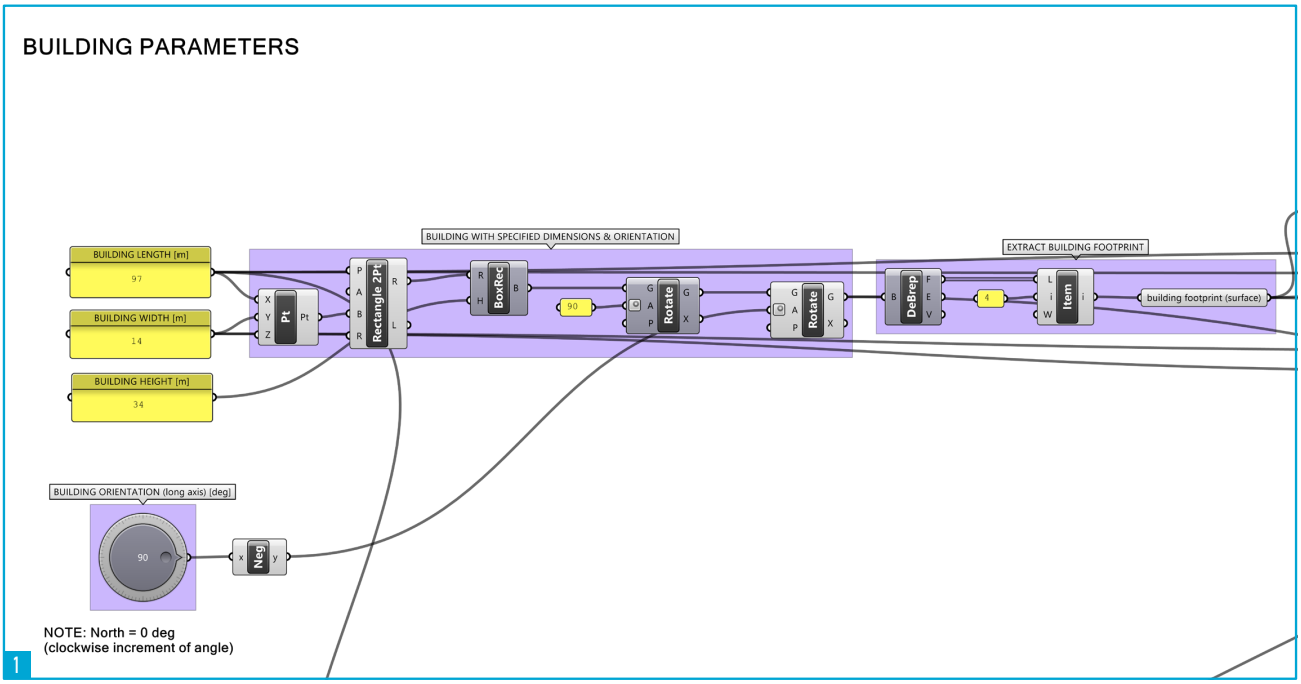

BUILDING PARAMETER INPUT

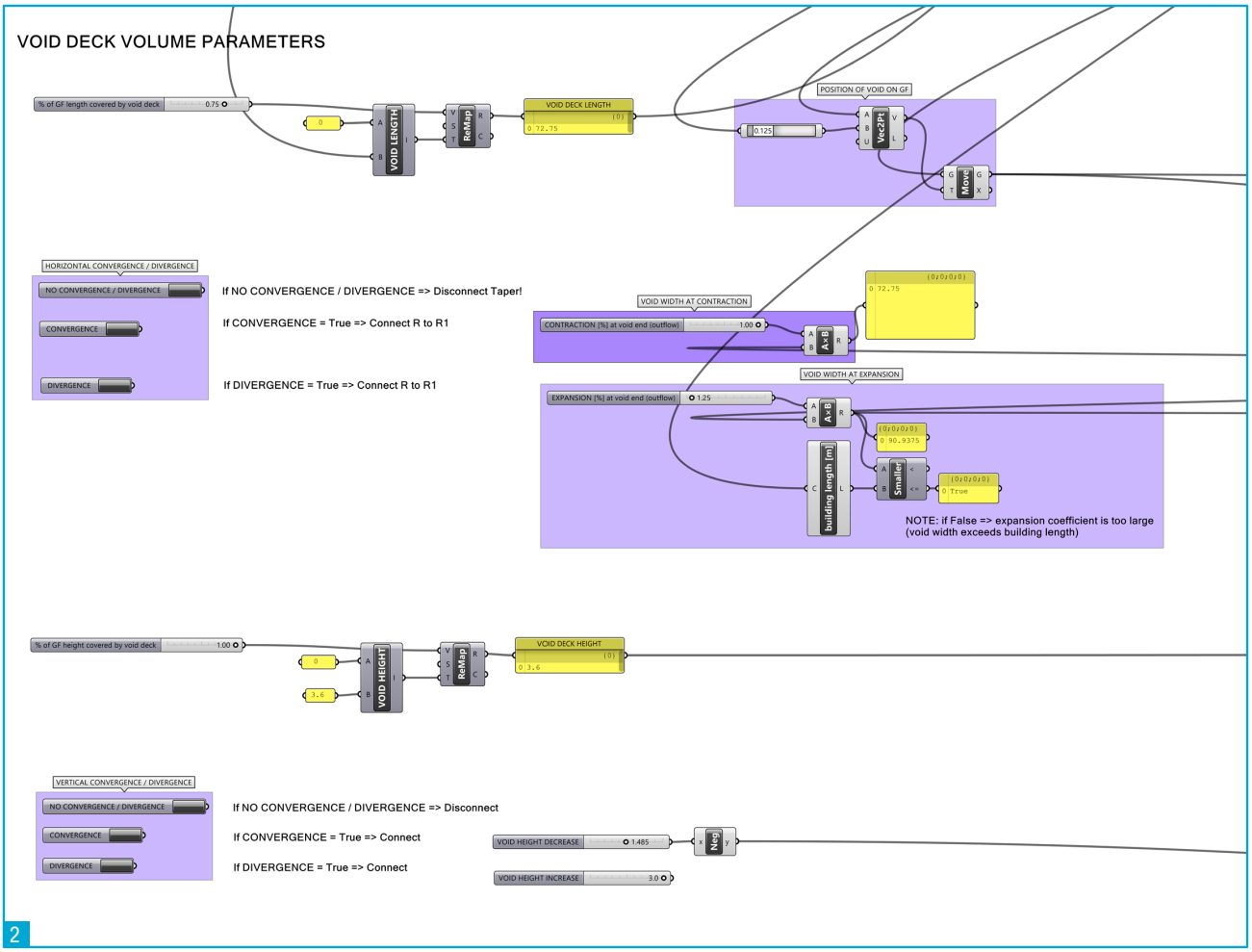

VOID DECK GEOMETRY PARAMETER INPUT

Figure 5.4: parametric building model – Grasshopper script breakdown (1)

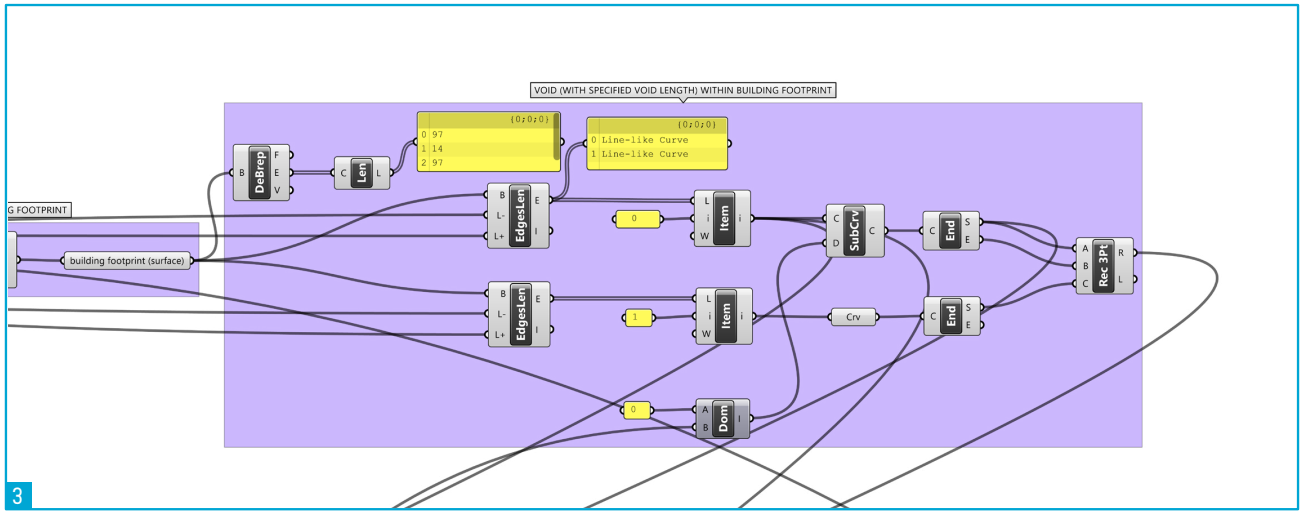

VOID DECK BASE GEOMETRY CREATION (with specified void length)

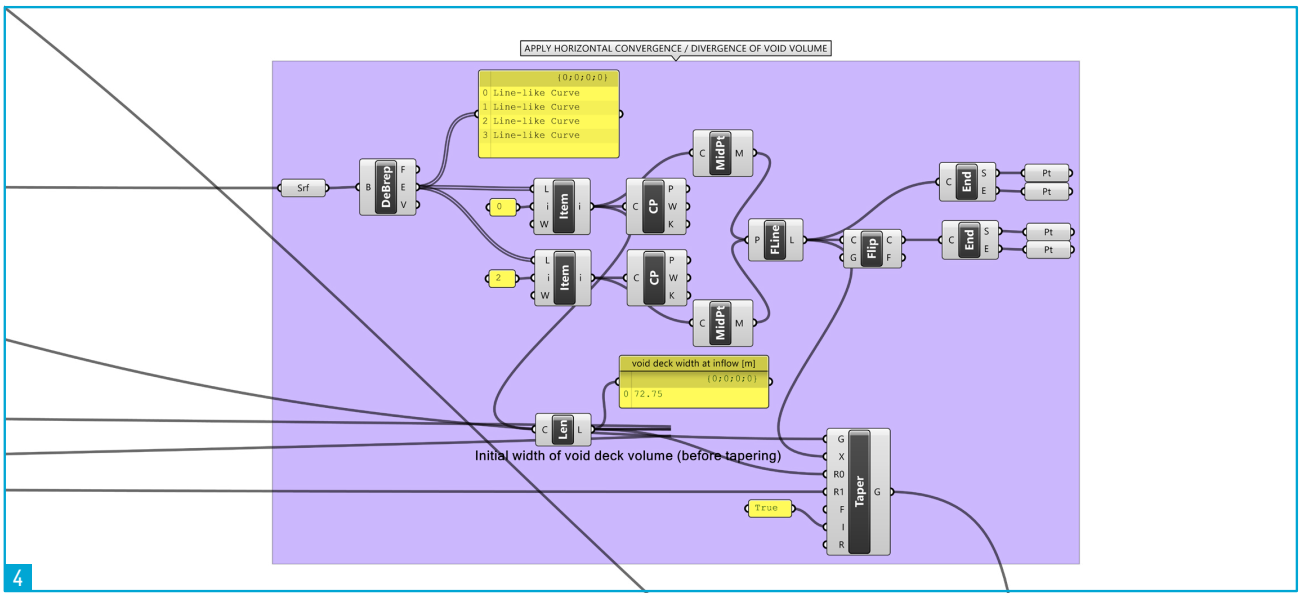

VOID GEOMETRY MODIFICATIONS: HORIZONTAL CONVERGENCE / DIVERGENCE

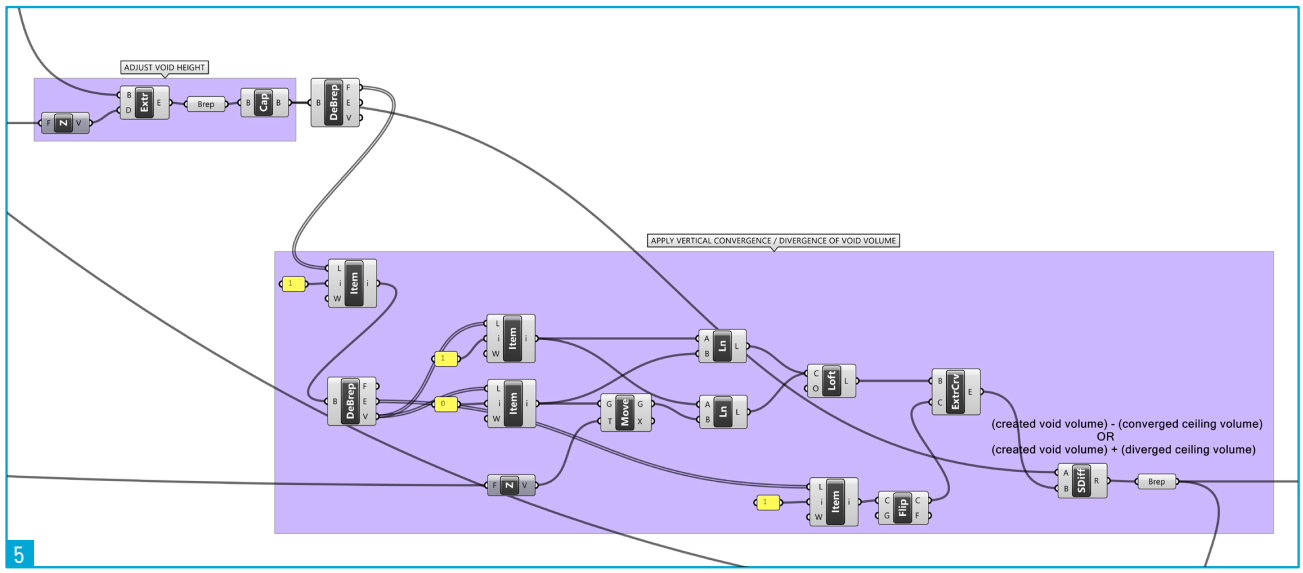

VOID GEOMETRY MODIFICATIONS: VOID HEIGHT & VERTICAL CONVERGENCE / DIVERGENCE

Figure 5.5: parametric building model – Grasshopper script breakdown (2)

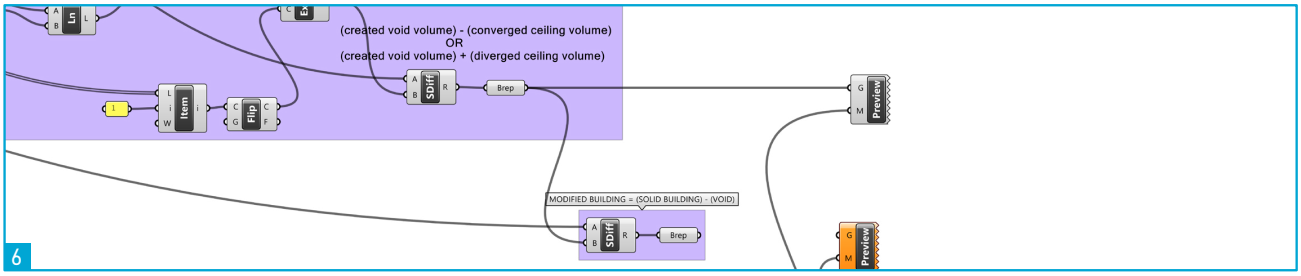

SUBTRACTION OF BUILDING VOLUME WITH CREATED VOID DECK VOLUME

Figure 5.6: parametric building model – Grasshopper script breakdown (3)

5.2 Void Geometry Design Variants

An overview of the void deck geometry variants generated with the parametric building model is given below (*figure 5.8*). Note that more details on the parameter settings per variant are given in *table 5.1*. The base case variant (variant 1) is a simple void deck of 3.6m height with no convergence or divergence in the horizontal nor in the vertical direction. As a starting point for the base case variant dimensions, a representative building in the study area (*figure 5.7*) was selected, as can be seen marked blue in the overview. This building's main axis is perpendicular to the North-South direction, which is representative for many of the buildings in the area which have void deck openings towards these prevailing wind directions.

The other variants, ranging from 2 up to 9 (with variant 2 and 3 both having 2 sub-variants to analyse the difference between straight and curved void deck walls) will be compared to the base case variant.

The main goal of the study with the single building model variants is to investigate the overall effect of different void deck geometries on the flow pattern around the building. Instead of making several of the same variant types but with different dimensions (e.g. several horizontally converging voids but with different angles), a study with more variation in geometry types was considered to be more interesting in this research. After all, the flow pattern effect observed from the single building simulation can be reinforced or weakened as wished in the urban-scale intervention by adjusting the parameters in the parametric urban model.

Figure 5.7: representative building in Clementi used as base case for the void deck study

REPRESENTATIVE BUILDING FOR VOID GEOMETRY VARIANT STUDY

building length = 97 m
building width = 14 m
building height = 34 m

1 BASE CASE: no horizontal / vertical convergence or divergence

2A horizontally converging void (straight taper)

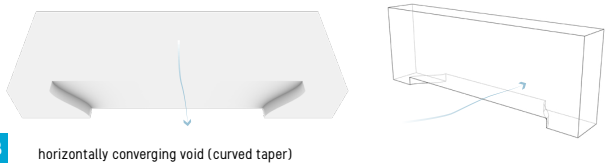

2B horizontally converging void (curved taper)

3A horizontally diverging void (straight taper)

3B horizontally diverging void (curved taper)

4 vertically converging void

5 vertically diverging void

6 horizontally & vertically converging void

7 horizontally converging & vertically diverging void

8 horizontally diverging & vertically converging void

9 horizontally & vertically diverging void

Figure 5.8: void geometry variants overview

Table 5.1 provides some more details on the parameter settings in the Grasshopper model for each variant.

Since many of the buildings in the study area have a void deck covering almost the entire ground floor – that is, except for the space reserved for staircases, elevators, technical rooms, apartments for people with mobility impairments and other required basic amenities –, a long void was the starting point for the base case. The percentage of the total ground floor (building) length covered by the void deck of the base case model was set to 75%, to account for these amenities while still keeping enough space at both building ends to play with horizontal convergence and divergence in the variants. The base case variant has a simple, straight, void (no horizontal or vertical convergence / divergence) with a height of 3.6m.

The contraction resp. expansion of the horizontally converging (variant 2A and 2B) and diverging (variant 3A and 3B) voids was assumed to be 25% in both cases. This allows for a fair comparison of the flow pattern effects. Both straight and curved walls are investigated.

The possible range for convergence is smaller in the vertical than in the horizontal direction. The void height decrease of the vertically converging void (variant 4) was determined based on practical considerations, since people should still be able to walk underneath. The height at the contraction was chosen to be 2.115m, which is a standard – though not smallest – door height. Starting from a void deck height of 3.6m at the inflow, this means a void height decrease of 1.485m at the outflow. Similar to the horizontal convergence/divergence cases, a fair comparison should be made between the vertically converging and diverging void deck. Therefore, a height difference of 1.485m between the inflow and outflow was also applied to the vertically diverging void, thus from 3.6m up to 5.085m.

Combinations of the aforementioned horizontally/vertically converging and diverging variants were then made, resulting in variant 6 to 9.

VOID GEOMETRY VARIANTS OVERVIEW		
VARIANT	**void geometry**	**description**
1	BASE CASE	• no convergence/divergence in horizontal nor vertical direction • % of ground floor length covered by void deck: 75% • % of ground floor height covered by void height: 100% (void deck height = 3.6m)
2A	horizontally converging void - straight taper	contraction at void outflow: 75% of void inflow
2B	horizontally converging void - curved taper	contraction at void outflow: 75% of void inflow
3A	horizontally diverging void - straight taper	expansion at void outflow: 125% of void inflow
3B	horizontally diverging void - curved taper	expansion at void outflow: 125% of void inflow
4	vertically converging void	void height decrease at outflow: 1.485m
5	vertically diverging void	void height increase at outflow: 1.485m
6	horizontally & vertically converging void	• horizontal contraction at void outflow: 75% of void inflow • void height decrease at outflow: 1.485m
7	horizontally converging & vertically diverging void	• horizontal contraction at void outflow: 75% of void inflow • void height increase at outflow: 1.485m
8	horizontally diverging & vertically converging void	• horizontal expansion at void outflow: 125% of void inflow • void height decrease at outflow: 1.485m
9	horizontally & vertically diverging void	• horizontal expansion at void outflow: 125% of void inflow • void height increase at outflow: 1.485m

Table 5.1: parameter settings of void geometry variants in single building Grasshopper model

5.3 Parametric Urban Model

The parametric single building model was further 'expanded' to an urban parametric void deck model for the entire study area. Instead of looking at a single building, this parametric model takes the volumes of all the buildings in the study area in Clementi as an input and allows one to apply void deck geometry modifications to specific building groups in the area. The building groups can be formed based on different building characteristics, such as building orientation in this case. They can also be grouped by sub-neighbourhood, for example. The combination of the single building Grasshopper model and the parametric urban model allows one to perform a quick test of the effect of a specific void deck geometry on the flow pattern underneath / around a single building, and to apply these void deck geometry modifications to specific building groups in the study area. The impact of these void deck modifications on the urban ventilation in the study area can then be tested in OpenFOAM.

The general structure of the parametric urban Grasshopper script (shown in *figure 5.10*) consists of four main groups:

A) Script section for buildings with void decks facing prevailing wind directions
B) Script section for buildings with void decks facing other wind directions
C) Group of buildings without void decks (excluded from the void deck modifications)
D) Special cases (to be treated separately)

Group A consists of buildings with their main axis perpendicular to wind directions North and South, which thus play an important role during both monsoon seasons, as well as those perpendicular to (North-) Northeast, which are of importance during the Northeast Monsoon. Group B, on the other hand, consists of buildings with void decks facing non-prevailing wind directions.

As the main goal is to analyse what influence a change in void deck geometry will have on the flow pattern in the area, the buildings which do not currently have a void deck will not be analysed in the parametric model.

The script is applicable to all buildings that have a longer and shorter axis as it needs to detect and sort e.g. edges according to their length to perform the void deck modifications. Point blocks with a square floorplan and buildings with a very irregular shape thus need to be treated separately if one wants to perform void deck modifications to those. In fact, some of the irregularly-shaped hybrid slab-point blocks only have a narrow corridor (e.g. to walk towards the lifts). Those were not regarded as void decks because they are not intended as spaces for interaction or outdoor activities.

The parametric script set-up consists of the following general steps:

STEP 1:
Split buildings consisting of parts with different orientations into separate parts as the script performs void modifications for building groups according to orientation

STEP 2:
Group buildings (parts) according to orientation w.r.t. wind directions

STEP 3:
Extract building footprints & bounding box

STEP 4:
Create basic void deck geometry

STEP 5:
Apply void deck geometry modifications

STEP 6:
Subtract final void deck geometry from building volume

Figure 5.9: parametric urban model - general steps

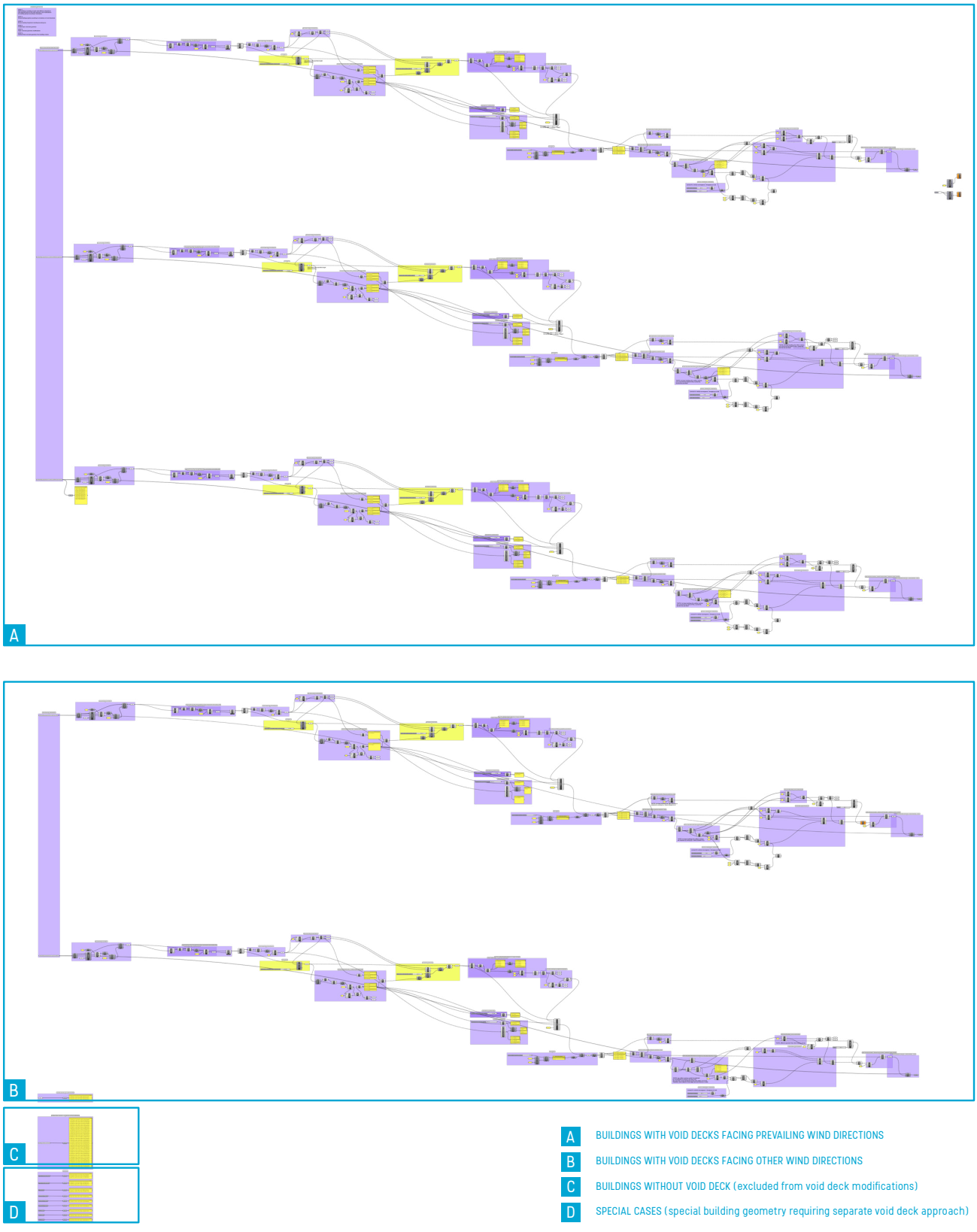

Figure 5.10: parametric urban model – Grasshopper script

Although the void deck modifications are performed based on the same functional principles (as shown in *figure 5.13*) for each of the building groups, there are some differences amongst them. The script could thus not simply be fully copied to all the building groups but had to be adjusted for each of them separately. This has to do with the orientation and length of the blocks.

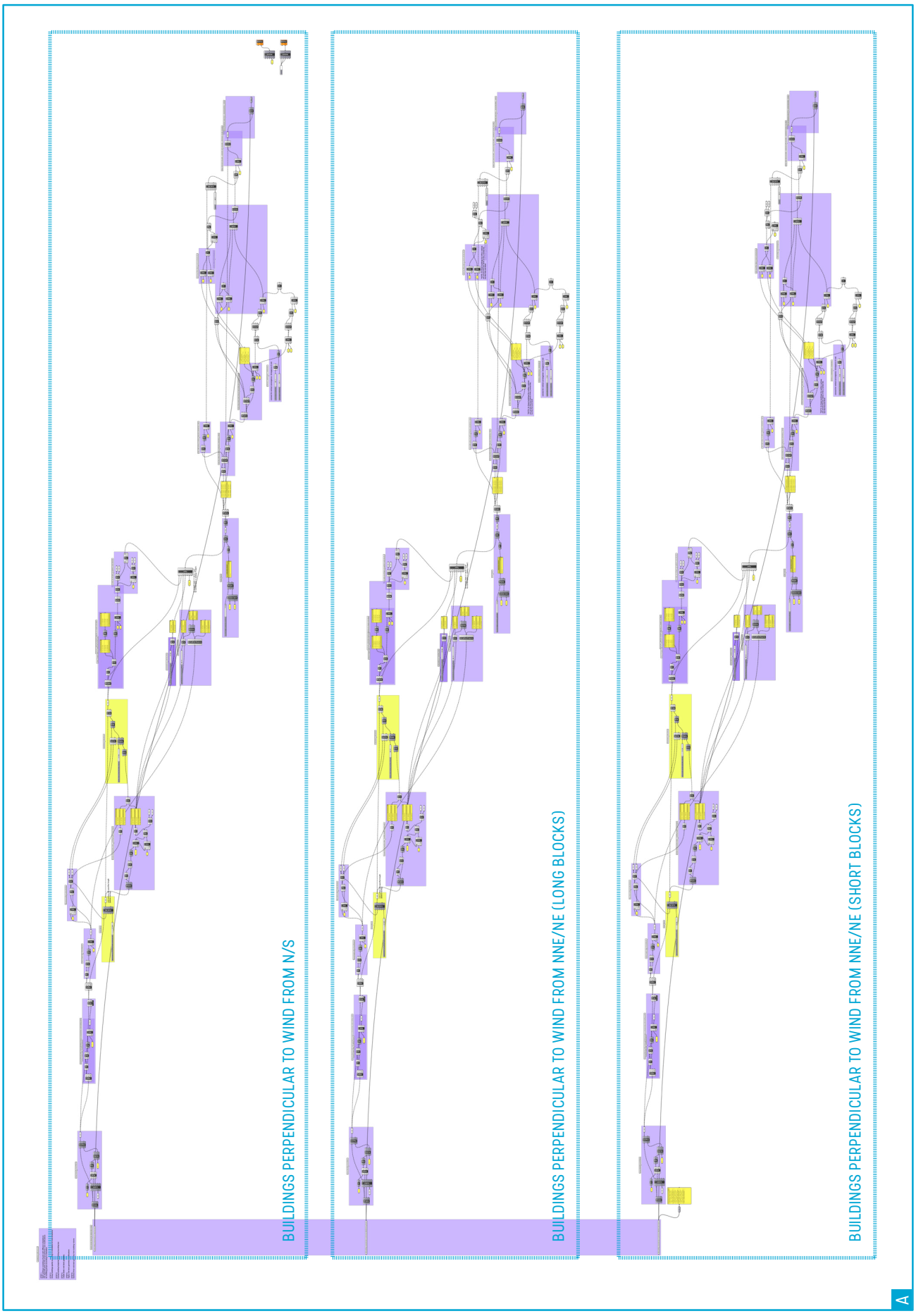

Figure 5.11: parametric urban model – Grasshopper script main components (A)

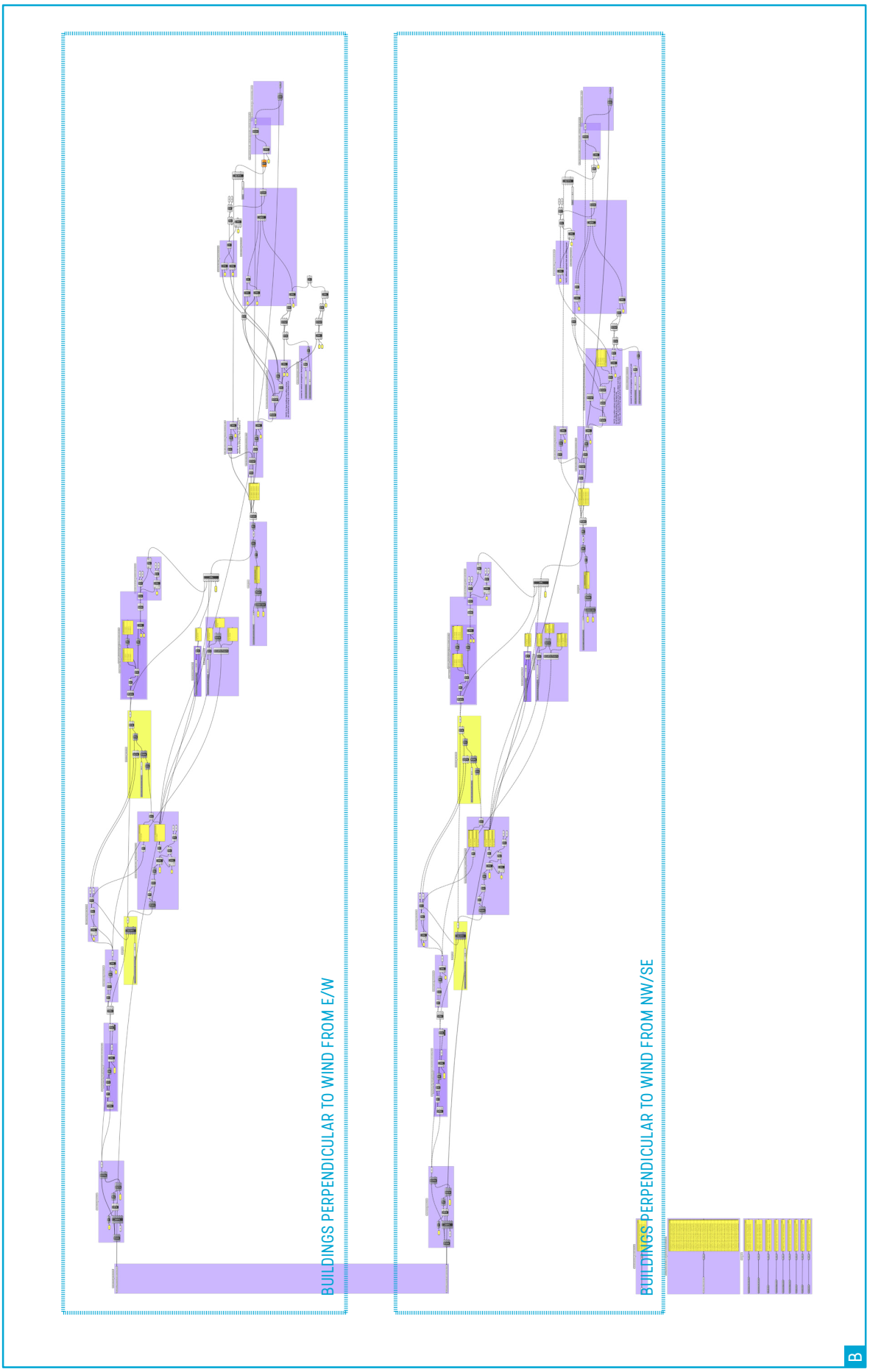

Figure 5.12: parametric urban model – Grasshopper script main components (B)

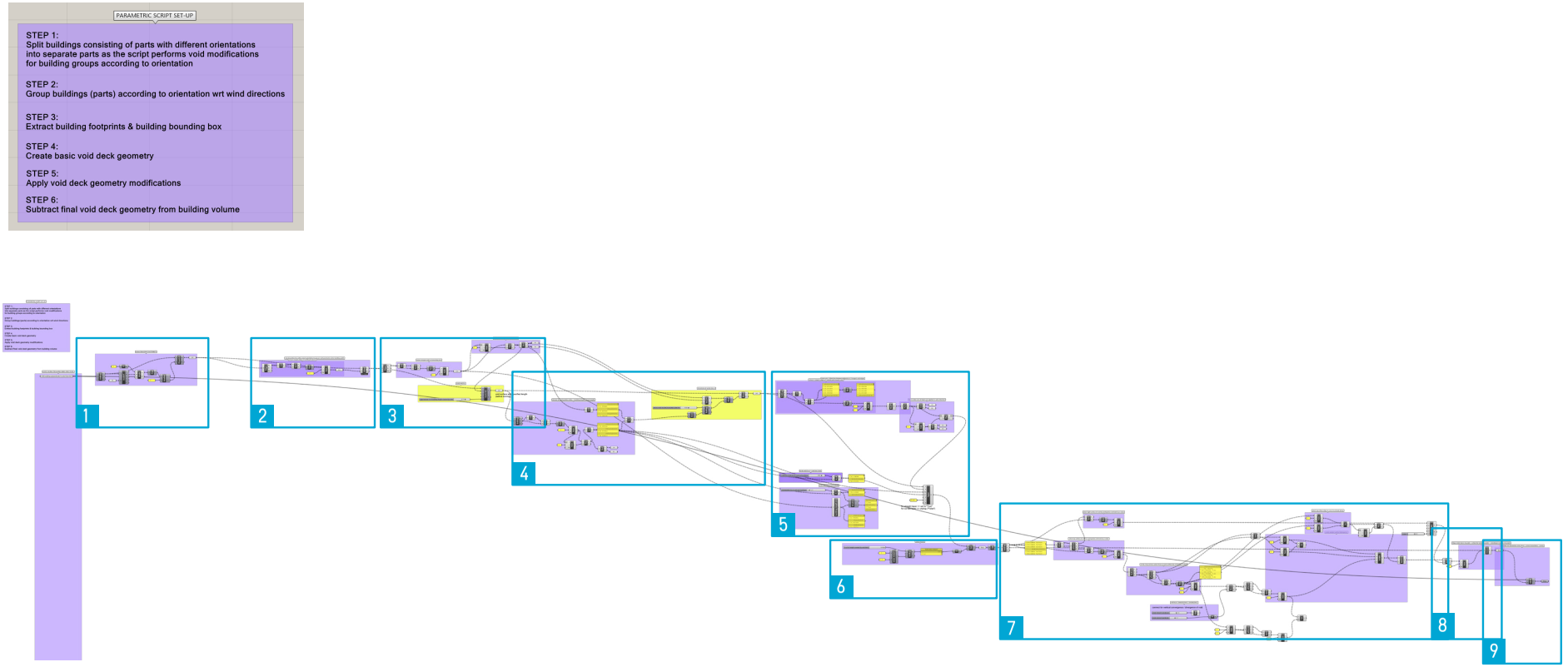

1 EXTRACTION OF BUILDING FOOTPRINT

2 CREATION OF BOUNDING BOX WITH CORRECT ORIENTATION

3 VOID DECK BASE GEOMETRY CREATION (SPECIFIED VOID LENGTH)

4 ADJUSTMENT OF VOID DECK POSITION

5 VOID GEOMETRY MODIFICATIONS: HORIZONTAL CONVERGENCE / DIVERGENCE

6 VOID GEOMETRY MODIFICATIONS: VOID HEIGHT

7 VOID GEOMETRY MODIFICATIONS: VERTICAL CONVERGENCE / DIVERGENCE

8 UNION OF CREATED VOID VOLUME & VERTICALLY DIVERGED VOLUME

9 SUBTRACTION OF BUILDING VOLUME WITH CREATED VOID DECK VOLUME

Figure 5.13: parametric urban model – Grasshopper script general steps per building group

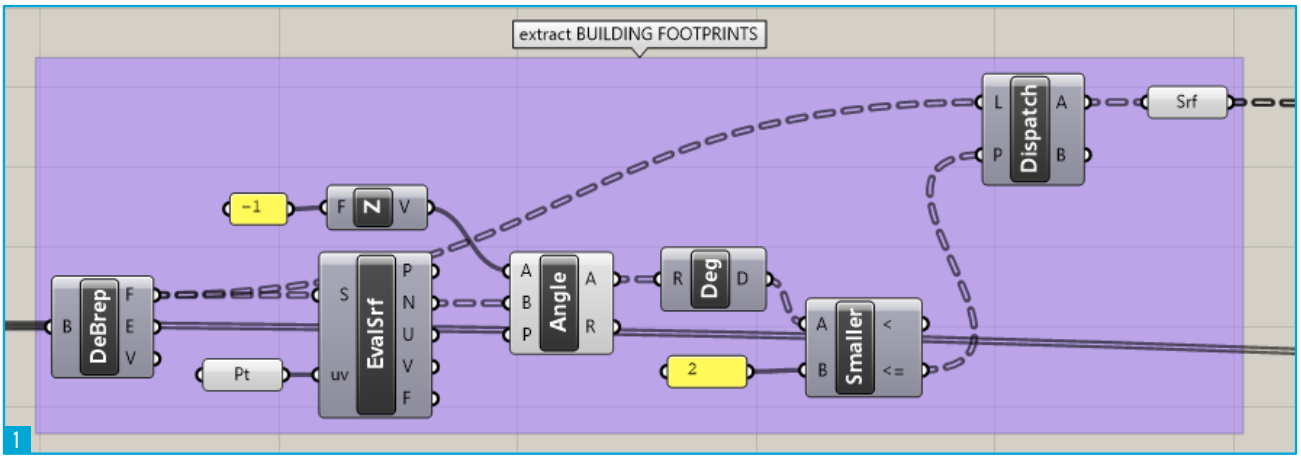

EXTRACTION OF BUILDING FOOTPRINT

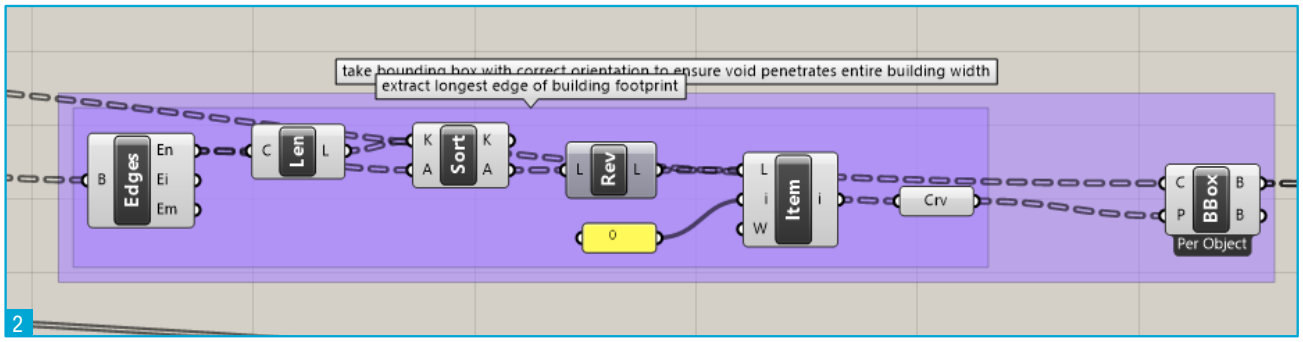

CREATION OF BOUNDING BOX WITH CORRECT ORIENTATION

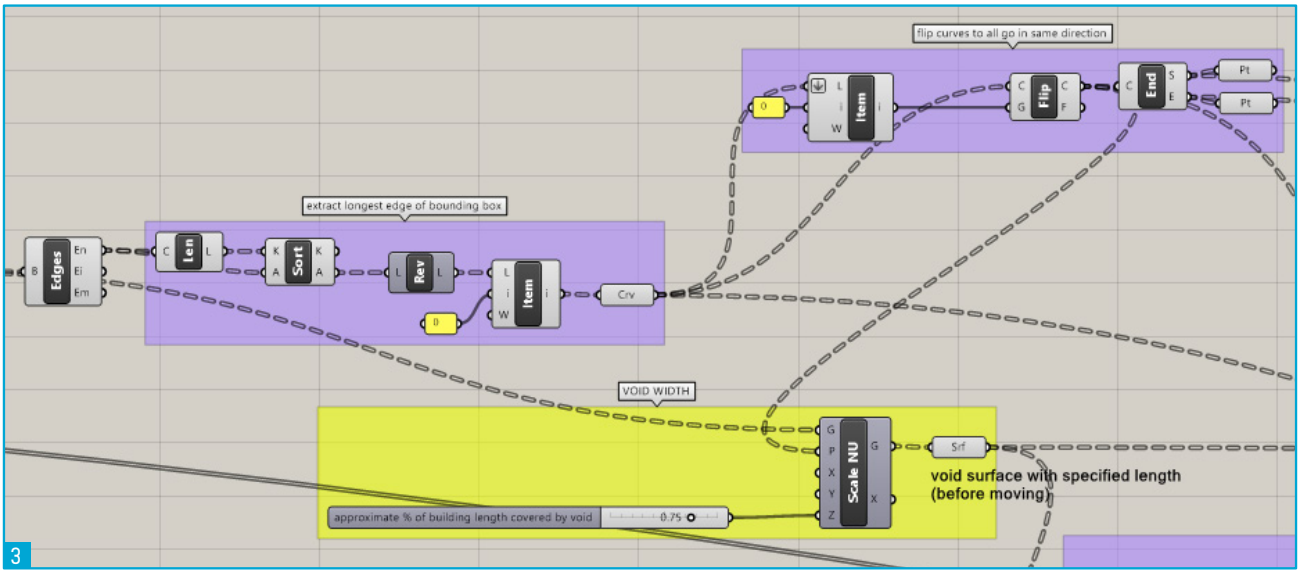

VOID DECK BASE GEOMETRY CREATION (SPECIFIED VOID LENGTH)

Figure 5.14: parametric urban model – Grasshopper script breakdown (1)

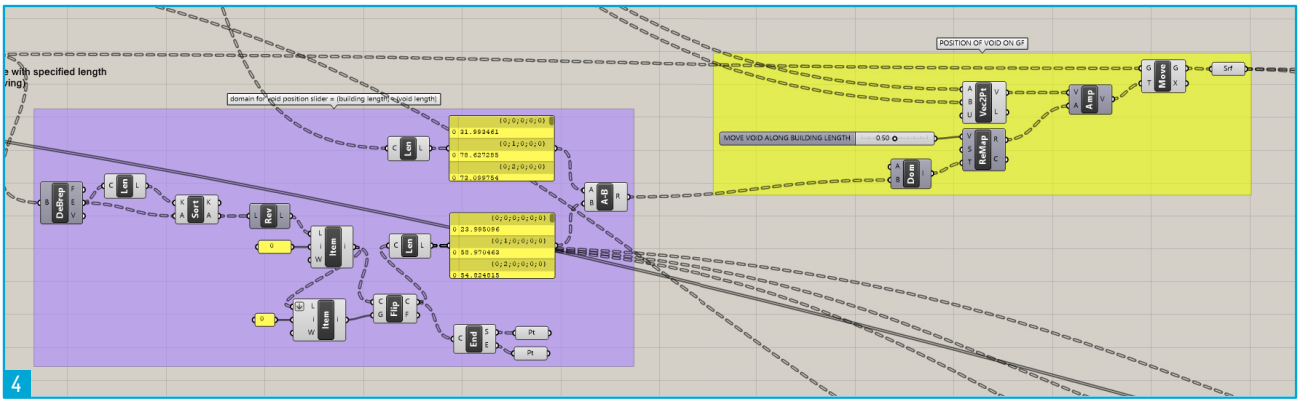

ADJUSTMENT OF VOID DECK POSITION

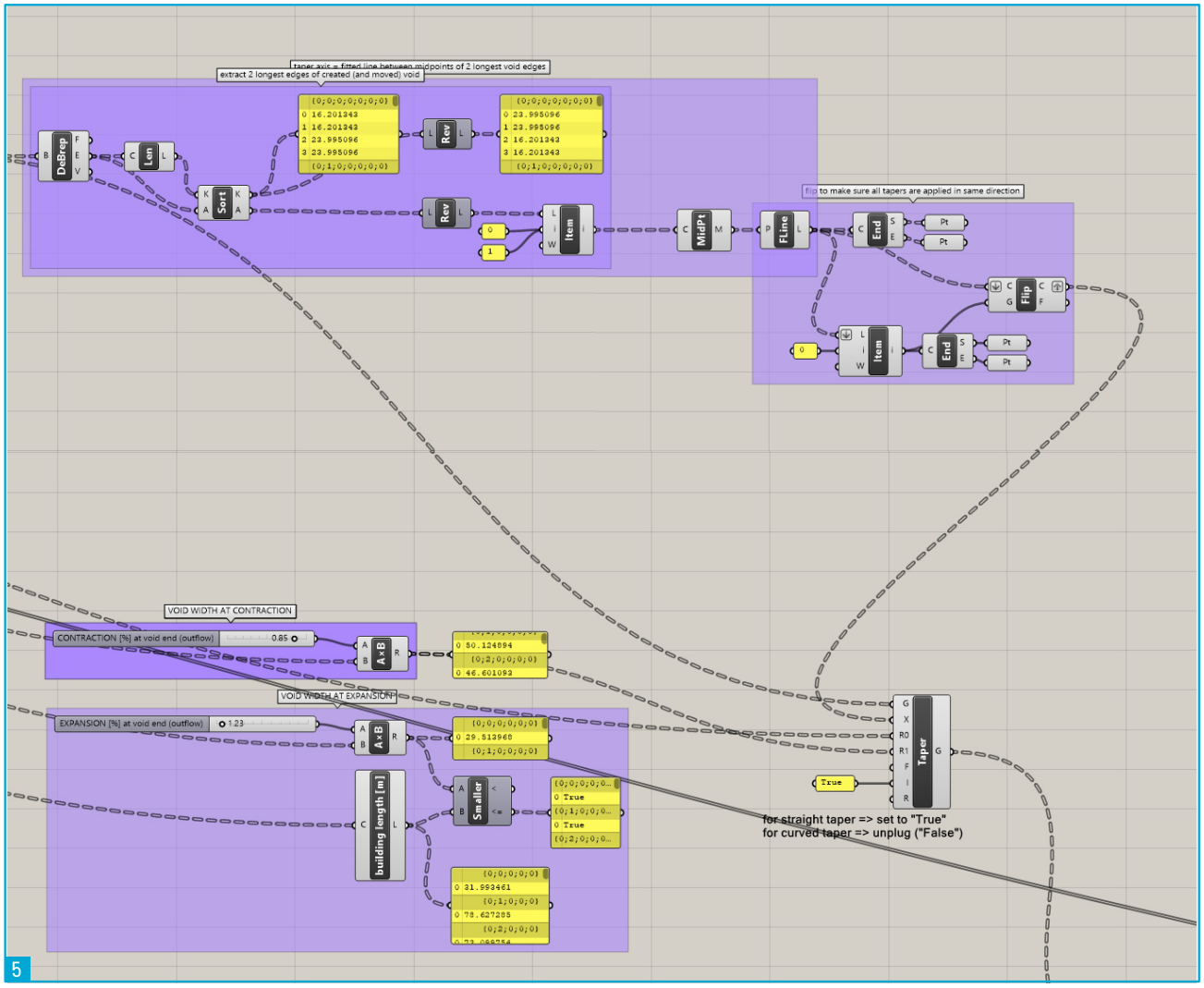

VOID GEOMETRY MODIFICATIONS: HORIZONTAL CONVERGENCE / DIVERGENCE

Figure 5.15: parametric urban model – Grasshopper script breakdown (2)

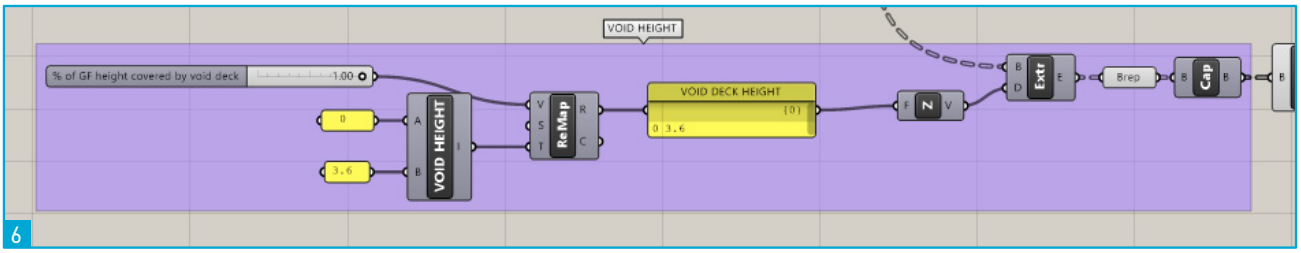

VOID GEOMETRY MODIFICATIONS: VOID HEIGHT

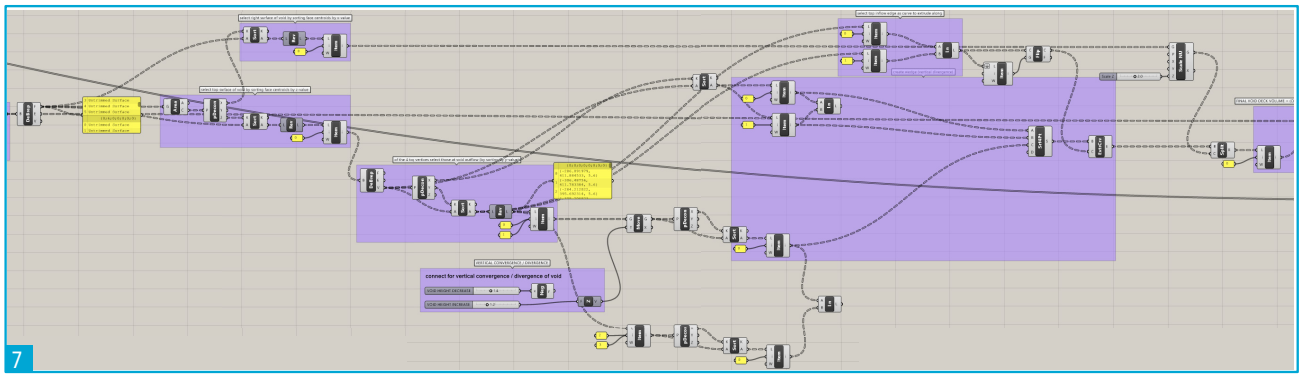

VOID GEOMETRY MODIFICATIONS: VERTICAL CONVERGENCE / DIVERGENCE

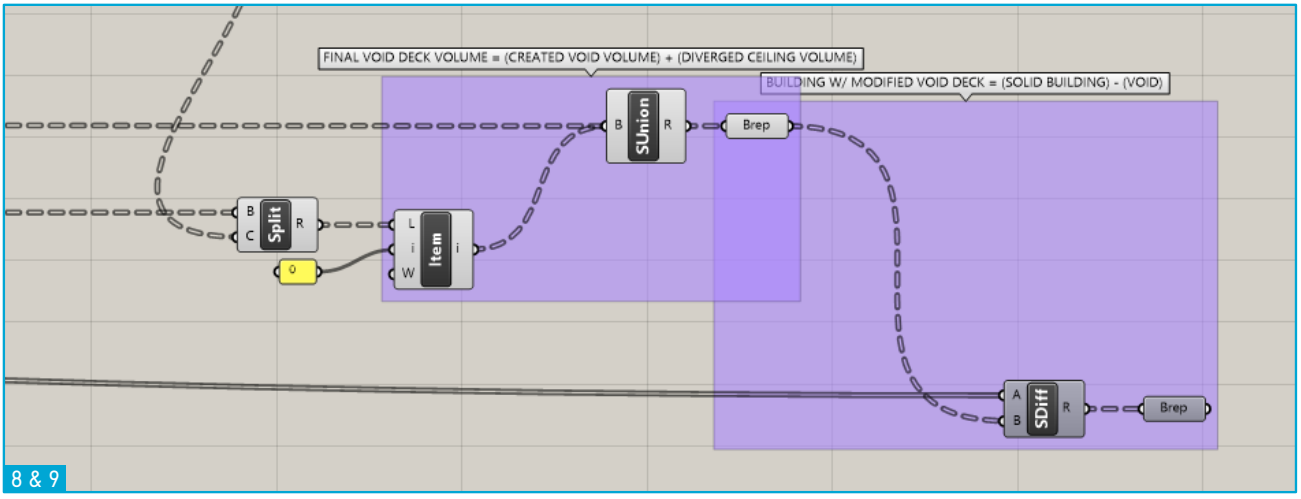

- UNION OF CREATED VOID VOLUME & VERTICALLY DIVERGED VOLUME
- SUBTRACTION OF BUILDING VOLUME WITH CREATED VOID DECK VOLUME

Figure 5.16: parametric urban model – Grasshopper script breakdown (3)

The diagram below shows the resulting five building groups to which void deck modifications can be performed independently from each other.

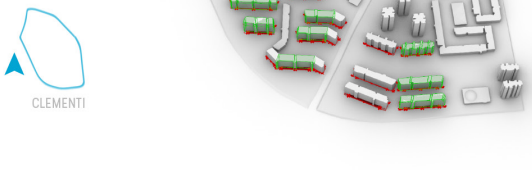

BUILDING GROUP 1: buildings perpendicular to wind from N/S

BUILDING GROUP 2: buildings perpendicular to wind from NNE/NE (long blocks)

BUILDING GROUP 3: buildings perpendicular to wind from NNE/NE (short blocks)

BUILDING GROUP 4: buildings perpendicular to wind from E/W

BUILDING GROUP 5: buildings perpendicular to wind from NW/SE

Figure 5.17: grouped buildings for urban-scale parametric void deck geometry intervention

The remaining buildings, consisting of group 6 and 7 as indicated below, are those which have been excluded from the parametric void deck modifications due to their complexity (which does not align with the standard parametric set-up and therefore requires a separate treatment) or the fact that they do not currently have a void deck.

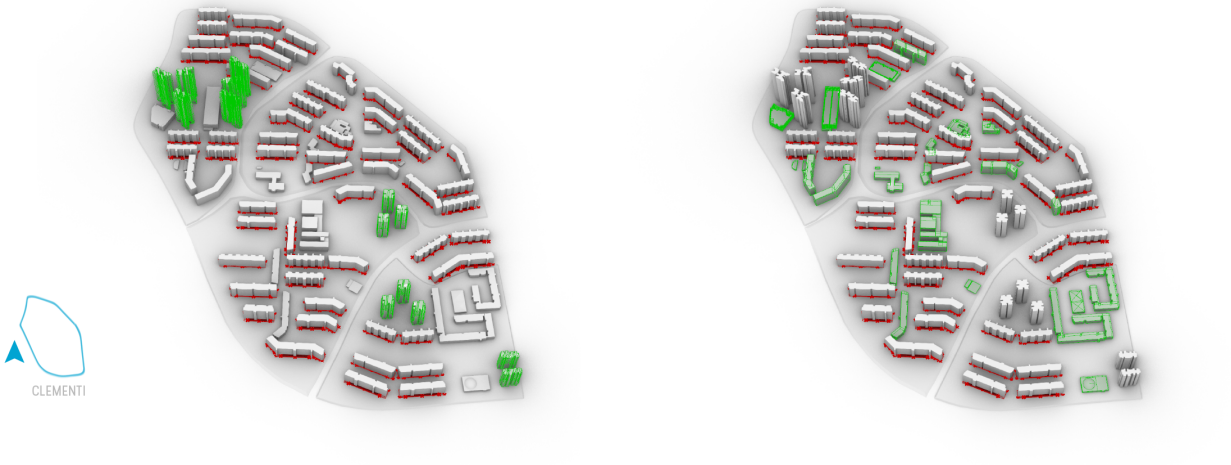

BUILDING GROUP 6: special cases

BUILDING GROUP 7: buildings without void deck

Figure 5.18: building groups excluded from parametric void deck geometry intervention

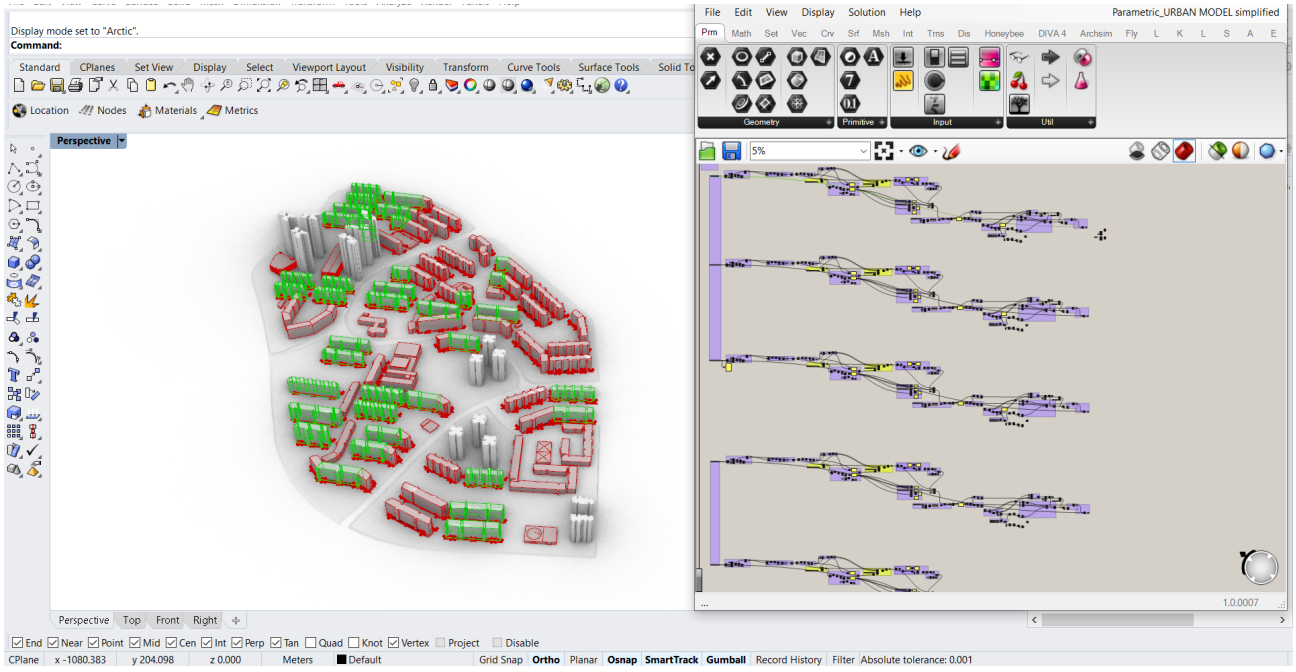

Figure 5.19: urban parametric model (Rhino & Grasshopper)

06

COMPUTATIONAL FLUID DYNAMICS SIMULATIONS

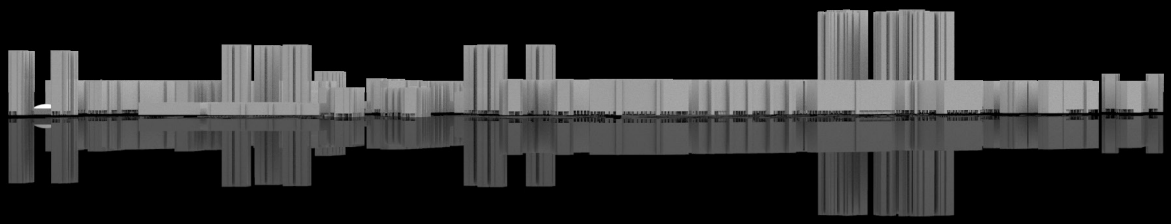

6.1 Simulation Set-Up

For the single building cases, which are used to compare the overall effect of different void deck geometries on the flow pattern around a building, we focus on simulating the wind direction perpendicular to the void deck opening. The representative building chosen for the base case has a void deck which aligns with the prevailing North and South wind direction. All the void deck geometry variants were simulated with a wind speed of 2.2 m/s from the South, which is representative for the Southwest Monsoon season. On the other hand, the urban simulations of the entire study area are performed for all three prevailing wind directions.

6.1.1 CFD Simulation Method & Governing Equations

The governing equations in CFD stem from the principles of conservation of mass, momentum (also known as Newton's second law) and energy, leading to the continuity, momentum and energy equations respectively (represented on a per-unit-volume basis in fluid mechanics). The instantaneous Navier-Stokes equations for an incompressible, viscous flow of a Newtonian fluid can thus be written as:

$$\frac{\partial u_i}{\partial x_i} = 0 \qquad (6.1)$$

$$\frac{\partial u_i}{\partial t} + u_j * \frac{\partial u_i}{\partial x_j} = -\frac{1}{\rho} * \frac{\partial p}{\partial x_i} + \frac{\partial}{\partial x_j}(2 * \nu * s_{ij}) \qquad (6.2)$$

$$\frac{\partial \theta}{\partial t} + u_j * \frac{\partial \theta}{\partial x_j} = \frac{1}{\rho * c_p} * \frac{\partial}{\partial x_j}\left(k * \frac{\partial \theta}{\partial x_j}\right) \qquad (6.3)$$

with

u_i = instantaneous velocity vector
x_i = instantaneous position vector
p = instantaneous pressure
θ = instantaneous temperature
t = time
ρ = density
ν = kinematic viscosity
c_p = specific heat capacity
k = thermal conductivity
$s_{ij} = \frac{1}{2} * \left(\frac{\partial u_i}{\partial x_j} + \frac{\partial u_j}{\partial x_i}\right)$ = strain rate tensor

The simulations are performed using the Reynolds-Averaged Navier-Stokes (RANS) method. This implies that the instantaneous values in these equations are decomposed into a mean and a fluctuating component (known as Reynolds decomposition), after which the equations are time-averaged (in case of a statistically steady flow; a flow in which the fluid properties do not change over time, so with local time derivatives equal to zero), also called steady RANS, as opposed to URANS (for unsteady/transient flow), in which they are ensemble-averaged. This is shown below.

$$u = U + u' \qquad (6.4\ a)$$

$$p = P + p' \qquad (6.4\ b)$$

$$\theta = \Theta + \theta' \qquad (6.4\ c)$$

Substitution results in the RANS equations (3D Reynolds-averaged Navier-Stokes equations for an incompressible flow of a Newtonian fluid):

$$\frac{\partial U_i}{\partial x_i} = 0 \tag{6.5}$$

$$\frac{\partial U_i}{\partial t} + U_j * \frac{\partial U_i}{\partial x_j} = -\frac{1}{\rho} * \frac{\partial P}{\partial x_i} + \frac{\partial}{\partial x_j}\left(2 * \nu * S_{ij} - \overline{u_j' u_i'}\right) \tag{6.6}$$

$$\frac{\partial \theta}{\partial t} + U_j * \frac{\partial \theta}{\partial x_j} = \frac{1}{\rho * c_p} * \frac{\partial}{\partial x_j}\left(k * \frac{\partial \theta}{\partial x_j} - \overline{u_j' \theta'}\right) \tag{6.7}$$

whereby

$S_{ij} = \frac{1}{2} * \left(\frac{\partial U_i}{\partial x_j} + \frac{\partial U_j}{\partial x_i}\right)$ = mean strain-rate tensor

The simulations are carried out using the steady-state SimpleFoam solver for incompressible turbulent flows from the OpenFOAM CFD toolbox, with the addition of the scalar transport equation for convection and diffusion. This allows the temperature to be included in the simulation model as a passive scalar, which is thus transported with the flow without buoyancy effects. This simplification as compared to more complex buoyant ventilation and heat transfer solvers like buoyantSimpleFoam can be justified since the temperature differences in the study area will be small and the Reynolds number is high. (Ferziger, Peric, & Street, 2020) First-order numerical schemes are used in the simulations, as represented in the fvSchemes dictionary in *Appendix D (OpenFOAM Files)*.

In this case, a turbulence model is used to represent the turbulent character of the flow. Although gases are theoretically compressible, air is considered as an incompressible fluid in building aerodynamics since the fractional change of absolute pressure is negligible for wind speeds below 100 m/s (Mach number below 0.3). (Blocken, 2019)

6.1.2 Turbulence Model

Since the conservation equations in RANS involve the Reynolds stresses and turbulent scalar flux due to averaging, the number of unknowns is larger than the number of equations. (Ferziger et al., 2020) The use of either LES or RANS (which are both not exact) to perform the simulations therefore requires a turbulence model to close the equations. In essence, the turbulence model describes the Reynolds stresses in terms of the known average quantities.

Turbulence models can generally be divided into two main groups: first-order and second-order closure models. While the first group uses the Boussinesq eddy-viscosity hypothesis to relate the unknown Reynolds stresses to the velocity gradients in the mean flow and the gradient-diffusion assumption to relate the turbulent heat flux (or turbulent mass flux) to the temperature gradient (or concentration gradient) in the mean flow by means of the turbulent heat (or mass) diffusivity, the second group implies the use of additional transport equations for these Reynolds stresses and turbulent heat/mass fluxes (*equations 6.9a and 6.9b below*). (Blocken, 2019) The second-order closure models are therefore more computationally demanding.

Boussinesq eddy-viscosity hypothesis:

$$-\overline{u_i' u_j'} = 2 * \nu_t * S_{ij} - \frac{2}{3} * k * \delta_{ij} \tag{6.8}$$

with

ν_t = turbulent viscosity

S_{ij} = time-averaged shear stress tensor

$\delta_{ij} = \begin{cases} 1 \ (for\ i = j) \\ 0 \ (for\ i \neq j) \end{cases}$ = Kronecker delta

Gradient-diffusion assumption:

$$-\overline{u_j'\theta'} = D_{\theta,t} * \frac{\partial \theta}{\partial x_j} \quad \text{(turbulent heat flux)} \qquad (6.9\ a)$$

$$-\overline{u_j'c'} = D_{c,t} * \frac{\partial c}{\partial x_j} \quad \text{(turbulent mass flux)} \qquad (6.9\ b)$$

with

$D_{\theta,t}$ = turbulent heat diffusivity
$D_{c,t}$ = turbulent mass diffusivity

The standard k-ε turbulence model, a first-order closure model based on the turbulent kinetic energy and the turbulent kinetic energy dissipation rate ε, will be used in this case. Two transport equations (for k and ε) for this turbulence model are added to the RANS equations, as given below.

$$u_j * \frac{\partial k}{\partial x_j} = \frac{\partial}{\partial x_j} * \left[\left(\nu + \frac{\nu_t}{\sigma_k}\right) * \frac{\partial k}{\partial x_j}\right] + P_k - \varepsilon \qquad (6.10)$$

$$u_j * \frac{\partial \varepsilon}{\partial x_j} = \frac{\partial}{\partial x_j} * \left[\left(\nu + \frac{\nu_t}{\sigma_\varepsilon}\right) * \frac{\partial \varepsilon}{\partial x_j}\right] + C_{\varepsilon 1} * \frac{\varepsilon}{k} * P_k - C_{\varepsilon 2} * \frac{\varepsilon^2}{k} \qquad (6.11)$$

with

P_k = turbulent production term

And the standard k-ε turbulence model coefficients $C_{\varepsilon 1}$, $C_{\varepsilon 2}$, σ_k and σ_ε set in OpenFOAM as follows:

$C_\mu = 0.09$ (coefficient for turbulent viscosity)
$C_1 = 1.44$ (model coefficient 1)
$C_2 = 1.92$ (model coefficient 2)
$sigmaEps = 1.11$

This turbulence model is robust and is the most widely used model thus far (very suitable for outdoor simulations), though it should be noted that it can only be applied to fully turbulent flows. (Blocken, 2019) The model only requires the specification of the initial and/or boundary conditions.

Despite its broad and convenient implementation, the standard k-ε turbulence model also has some disadvantages for simulations of flows around buildings. For example, the flow separation and recirculation regions at the roof and sides of buildings is usually underestimated due to an overestimation of the production of turbulent kinetic energy k (mean kinetic energy per unit mass of the eddies in the turbulent flow) around the frontal and side corners. (Blocken, 2019) On the other hand, the velocity and size of the recirculation vortex behind buildings tends to be overestimated. (Blocken, 2019) This is due to an underestimation of the turbulent kinetic energy in this region. These need to be taken into consideration while interpreting the results from the CFD simulations.

6.1.3 Computational Model

6.1.3.1 Computational Domain & Roughness Areas

The tallest building height in the simulation model is 118 m. The minimum domain dimensions based on the *COST 732 Best Practice Guideline for the CFD Simulation of Flows in the Urban Environment* (COST Office – Carissimo, Franke, Hellsten, & Schlünzen, 2007) can then be determined as follows:

$$H_{domain} = 6 * H_{max} = 6 * 118m = 708m$$

$$D_{lat.boundary\ domain\ to\ model} = 5 * H_{max} = 5 * 118m = 590m \quad \text{(on both sides)}$$

$$D_{inflow\ boundary\ to\ model} = 5 * H_{max} = 5 * 118m = 590m$$

$$D_{outflow\ boundary\ to\ model} = 15 * H_{max} = 15 * 118m = 1770m$$

Next, this first generated computational domain still needs to be assessed on compliance with the blockage ratio requirements specified by Tominaga, Mochida, Yoshie, Kataoka, Nozu, Yoshikawa, Shirasawa (2008) and Blocken (2015), as summarized below.

- Max. blockage ratio:

$$BR = \frac{A_{frontal,buildings}}{A_{cross-section,domain}} < 3\% \qquad \text{(for CFD simulations)} \qquad (6.12)$$

Note that for wind tunnel testing, the requirement is less stringent (BR ‹ 5%).

- Directional blockage ratio:

Decomposition of blockage ratio and 3% limit in horizontal and vertical lateral direction, where the limit for each is the square root of 3% (≈17%).

$$BR_L = \frac{L_{building}}{L_{domain}} \leq 17\% \qquad (6.13\ a)$$

$$BR_H = \frac{H_{building}}{H_{domain}} \leq 17\% \qquad (6.13\ b)$$

As mentioned in the climate analysis *(see section 3.1)*, there are three prevailing wind directions in Singapore: north, north-northeast and south. The CFD-simulations will be performed for these prevailing wind directions. The minimum computational domain requirements thus result in three computational domains which are equal in size (as the minimum dimensions depend on the maximum building height in the modelled area) but with a different orientation and location (of the borders). In principle, this would imply that three different meshes should be created. In order to save on computational time (especially considering the fact that the grid generation is usually one of the most time-consuming parts in CFD), the N and NNE meshes can be combined into a single mesh thanks to their close orientation. As such, two meshes are created: one for the N- and NNE-wind directions and one for the S-direction.

The following steps were followed to determine the final computational domains for the simulations:

1) Determine computational domain size for the wind direction (or both directions in the case of the combined N & NNE domain) based on the minimum dimension requirements (depending on the maximum building height in the modelled area)
2) Check the blockage ratio requirements (maximum blockage ratio and directional blockage ratios in horizontal and vertical sense)
3) Adjust the computational domain size accordingly

=› For wind from S-direction:

The initial domain that was constructed based on the minimum dimension requirements (depending on H_{max}) for the case with wind from the South did not meet the blockage ratio requirements. The vertical directional blockage ratio criterion was met, but the maximum blockage ratio and horizontal directional blockage ratio requirements were not. Therefore, we know that the height of the computational domain does not need to be adjusted. Instead, the width of the domain needs to be adjusted (to meet the maximum blockage ratio requirement since this depends on the frontal area of the buildings and box) and so does the length of the domain (to meet the horizontal directional blockage requirement). The Grasshopper script below *(figure 6.1)* shows the blockage ratio checks that were performed.

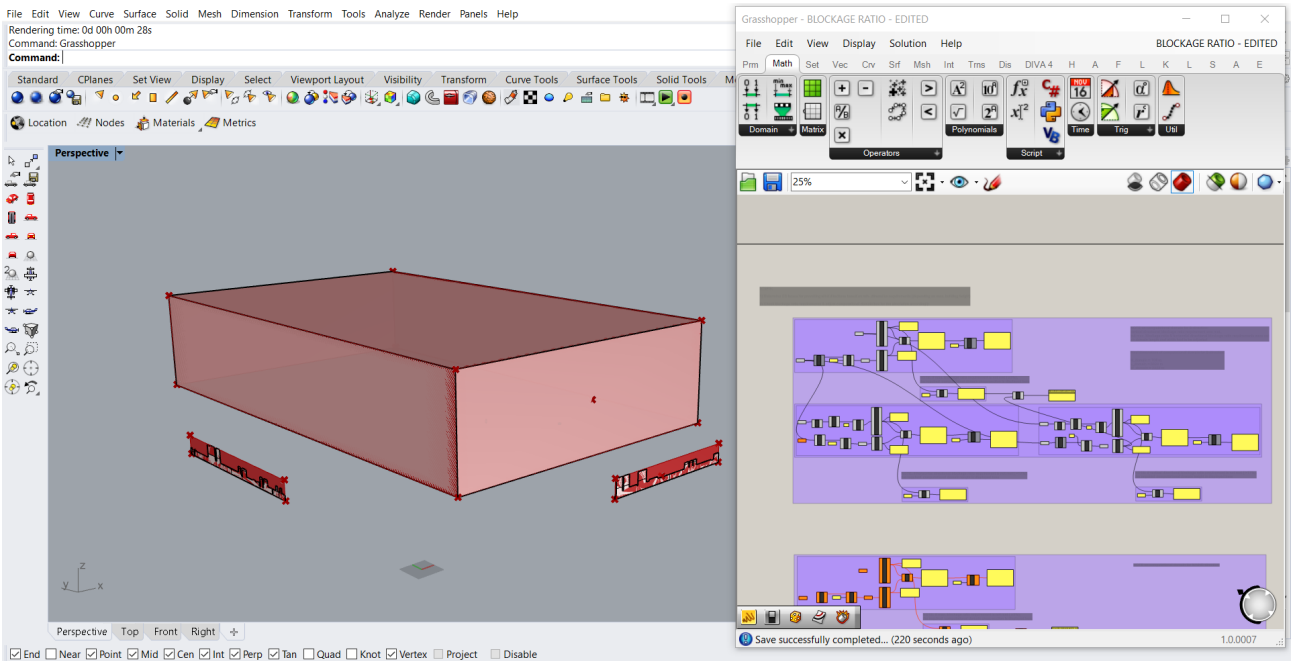

STEPS:

1) Determine CD boxes for prevailing wind directions based on min. dimension requirements (depending on max. building height)

2) Check blockage ratio requirements & adjust computational domain box for the simulation accordingly

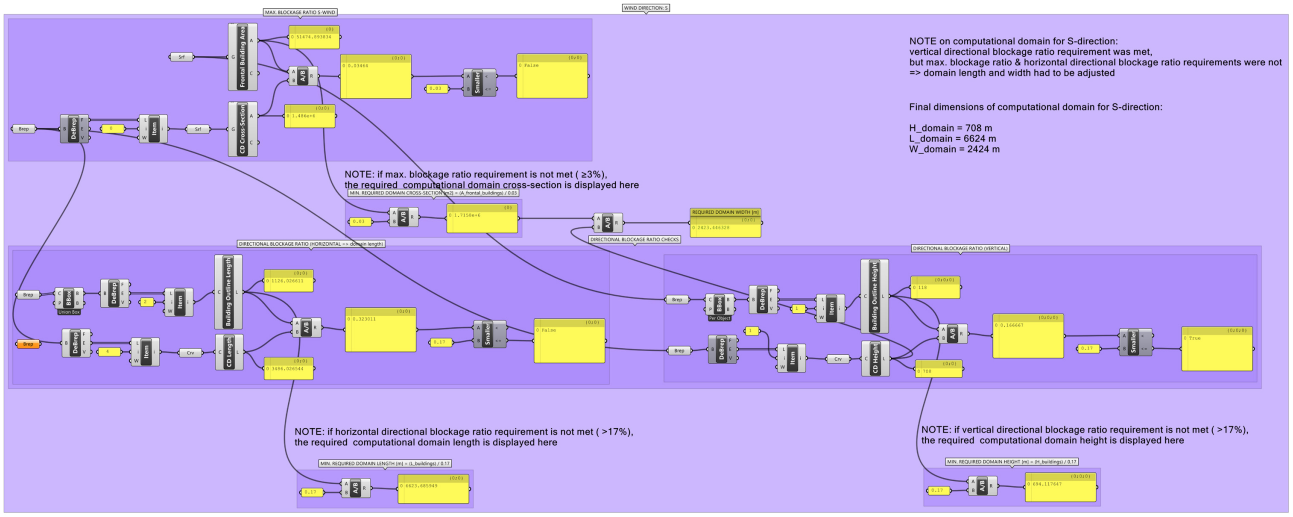

Figure 6.1: maximum and directional blockage ratio checks of the computational domain for S-wind (Grasshopper & Rhino)

The required minimum domain length and width to comply with these are calculated in the Grasshopper script. Next, the domain was adjusted. Note that, in scaling the computational domain dimensions, the ratios of the upstream and downstream distances were maintained. The final domain dimensions after the adjustments are:

Domain width = 2424m
Domain length = 6624m
Domain height = 708m

The domain for the simulations with wind from S is displayed in *figure 6.2*.

=› For wind from N- & NNE-direction:

Note that the required size for the computational domain for wind from the N-direction (in order to comply with both the maximum blockage ratio as well as the directional blockage ratios) is equal to the final defined domain size for wind from the S-direction since these are opposite.
As the simulations for the prevailing N- and NNE-directions are combined into a single mesh, their required domain size is defined by the combination of the minimum size for N-wind and NNE-wind (*figure 6.3*).

The final dimensions of the combined domain for the N and NNE wind simulations are:

Domain width = 4758m
Domain length = 7049m
Domain height = 708m

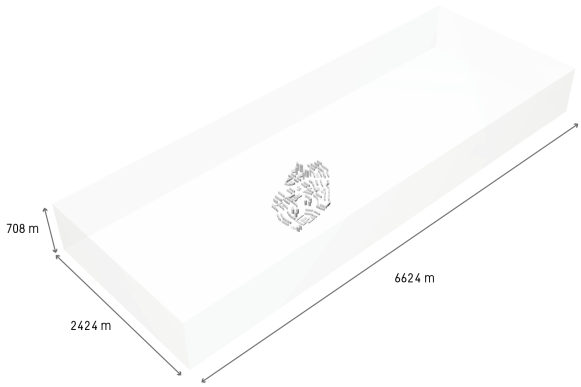

Figure 6.2: adjusted domain size for wind from S-direction based on blockage ratio requirements specified in Blocken (2015)

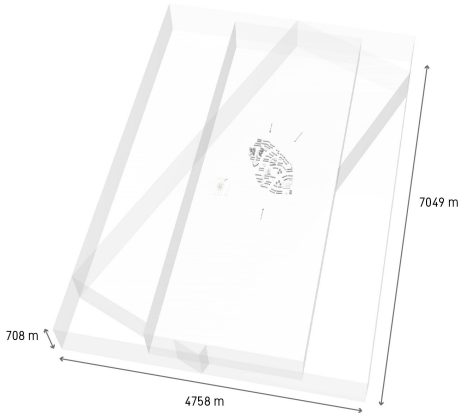

Figure 6.3: final domain for combined mesh for N- & NNE-wind

=› **Division into roughness patches:**

The area at and around the urban model can be regarded as a patchwork in which each patch has its own surface characteristics. As explained by Stull (1988), when air moves from one to another surface, the flow is modified and each of these patches leads to the establishment of their own internal boundary layer (IBL). This results in several internal boundary layers being formed within internal boundary layers.

Having adjusted the computational domain to meet the blockage ratio requirements, the roughness parameters can now be determined for each of the roughness patches. This will be done according to the guidelines in *Computational Fluid Dynamics for Urban Physics: Importance, scales, possibilities, limitations and ten tips and tricks towards accurate and reliable simulations* by Blocken (2015).

The guidelines state that the roughness should be defined in five distinct areas, four of which are located inside the computational domain and one upstream of it. The aerodynamic roughness length of these terrain patches is determined according to the Davenport-Wieringa roughness classification, shown in *figure 6.4*.

	z_0 (m)	Landscape description
1	0.0002 Sea	Open sea or lake (irrespective of the wave size), tidal flat, snow-covered flat plain, featureless desert, tarmac, concrete, with a free fetch of several kilometres.
2	0.005 Smooth	Featureless land surface without any noticeable obstacles and with negligible vegetation; e.g. beaches, pack ice without large ridges, morass, and snow-covered or fallow open country.
3	0.03 Open	Level country with low vegetation (e.g. grass) and isolated obstacles with separations of at least 50 obstacle heights; e.g. grazing land without windbreaks, heather, moor and tundra, runway area of airports.
4	0.10 Roughly open	Cultivated area with regular cover of low crops, or moderately open country with occasional obstacles (e.g. low hedges, single rows of trees, isolated farms) at relative horizontal distances of at least 20 obstacle heights.
5	0.25 Rough	Recently-developed "young" landscape with high crops or crops of varying height, and scattered obstacles (e.g. dense shelterbelts, vineyards) at relative distances of about 15 obstacle heights.
6	0.50 Very rough	"Old" cultivated landscape with many rather large obstacle groups (large farms, clumps of forest) separated by open spaces of about 10 obstacle heights. Also low large vegetation with small interspaces such as bush land, orchards, young densely-planted forest.
7	1.0 Closed	Landscape totally and quite regularly covered with similar-size large obstacles, with open spaces comparable to the obstacle heights; e.g. mature regular forests, homogeneous cities or villages.
8	≥ 2.0 Chaotic	Centres of large towns with mixture of low-rise and high-rise buildings. Also irregular large forests with many clearings.

Figure 6.4: updated Davenport-Wieringa roughness classification. From Computational Fluid Dynamics for Urban Physics: Importance, scales, possibilities, limitations and ten tips and tricks towards accurate and reliable simulations (Building and Environment 2015(2015 01 02), by Blocken, 2015. (doi: 10.1016/j.buildenv.2015.02.015)

A summary of the characteristics of each of the roughness areas, translated into the required roughness parameters for the study of Clementi, is given in the tables and images below.

	ROUGHNESS AREAS FOR PREVAILING WIND FROM SOUTH				
	location	general roughness area characteristics	terrain characteristics	roughness class	aerodynamic roughness length
ROUGHNESS AREA 1	fetch of 5-10km upstream of computational domain	• long distance necessary for ABL to adjust to underlying terrain roughness, but roughness can therefore be at least 1 class off due to heterogeneous terrain characteristics over long patch • determines inlet parameters • based on Davenport / Wieringa roughness classification	• area stretches southwards from harbour terminal Pasir Panjang across Singapore Strait water channel • includes industrial (Bukom) and offshore landfill (Semakau) islands	1 (sea)	$z_{0,1} \approx 0.0040$ m (value near upper boundary of roughness class to take effect of islands into account)
ROUGHNESS AREA 2	upstream area inside computational domain	• objects not within area of interest, so can be modelled implicitly (simplified) => less grid cells required • based on Davenport / Wieringa roughness classification	• large variation in building heights and very few open spaces • area includes part of industrial port; West Coast Park; newly developed area with buildings up to 40 storeys tall; NUS Kent Ridge campus; low-rise residential area with trees densely spread in between detached houses	7 (closed)	$z_{0,2} \approx 1.0$ m
ROUGHNESS AREA 3	ground surface of modelled study area	• small-scale topographic features (e.g. sidewalks, benches, fences, trees etc.) modelled implicitly (simplified): included as surface roughness based on Davenport / Wieringa roughness classification)	• quite closely built-up area, except for Ulu Pandan Park Connector southeast of modelled study area • mostly low-rise buildings to the west of model and 16-storey tall buildings to the east • similar roughness as area 2	7 (closed)	$z_{0,3} \approx 1.0$ m
ROUGHNESS AREA 4	surfaces of modelled buildings / structures in study area	• buildings (void decks in particular) modelled explicitly (simplified) • implemented in k and ε wall functions for rough walls and high Re-flows	N/A (see wall function description)	N/A (see wall function description)	N/A (see wall function description)
ROUGHNESS AREA 5	downstream area inside computational domain	• area of less importance (limited upstream aerodynamic disturbance by downstream terrain features) • based on Davenport / Wieringa roughness classification	• relatively large obstacle groups separated by scattered green patches with high density of trees • size of nature coverage similar to urban coverage • lower roughness than area 2 and 3	6 (very rough)	$z_{0,5} \approx 0.50$ m

Table 6.1: specification of roughness areas for simulation with wind from S

Figure 6.5: roughness area 1 (upstream of computational domain) for simulation with wind from South

Figure 6.6 (next page): roughness areas inside computational domain for simulation with wind from South


COMPUTATIONAL DOMAIN (TOP VIEW)
ROUGHNESS AREA 5
modelled building area
in computational domain
= ROUGHNESS AREA 4
ROUGHNESS AREA 3
ROUGHNESS AREA 2
ROUGHNESS AREA 1
Google
Imagery ©2019 Google, Maxar Technologies, Map data ©2019 G

	ROUGHNESS AREAS FOR PREVAILING WIND FROM NORTH / NORTH-NORTHEAST				
	location	general roughness area characteristics	terrain characteristics	roughness class	aerodynamic roughness length
ROUGHNESS AREA 1	fetch of 5-10km upstream of computational domain	• long distance necessary for ABL to adjust to underlying terrain roughness, but roughness can therefore be at least 1 class off due to heterogeneous terrain characteristics over long patch • determines inlet parameters • based on Davenport / Wieringa roughness classification	• eastern half of area is mostly covered by Bukit Timah Nature Reserve and Central Water Catchment Nature Reserve • western half of area is industrial / residential with large variation in building heights • northern part includes water reclamation plant and horse racing track • large obstacle groups as well as open spaces (east side)	6 (very rough)	$z_{0,1} \approx 0.50$ m
ROUGHNESS AREA 2	upstream area inside computational domain	• objects not within area of interest, so can be modelled implicitly (simplified) => less grid cells required • based on Davenport / Wieringa roughness classification	• western part of area is mostly industrial (including water reclamation plant, military training camp, logistics companies, manufacturing facilities); eastern part primarily residential (mainly low-rise) • large obstacle groups separated by scattered green patches	6 (very rough)	$z_{0,2} \approx 0.50$ m
ROUGHNESS AREA 3	ground surface of modelled study area	• small-scale topographic features (e.g. sidewalks, benches, fences, trees etc.) modelled implicitly (simplified): included as surface roughness based on Davenport / Wieringa roughness classification)	• quite closely built-up area, except for Ulu Pandan Park Connector to southeast and small portion of Pandan reservoir to west of modelled study area	7 (closed)	$z_{0,3} \approx 1.0$ m
ROUGHNESS AREA 4	surfaces of modelled buildings / structures in study area	• buildings (void decks in particular) modelled explicitly (simplified) • implemented in k and ε wall functions for rough walls and high Re-flows	N/A (see wall function description)	N/A (see wall function description)	N/A (see wall function description)
ROUGHNESS AREA 5	downstream area inside computational domain	• area of less importance (limited upstream aerodynamic disturbance by downstream terrain features) • based on Davenport / Wieringa roughness classification	• large variation in building heights and limited open spaces • area includes part of industrial port and Singapore Strait waterway; West Coast Park; newly developed area with buildings up to 40 storeys tall; NUS Kent Ridge campus; low-rise residential area with trees densely spread in between detached houses	7 (closed)	$z_{0,5} \approx 1.0$ m

Table 6.2: specification of roughness areas for simulation with wind from N/NNE

Figure 6.7: roughness area 1 (upstream of computational domain) for simulation with wind from North/North-North-east

Figure 6.8 (next page): roughness areas inside computational domain for simulation with wind from North/North-Northeast


COMPUTATIONAL DOMAIN (TOP VIEW)
ROUGHNESS AREA 1
ROUGHNESS AREA 2
modelled building area
in computational domain
ROUGHNESS AREA 4
ROUGHNESS AREA 3
ROUGHNESS AREA 5

Apart from these general roughness areas of the ground plane (upstream of the domain and bottom boundary of the domain), a z0-value was also assigned to the elevated terrain of the study area. While the z0-values of the former implicitly modelled areas were determined based on all their roughness elements (buildings, vegetation etc.), the latter was only based on the vegetation characteristics as the buildings on top of this elevated terrain are listed separately in the boundary field. The elevated terrain is mostly covered by grass, with trees of various sizes scattered in between the buildings. This roughness lies in between roughness class 3 (open) and 4 (roughly open) and is therefore assumed to be 0.06m.

6.1.3.2 Initial & Boundary Conditions

The initial and boundary conditions are summarized in this section. The complete list of all the input files in the OpenFOAM simulation can be found in *Appendix D*.

A fully-developed neutrally stratified ABL flow is assumed at the inlet, with typical wind speed U, k and ε inlet profiles according to Richards and Hoxey (1993) as follows:

$$U = \frac{u_*}{\kappa} ln\left(\frac{z + z_0}{z_0}\right) \tag{6.14}$$

$$k = \frac{u_*^2}{\sqrt{C_\mu}} \tag{6.15}$$

$$\varepsilon = \frac{u_*^3}{\kappa(z + z_0)} \tag{6.16}$$

with:

κ = 0.41 (von Kármán constant);
U = wind speed measured at reference height z [m/s];
z_0 = aerodynamic roughness length upstream of computational domain [m];
u^* = friction velocity [m/s]

The wind velocity at the reference height was based on the Annual Climatological Report 2017 by the Meteorological Service Singapore. This report includes measurements for the year 2017 as well as averaged statistics over the period 1981-2010. The latter were used for the wind-speed input for the Southwest Monsoon (June - September) and Northeast Monsoon months (December - March) respectively.

					average
Southwest Monsoon	June	July	August	September	
	2.0	2.4	2.5	2	**2.2**
Northeast Monsoon	December	January	February	March	
	2.2	2.9	3.0	2.3	**2.6**

Table 6.3: 1981-2010 average wind speed measurements [m/s] for Southwest and Northeast Monsoon months (Changi Climate Station, from "Annual Climatological Report 2017" by Meteorological Institute Singapore, 2017)

A wind speed of 2.2 m/s and 2.6 m/s (Changi Climate Station wind sensor at 10m height) was thus specified in the ABL conditions for the wind inlet profile with wind from the South and (North-)Northeast respectively. Moreover, the z0-values upstream of as well as inside the domain of all the ground / terrain patches need to be specified in the ABL conditions as these influence the wind profile over the terrain. An elaborate description of the z0-values was given in the previous section.

The boundary conditions used in the simulations are summarized hereafter. For the full specifications of the boundary conditions, please refer to *Appendix D (OpenFOAM Files)*.

	pressure p		velocity U	
	boundary condition	value	boundary condition	value
inlet	zeroGradient	-	atmBoundaryLayerInletVelocity	inlet wind speed profile based on specified ABLConditions
outlet	uniformFixedValue	constant pressure (0, as specified in initialConditions)	inletOutlet	inletValue: uniform (0 0 0); value: uniform flowVelocity specified in initialConditions
ground / terrain	zeroGradient	-	noSlip	-
top	symmetry	-	symmetry	-
sides	symmetry	-	symmetry	-
buildings	zeroGradient	-	noSlip	-

Table 6.4: general boundary conditions

	turbulent kinetic energy k		turbulent kinetic energy dissipation ε (epsilon)		turbulent kinematic viscosity (nut)	
	boundary condition	value	boundary condition	value	boundary condition	value
inlet	atmBoundaryLayerInletK	k inlet value based on specified ABLConditions	atmBoundaryLayerInletEpsilon	ε inlet value based on specified ABLConditions	calculated	uniform 0
outlet	inletOutlet	inletValue: uniform turbulentKE (specified in initialConditions)	inletOutlet	inletValue: uniform turbulentEpsilon (specified in initialConditions)	calculated	uniform 0
ground / terrain	kqRWallFunction	uniform turbulentKE (specified in initialConditions)	epsilonz0WallFunction	uniform turbulentEpsilon (specified in initialConditions and dependent on z0-value)	nutkAtmRoughWallFunction	uniform 0.0 with z0-value specified in ABLConditions
top	symmetry	-	symmetry	-	symmetry	-
sides	symmetry	-	symmetry	-	symmetry	-
buildings	kqRWallFunction	uniform turbulentKE (specified in initialConditions)	epsilonWallFunction	inletValue: uniform turbulentEpsilon (specified in initial conditions)	nutkWallFunction	uniform 0.0

Table 6.5: turbulence boundary conditions

The approach flow is modelled parallel to the lateral boundaries of the domain. A symmetry boundary condition was thus assigned to the top and side boundaries of the domain for all the variables.

Velocity boundary conditions

The inlet wind speed profile is computed based on the ABL conditions. The outlet boundary was placed far enough from the study area not to have an influence upstream. As such, the flow at the outlet can be assumed to be fully developed, with all flow variable derivatives equal to 0. The fluid velocity at all the walls (ground, terrain, buildings) is equal to the wall velocity (zero), following the no-slip boundary condition.

Pressure boundary conditions

A constant, zero, static pressure condition is imposed at the outlet boundary, while a zero normal (perpendicular to the patch) pressure gradient (Neumann) boundary condition is applied to the walls (ground, terrain, buildings).

Turbulent kinetic energy boundary conditions

The kqRWallFunction is applied to all the walls in the boundary field, namely the ground boundary, the terrain and the buildings. This wall function for rough walls is applicable to situations with a high Reynolds number (Liu, 2017), which is characteristic for the turbulent flow around buildings in urban environments. The inlet boundary condition for k is determined from the ABL conditions set in OpenFOAM. It is calculated as:

$$k = \frac{u_*^2}{\sqrt{C_\mu}} \qquad (6.17)$$

Turbulent kinetic energy dissipation boundary conditions

The selected ε wall function for the ground / terrain – epsilonz0WallFunction – is based on the z0-value of the terrain as specified in the ABL conditions, while the wall function for the buildings – epsilonWallFunction – is based on ε and G (production term). The latter is typically used for high-Re flows.

The boundary condition for ε at the inlet is determined from the specified ABL conditions as:

$$\varepsilon = \frac{u_*^3}{\kappa(z + z_0)} \qquad (6.18)$$

Turbulent kinematic viscosity boundary conditions
The inlet and outlet of the domain have the "calculated" boundary condition. This implies that the value for ν_t depends on the values of k and ε and is calculated from:

$$\nu_t = C_\mu * \frac{k^2}{\varepsilon} \qquad (6.19)$$

Where C_μ denotes the turbulence model constant, which is equal to 0.09.
The wall function for ν_t applied to the ground and terrain boundaries is the nutkAtmRoughWallFunction, which is based on the z0-value of the terrain parts specified in the ABL conditions. The wall function for the buildings – nutkWallFunction –, on the other hand, is based on the turbulent kinetic energy k.

The temperature boundary conditions are described separately below.

Temperature boundary conditions
The inlet air temperature was determined based on available measurements for the most recent year obtained from the Changi Climate Station. Although temperature measurements were also available for the average of period 1981–2010, using data of the most recent year is more appropriate in this study as rising temperatures due to climate change emphasize the importance of effective urban ventilation. The table below shows the average yearly air temperature (27.7°C = 300.7K), as specified for the inlet temperature in the boundary conditions in OpenFOAM, determined from the monthly data for the year 2017.

Jan	Feb	March	April	May	June	July	Aug	Sept	Oct	Nov	Dec	**average**
26.9	26.9	27.4	27.8	28.5	28.5	28.3	28.1	28.0	27.9	27.1	27.0	**27.7**

Table 6.6: monthly reported temperature measurements [°C] for 2017 (Changi Climate Station, from "Annual Climatological Report 2017" by Meteorological Institute Singapore, 2017) and average yearly air temperature

The transport properties of the fluid corresponding to this air temperature were set as follows.

Air temperature T_{air} [K]	Prandtl number Pr [-]	Thermal diffusivity a=k/(ρ*c) [m²/s]
300	0.707	$22.07*10^{-6}$

Table 6.7: properties of dry air at 300K (at 1 atm = 1.013 bar = 101325 Pa). From: "Engineering ToolBox", 2005 (https://www.engineeringtoolbox.com/dry-air-properties-d_973.html).

The 3D-model was split into separate parts and reasonable surface temperatures were assigned to each of them to analyze the convective heat transfer over the surfaces. The surface temperature boundary conditions for the buildings, the ground plane and the terrain patches were determined based on research outcomes from a study by Philipp (2019) as part of the *Cooling Singapore* project. In this research, land surface temperature data from satellite-based remote sensing *(figure 6.9)* were related to the Local Climate Zones (LCZ) map of Singapore *(figure 6.10),* which was developed in another recent study by Mughal, Li, Yin, Martilli, Brousse, Dissegna, & Norford (2019).

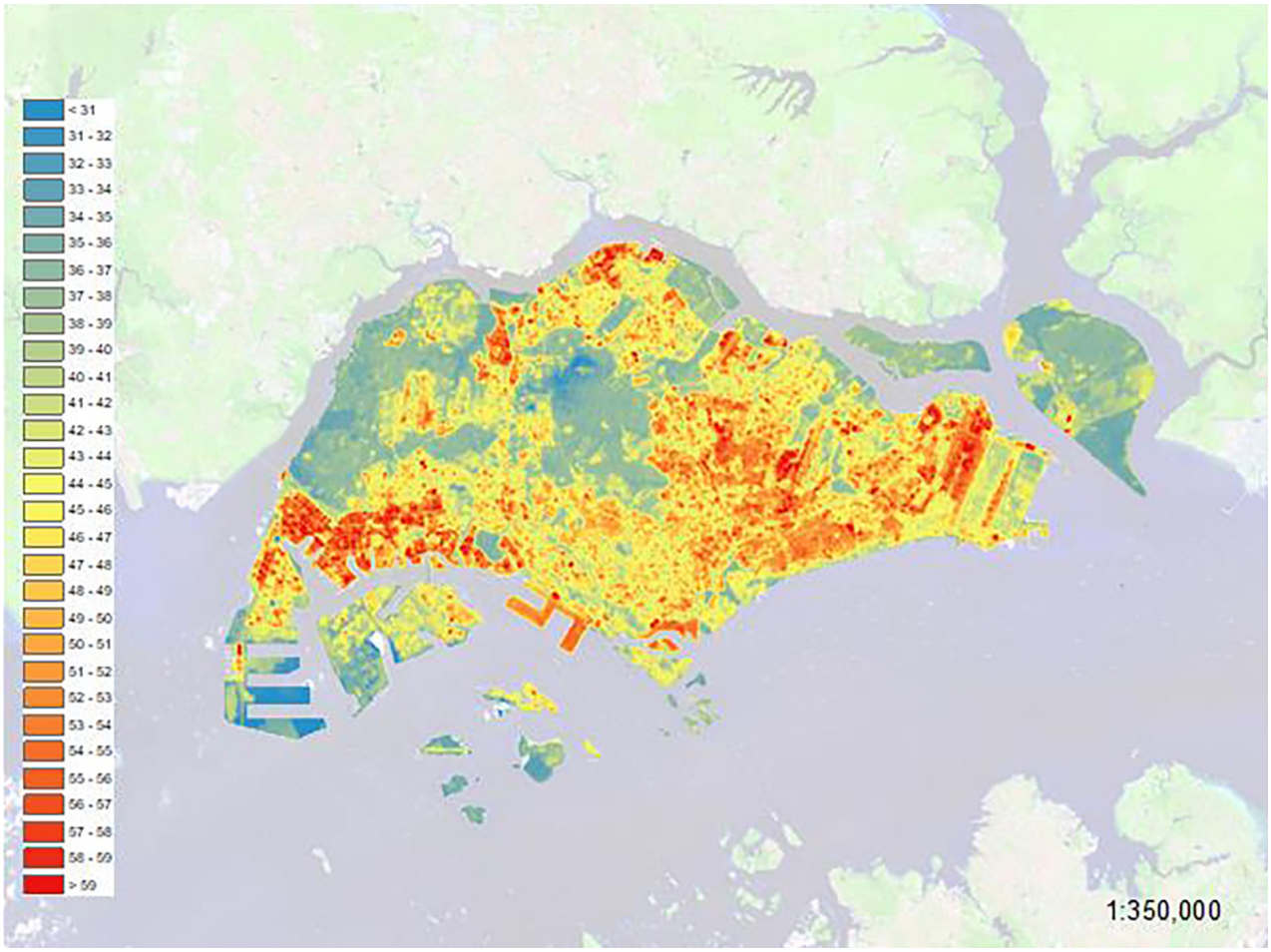

Figure 6.9: remote sensing day-time image (24 May 2018, 11:15 a.m.) of surface temperatures in Singapore. From Surface Urban Heat Island (S-UHI) investigations using remote sensing (Singapore-ETH Centre, Cooling Singapore), by Philipp, 2019. (https://doi.org/10.3929/ethz-b-000372356)

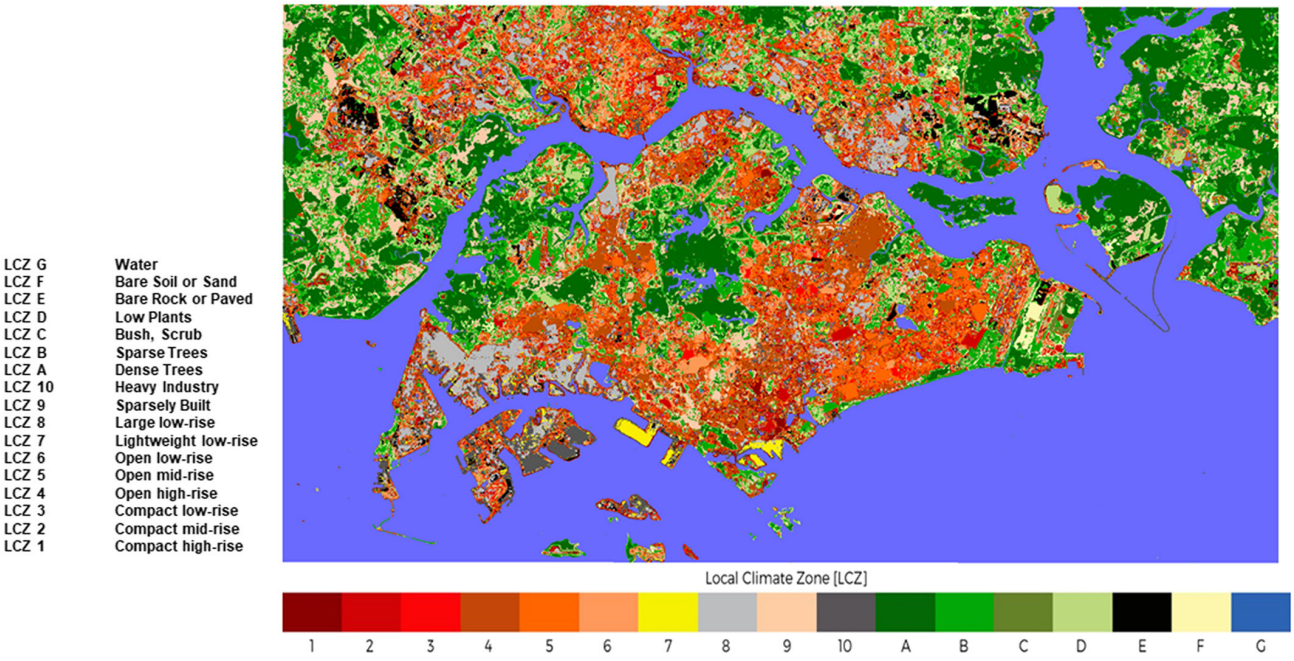

Figure 6.10: Local Climate Zones map Singapore. From High-Resolution, Multilayer Modeling of Singapore's Urban Climate Incorporating Local Climate Zones. In Journal of Geophysical Research: Atmospheres, 124, 7764-7785, by Mughal et al., 2019. (https://doi.org/10.1029/2018JD029796)

The resulting average surface temperatures (based on remote sensing satellite-based data of 24 May 2018, 11:15 a.m.) for Singapore in relation to the Local Climate Classification (developed by Oke and Stewart, 2012) are represented in *figure 6.11*.

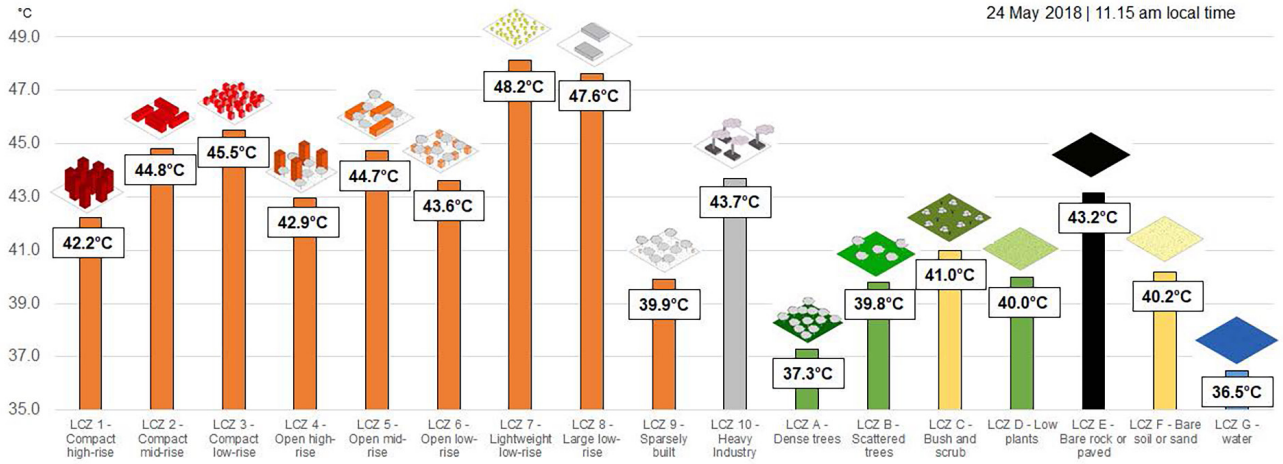

Figure 6.11: day-time average surface temperature for LCZ. From Surface Urban Heat Island (S-UHI) investigations using remote sensing (Singapore-ETH Centre, Cooling Singapore), by Philipp, 2019. (https://doi.org/10.3929/ethz-b-000372356)

The output from the abovementioned studies (*figure 6.11* in particular) was used to make reasonable assumptions for the temperature boundary conditions of the surfaces (ground/bottom boundary of computational domain, terrain patches and building surfaces) specified in OpenFOAM for the study area in Clementi. This was done by classifying the respective areas of the computational model according to the local climate zone (LCZ) that best matches the surface properties of the area. The definitions and climate zone properties provided in the LCZ datasheets of the supplement to the *Local Climate Zones for Urban Temperature Studies* paper by Oke and Stewart (2012) were consulted to determine the LCZs. The 3D model parts with their main properties and the corresponding LCZ are listed in *Appendix C (Local Climate Zones Clementi)*.

The surface temperatures of the terrain roughness areas upstream and downstream of the modelled area (indicated previously in this report as roughness area 2 and 5 respectively) have been chosen in accordance with their aerodynamic roughness length from the Davenport-Wieringa classification, as specified in *section 6.1.3.1*. A relation between the aerodynamic roughness length classes and the local climate zones is given by Oke and Stewart (2012) in *table 6.8*.

TABLE 5. Davenport classification of effective terrain roughness. Correspondence with LCZs is given for each Davenport class.

Davenport class	Roughness length, z_0 (m)	Landscape description	LCZ correspondence
1. Sea	0.0002	Open water, snow-covered flat plain, featureless desert, tarmac, and concrete, with a free fetch of several kilometers.	E, F, G
2. Smooth	0.0005	Featureless landscape with no obstacles and little if any vegetation (e.g., marsh, snow-covered or fallow open country).	E, F
3. Open	0.03	Level country with low vegetation and isolated obstacles separated by 50 obstacle heights (e.g., grass, tundra, airport runway).	D
4. Roughly open	0.10	Low crops or plant covers; moderately open country with occasional obstacles (e.g., isolated trees, low buildings) separated by 20 obstacle heights.	7, C, D
5. Rough	0.25	High crops, or crops of varying height; scattered obstacles separated by 8 to 15 obstacle heights, depending on porosity (e.g., buildings, tree belts).	5–10, B, C
6. Very rough	0.5	Intensely cultivated landscape with large farms and forest clumps separated by 8 obstacle heights; bushland, orchards. Urban areas with low buildings interspaced by 3 to 7 building heights; no high trees.	2, 3, 5, 6, 9, 10, B
7. Skimming	1.0	Landscape covered with large, similar-height obstacles, separated by 1 obstacle height (e.g., mature forests). Dense urban areas without significant building-height variation.	2, 4
8. Chaotic	≥ 2	Landscape with irregularly distributed large obstacles (e.g., dense urban areas with mix of low and high-rise buildings, large forest with many clearings).	1, 4, A

Table 6.8: correspondence of Davenport-Wieringa roughness classes with local climate zones (LCZs). From Local Climate Zones for Urban Temperature Studies. In American Meteorological Society, 1879–1900), by Oke & Stewart, 2012. (https://doi.org/10.1175/BAMS-D-11-00019.1)

For the simulation with wind approaching from the South direction, the roughness areas 2 and 5 were characterized by an aerodynamic roughness length z_0 of 1.0m and 0.5m, which translates to LCZ 2/4 and 2/3/5/6/9/10/B respectively. Since these upstream and downstream areas were not modelled explicitly, with a uniform aerodynamic roughness length over the entire surface, the areas are also simplified for the surface temperature boundary conditions by taking a uniform surface temperature over the entire upstream and downstream area. Although the upstream roughness area has both high- and low-rise buildings, the buildings directly upstream are mostly high-rise, so we classify the entire patch as LCZ 4 (open high-rise) for simplification purposes. The corresponding surface temperature according to *figure 6.11* is 42.9°C, which is inserted as the domain's bottom surface boundary condition upstream of the modelled area. The downstream area, on the other hand, is mostly characterized by low-rise buildings. The local climate zone that best describes this area is LCZ 6 (open low-rise), with a corresponding temperature boundary condition of 43.6°C for the domain's bottom surface.

An overview of the LCZs and their corresponding temperature boundary conditions in the computational model is given in *figures 6.12 and 6.13*.
It should be noted that, since these surface temperature boundary conditions are determined using the diagram (*figure 6.11*) which relates the local climate zones to remote sensing surface temperatures based on measurements of 24 May 2018 at 11:15 a.m., these simulation settings are not accurate for the entire year and every sun position, although the *climate data part in section 3.1* showed that the temperature fluctuations over the months are rather small (ΔT_{max} = 1.8°C). However, since May and June are the months with the highest monthly temperature in Singapore (*see climate data part 3.1*), these case boundary conditions are representative for a day-time analysis of urban ventilation.

Figure 6.12: LCZs and surface temperature boundary conditions in study area

Figure 6.13 (next page): assigned surface temperature boundary conditions of 3D-model parts and bottom patch of computational domain based on LCZs (GIF-animation in presentation)

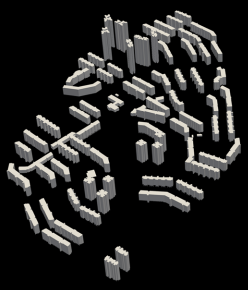

LCZ 4
42.9 °C

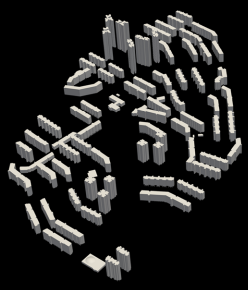

LCZ 6
43.6 °C

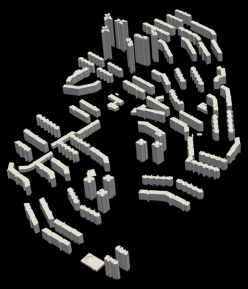

LCZ 5
44.7 °C

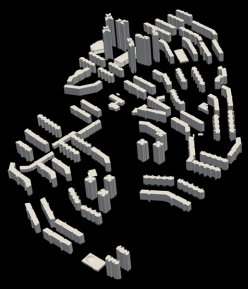

LCZ 5
44.7 °C

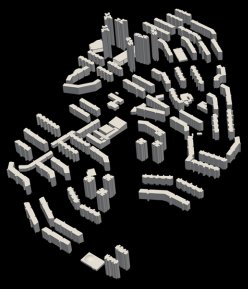

LCZ 2
44.8 °C

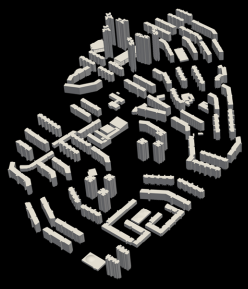

LCZ 8
47.6 °C

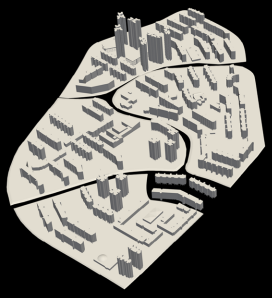

LCZ B
39.8 °C

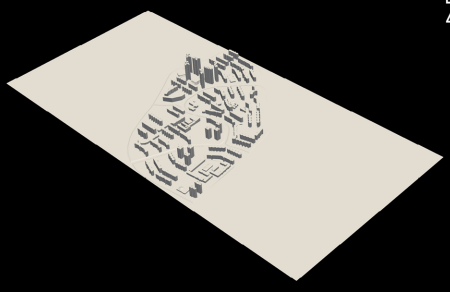

LCZ E
43.2 °C

LCZ 6
43.6 °C

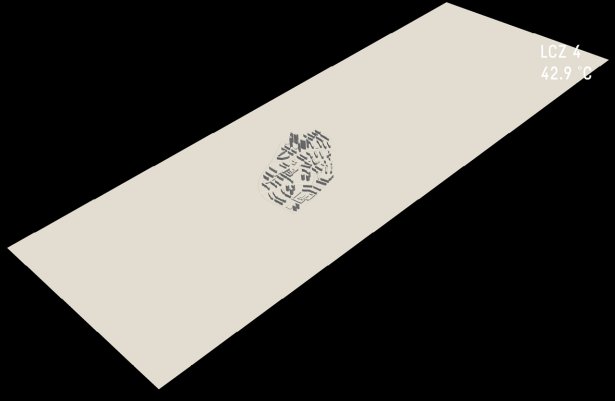

LCZ 4
42.9 °C

6.1.3.3 Simulations Convergence

The generation of the computational mesh for the simulations is a time-consuming, yet very important aspect in CFD. Attention should be paid to both the size (thus, the resolution) and shape of the grid to ensure a high-quality grid. (Blocken, 2019) A grid convergence analysis is indispensable to ensure that the results obtained from the CFD simulations are grid-independent.
Two types of convergence analyses are performed and described below.

a) Grid independence study

A grid-independent solution is one where further division of the control volumes (grid) does not lead to significant changes in the variable value (e.g. the velocity at a certain point around the building). In this study, the quality of the grid is particularly important at the void decks. The grid convergence analysis has therefore been performed by placing a probe at pedestrian height (1.75m) at the centre of the void deck of the building. In the urban case, this was done for 30 buildings in the study area in order to get an idea of where in the study area the results were reliable. The data at these probe locations were sampled for three systematically refined grids – starting from a relatively course grid (with locally a higher mesh refinement level at the building geometry and in the lowest part of the whole computational domain) which complies to the guideline of a minimum of 10 cells along each building dimension; and refining by a constant refinement factor of $\sqrt{2}$ – and compared to analyse the grid sensitivity of the simulation results.

The graph below (*figure 6.14*) shows the grid convergence analysis for the single building case simulations; created by plotting the probe results of the last time step for different mesh refinements.

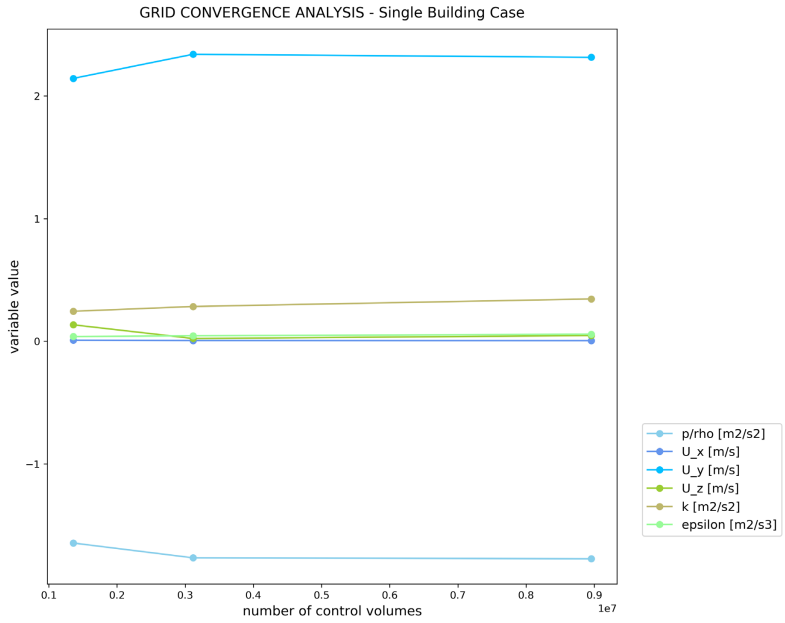

Figure 6.14: grid convergence analysis for single building case simulations

The medium-sized grid (with 10m/$\sqrt{2}$ =7.07m per cell in each direction for the background mesh, resulting in a mesh of 3,114,929 cells in total) was chosen for the simulations of the single building cases as further refinement of the grid does not lead to significant changes in the variable values.

The mesh creation for the urban case simulations followed a more elaborate process as the building void decks were modelled as detailed as possible to get an accurate representation for the simulation of the urban ventilation in the current situation. Considering the complexity of this model, the mesh was adjusted in several steps, looking at more aspects than just the cell dimensions of the background mesh in the blockMeshDict of OpenFOAM. The final mesh was chosen based on how well the void deck elements are represented in the mesh and on the corresponding computational implications (mesh size, computational

time) for the simulations. The background mesh (generated with blockMesh) is denoted as level 0. Every next refinement level implies that the cells are split in half in each direction, thus leading to a doubling of the number of cells in each direction (*see figure 6.15*).

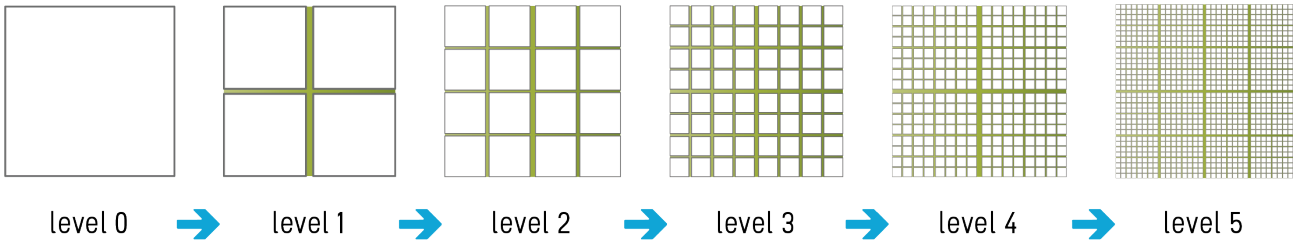

Figure 6.15: sequential mesh refinement levels in OpenFOAM

Starting with a background mesh of 36m per cell in x,y,z-direction, the grid was refined by a factor of √2 in several steps. The refinement level of the refinement boxes was also adjusted several times, as well as some other settings. The meshes generated in OpenFOAM were visualized in ParaView, some of which are shown in *figure 6.16*. The top left image shows how the geometry of the imported 3D-model was detected in OpenFOAM, by running the surfaceFeatures command. To assess the mesh quality, one can thus compare each of the visualized meshes to this detected model.

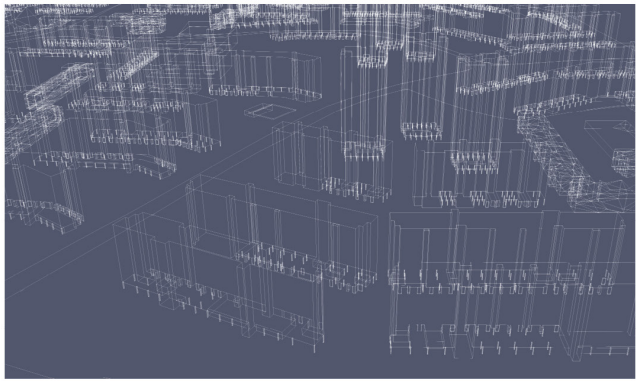

surfaceFeatures (detected geometry from imported 3D-model)

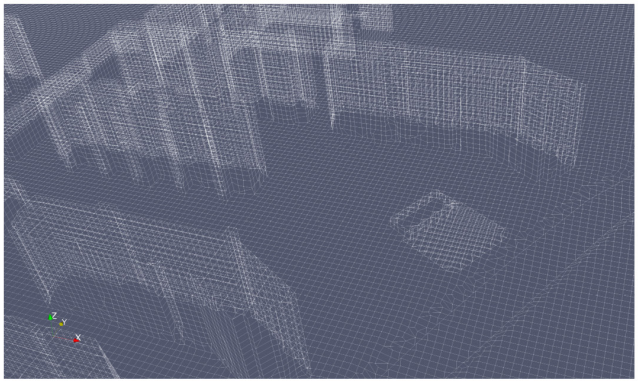

urban mesh M1.2

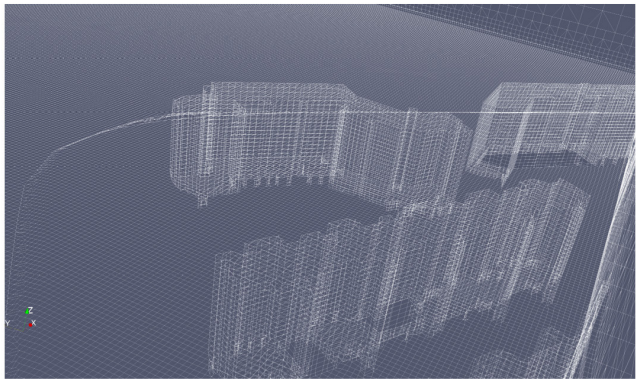

urban mesh M1.3

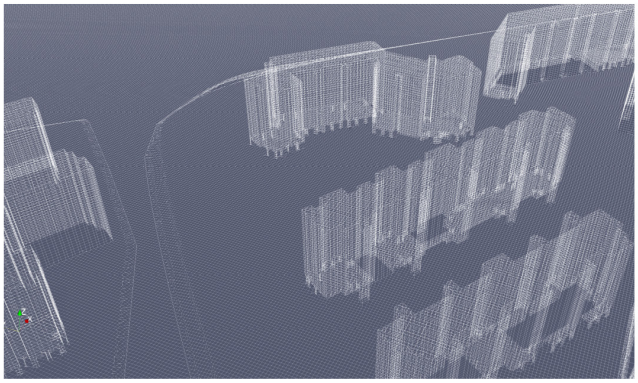

urban mesh M1.4

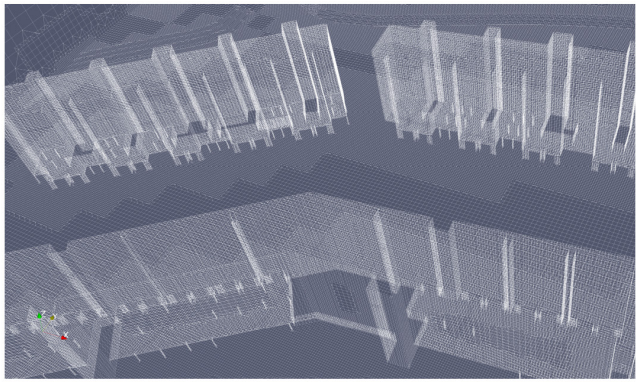

urban mesh M1.5

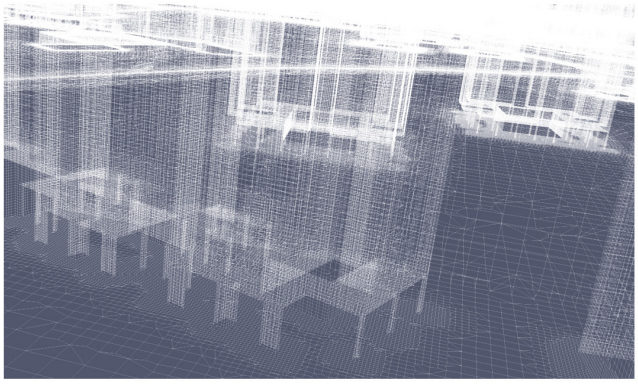

urban mesh M1.6

Figure 6.16: visualized mesh refinements for urban case simulations (current situation)

The coarser meshes were eliminated during the qualitative mesh check (by visual inspection of the mesh) as these did not properly capture the void deck features and thus did not qualify to analyse the flow pattern around the void decks. The final mesh settings for the urban case are shown in *table 6.9* below.

background mesh cell size (blockMeshDict set-up)	grid refinement settings (snappyHexMeshDict set-up) *	number of cells in mesh
36m/(√2*√2) = 18m per cell in x,y,z-direction	box 1: refinement level 4 box 2: refinement level 3 box 3: refinement level 5 buildings: refinement level 5	≈ $32*10^6$

* refinement box 1: refinement box for 6 hybrid (complex-shaped) buildings
refinement box 2: box at start of terrain outline
refinement box 3: void decks refinement box of 2m (terrain) +3.7m (coverage of void decks) height covering whole domain

Table 6.9: urban case – final mesh settings

The detailed mesh settings, as well as the computational times and CPU usage are reported at the end of *Appendix D (OpenFOAM-files)*.

The refinement level of box 3, which is located in the lowest part, spanning over the whole domain, determines how refined the mesh will be at the void decks. This means that the regular cells (note: the shape of these cells is deformed in the next refinement step: surface snapping) of the castellated mesh around the geometry in the lowest part of the domain, where the void decks are situated, will have a dimension of 0.56m in x,y,z-direction (assuming simpleGrading (1 1 1) in the base mesh). In that case, the centroid of the cell closest to the bottom wall is at 0.28m height, which respects the $y_P > z_{0,terraingrass}$ grid refinement rule, as $z_{0,terraingrass}$ = 0.06m.

b) Residuals convergence

Once the appropriate refinement level of the grid has been chosen, the convergence with respect to the number of iterations can be analyzed for the simulation with that grid. This convergence analysis is typically performed to reduce errors in iterative solution methods. By plotting time (number of iterations) versus the values of the variables of importance (p, U, k, ε, T) it becomes visible how fast each of the variables converge. The convergence criterion for each of the residuals is set in the fvSolution dictionary. The solver will stop running once the residual for each variable reaches a value below the tolerance that was set.

The change of the variable values at the probe location over time (with increasing number of iterations) during the simulation is shown in *figure 6.17* on the left. As can be seen from both plots, the simulation results have converged after approximately 450 iterations, with no further significant changes. The residuals for each of the variables with respect to the number of iterations are plotted on the right. After approximately 450 iterations, the residuals have dropped almost completely to zero, which means that the deviation of the numerical iterative simulation results from the exact solution (i.e. the error) has become extremely small. As can be seen from the graph, of all the variables being solved in the system of equations, the cell residual values for pressure converge slowest.

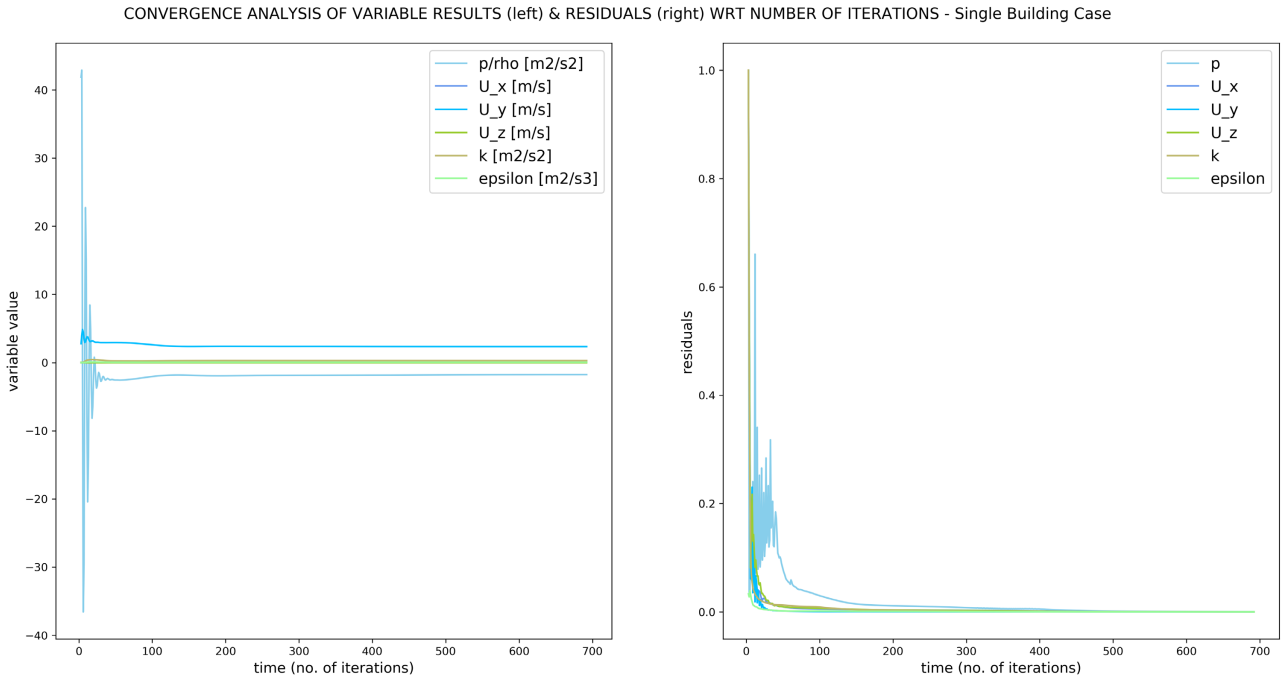

Figure 6.17: convergence analysis with respect to number of iterations for single building case simulations

The convergence analysis of the residuals with respect to the number of iterations for the urban case (with the void decks in their current state) is shown in *figure 6.18* below.

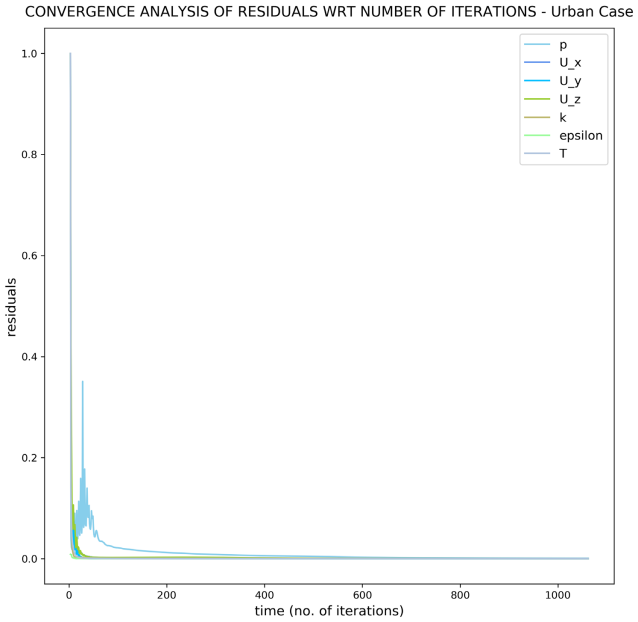

Figure 6.18: convergence analysis with respect to number of iterations for urban case simulations

As mentioned earlier, 30 probes were set inside void decks in the whole area to monitor the convergence during the simulation. These were grouped as follows:

- PROBE SET 1: probes in void decks of buildings at main street level (probe height = 0m + 1.75m)
- PROBE SET 2: probes in void decks of buildings on “NW terrain island” (probe height = 2m + 1.75m)
- PROBE SET 3: probes in void decks of buildings on “SE terrain island” (probe height = 2m + 1.75m
- PROBE SET 4: probes in void decks of buildings on “NE terrain island” (probe height = 2m + 1.75m)
- PROBE SET 5: probes in void decks of buildings on “SW terrain island” (probe height = 2m + 1.75m)

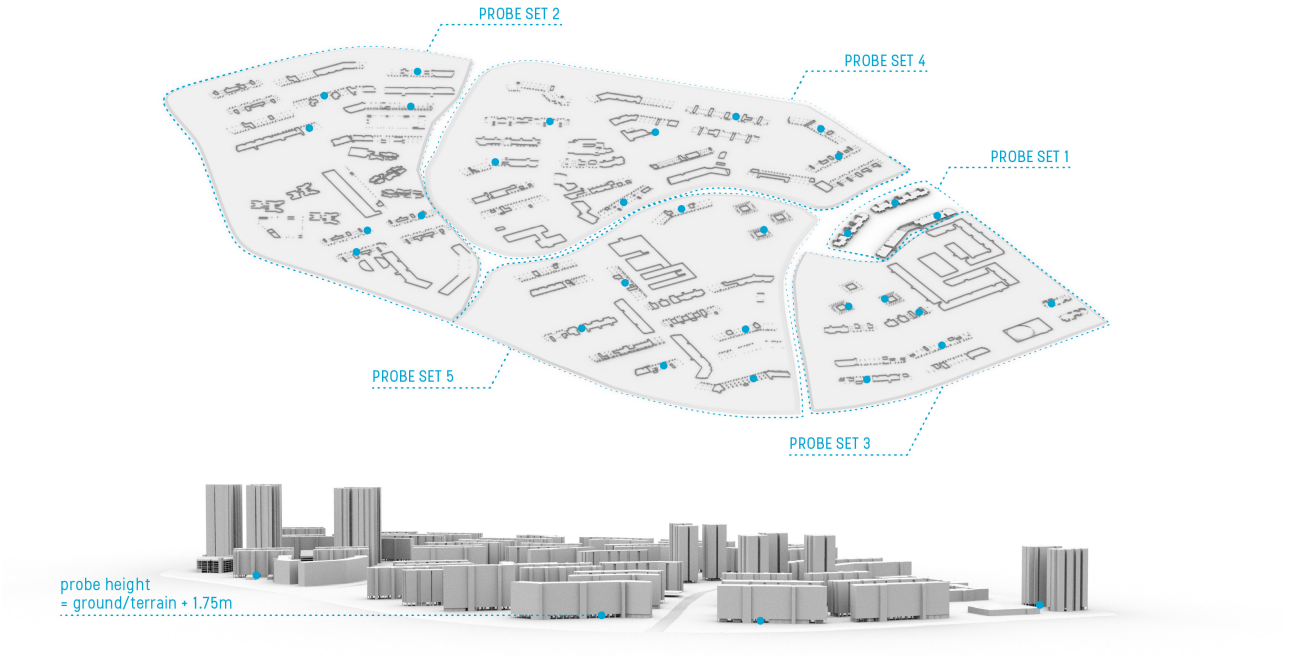

Figure 6.19: probe locations

Per probe set, the variable values were plotted for one randomly chosen probe, as shown in the subsequent *figures 6.20 to 6.24*. All probes show a clear convergence towards the end of the simulation.

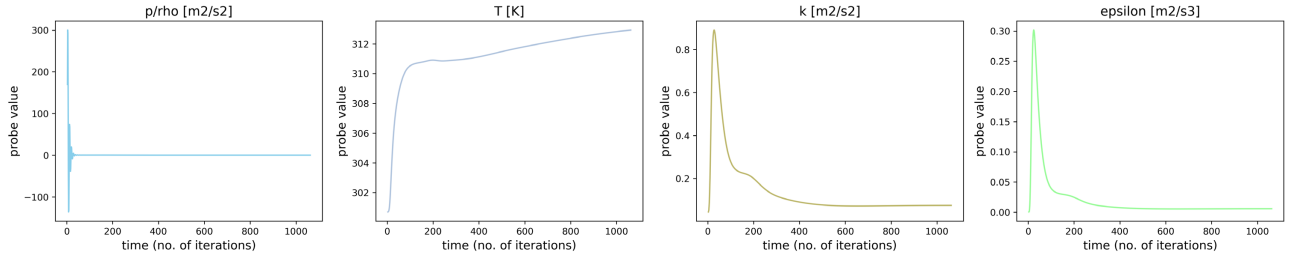

Figure 6.20: PROBE SET 1 convergence: probes in void decks of buildings at main street level (probe height = 0m + 1.75m)

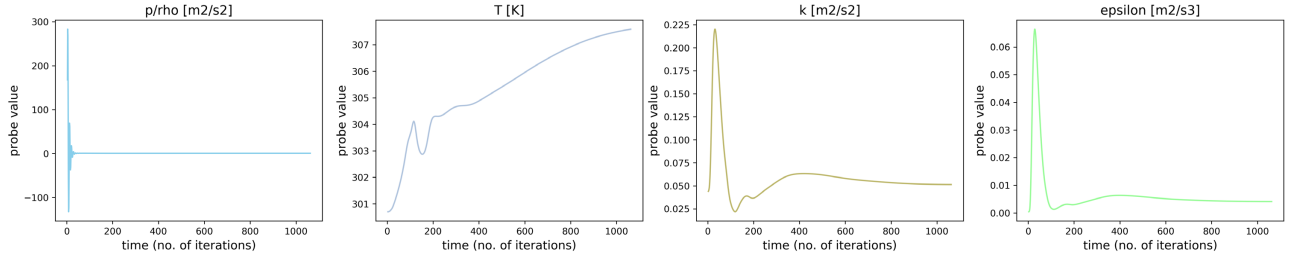

Figure 6.21: PROBE SET 2 convergence: probes in void decks of buildings on "NW terrain island" (probe height = 2m + 1.75m)

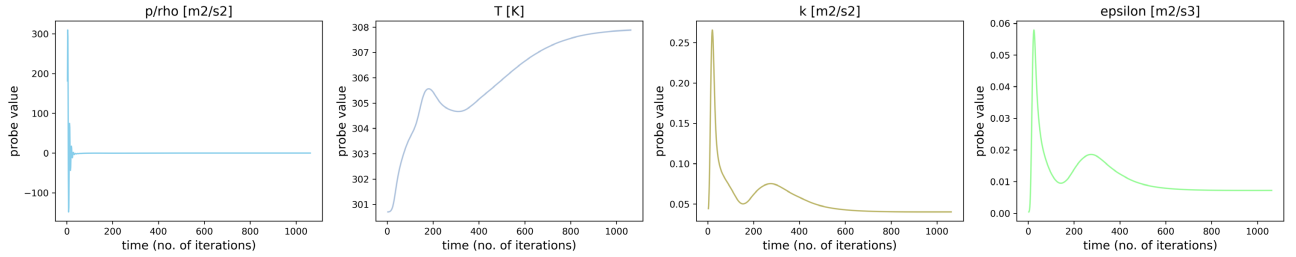

Figure 6.22: PROBE SET 3 convergence: probes in void decks of buildings on "SE terrain island" (probe height = 2m + 1.75m)

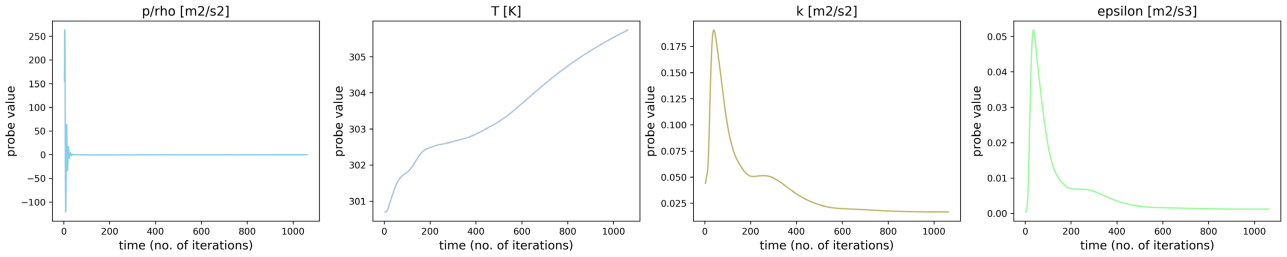

Figure 6.23: PROBE SET 4 convergence: probes in void decks of buildings on "NE terrain island" (probe height = 2m + 1.75m)

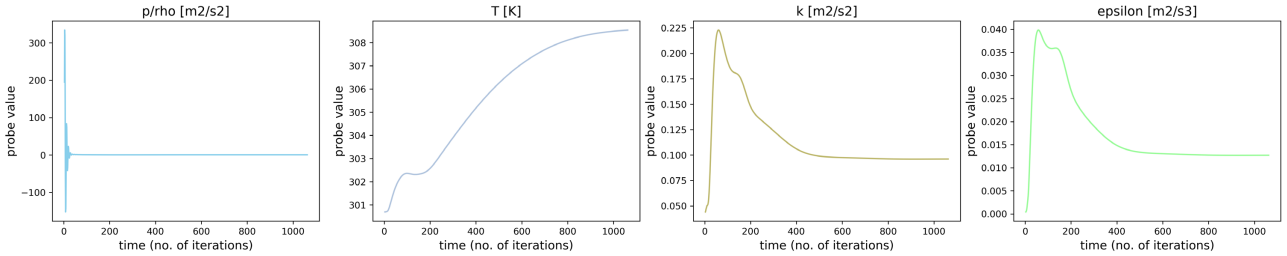

Figure 6.24: PROBE SET 5 convergence: probes in void decks of buildings on "SW terrain island" (probe height = 2m + 1.75m)

6.2 Simulation Results

The results from the single building and urban case simulations are displayed here and will be discussed in the next section. All the plots in this section were created in ParaView.

6.2.1 Single Building Case – Void Geometry Variants

Starting with the single building cases, the plots below show the top-view results for the wind speed at pedestrian height (1.75m from the ground).

One additional simulation was run for an empty case, thus with the same settings as all the variant cases, but excluding the building model. This was done to analyse the impact of a building with a certain void deck design on the flow pattern, as compared to the case where this building would not have been present. This is expressed as the amplification factor K, which is defined as the ratio of the mean wind speed at a certain point for the case with the building with the void deck and the mean wind speed at the same point for the case without the building:

$$K_{\text{point P; building with void deck design } i} = \frac{U_{\text{point P; building with void deck design } i}}{U_{\text{point P; without building}}} \qquad (6.20)$$

Note that, since the snappyHexMesh refinement step was not done for the empty case – as no geometry STL-file exists in that case –, one should make sure that the same level of grid refinement is obtained in the empty case and the variant cases to avoid mesh uncertainties. To ensure this, we split the computational domain into an upper and lower hexahedral block; the lowest one having a height of 4m, for which the background mesh (blockMeshDict) was refined to the same level as that of the variant case simulations that were run with snappyHexMesh.

Contour plots of the amplification factor were made for each of the design variants, as shown in *figure 6.26*. The amplification factor at the centre of the void deck (at 1.75m height) is marked in the plot.

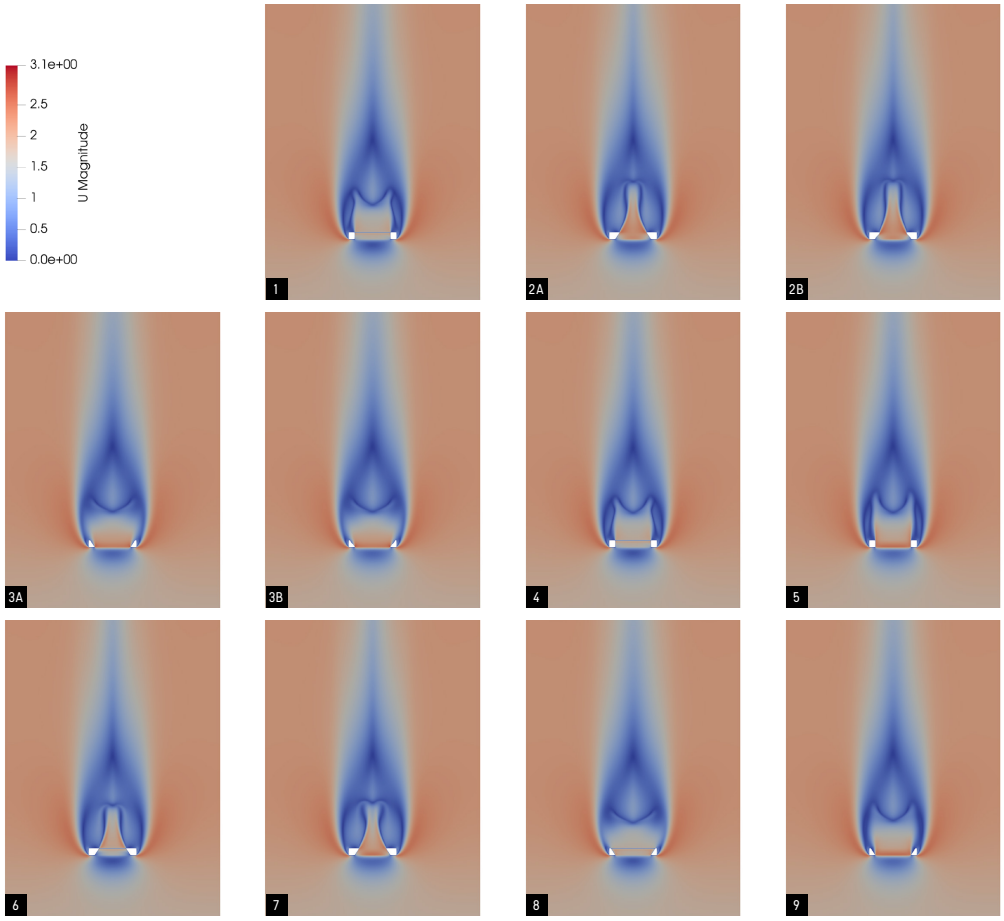

Figure 6.25: horizontal plane results for U at pedestrian level (1.75m height)

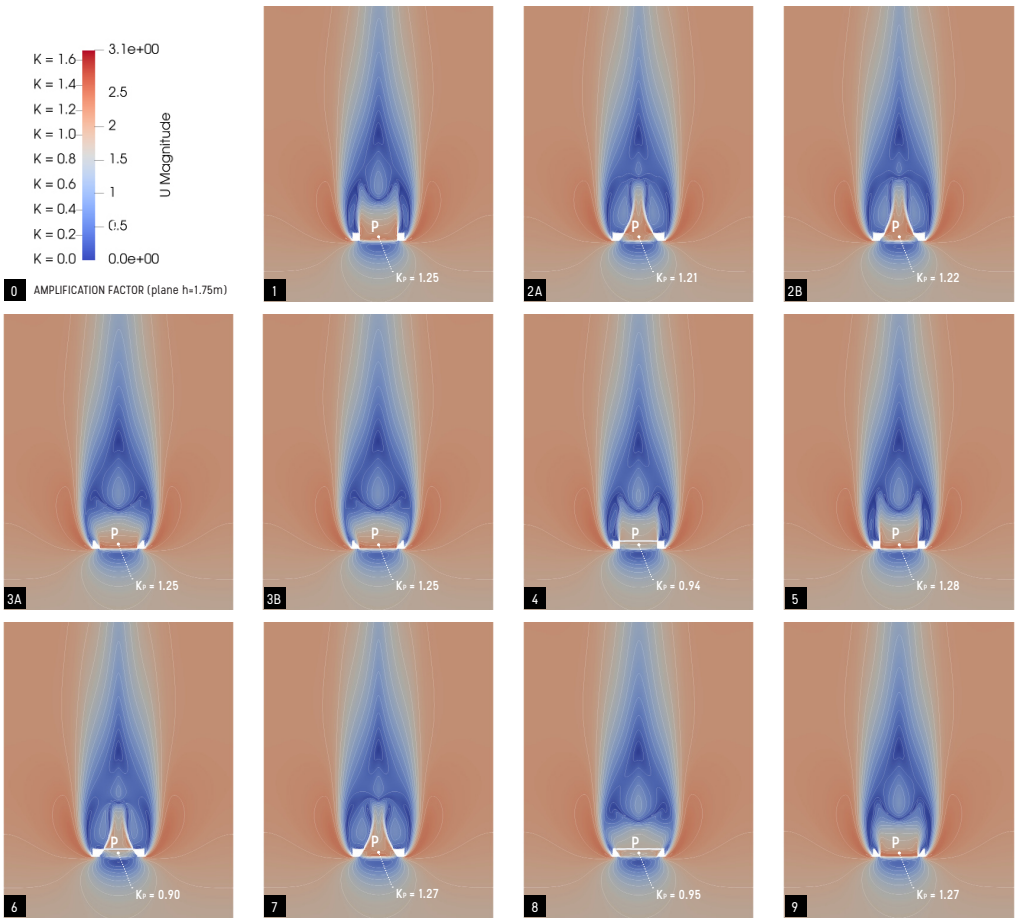

Figure 6.26: contour plots of amplification factor K at pedestrian level (1.75m height)

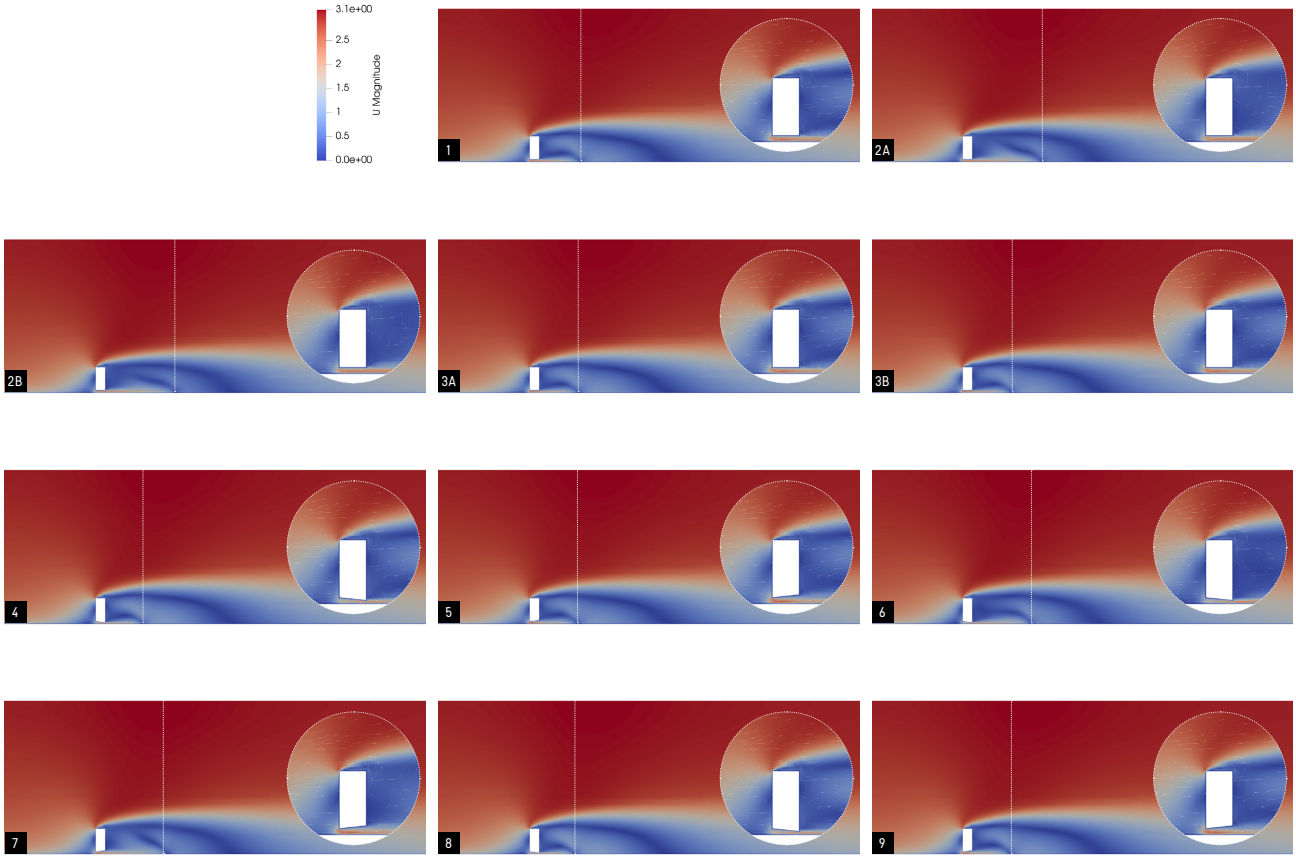

Figure 6.27: vertical plane (at centre of void deck) results for U & zoom of U vector glyph plot

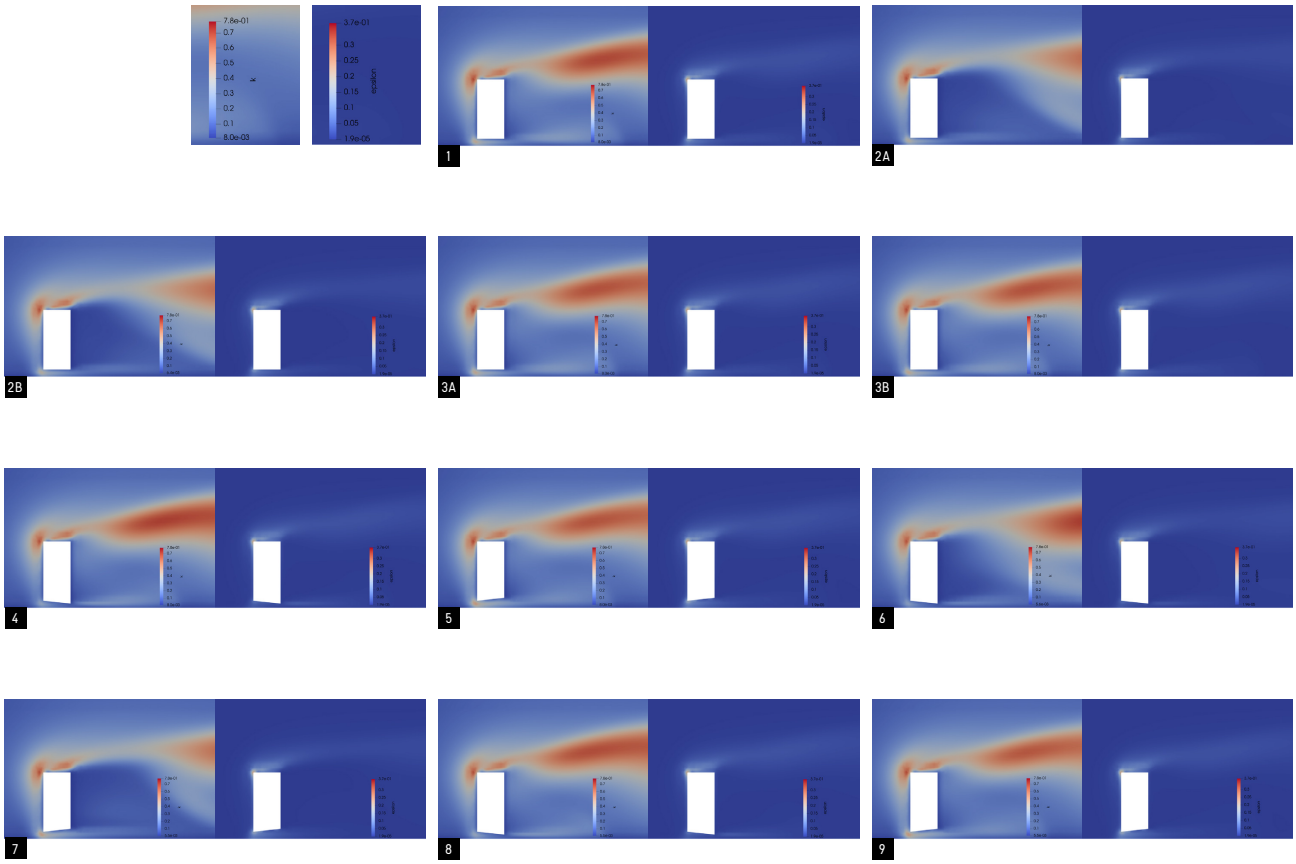

Figure 6.28: vertical plane (at centre of void deck) results for k and ε

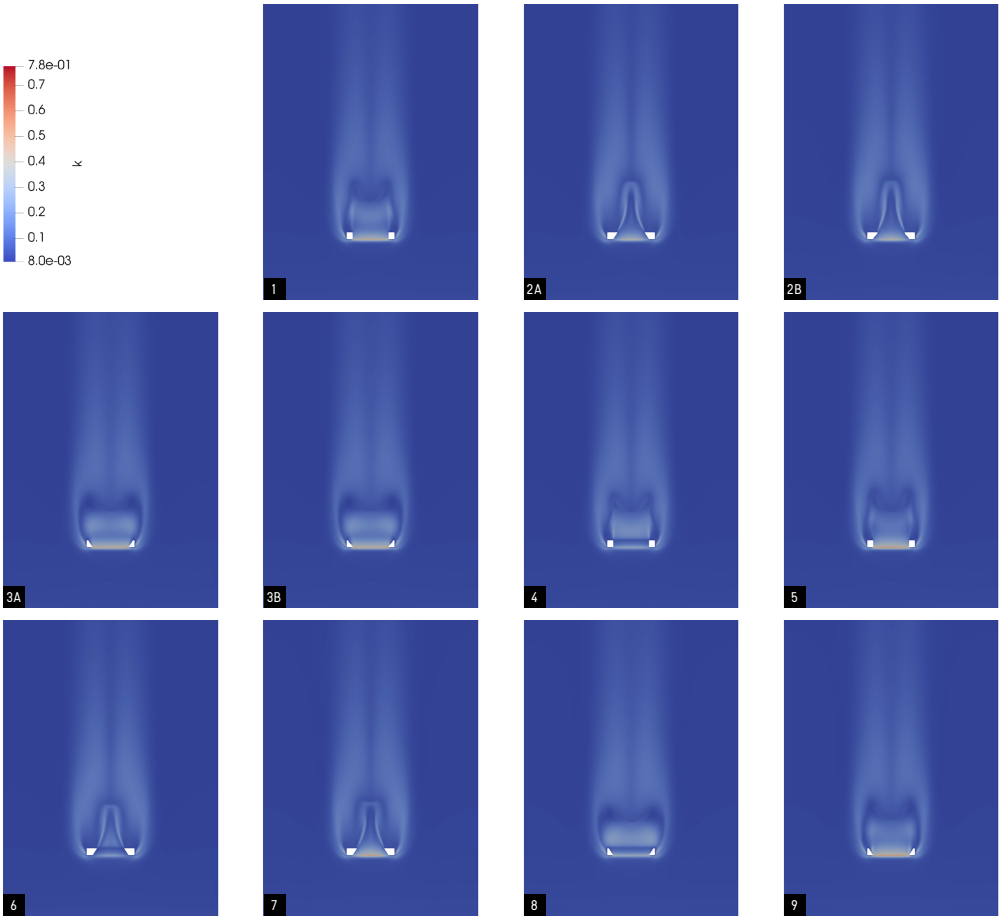

Figure 6.29: horizontal plane results for k at pedestrian level (1.75m height)

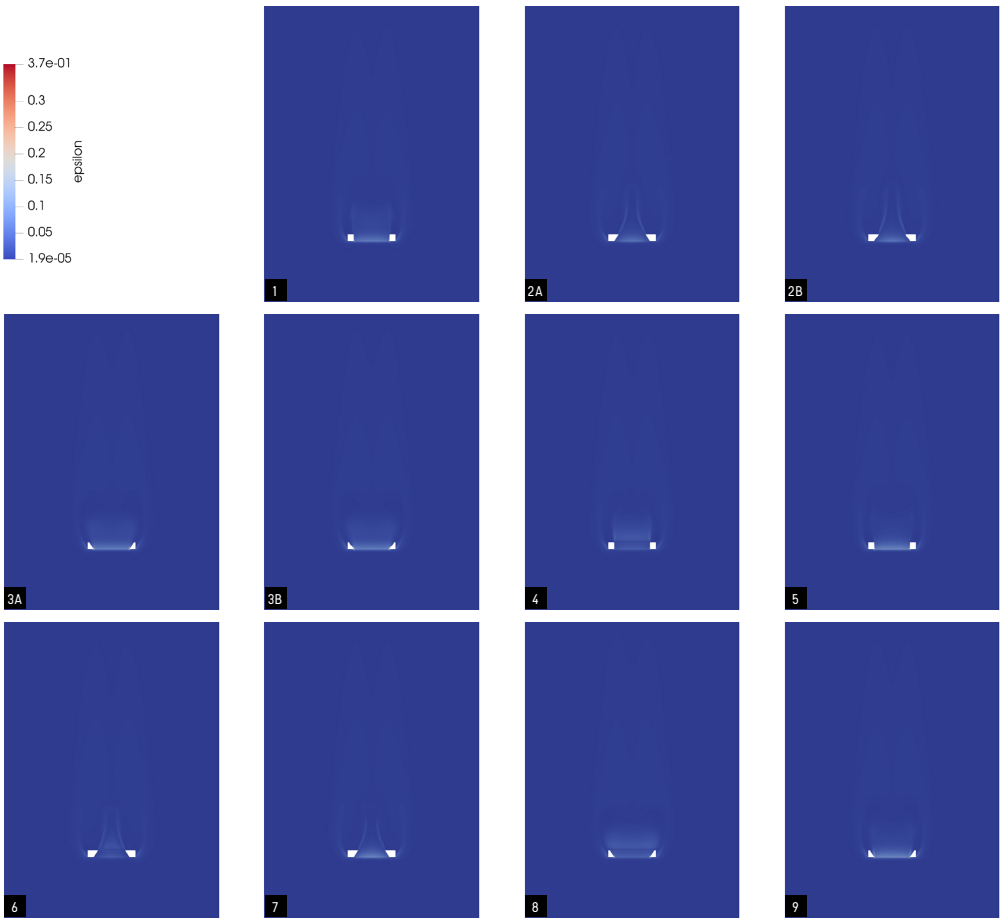

*Figure 6.30: horizontal plane results for **ε** at pedestrian level (1.75m height)*

6.2.2 Urban Case – Current Situation

The sampled results for U and T at 1.75m height above the elevated terrain are shown below for the three considered wind directions.

Figure 6.31: prevailing wind from North – U at pedestrian level (z = +3.75m)

Figure 6.32: prevailing wind from North – T at pedestrian level (z = +3.75m)

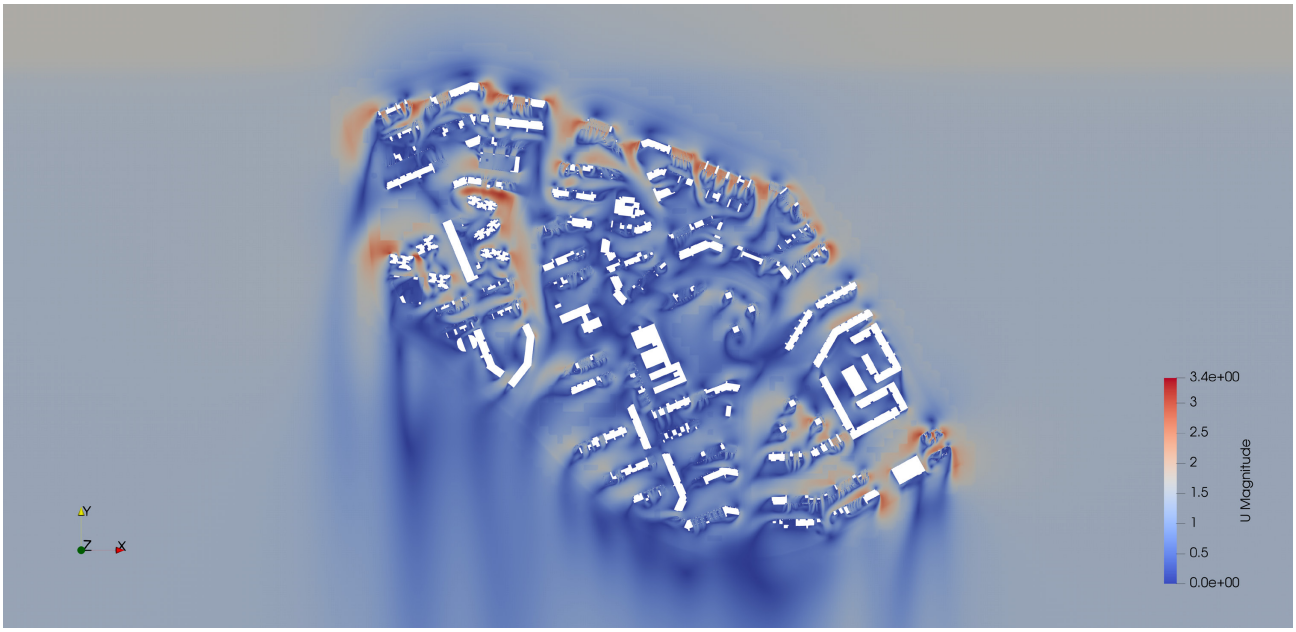

Figure 6.33: prevailing wind from North-Northeast – U at pedestrian level (z = +3.75m)

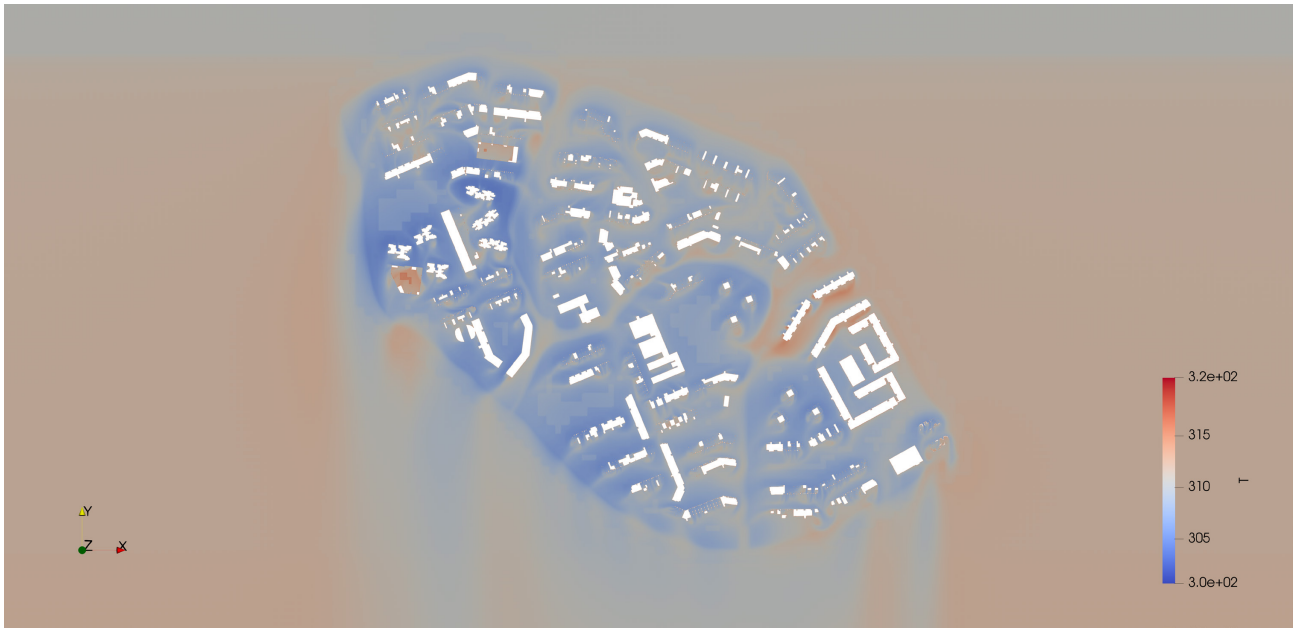

Figure 6.34: prevailing wind from North-Northeast – T at pedestrian level (z = +3.75m)

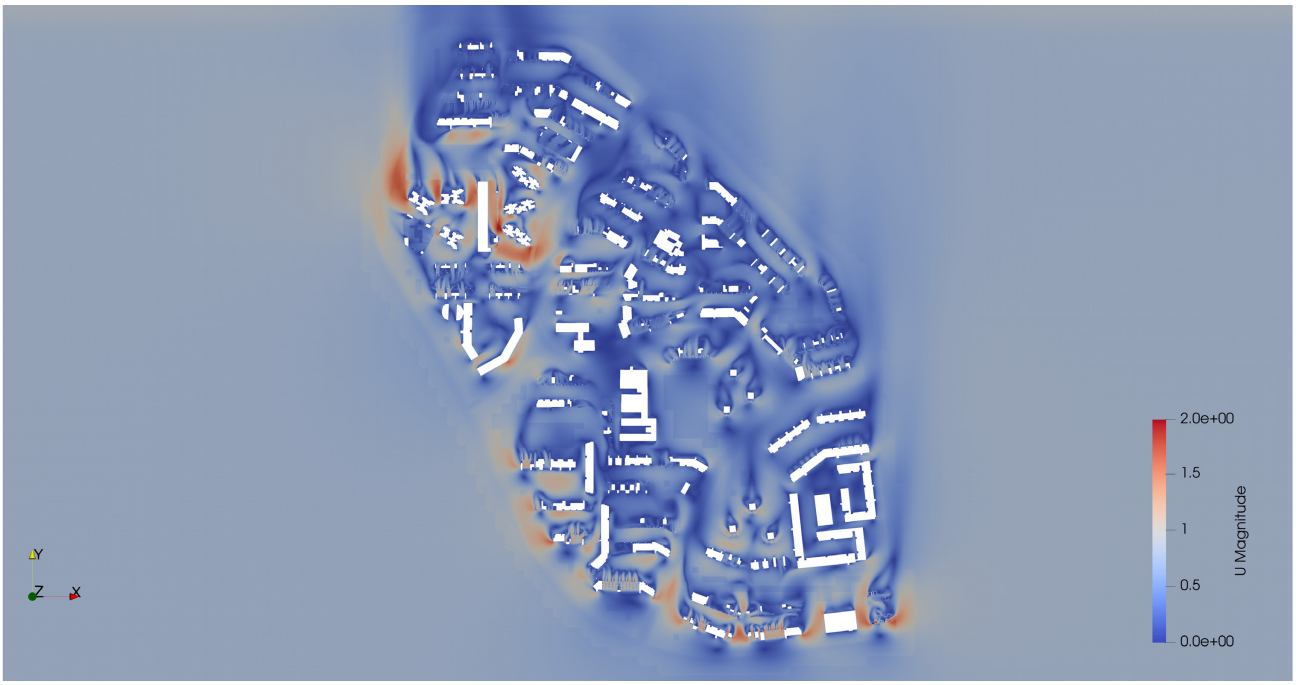

Figure 6.35: prevailing wind from South – U at pedestrian level (z = +3.75m)

Figure 6.36: prevailing wind from South – T at pedestrian level (z = +3.75m)

6.3 Discussion of Simulation Results

6.3.1 Single Building Case – Void Geometry Variants

The horizontal flow pattern around the building at pedestrian height (*see figure 6.25*) shows clear differences amongst the different void deck designs. Looking at the the flow pattern, two groups can be distinguished: void decks which lead to a funnel-shaped area of increased velocity in the wake behind the building (void deck variants 2A, 2B, 6 and 7), and those with an accelerated flow along (almost) the whole building length (void deck variants 1, 3A, 3B, 4, 5, 8 and 9). The **funnel-shaped** flow acceleration in the horizontal velocity field occurs as a result of **horizontal convergence** of the void deck, which is a common characteristic of variants 2A, 2B, 6 and 7. While the group of void decks with horizontal convergence overall seems to lead to a more significant increase in wind speed downstream of the void deck, this high-velocity flow is concentrated over a limited, funnel-shaped, area. This may have positive or negative consequences in terms of urban planning, depending on which functions are located behind the building. For example, if there is a pedestrian route along the building length behind the building, this sudden, very localized, increase in wind speed may be perceived as unpleasant while walking past it. In that case, a **more even spread** of slightly increased wind speeds along the building length, as obtained with a **horizontally diverging** geometry, would be more desirable. On the other hand, if the urban function downstream of the void deck involves a high level of physical activity (such as a sports field) which, according to wind comfort criteria such as those of Lawson, tolerate – and in case of a tropical climate even desire – higher wind speeds, the funnel-shaped flow acceleration pattern might be more suitable. When comparing the horizontally converging and diverging void decks with straight walls to those with curved walls, there is hardly any difference in the flow pattern. Thus, the choice of either straight or curved tapered void decks remains a question of architectural preference.

High wind speeds at the building corners where the flow separates (commonly referred to as corner streams) occur in all cases. This is where significant turbulence is generated, leading to increased turbulent kinetic energy (k) as can be seen in *figure 6.29*. The highest level of turbulence occurs at the edge of the building where the air flows into the void deck. At pedestrian height, the turbulence at this edge is most pronounced in variants 3A, 3B, 5, 7 and 9. The latter three all diverge vertically from the inflow towards the outflow of the void deck. The high value of k may thus be caused by the sudden change from

a completely unconfined flow upstream of the building, part of which is being pushed into the void of a limited height at the inflow. Downstream of the void deck, the flow is also more turbulent than the flow upstream and around the sides of the building. The pattern of k, as well as that of the turbulent kinetic energy dissipation rate ε, clearly follows that of the velocity magnitude described before. In the vertical plane (*figure 6.28*), it becomes clear that the largest region of high turbulence is caused by the separation at the frontal corner of the roof of the building. The energy of the turbulent fluctuations at the void decks is much lower in comparison. The vertical cutting plane shows that the highest turbulence occurs at the frontal top edge of the vertically diverging void decks.

By means of the amplification factor, one can analyse the effect of a particular building on the outdoor ventilation. If K › 1, the mean wind speed, and thus the urban ventilation, is augmented due to the presence of the building with the void deck. On the other hand, a K ‹ 1 implies a reduction in urban ventilation due to the building.

Looking at the centre of the void deck at a height of 1.75m above the ground (marked by point P), one can observe an increase in the velocity as compared to the empty case in almost all the variants, except for the buildings with void deck 4, 6 and 8. All the other void deck geometries will thus likely have a positive influence on the outdoor thermal comfort. The **highest amplification factors** were sampled in the **vertically diverging void decks**. There is a clear consistency in the cases with **K ‹ 1**, as these are all **convergent void decks in the vertical direction**. Since the lowest void deck height is at the edge of the void deck where the air flows out, the air thus mainly speeds up downstream of the void deck, rather than inside the void deck. Since the void decks serve as a community space, purposefully integrated underneath the building to provide a place with an enhanced microclimate for people, void decks 4, 6 and 8 would not be very suitable as they do not lead to increased wind speeds inside the void deck, but only – to a limited degree – downstream of it. In the vertical plane results for U, one can clearly see the difference with the other void deck designs, which do lead to a flow acceleration through the void deck. A recirculation flow at the leeward side of the building can be observed from the U-vector glyph plot. Another thing to notice from the vertical plane results is the difference in the distance to where the accelerated flow extends behind the building, as indicated by the white dotted line. The building wake itself, which is characterized by low velocities, extends much further behind the building.

The overview below relates the flow pattern of the different void deck geometries to what it may mean for urban planning.

DESCRIPTION OF FLOW PATTERN

VARIANT	INSIDE VOID DECK	DOWNSTREAM OF VOID DECK	AMPLIFICATION FACTOR AT CENTRE OF VOID DECK	SUGGESTIONS WITH REGARD TO URBAN PLANNING
1 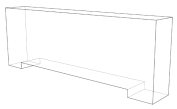	 no significant velocity gradients inside void deck (steep gradient right before entry of void deck)	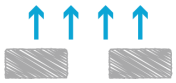 even spread of accelerated flow along length	 K › 1 => urban ventilation ↑ due to presence of building with void deck	 adjacent walking route along building
2A 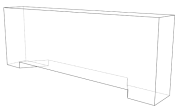	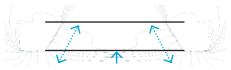 steepest velocity gradient at middle of void deck (entry); more gradual change along edges of void deck walls	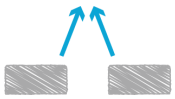 funnel-shaped area of accelerated flow	 K › 1 => urban ventilation ↑ due to presence of building with void deck	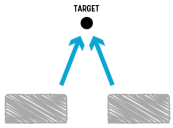 direct accelerated flow towards target
2B 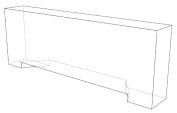	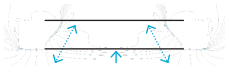 steepest velocity gradient at middle of void deck (entry); more gradual change along edges of void deck walls	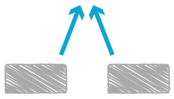 funnel-shaped area of accelerated flow	 K › 1 => urban ventilation ↑ due to presence of building with void deck	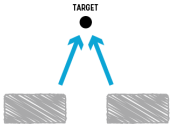 direct accelerated flow towards target
3A 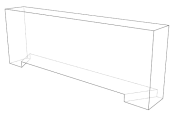	 largest velocity gradients at edges of void deck walls (also steep gradient right before entry of void deck)	 even spread of accelerated flow along length	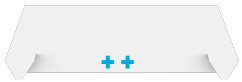 K › 1 => urban ventilation ↑ due to presence of building with void deck	 adjacent walking route along building
3B 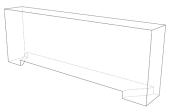	 largest velocity gradients at edges of void deck walls (also steep gradient right before entry of void deck)	 even spread of accelerated flow along length	 K › 1 => urban ventilation ↑ due to presence of building with void deck	 adjacent walking route along building
4 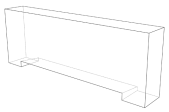	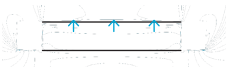 steepest velocity gradient upon flow exit from void deck	 even spread of accelerated flow along length	 K ‹ 1 => urban ventilation ↓ due to presence of building with void deck	 not suitable for microclimate enhancement inside void deck
5 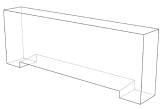	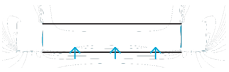 steepest velocity gradient upon flow entry in void deck	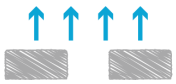 even spread of accelerated flow along length	 K › 1 => urban ventilation ↑ due to presence of building with void deck	 adjacent walking route along building
6 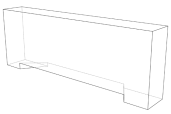	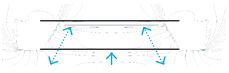 steepest velocity gradients at entry and along edges of void deck walls	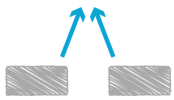 funnel-shaped area of accelerated flow	 K ‹ 1 => urban ventilation ↓ due to presence of building with void deck	 not suitable for microclimate enhancement inside void deck
7	steepest velocity gradient right before entry; inside void deck steepest along edges of void deck walls	funnel-shaped area of accelerated flow	K › 1 => urban ventilation ↑ due to presence of building with void deck	direct accelerated flow towards target
8	steepest velocity gradient upon flow exit from void deck; smaller gradient inside void deck	even spread of accelerated flow along length	K ‹ 1 => urban ventilation ↓ due to presence of building with void deck	not suitable for microclimate enhancement inside void deck
9	steepest velocity gradient upon flow entry in void deck	even spread of accelerated flow along length	K › 1 => urban ventilation ↑ due to presence of building with void deck	adjacent walking route along building

Figure 6.37: description of flow pattern

6.3.2 Urban Case – Current Situation

The results for U at pedestrian level clearly show an increase in the mean wind speed inside and downstream of the void decks. This wind-induced effect is more pronounced at some void decks than at others. Interestingly, especially the small void deck elements, such as the columns inside the void decks, create narrow streams of increased wind speeds downstream of the void decks.

Apart from the magnitude of U, the void decks also clearly impact the direction of the urban flow. From the results, it can be observed that the void decks can help at guiding the flow in a particular direction (see *figure 6.38*). This is an interesting observation with regard to urban planning as it means one can 'craft' the geometry of the void deck elements such that the flow will be directed towards particular locations. Examples are locations with outdoor functions which demand a higher wind speed to stimulate the convective surface heat transfer from the body, such as functions involving an intense activity level (e.g. sports fields, cycling and running trails). This also gives architects the opportunity to experiment with the architectural shape of the wind-inducing and wind-guiding void deck features.

Other than the void decks, the – more recently built – complex-shaped hybrid blocks highly impact the direction of the flow as well, leading to a swirling-pattern. While the void decks clearly guide the flow into one particular direction, the hybrid blocks seem to 'confuse' the wind direction through enhanced flow mixing. The orientation and configuration of these blocks with respect to one another are leading factors for the flow pattern around these hybrid buildings.

Figure 6.38: influence of void decks on magnitude and direction of U (shown for prevailing wind from North – U at pedestrian level (z = +3.75m))

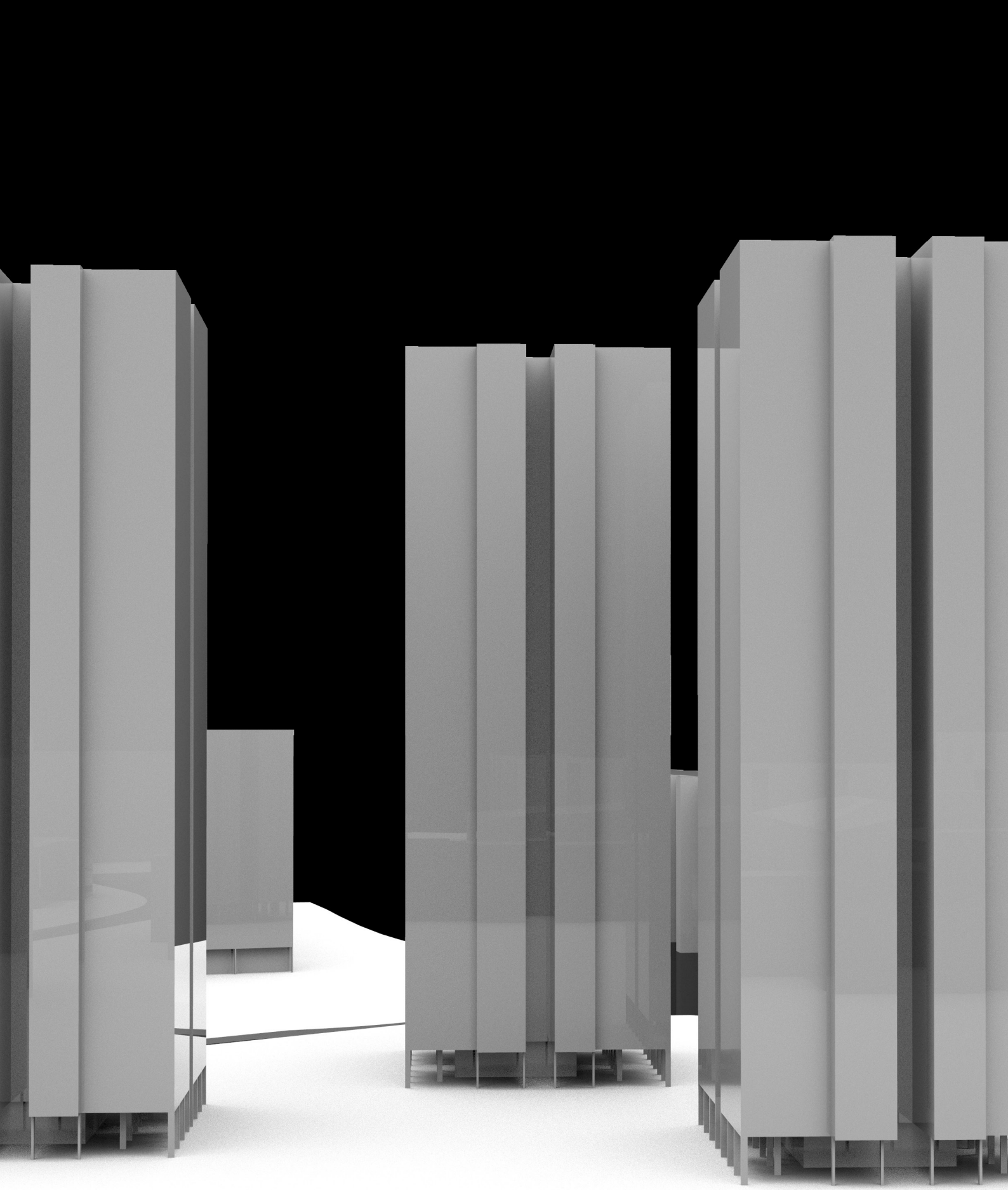

07

COMFORT ASSESSMENT

In this chapter, the simulated wind climate will be mapped onto the current urban activity pattern in the study area. An assessment of the outdoor thermal and pedestrian wind comfort will then be done in relation to this current activity pattern.

7.1 Current Activity Pattern

To assess the potential application of void deck wind strategies, an inventory of the main types of outdoor activities in the study area was completed and shown in the map below (*figure 7.1*). The outdoor functions were categorized, taking into account the different comfort requirements. For example, a running and cycling trail will impose more stringent thermal comfort, and less stringent wind comfort, requirements than the more stationary activities, such as frequent and occasional sitting.

As can be seen on the map, the void decks are mostly used for outdoor occasional sitting, with a nice spread of playgrounds, sports fields and outdoor gyms in between the buildings. The number of locations characterized as frequent outdoor seating area (such as outdoor cafés and restaurants) is limited in this residential area. The public transport transits (e.g. bus and MRT) were also marked on the map as these widely-used amenities in Singapore can be considered as zones where walking and occasional sitting are common.

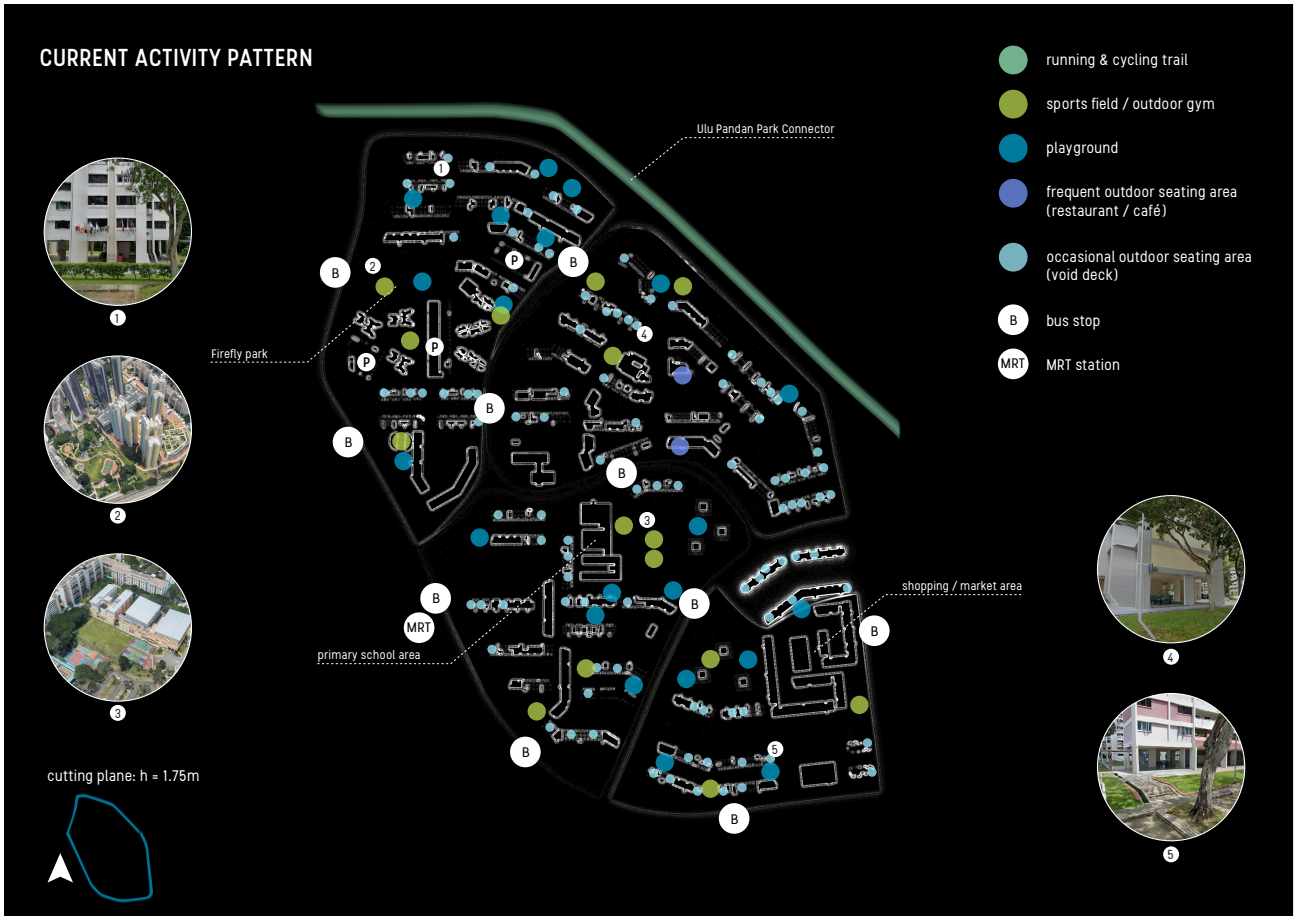

Figure 7.1: map with current outdoor activities in study area

7.2 Thermal Comfort Assessment

The thermal comfort assessment for this case is performed based on the empirical Temperature-Humidity Index THI since this index was specifically developed for warm-humid regions and the required parameters can be obtained using the simpleTFoam solver in OpenFOAM. However, the thermal discomfort threshold is adapted to take the increased tolerance as a result of acclimatization and adaptive behaviour into account, being therefore raised to 31°C following Lee et al.'s (as cited in Heng & Chow, 2019) recommendation. The resulting adapted THI classification used for the assessment is shown below (*table 7.1*).

THI range	perceived comfort
21˚C ≤ THI ≤ 24˚C	comfortable for vast majority of people
24˚C < THI ≤ 31˚C	acceptable for most people
THI > 31˚C	uncomfortably hot

Table 7.1: THI comfort limits (calibrated to Singapore's local context)

Using the empirical formula for THI developed by Emmanuel (2005), the obtained temperature results for the urban case can be assessed against these THI comfort classes.

$$THI = 0.8 * T_a + \frac{RH * T_a}{500} \qquad [°C] \qquad (7.1)$$

with

T_a = air temperature [°C]
RH = relative humidity [%]

The average yearly relative humidity of 83.9% (Meteorological Service Singapore, 2019 – *see Climate Analysis section 3.1*) is used as it was explained earlier that no significant differences occur between the different months.

A contour plot is generated based on the THI classes as follows:

- THI class 1 (locations where the vast majority of people feel thermally comfortable):
  $T_a \leq 24.8°C = 297.8K$
- THI class 2 (locations which are thermally acceptable to most people):
  $24.8°C = 297.8K < T_a \leq 32.0°C = 305.0K$
- THI class 3 (locations which are perceived as uncomfortably hot to the vast majority):
  $T_a > 32.0°C = 305.0K$

Wind from Prevailing Wind Direction N

Since all the air temperatures sampled at pedestrian height are higher than 297.8K, the category of people feeling 'thermally comfortable' is not represented here. The remaining question is thus whether people would perceive the outdoor environment as 'thermally acceptable' or not. Those areas which would be perceived as thermally acceptable to the majority of people are marked by the white contours below. These are mostly located in the vicinity of the complex-shaped buildings. Although the terrain vegetation clearly has a big influence on the occurring air temperatures at pedestrian height, the study area is still perceived as uncomfortably hot by most people for the simulated time.

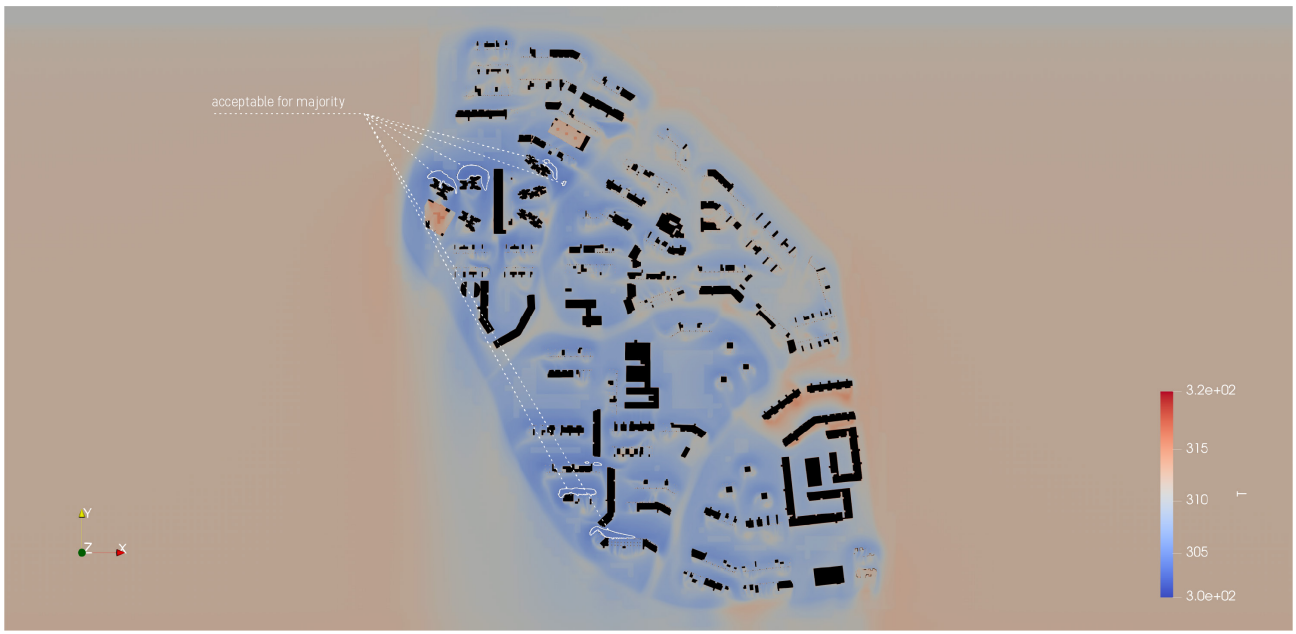

Figure 7.2: wind from N – highlighted areas with white contour [297.8 K ‹ T_a ≤ 305.0 K] => thermally acceptable for most people; all other areas uncomfortably hot

Wind from Prevailing Wind Direction NNE

The case with wind from North-Northeast shows a similar conclusion: the few thermally acceptable areas are situated around the hybrid towers. The convective heat transfer, and thus the resulting air temperature field, are clearly impacted by the complex shape of these towers. The thermally acceptable region around the most upstream-located of these hybrid towers (for the case with wind from NNE) has now become about six times as large while the other thermally comfortable areas have reduced in size compared to the case with wind from North.

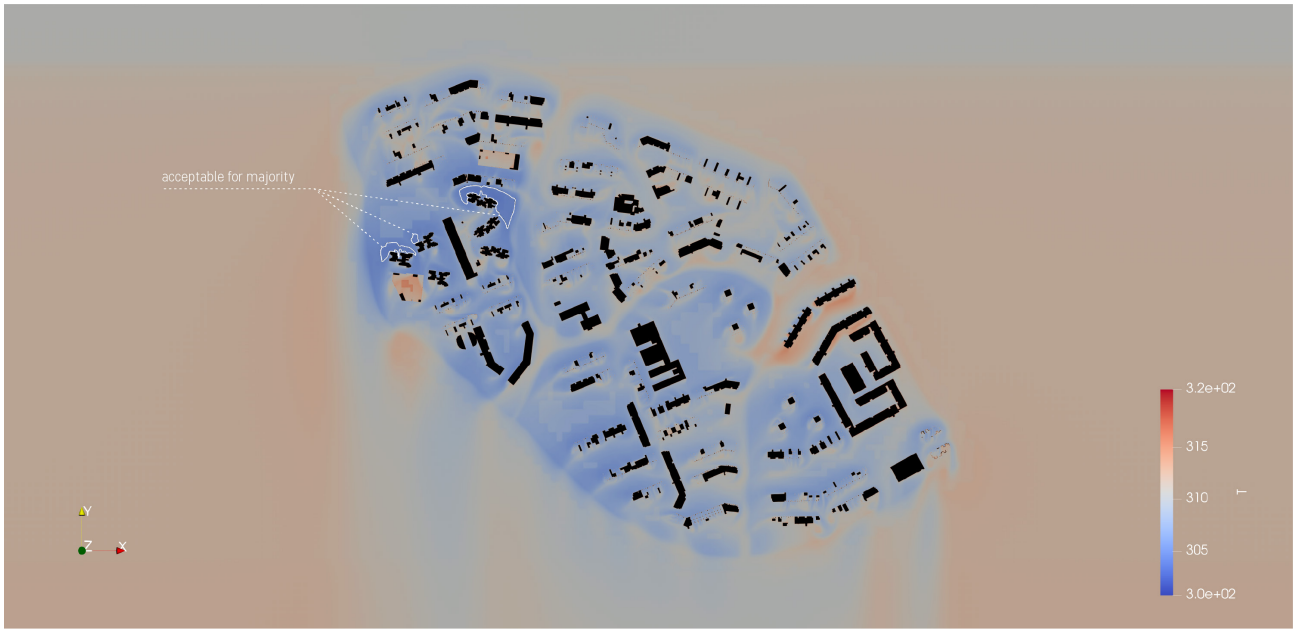

Figure 7.3: wind from NNE – highlighted areas with white contour [297.8 K ‹ T_a ≤ 305.0 K] => thermally acceptable for most people; all other areas uncomfortably hot

Wind from Prevailing Wind Direction S

The case with wind from South does not show any thermally acceptable areas around the hybrid towers. Only a few small areas at the downstream edge of the study area are marked as having thermally acceptable conditions.

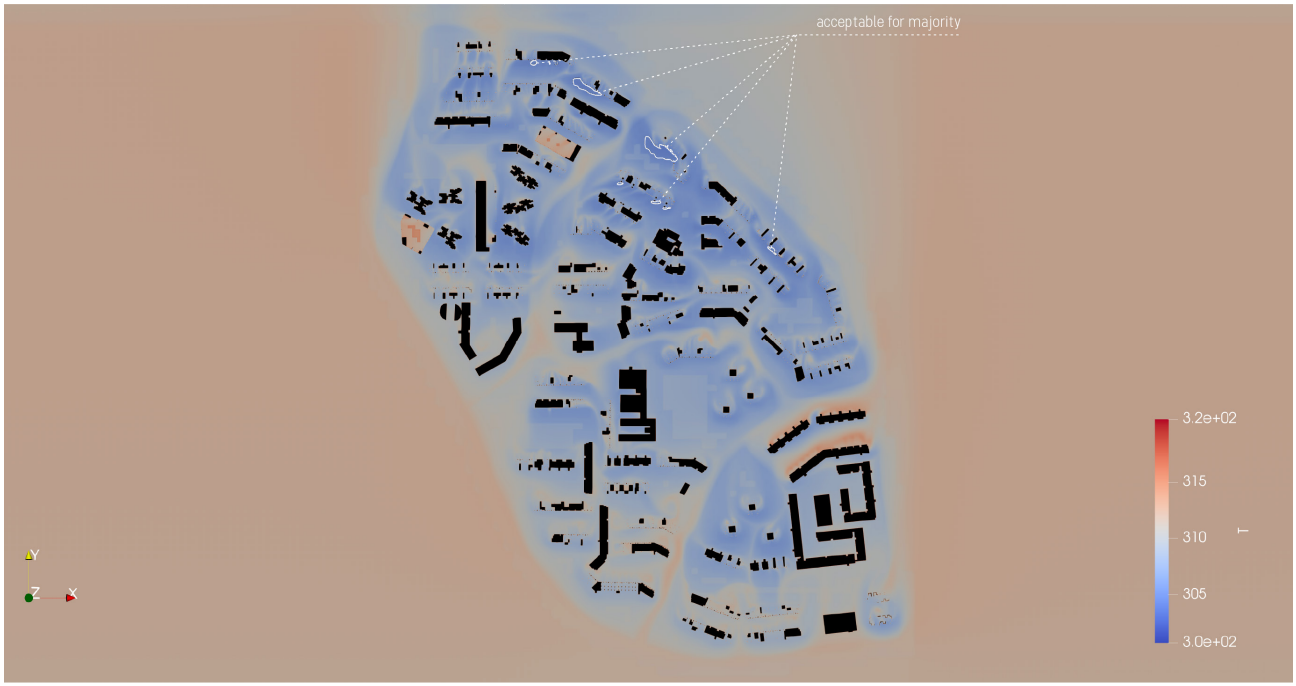

Figure 7.4: wind from S – highlighted areas with white contour [297.8 K ‹ T_a ≤ 305.0 K] => thermally acceptable for most people; all other areas uncomfortably hot

All the simulations showed that the air temperatures above the vegetated terrain are lower than those above the surrounding paved areas as a result of convection over these lower-temperature surfaces. Next to the terrain vegetation, the void decks also lead to a cooling effect. This becomes clearer when a larger number of temperature contours is plotted, as shown below for the case with prevailing wind from North-Northeast. Ten contour lines are spaced linearly over the total temperature range of 19.9K.

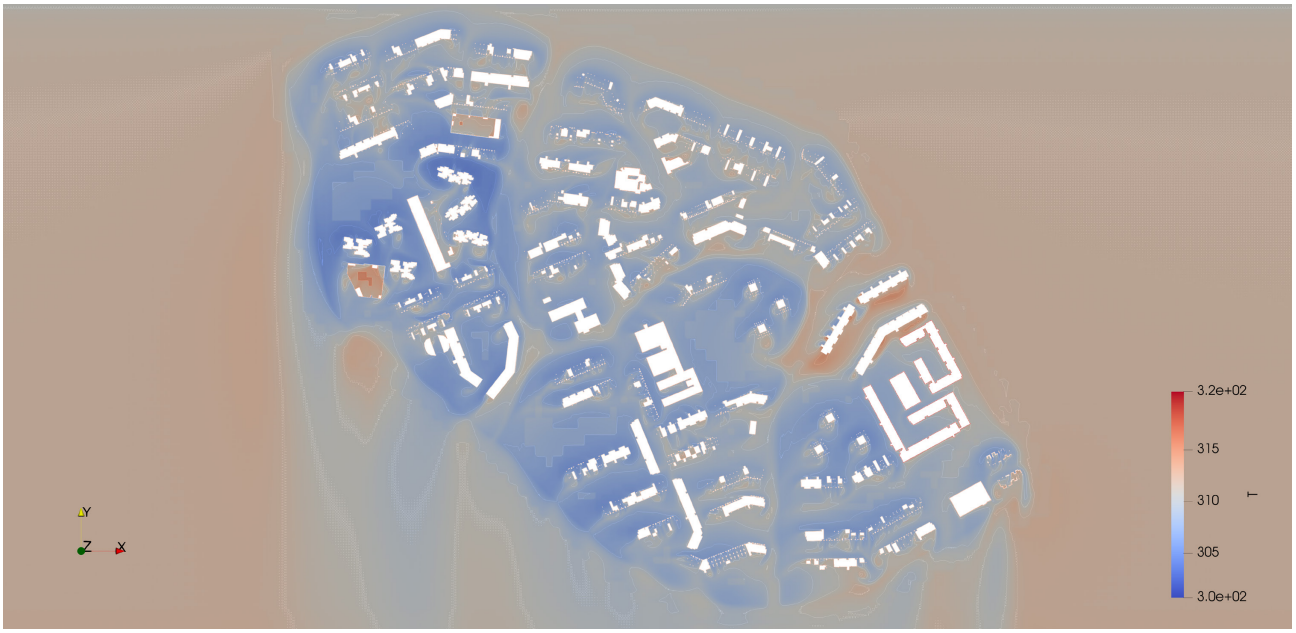

Figure 7.5: temperature contours around buildings

One can observe lower-temperature contours around the buildings. Zooming in on the void decks, the cooling effect becomes more apparent, with low-temperature contours following the void deck openings *(figure 7.6)*.

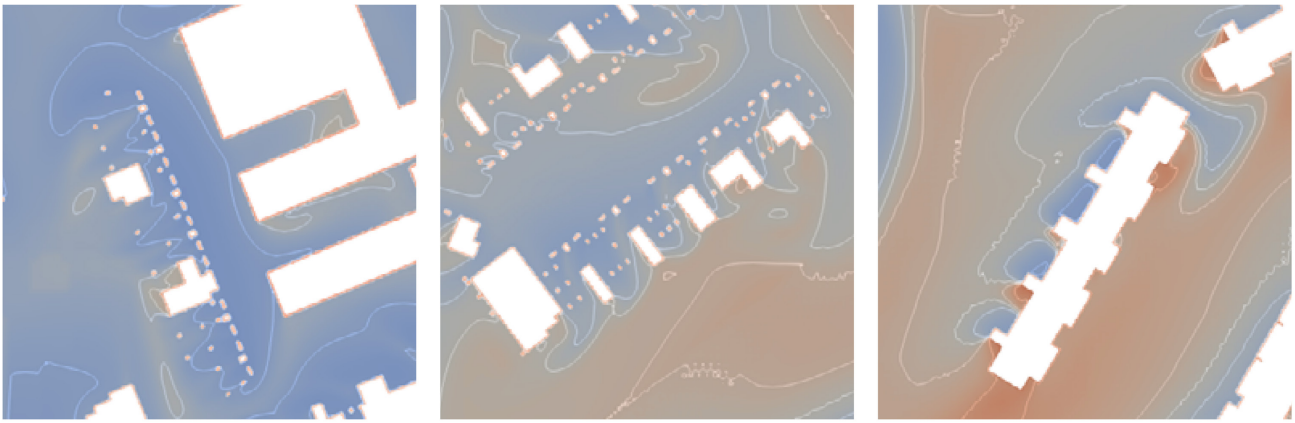

Figure 7.6: temperature contours zoomed – cooling effect of void deck openings (corresponds to colorbar figure 7.5)

7.3 Pedestrian Wind Comfort Assessment

As mentioned in *section 3.6.2*, the urban-case results for U will be assessed against the wind comfort criteria developed by the city of London and RWDI as these provide an elaborate distinction between various outdoor functions.

category	mean & GEM wind speed	max. exceedance probability	description of (dis)comfort category
frequent sitting	2.5 m/s	5%	acceptable for frequent outdoor sitting use, e.g. restaurant, café
occasional sitting	4 m/s	5%	acceptable for occasional outdoor seating, e.g. general public outdoor spaces, balconies and terraces intended for occasional use
standing	6 m/s	5%	acceptable for entrances, bus stops, covered walkways or passageways beneath buildings
walking	8 m/s	5%	acceptable for external pavements, walkways
uncomfortable	> 8 m/s	5%	not comfortable for regular pedestrian access
unsafe	15 m/s	0.022%	unsafe wind conditions for both pedestrians and cyclists

*Table 7.2: wind comfort criteria used in the urban case assessment. Adapted from **Wind microclimate guidelines for developments in the city of London**, by City of London Corporation, 2019.*

The contour plots for pedestrian wind comfort based on the abovementioned criteria are shown below for prevailing wind from North, North-Northeast and South respectively. The average Northeast Monsoon wind speed used as the reference inlet speed is higher than that of the Southwest Monsoon (2.6 m/s vs. 2.2 m/s), but the upstream aerodynamic roughness length of the former cases is significantly higher than that of the latter case. Evidently, this impacts the steepness of the wind profile at the inlet. It is therefore important to simulate all three to determine which one is more critical in terms of pedestrian wind comfort.

Wind from Prevailing Wind Direction N

The highlighted areas in *figure 7.7* below are those which exceed certain thresholds for pedestrian wind comfort and are therefore not suitable for all outdoor activities. The areas marked by a white contour lie within the range of 2.5 m/s to 4.0 m/s and are thus acceptable for occasional outdoor sitting, standing and walking, but not for frequent outdoor sitting. There is one location (in between two tall hybrid towers; marked by the red contour line) at which the threshold of 4.0 m/s is exceeded. At this location, outdoor sitting (both frequent and occasional) is thus not recommended at all. As could be seen from the current activity map, a sports field and outdoor gym are located just upstream of and in between the towers. As higher wind speeds are tolerable, and lower temperatures are desirable, for more active types of activities, there are no major problems in this case. No seating areas (e.g. benches) are placed here. All other areas are comfortable for each of the assessed outdoor activities (frequent and occasional outdoor sitting, standing, walking, cycling).

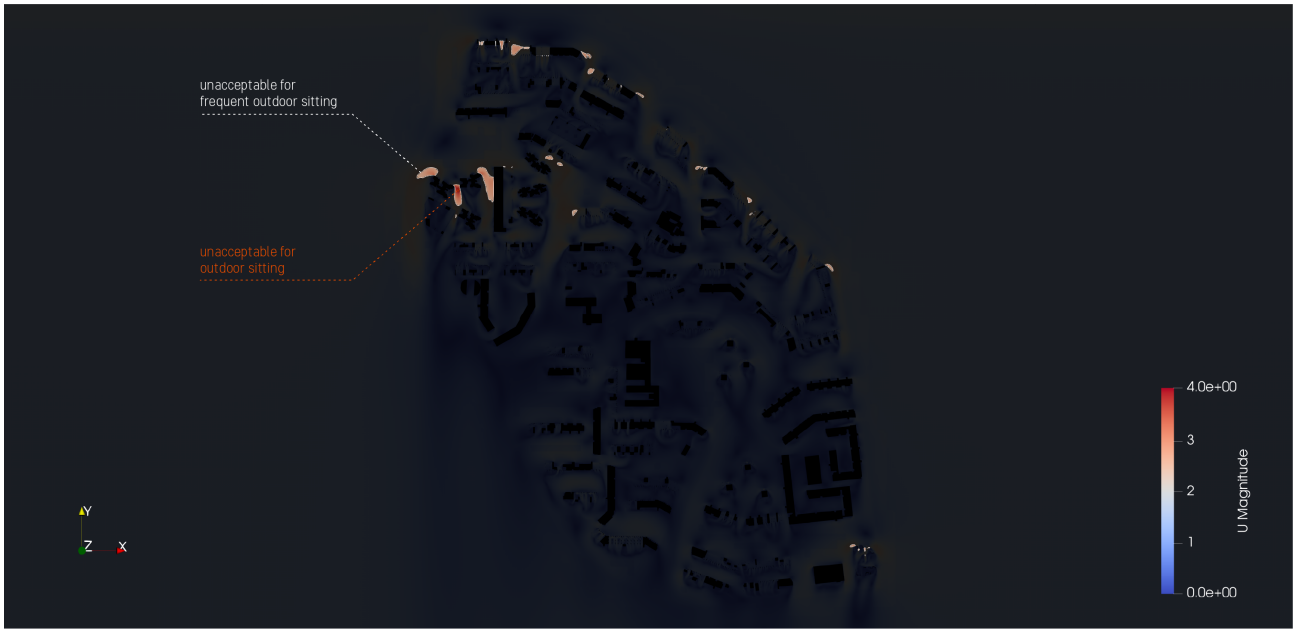

Figure 7.7: wind from N – highlighted areas with white contour [2.5 m/s ‹ U ≤ 4.0 m/s] => not acceptable for frequent outdoor sitting; highlighted area with red contour [4.0 m/s ‹ U ≤ 6.0 m/s] => not acceptable for outdoor sitting

Wind from Prevailing Wind Direction NNE

For the case with wind from North-Northeast, the pedestrian wind conditions are overall suitable for each of the assessed outdoor activities, except for the few locations marked below which are unsuitable for frequent outdoor sitting. These are mostly located around the hybrid towers and at the upstream edge of the study area.

Figure 7.8: wind from NNE – highlighted areas [2.5 m/s ‹ U ≤ 4.0 m/s] =› not acceptable for frequent outdoor sitting

Wind from Prevailing Wind Direction S

For the case with an approaching flow from the South (Southwest Monsoon), the velocity results at pedestrian height were all below 2.5 m/s. Hence, no pedestrian wind discomfort problems are expected to occur in the study area under these conditions and all of the assessed outdoor activities can be performed. As such, no pedestrian discomfort plot is to be displayed here.

The fact that the overall pedestrian wind comfort in the current situation is very good while there are very few locations with thermally acceptable conditions indicates that there is still a lot of room for wind velocity-inducing measures for the void decks. In other words, for the urban-scale intervention more focus can be put on the application of void deck geometries which lead to an increase in wind speed inside and around the void decks, rather than on those which slow down the airflow. Occasional outdoor sitting and walking, which are the two outdoor activity comfort classes mostly related to void deck usage, do not show any problems related to wind comfort in the study area. In fact, the pedestrian comfort assessment shows that almost all locations in the study area are suitable for each of the assessed outdoor activities. In terms of urban planning, this leaves a lot of opportunities for the planning of future developments and outdoor functions. It should be noted, however, that the pedestrian wind comfort does not necessarily need to achieve the highest level for all activities. In fact, that would limit the potential enhancement of the outdoor thermal comfort in the area.

It is the combination of pedestrian wind comfort and thermal comfort which defines how comfortable the wind microclimate in a particular location is. The next chapter will deal with the comfort level of the study area based on the combined assessment of the outdoor thermal and pedestrian wind conditions, indicating the mismatch between both.

Since the simulations were only performed for the three prevailing wind directions during the monsoon seasons, no extensive 16-direction comfort evaluation for an entire year based on the Weibull probability distribution was performed. Besides, there was a lack of available hourly wind statistics to determine the required Weibull parameters per wind direction. However, the ultimate goal of this research is not to carry out a comfort evaluation for the whole year in the area, but to analyse what effect different void deck geometries would have on the wind speed and temperature distributions and thus on the thermal and pedestrian wind comfort for various activities in the area. For this purpose, it was sufficient to perform the steady-state simulation for the same instance using the same input settings but with the different geometries. A comparison could then be made between the flow pattern in the current situation and that after making changes to the void decks of the buildings, which is elaborated on in the following chapters.

7.4 Identification of Mismatch Locations

The current case with prevailing wind from the South showed no locations with pedestrian wind discomfort. The cases with the other two prevailing wind directions both showed some locations with pedestrian wind discomfort. All three cases showed outdoor thermal discomfort. The mismatch locations, which are characterized by a good pedestrian wind comfort and a bad thermal comfort or vice versa due to the negative correlation between the occurring wind speeds and the sampled air temperatures, are shown in the images below. The discomfort locations are here defined as those which fall under THI class 3 (THI › 31°C, perceived as uncomfortably hot to most people in Singapore) and/or those where pedestrian wind discomfort occurs for one or more of the assessed outdoor activities.

In the following plots, the discomfort and comfort locations are marked in colour and projected on the grayscale results plane of U and T.

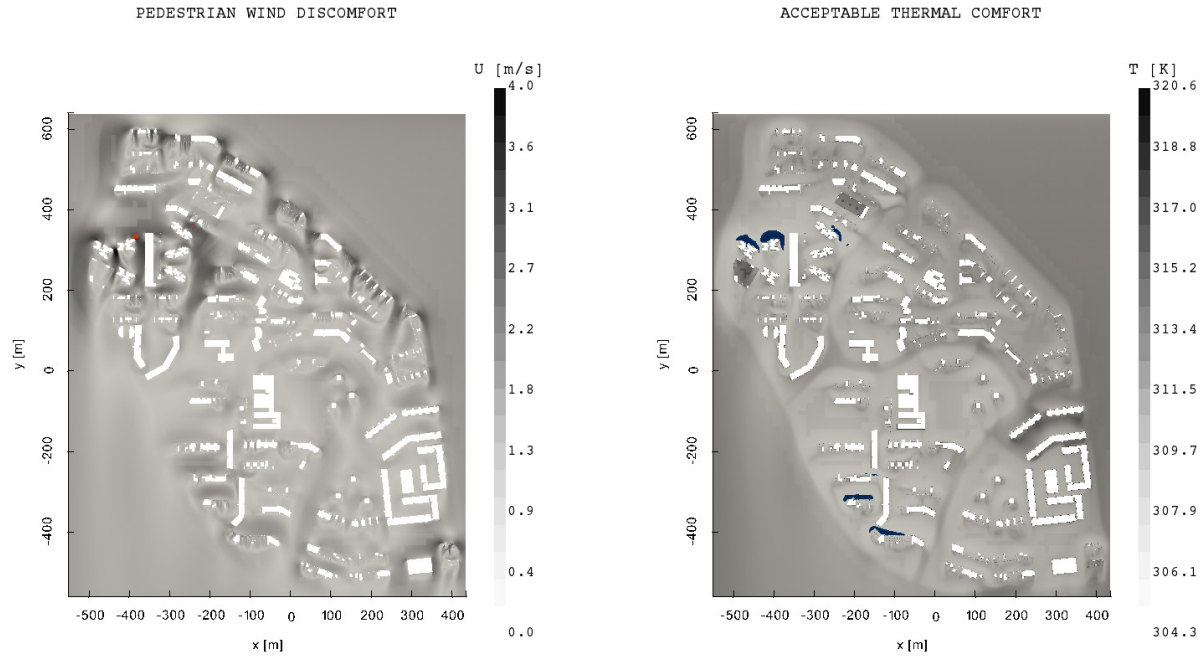

Figure 7.9: wind from N – pedestrian wind discomfort (discomfort locations marked in red) vs. acceptable thermal comfort (acceptable comfort locations marked in blue)

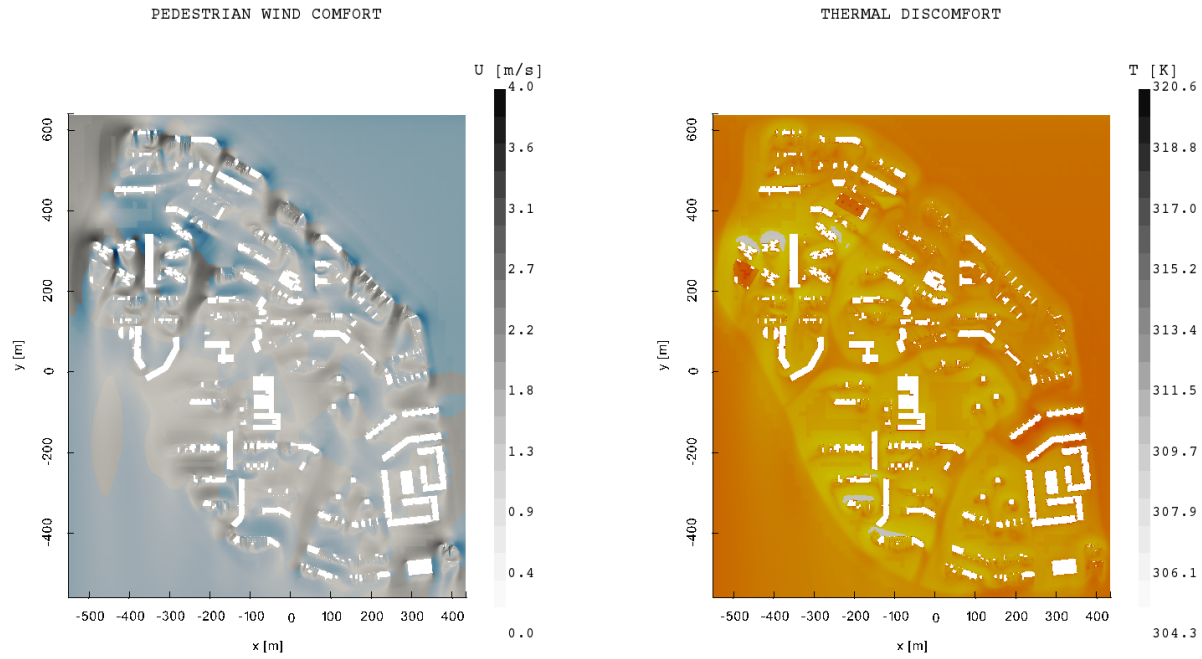

Figure 7.10: wind from N – pedestrian wind comfort (comfort locations marked in blue vs. thermal discomfort (discomfort locations marked in orange)

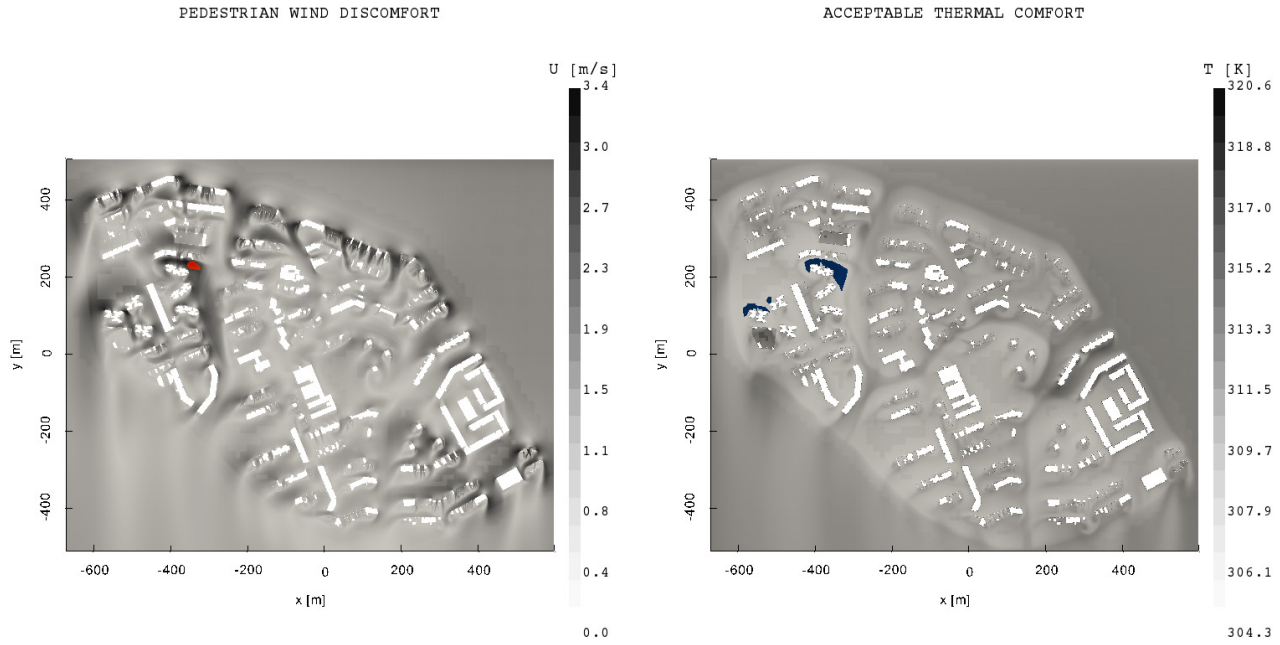

Figure 7.11: wind from NNE – pedestrian wind discomfort (discomfort locations marked in red) vs. acceptable thermal comfort (acceptable comfort locations marked in blue)

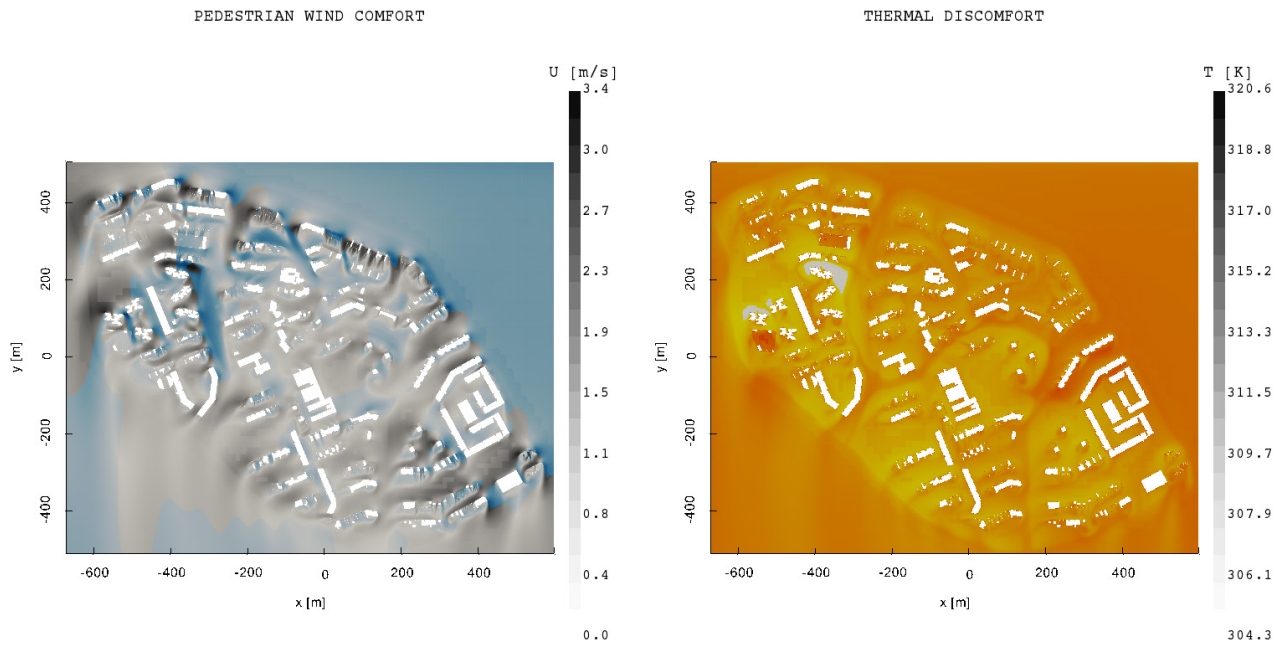

Figure 7.12: wind from NNE – pedestrian wind comfort (comfort locations marked in blue) vs. thermal discomfort (discomfort locations marked in orange)

The mismatch is clearly portrayed in the plots. This marks the importance to perform these types of wind microclimate analyses in a tropical environment as Singapore, taking into account both the pedestrian comfort and thermal comfort effects of the wind.

08

INTERVENTION

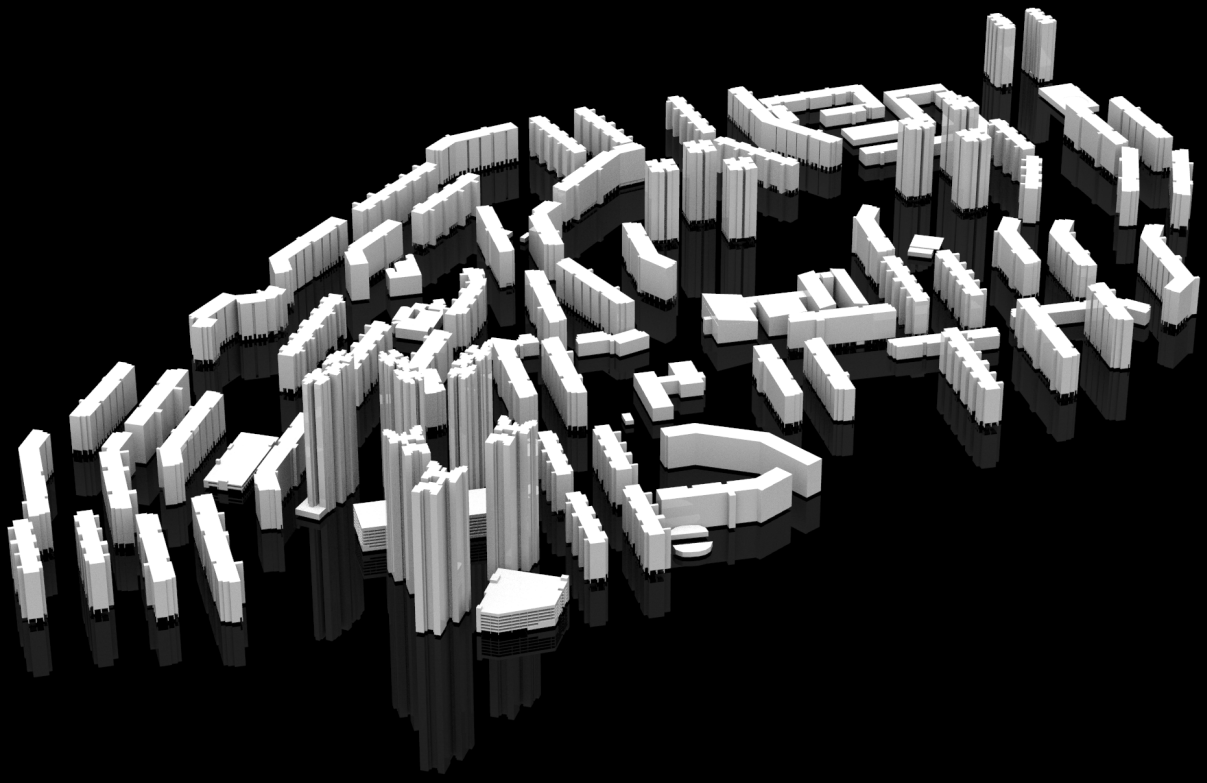

While the simulations of the current situation showed thermal discomfort for all of the analysed prevailing wind directions, the case with approaching flow from the North was most critical in terms of pedestrian wind comfort. These wind conditions are thus governing for the post-intervention flow assessment, so the simulations with modified void decks were performed with an approaching flow from the North. In this regard, the most interesting building groups for the intervention are those with a void deck facing this wind direction.

The first step was to select a void deck geometry based on the parametric geometry study performed on a single building (*section 5.2*). Those geometries which led to the highest amplification factor in the void deck are most interesting for the intervention because they are the best-case scenario in terms of thermal comfort and the worst-case scenario in terms of pedestrian comfort, which is not a concern for the current study. Thus, by going for the most 'extreme', i.e. the most speed-amplifying, void deck option, a better idea can be obtained of how and to which extent the void decks would affect the imbalance between the thermal and pedestrian comfort in the area. The highest amplification factors were obtained for the vertically diverging void decks:

- variant 5: vertically diverging void deck
- variant 7: horizontally converging and vertically diverging void deck
- variant 9: horizontally and vertically diverging void deck

Since variant 7 leads to a funnel-shaped area of amplified speed, it is more suitable in cases where the aim is to improve the wind conditions at one particular location instead of at a district scale.

A comparative study of variant 5 and 9 was subsequently carried out. In order to get a good coverage of the entire void deck, a total of 75 probes were placed at pedestrian height and the amplification factors were calculated at each location based on the sampled wind speed results. This is shown in *figure 8.1* (inflow edge at y=0). Overall, one can observe a similar pattern, namely with the highest amplification factors at the inflow edge and reducing towards the higher (vertically diverged) outflow edge.

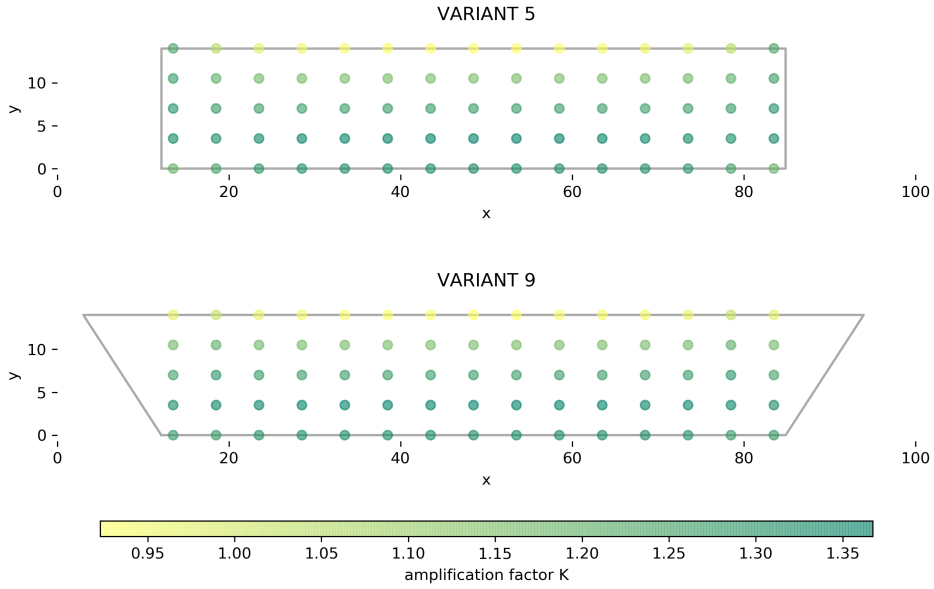

Figure 8.1: computed amplification factors at 75 probes (at 1.75m height) in void deck variant 5 and 9

By overlaying them and computing the difference, more insight can be gained. The probes marked in green in the void deck plan view below are those where the amplification factor of variant 5 (sampled at pedestrian height) is larger than that of variant 9, while the red ones are the locations where variant 9 led to a higher value. Note that the two triangular areas at both sides of variant 9 (which diverges horizontally as well), had an amplification factor K<1 (in fact, close to 0), as could be seen in *figure 6.26 (contour plots of amplification factor K at pedestrian level (1.75m height))*, meaning that the flow is not amplified there. At

most (49 out of the 75) probe locations, variant 5 leads to a higher amplification factor. The difference is most significant at the outflow corners. The centre region of the void deck, which is important in terms of the functionality of the void deck, also has a higher value for variant 5 than for variant 9. The latter, on the other hand, scores better at the inflow corners. Overall, we can conclude that void deck geometry **variant 5 leads to a more amplified pedestrian-level flow** at most locations in the void deck. This geometry variant is therefore chosen for the urban-scale void deck intervention.

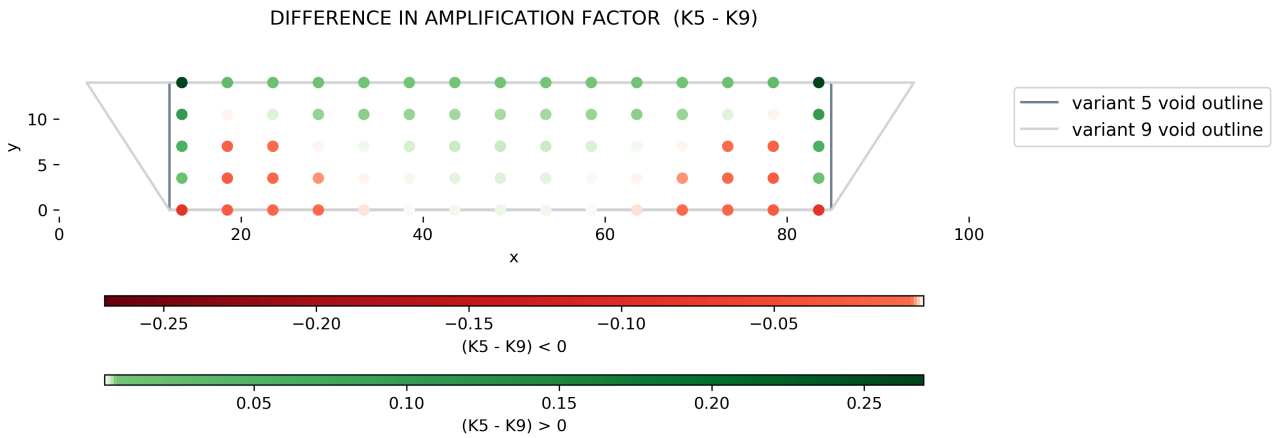

Figure 8.2: difference in amplification factors at 75 probes (at 1.75m height) in void deck variant 5 and 9. Green probes indicating highest amplification factor for variant 5 and red ones for variant 9 respectively.

Two intervention cases are analyzed with the chosen void deck geometry:

1) Modification of void decks facing N (building group 1)
2) Modification of void decks facing N and NE (building groups 1, 2 and 3)

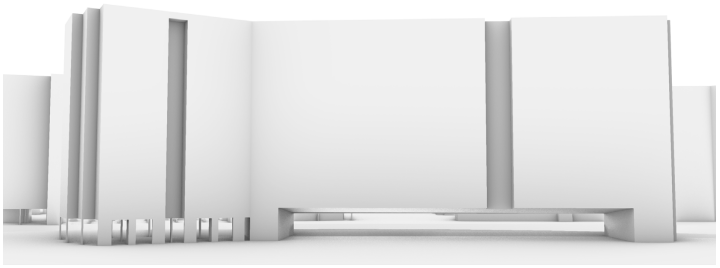

Figure 8.3: N-facing void decks modified; other oriented building parts unmodified

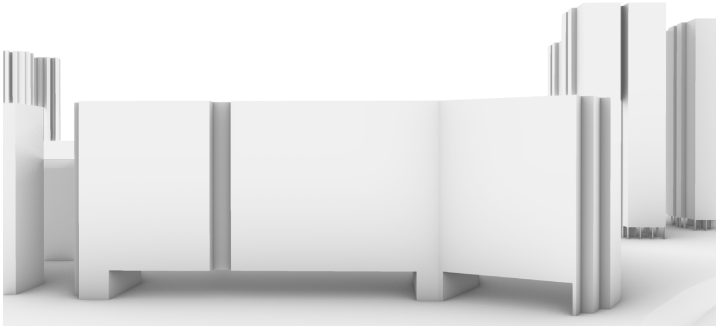

Figure 8.4: N- and NE-facing void decks modified

09

POST-INTERVENTION COMFORT ASSESSMENT

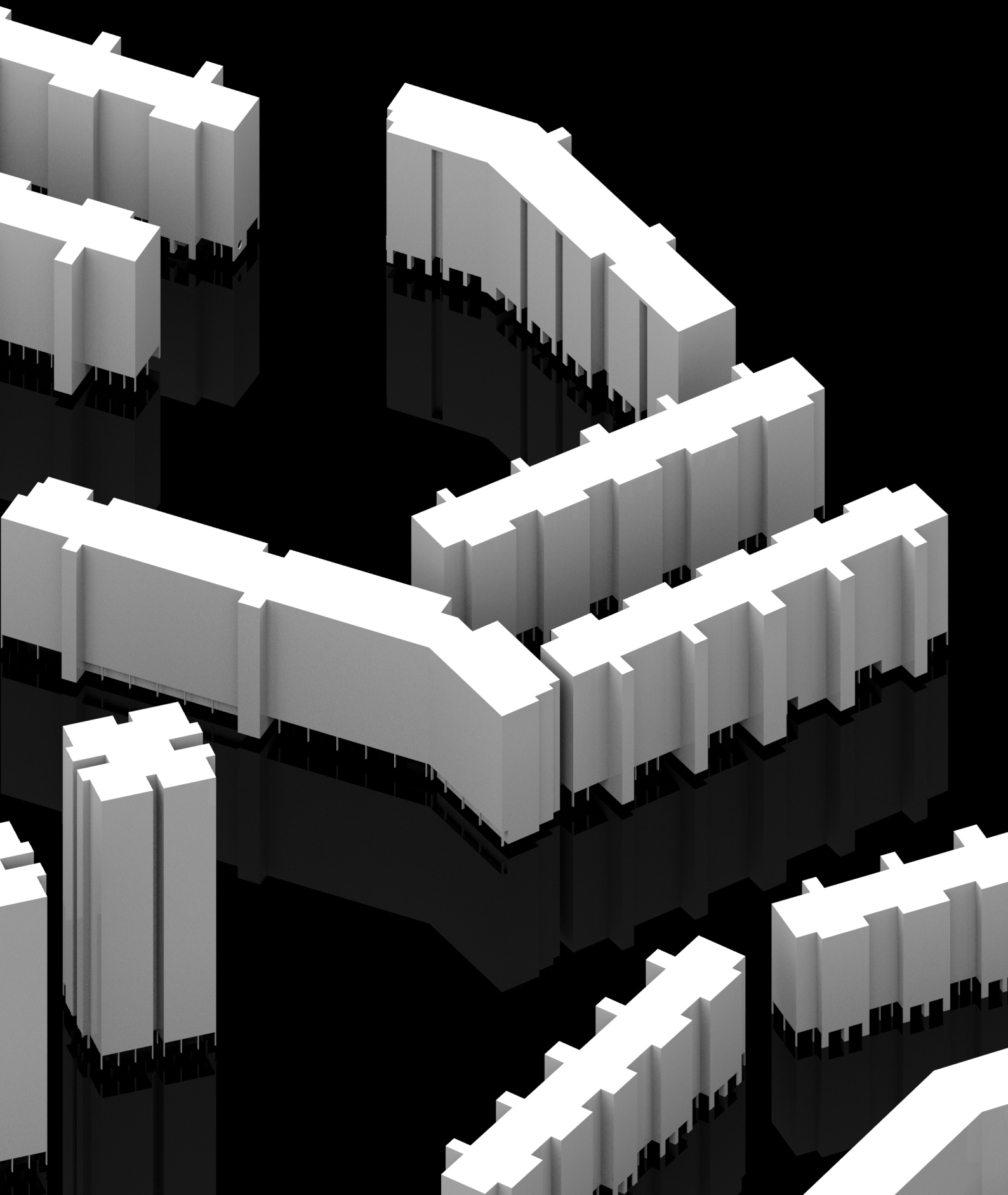

The outdoor comfort assessment based on the Temperature-Humidity Index and London's pedestrian wind comfort criteria was carried out in order to get an idea of the existing imbalance between outdoor thermal and pedestrian comfort in Clementi, Singapore, and how this might affect the outdoor activities. In this chapter, the impact of the urban-scale void deck intervention is analysed. When making a comparison before and after an urban microclimate strategy, or between different urban cooling measures, it makes more sense to express the impact in terms of the changes in U and T rather than comparing the comfort class before and after the intervention because the range between the various comfort classes is quite large. For example, the temperature difference between the THI classes is 7.2 K (or 7.2°C), which is a very large range. Needless to say, a temperature decrease of 7.2 K through a passive urban cooling measure, such as a slight change in void deck geometries, is unrealistic. It is therefore highly unlikely that the assessed area would suddenly fall under a different outdoor comfort class. However, this certainly does not mean that the impact of the urban microclimate strategy is insignificant, as will be shown in this chapter. We therefore focus on the impact of the void deck modifications on the wind speed and temperature distributions in the following section 9.1. A post-intervention assessment based on the comfort classes is still presented for reference in section 9.2 and 9.3.

9.1 Post-Intervention Urban Simulation Results

The effect of the modified void decks on the flow pattern was determined by subtracting the velocity magnitudes and temperatures of the current situation from those of the intervention cases:

$$\text{void decks effect on } T = T_{\text{modified void decks}} - T_{\text{current situation}} \quad (9.1)$$

$$\text{void decks effect on } U = U_{\text{modified void decks}} - U_{\text{current situation}} \quad (9.2)$$

Note that, to be able to compare the pre- and post-intervention results, the point/cell array data from the mesh of the current situation simulation had to be resampled onto the mesh with the modified void decks since two different meshes had been generated with snappyHexMesh due to the different geometries.
The effect of the void deck interventions on the velocity and temperature is presented below, whereby a positive value for ΔU or ΔT denotes an increase and a negative value a decrease in the locally sampled wind speed or air temperature respectively.

INTERVENTION 1: modified void decks facing wind from N

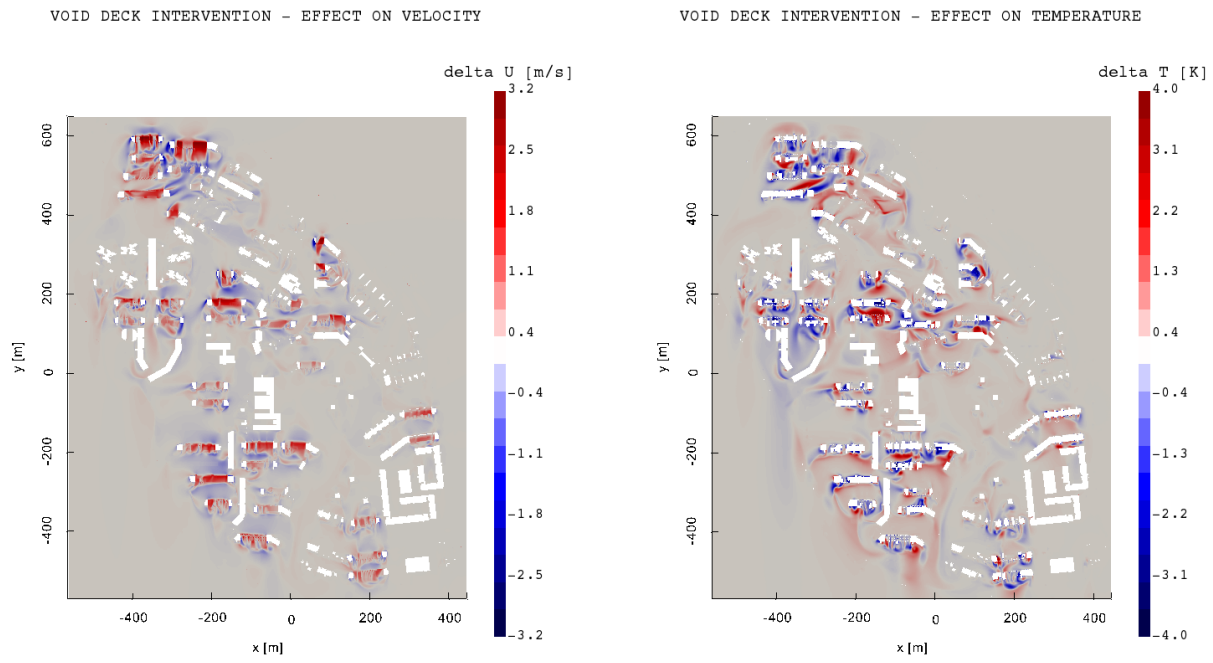

Figure 9.1: impact of void deck modifications on U and T (intervention 1: N-facing void decks modified)

INTERVENTION 2: modified void decks facing wind from N and NE

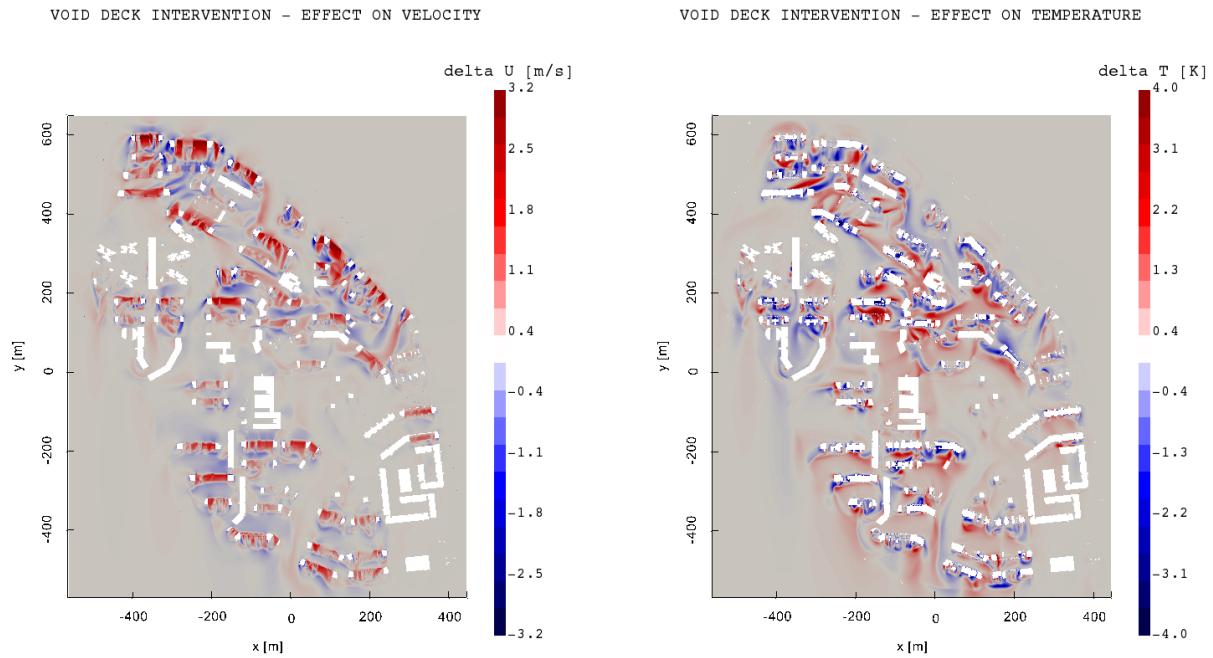

Figure 9.2: impact of void deck modifications on U and T (intervention 2: N- and NE-facing void decks modified)

The plots clearly show an effect of the modified void decks on the flow pattern. An increase in wind speed can be observed in almost all the modified void decks. The maximum observed wind speed increase is 3.2 m/s. Needless to say, this maximum difference occurs at a previously closed building volume which now has a vertically diverging void. Considering the inlet wind speed of 2.6 m/s at a reference height of 10m, this wind speed increase from 0 m/s to 3.2 m/s at pedestrian height due to the vertically diverging void deck is still notable. At some buildings we can also observe an increase in wind speed in void volumes which were already open before the intervention. Some examples are marked below (*figure 9.3*). This indicates that **the applied vertical divergence of the void deck does indeed amplify the flow speed as compared to a non-diverging void deck**, as was also observed in the void geometry study of a single building.

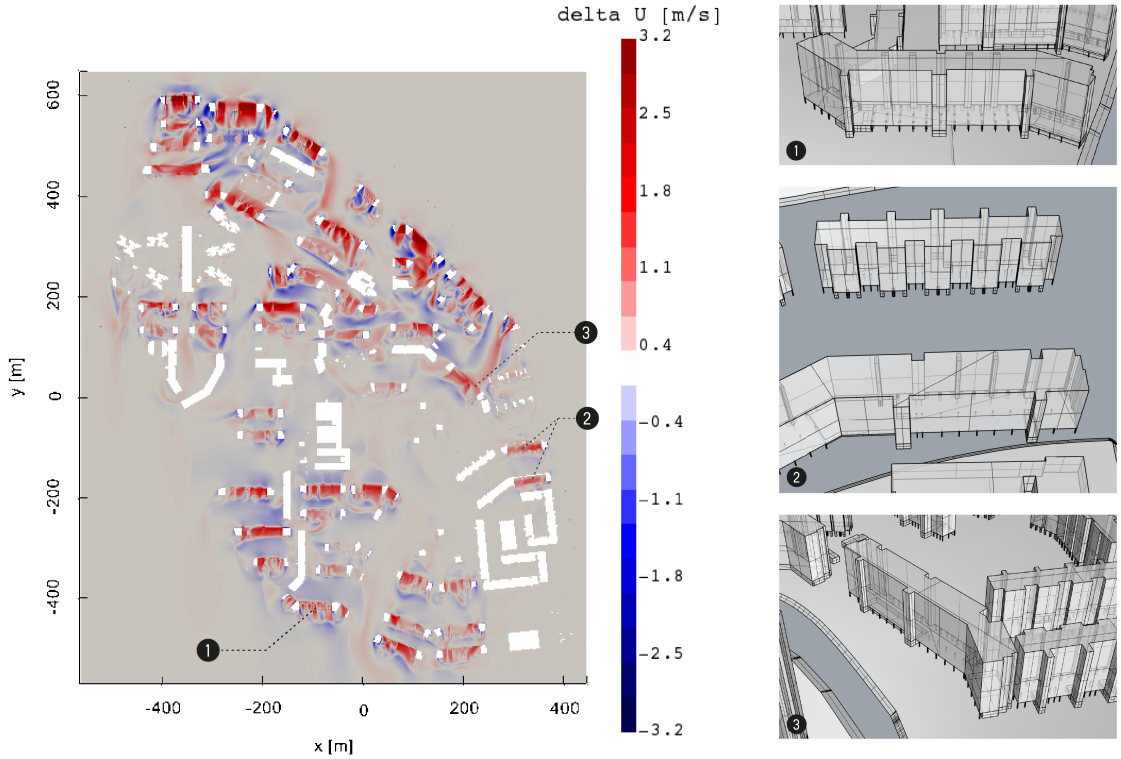

Figure 9.3: examples of U increase at some previously open volumes

The red areas in the void deck impact plots are clearly located inside the void decks and some of them extend to a certain distance downstream of the void deck. In that case, the amplified wind speeds do not only affect the microclimate inside the void deck, but can also be experienced by pedestrians walking in the street behind the building. Some light blue areas, denoting a slight decrease in wind speed, can be observed in between the buildings. The corner streams at the sides of the buildings, which are generally characterized by high wind speeds, are weakened at some locations.

The observed effects of the void deck modifications on the wind speed clearly translate into an effect on the air temperature. The modified void decks at which an increase in wind speed was observed are marked by a ΔT below zero, which indicates the cooling effect of the void deck modifications on the local air temperature. A temperature decrease exceeding 1.5K can be observed in the void decks. Apart from the void decks, the flow pattern around the buildings is altered as well. The most densely-built areas, where the distance in between the buildings is lowest, are most marked in the ΔT-plot. The temperature differences in these areas are more extreme than in others; showing alternating swirls of cooled and heated air in the wakes of the buildings. This may be attributed to the short building-to-building distance over which the thermal exchanges of the cooled air leaving the void decks and the hot surface temperatures of the buildings take place.

In order to gain some more insight in how the air temperatures were affected in the buildings which already had a void deck, the values before and after the modifications were sampled at a number of probes. The probes were placed in every void deck of the intervention case as well as in between some of the closely-packed buildings where the ΔT-plot showed some significant changes, amounting to a total of 216 probes. Since we are particularly interested in the changes in void decks which already existed before the intervention (but which were modified to a vertically divergent geometry), the probes in formerly closed volumes were filtered out. The resulting 159 probes are shown in *figure 9.4* below with their respective ΔT-value. In total, 94 probes showed a decrease, while 65 led to an increase in air temperature after the modifications. As can be seen from the plot, most of the probes which increased in temperature are, however, located in between the buildings rather than inside the void decks. Overall, the modified void deck geometries thus lead to a cooling effect at the majority of the probes.

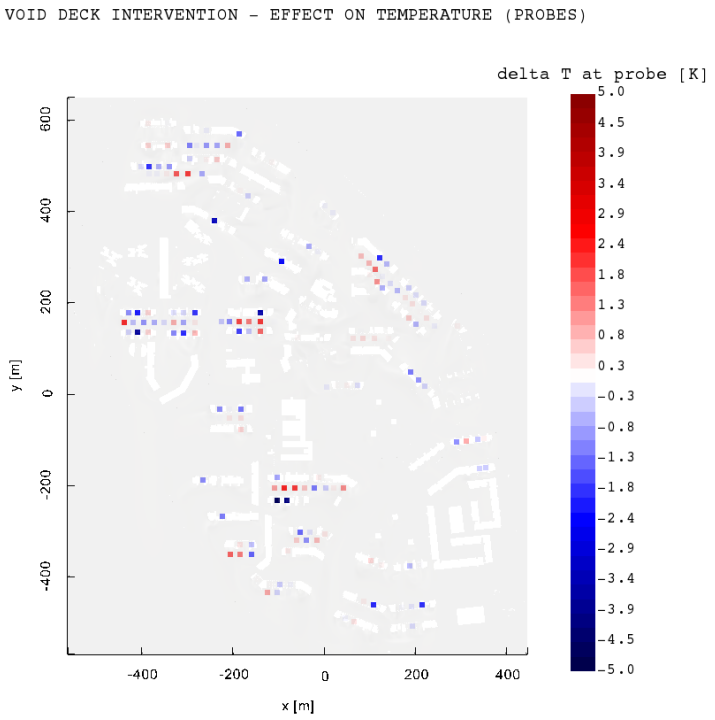

Figure 9.4: ΔT at probes after intervention 2

The north-alignment of the void decks can be expected to have a similar positive effect with an approaching flow from the south. The results show that applying the proposed geometry modifications to the buildings with a void deck facing Northeast as well (intervention 2), has a similar effect as on those facing North when simulating with an approaching flow from the North. Since the prevailing wind directions are North, South – which are on the same axis – and North-Northeast, this means that the void decks will positively affect the wind microclimate in the commonly used void deck spaces during both monsoon seasons. In order to achieve an enhanced wind microclimate inside these communal spaces all year round, it would thus be good to apply these flow-inducing void deck geometries to the building groups with void decks facing the North-South axis as well as those facing the (North-)Northeast direction.

9.2 Thermal Comfort Assessment

Despite the observed temperature differences after the intervention, the areas marked as "acceptable to the majority of people" increased only very slightly (almost negligibly) in size as compared to the existing situation. The large range between the comfort assessment classes is thus not able to capture the observed temperature effects, as was explained in the introduction of this chapter.

INTERVENTION 1: modified void decks facing wind from N

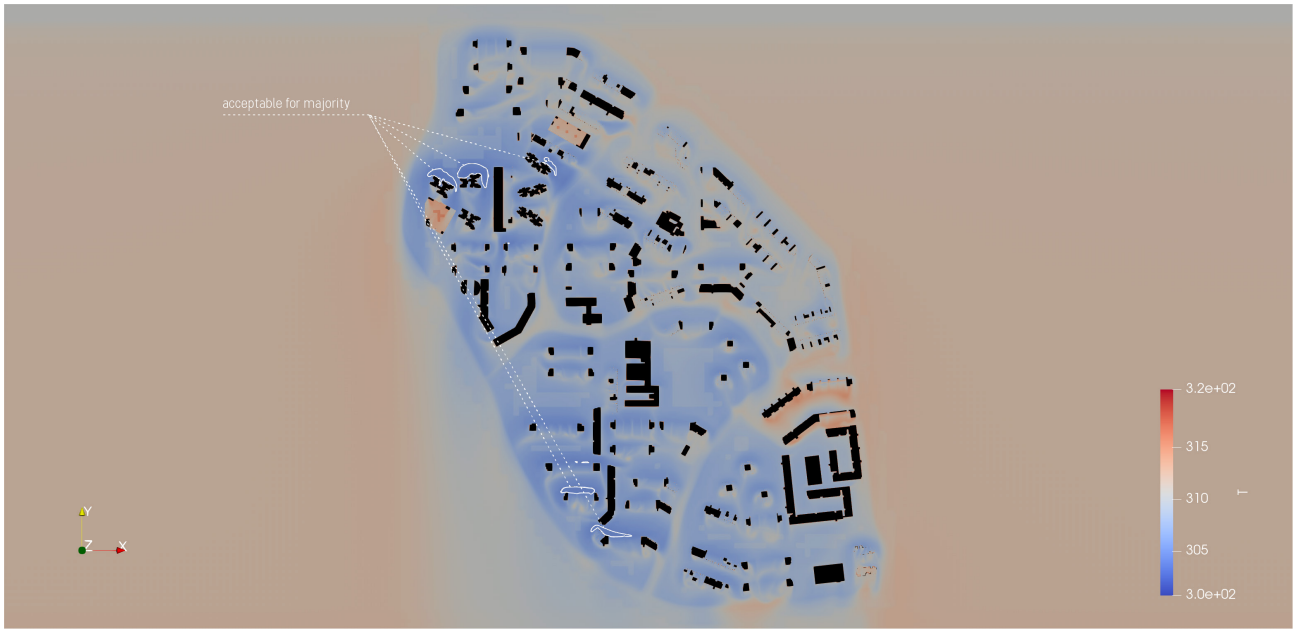

Figure 9.5: intervention case 1 – highlighted areas with white contour [297.8 K ‹ T_a ≤ 305.0 K] =› thermally acceptable for most people; all other areas uncomfortably hot (simulation with wind from N)

INTERVENTION 2: modified void decks facing wind from N and NE

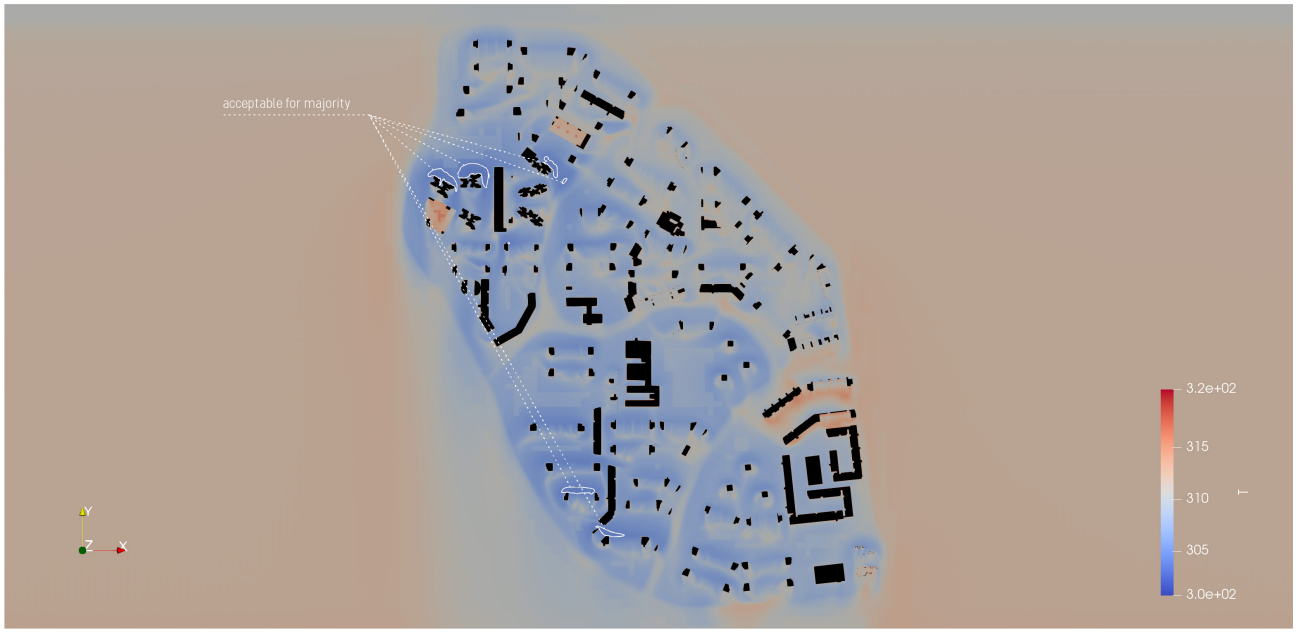

Figure 9.6: intervention case 2 – highlighted areas with white contour [297.8 K ‹ T_a ≤ 305.0 K] => thermally acceptable for most people; all other areas uncomfortably hot (simulation with wind from N)

9.3 Pedestrian Wind Comfort Assessment

Although the void deck modifications showed a clear increase in wind speeds, the assessment against the London pedestrian comfort criteria remains very similar to that of the current situation. The size of the discomfort areas has increased, although to a very limited extent. The modified void decks at the northern, and north-eastern (in case of intervention 2), inflow edge exceed the comfort threshold for frequent outdoor sitting, though no strict conclusions can be drawn about the outer building row. Overall, we can conclude that the field for U is not negatively affected by the applied void deck modifications to such an extent that it would cause pedestrian comfort problems

INTERVENTION 1: modified void decks facing wind from N

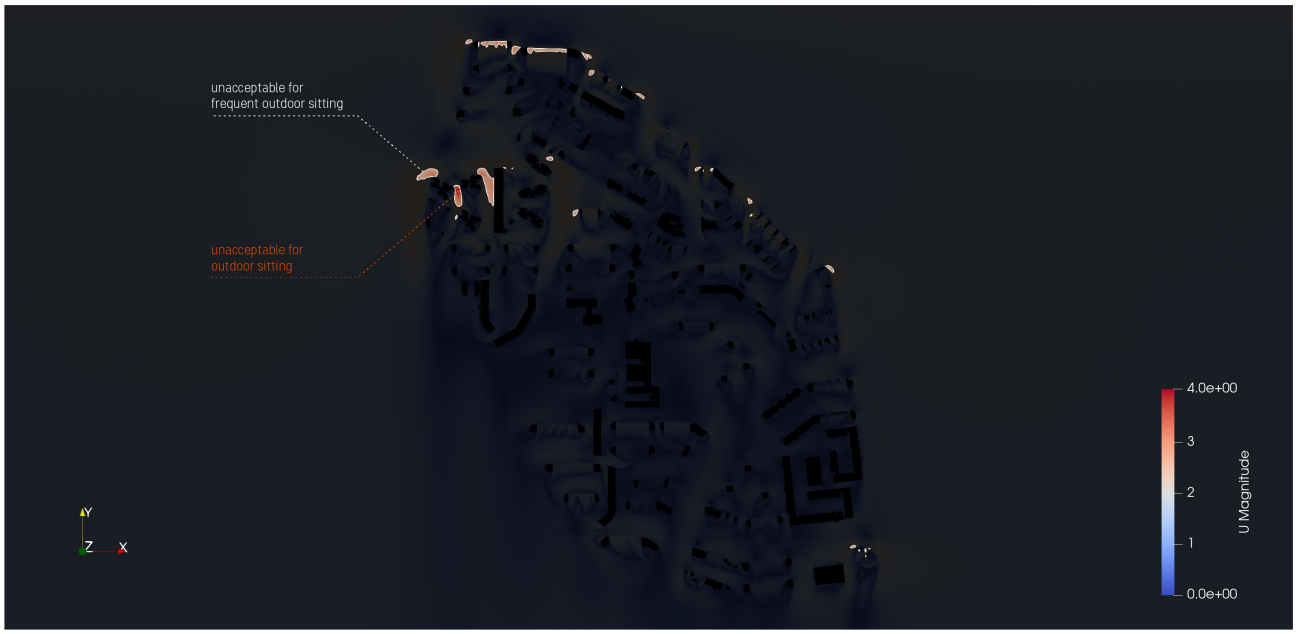

Figure 9.7: intervention case 1 – highlighted areas with white contour [2.5 m/s ‹ U ≤ 4.0 m/s] => not acceptable for frequent outdoor sitting; highlighted area with red contour [4.0 m/s ‹ U ≤ 6.0 m/s] => not acceptable for outdoor sitting (simulation with wind from N)

INTERVENTION 2: modified void decks facing wind from N and NE

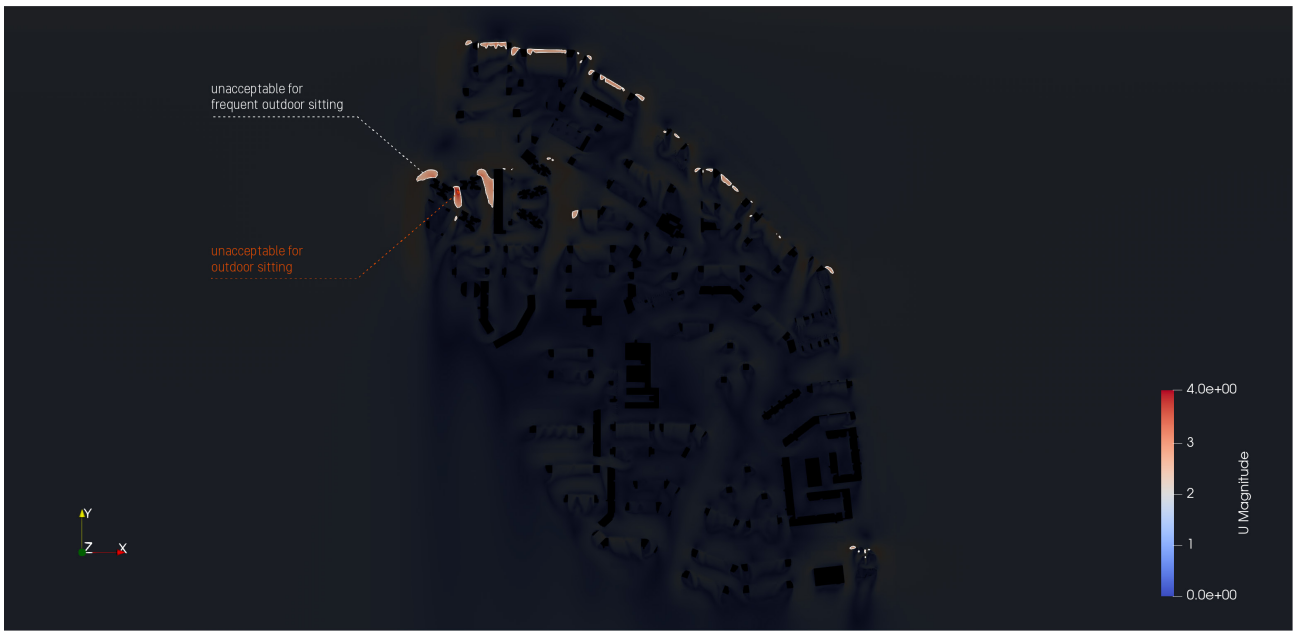

Figure 9.8: intervention case 2 – highlighted areas with white contour [2.5 m/s ‹ U ≤ 4.0 m/s] => not acceptable for frequent outdoor sitting; highlighted area with red contour [4.0 m/s ‹ U ≤ 6.0 m/s] => not acceptable for outdoor sitting (simulation with wind from N)

In conclusion, the comfort range of outdoor comfort assessments is rather large and the limits are quite high. As such, even if the wind speed and temperature differences after an intervention are clearly visible (and not insignificant), this does not directly imply that the new outdoor conditions will suddenly fall under a different comfort class. For example, the temperature difference between the THI classes is 7.2 K (or 7.2 °C), which is a very large range. Ideally, comfort classes with smaller ranges should thus be developed to be able to make outdoor comfort comparisons of different urban interventions. The high complexity of the outdoor climate, due to a much higher temporal and spatial variation of the outdoor conditions as compared to indoor room models, requires the formulation of clearly defined locally adjusted comfort scales. While some cities or institutions have developed their own locally adapted pedestrian wind comfort criteria, outdoor guidelines and criteria remain scarce, especially for outdoor thermal comfort. At present, it thus more insightful to express the impact of urban cooling strategies for comparisons in terms of the changes in wind speed and temperature.

The void deck modifications clearly resulted in an increase in wind speed and a decrease in air temperature in the void decks. Even though the conditions have not shifted to a different comfort assessment class, the observed wind speed and temperature differences can still be expected to be perceivable by pedestrians. **Wind speed-amplifying void decks were thus shown to be an effective urban cooling measure for Singapore's tropical climate**, but in order to further enhance the outdoor thermal comfort, they should be used in combination with other passive cooling strategies in urban design, such as high-SRI (Solar Reflectance Index) materials, evaporative cooling through the implementation of water bodies and vegetation.

The demonstrated workflow aids and speeds up the optimization process of void deck geometries to enhance the urban wind microclimate. The same methodology is also applicable in the optimization process of other building features (e.g. canopies and podia) that may affect the wind microclimate.

10

CONCLUSION

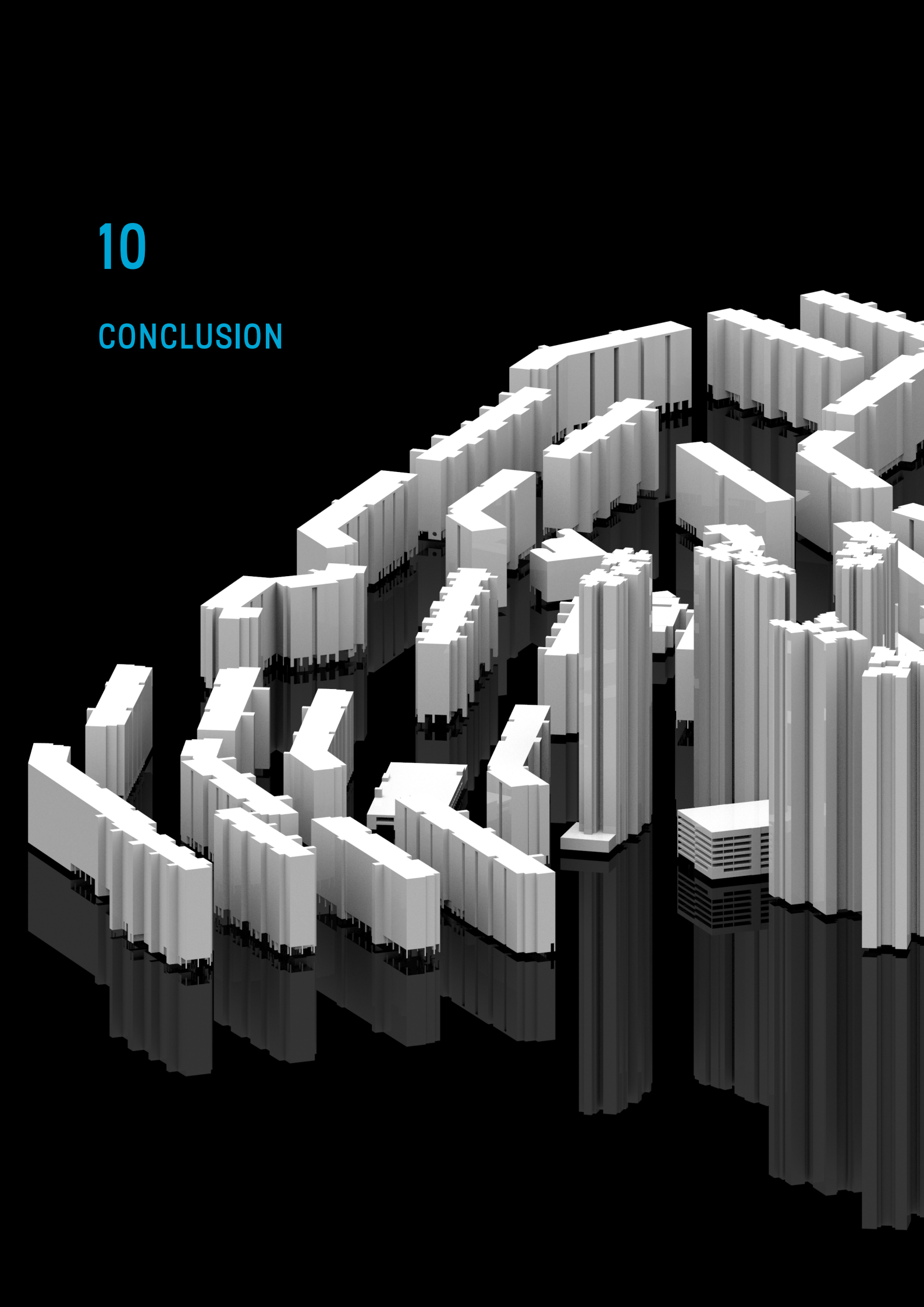

This research has demonstrated how a combined computational design and simulation approach can be implemented to analyse and optimize the design of void deck geometries with the aim to enhance the urban wind microclimate in a tropical environment, with a particular focus on the establishment of a good balance between outdoor thermal and pedestrian wind comfort. The research was carried out starting with a climate analysis and an extensive literature study on void decks, outdoor thermal and pedestrian wind comfort, followed by a parametric study of various void deck geometries and how these impact the flow pattern around a building. Next, a CFD simulation of the study area with the existing building void decks was performed for the three prevailing monsoon wind directions to analyse the current wind microclimate. The conclusions of the void deck geometry study of the single building and the current wind comfort conditions in the study area were combined into an urban parametric model which allows one to perform void deck modifications in an entire urban area based on specific building characteristics, such as building orientation. Using this parametric model, an urban-scale design intervention was made on the void deck geometries with the aim to enhance the wind microclimate in Clementi. The research concluded with a post-intervention CFD simulation to assess the effectiveness of the proposed void deck modifications with respect to the outdoor thermal and pedestrian wind comfort in the neighbourhood. Below, an answer to the formulated research questions is given one by one based on conclusions drawn from the entire research.

Which void deck geometries and configurations have been applied to existing buildings in Singapore?

The research initiated with an inventory of existing void decks in Singapore and how these evolved in time. The analysis showed **differences between void decks both in terms of orientation, size or 'porosity level' (ratio between void volume and closed volume of the ground floor) and void deck elements**. While the void decks of the older HDB buildings primarily face the prevailing North and South wind directions, those of later estates show more variation in their orientation due to the increased demand for privacy, which led to the emergence of more enclosed building clusters. Besides the increase in complexity of building shapes – from long slab blocks to hybrid (slab-)point blocks – newer buildings also show a significant increase in height. While the older HDB buildings extended more in the horizontal direction, the newer ones thus extend more in the vertical direction. These changes have led to a large reduction of the average building footprint and thus also of the void deck size. Lastly, the inventory showed that while some void decks are literally just a 'void', with only some structural elements, others have been furnished with benches and recreational elements. Evidently, the addition of these elements has an influence on the flow pattern inside and downstream of the void decks.

The void decks in Clementi, the study area of this research, mostly date back to the 1970s and are thus characterized by their large size and simple, rectangular layout. However, the study area also includes some recently developed buildings which have a much-reduced void deck size, in some cases being just a corridor to the elevators. This variety in void deck orientations and sizes made Clementi a representative area to focus on in this research, allowing us to draw conclusions for buildings in other parts of Singapore. Most of the buildings have their void deck aligned with one of the prevailing wind directions (N, NNE and S), which made it particularly interesting for this urban ventilation topic.

How do current void deck designs affect wind flow patterns for urban ventilation in Singapore with regard to thermal comfort?

Although the thermal comfort was found to be bad in the entire study area, with just a few places marked as thermally acceptable to most people, the temperature contour plot showed that the **void decks do have a cooling effect** on the locally sampled air temperatures. However, since the hybrid (complex-shaped) towers in the study area led to a much higher local wind speed increase than the amplified wind speeds inside the void decks, the thermal comfort improvement inside the void decks seemed relatively low in comparison. It is therefore recommended to combine this downdraught effect of tall buildings, leading to increased wind speeds at pedestrian height, with wind speed-amplifying void deck geometries and other urban cooling strategies such as high-SRI materials and evaporative cooling to enhance the outdoor thermal comfort in Singapore's tropical climate.

What are the effects of current void deck designs on pedestrian wind comfort?

The climate analysis indicated that wind speeds in Singapore are generally low due to the city state's proximity to the equator (Acero & Ruefenacht, 2017). Besides the low average measured monsoon wind speeds (2.2 m/s for the Southwest and 2.6 m/s for the Northeast Monsoon respectively, as based on 1981–2010 measurements by the Meteorological Service Singapore) used for the inlet boundary conditions, the urbanized context also requires a relatively high aerodynamic roughness length in the simulations, which further hinders urban ventilation. Although the urban simulation clearly showed that the void decks help to increase the wind speed up to a certain distance downstream, they were not amplified to such an extent that they would cause pedestrian wind comfort problems. In fact, the **pedestrian wind comfort in the entire area was found to be very good**, with acceptable conditions for each of the assessed outdoor activities (frequent and occasional outdoor sitting, standing, walking, running). Extra **wind-inducing measures could thus be explored, focusing on those void deck geometries which lead to the highest amplification factors** and the desired flow pattern for the urban function downstream of the void deck.

Where do significant mismatches between urban ventilation and pedestrian comfort occur?

The current wind microclimate in the study area is characterized by a **strong imbalance between outdoor thermal and pedestrian wind comfort**. Whilst the occurring wind conditions make the area attractive to practically all outdoor activities (frequent and occasional outdoor sitting, standing, walking and running) in terms of pedestrian wind comfort, the thermal comfort assessment showed a very different pattern, with only a few spots being thermally acceptable to the majority of people.

The mismatch between the outdoor thermal and pedestrian wind comfort was clearly portrayed in the mismatch (comfort-discomfort) plots. The **most notable mismatch locations were located around the complex-shaped tall towers in the study area**, where the pedestrian comfort was worst and the thermal comfort best, leading to the strongest negative correlation between the air temperatures and wind speeds. The observed mismatch marks the importance to perform these types of wind microclimate analyses in a tropical environment as Singapore, taking into account both the pedestrian comfort and thermal comfort effects of the wind.

Which design strategies can be adopted to enhance Singapore's urban ventilation for outdoor thermal comfort while ensuring good pedestrian comfort?

The research included a parametric study in which a total of ten void deck geometries were created. While the base case variant was a simple void deck with straight walls, the other geometries were either converging or diverging horizontally or vertically, or any combination of these. Each of the variants were tested by means of a CFD simulation of the flow pattern inside/around a building incorporating that particular void deck. The vertically converging void decks were regarded as unsuitable for wind microclimate enhancement in Singapore as their low amplification factor ($K<1$) indicated no increase in wind speed inside the void deck. All other geometry variants showed a good potential for wind speed – and thus convective surface heat transfer – enhancement. The highest sampled values of K at the centre of the void deck were obtained for the vertically diverging variants. In fact, the building with a simple rectangular void deck (base case variant), as widely found in Singapore, was found to be quite effective, with a wind speed enhancement of 25% as compared to a probe at the same location in the absence of the building. A further distinction could be made in terms of the flow pattern. A horizontally converging void deck geometry was found to be effective at directing the urban ventilation towards locations/activities requiring more convective surface heat transfer – while tolerating higher wind speed levels in terms of pedestrian comfort – (such as sports fields) due to the funnel-shaped induced wind speed region downstream. Similarly, the urban simulation of the current situation showed that small void deck elements, such as columns, help to guide the flow to target locations as they create narrow streams of increased wind speeds downstream of the void decks. A horizontally diverging void deck, on the other hand, leads

to a more evenly spread region of accelerated flow along the void length and is therefore more suitable for e.g. walking routes adjacent to buildings.

The **vertically diverging void deck variant was chosen for the urban-scale void deck intervention** as it led to the highest amplification factor in the void deck. Applying this geometry at all the building parts facing the simulated wind direction led to a wind speed increase and temperature decrease in almost all the void decks. While the amplified wind speed region extended a bit downstream of some void decks, other areas in between the buildings showed a slowed down wind flow. The temperature effects were more extreme at the more closely-packed areas with a smaller distance in between the buildings. Overall, we can conclude that **the void deck modifications did not only affect the local wind microclimate inside the void decks, but also altered the wind microclimate in between the buildings**.

This leads to the following conclusion for the main research question, which read as follows.

How can the geometry design of void decks be optimized to enhance urban ventilation for outdoor thermal comfort in Singapore while ensuring good pedestrian comfort?

The observed mismatch between pedestrian wind and outdoor thermal comfort marks the need to seek a good balance between the desired increased wind speed for its cooling effect and the maximum allowable wind speed that can be tolerated to perform different outdoor activities in a tropical climate. To this end, a combined computational design and simulation approach, as demonstrated in this work, could be useful to architects, urban planners and engineers in the design process of future urban developments to ensure a good wind microclimate. The **steps in this proposed design methodology** are shown in the *diagram on the next page*. While this research focused on the geometry of void decks, the same methodology coupling parametric design and CFD is also **applicable in the optimization process of other building features which may affect the urban wind microclimate**, such as canopies and building podiums.

COMPUTATIONAL DESIGN & SIMULATION WORKFLOW FOR URBAN WIND MICROCLIMATE ENHANCEMENT

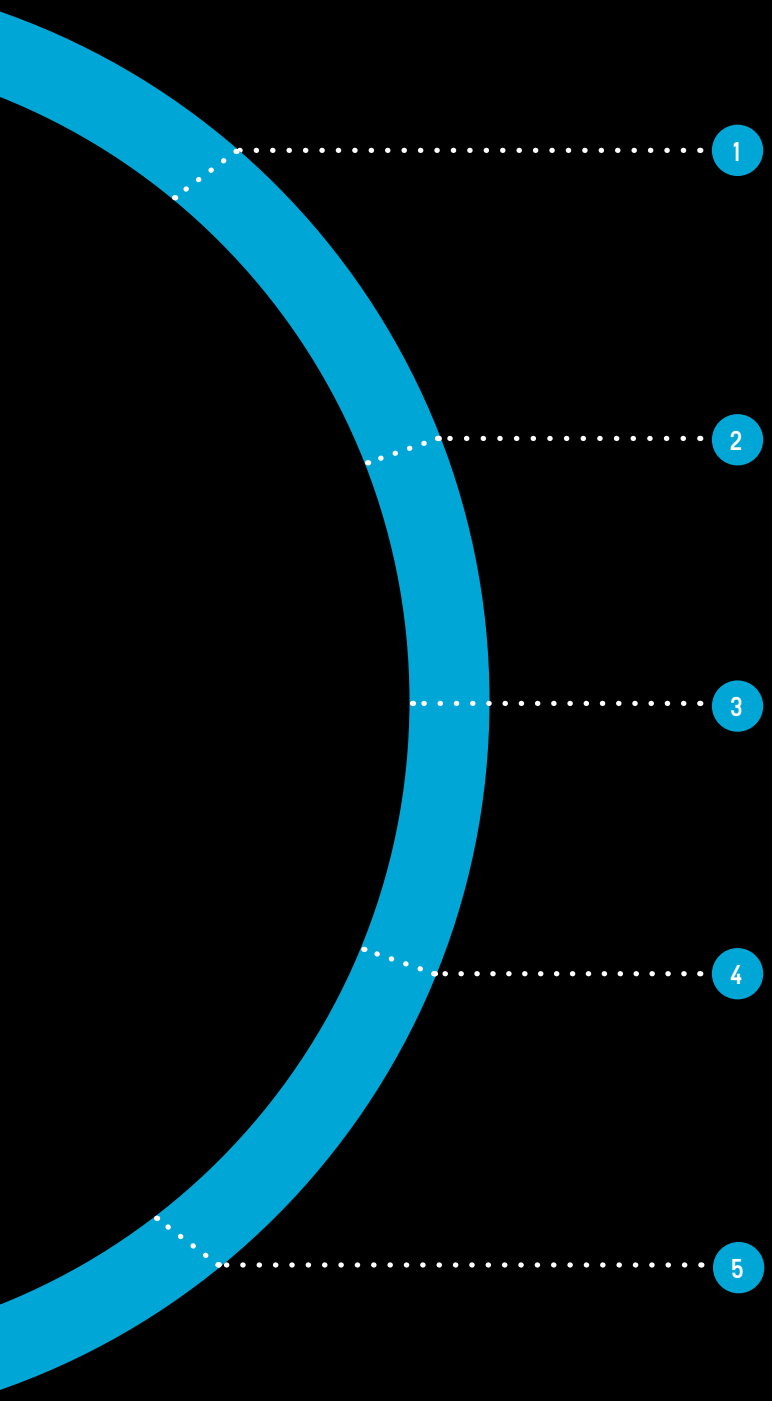

1

PARAMETRIC SMALL-SCALE TESTS

Perform simple CFD-tests on parametric single-building model

2

PARAMETRIC LARGE-SCALE INTERVENTION

Apply modifications to building groups in parametric urban model

3

URBAN INTERVENTION CFD-SIMULATION

Perform urban intervention CFD-simulation and analyze results

4

NON-PARAMETRIC LOCAL INTERVENTION

Apply (non-parametric) modification at particular location based on results from small-scale tests and specific activity comfort requirements

5

LOCAL INTERVENTION CFD-SIMULATION

Perform local intervention CFD-simulation and evaluate

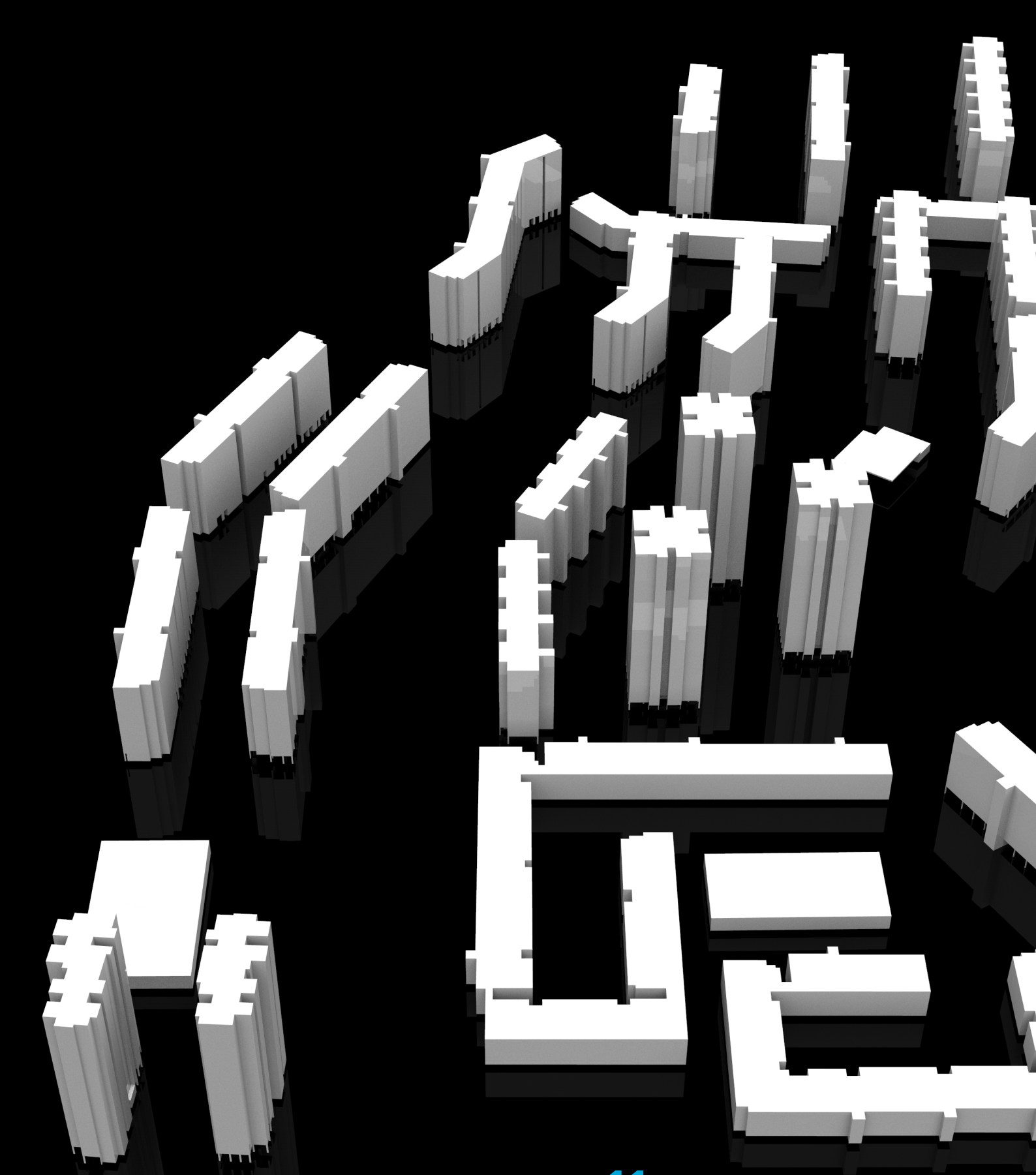

11

RECOMMENDATIONS

General recommendations for further development of the research

- All the simulations in this study were performed as RANS. In case more computational resources and time would be available, simulations for the further developments proposed here could be done using more advanced CFD approaches such as LES in reduced areas of interest. Besides, in case on-site measurements could be done or an ABL wind tunnel would be available for use, the CFD simulation results could be validated with these on-site measurements and/or wind tunnel tests.

- Although the thermal index used in the outdoor thermal comfort assessments (THI) is very suitable for tropical climates like Singapore's, it assesses thermal comfort solely on the basis of air temperature and relative humidity. The effect of wind speed is obviously also taken into consideration in this research by using a solver for convective surface heat transfer to solve the temperature field based on the occurring wind speeds in the area. The air temperatures used in the THI assessment are thus derived from simulations which take the cooling effect of the wind speeds into account. However, it would be interesting to do a more 'complete' thermal assessment (such as PET) based on more parameters, including e.g. mean radiant surface temperatures. However, this requires a lot of data from e.g. measurements on all surfaces in the area as the radiant temperatures highly depend on e.g. surface orientation, inclination, view factors and time of the day. In this case, assumptions were made for the surface temperatures to compute the convective heat transfer by linking the local climate zones in the study area to remote sensing measurements, which by all means involves uncertainties. No radiation model was included in the simulation as this requires more radiation data which were not available for this case. The applied surface temperatures were relatively high to account for the effects of solar heat gain and radiative heat transfer between the various surfaces in the area.

- In this case, no major local wind discomfort problems were found with respect to the local activities in the study area (current activity map). On the other hand, the thermal comfort was found to be bad in the entire study area, rather than at some specific spots. As such, step 4 and 5 of the proposed design methodology in the diagram were not carried out here. Repeating the process for another study area where specific local wind problems occur would thus be interesting to also include these steps and to perform a few local, non-parametric, void deck modifications depending on the specific requirements of the outdoor activities / functions at those locations.

- Although the void deck modifications clearly showed an impact on the sampled wind speeds and air temperatures in the void decks as well as around the buildings in the study area, the large value range between the outdoor comfort assessment classes was not able to capture these differences. In order to compare the effects of various urban interventions, more locally adapted outdoor comfort assessment scales with smaller ranges between the classes need to be established by cities and governmental institutions to formulate clear guidelines. The high complexity of outdoor conditions and the large range in people's comfort perceptions complicates this.

Recommendations for further development of the urban parametric void deck model

- The parametric void deck model (building scale) took 25% of the ground floor area into account as being "closed", thus with a void deck covering the remaining 75%. This assumption was based on the fact that most of the buildings in the study area have a large void deck, but a certain area on the ground floor is always reserved for amenities like staircases and technical rooms. In the urban parametric void deck model, this closed volume was placed at both ends of the building, thus with the void deck in the middle of the building. The void deck volume in the urban parametric model can be moved along the building length though. Further development of the urban parametric void deck model could explore more options for the location of the closed volumes; splitting them and moving them around in different configurations.

- To show the functionalities of the urban parametric model, the buildings in the study area were grouped by orientation and the void deck geometries were then adjusted per orientation group. However, the buildings can, of course, be grouped based on many other characteristics. Further studies on air flows in Singapore could explore void deck adjustments based on other building characteristics, such as distance between

buildings or building height. Also, if the simulation results of an area in its current situation show particular spots where flow velocities are too high or too low, the surrounding buildings in that particular place could be added to one group for which a flow-decelerating/-accelerating void deck geometry is chosen.

Recommendations for the coupling of urban 3D models with OpenFOAM CFD simulations and parametric design

- This urban parametric model was developed to illustrate how the combination of CFD with parametric models can help urban planners and architects to explore and test different void deck design variants for various areas or buildings to ultimately make better wind-informed design decisions. The study focused on the Clementi area (for which an OSM data file was downloaded from OpenStreetMap), but it would be highly desirable to expand this model for an entire city. Although the 3D city model itself can easily be generated using the Elk plugin for Grasshopper, turning the 3D-buildings into a parametric model can still be a bit inconvenient due to inconsistencies in how the object elements are detected. Thus, further research should be done on the coupling of automatically generated 3D city models with parametric design tools like Grasshopper. Automatically detecting and categorizing object elements will speed-up the proposed workflow considerably.
  Besides, the software used in this work consists of both open-source (OpenFOAM, Grasshopper, Grasshopper plugins) and commercial (Rhino) software. Ideally, an efficient workflow should be sought based on open-source tools that can perform all the above mentioned tasks.

- The terrain was modelled implicitly (very simplified) to get a correct representation of the elevated building position relative to the surrounding roads and to include the effect of the terrain geometry on the flow through the urban environment. The integration of a digital elevation model (DEM) would be an interesting future development to improve the accuracy of the terrain topography in the simulation model. This would be especially relevant for simulations of areas with a lot of height differences and slopes in the terrain. Currently, DEMs of urban environments are not widely available yet.

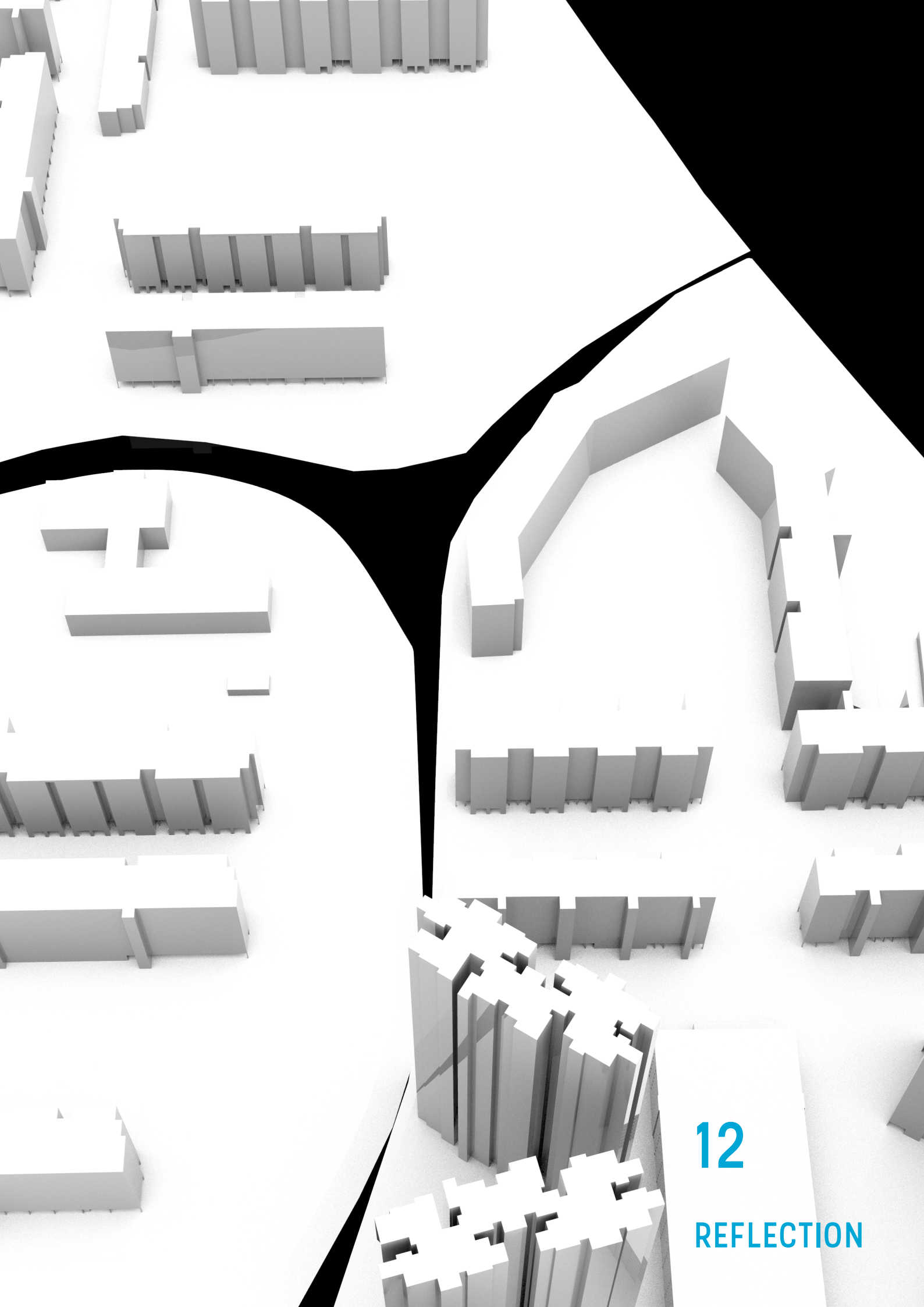

12

REFLECTION

Relationship Between Research Project, Master Track and Master Programme

The graduation topic of this thesis lies at the intersection of the Building/Urban Physics, Climate Design and Design Informatics fields of the Building Technology programme and the Architectural Engineering + Technology Department. Computational tools are used both in the design (Grasshopper as the main parametric / computational design tool) as well as the engineering aspects (OpenFOAM as the CFD tool for the urban flow assessment) of the research. Considering the urban challenges of today and in the future due to climate change, research on urban ventilation is essential to cope with heat stress. Enhanced urban ventilation will not only help to ensure a comfortable outdoor climate in cities, but may also positively affect indoor ventilation. The theme of climate design and sustainability is thus well-represented in the thesis topic.

The focus within the Building Technology master programme lies on performance-based design, in which the design of a building element is optimized to achieve a high specific performance. In this case, the building element is the void deck and the performance-based design task entails the optimization of its geometry for urban aerodynamics, i.e. with the aim to enhance the urban ventilation in the study area.

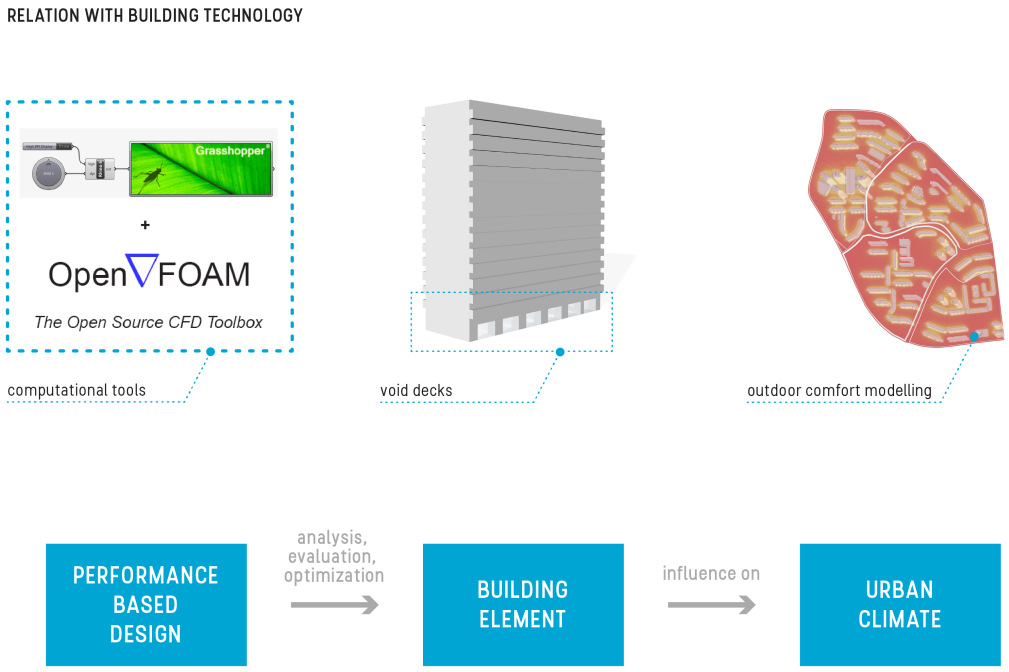

Figure 12.1: relation with Building Technology

The research demonstrates a workflow based on computational design and simulation that includes the three branches of Architecture, Urbanism and Building Sciences.

Relationship Between Research & Design

Both a research-through-design and a design-through-research methodology are used in this thesis. The former entails the use of parametric design to generate different void deck geometry design variants. These were then assessed and the findings of this sub-research were used to make better informed decisions for the urban case design intervention. The latter methodology was thus implemented by using the research findings from the single building simulations of the different void deck designs to make a proposal for void deck design interventions of buildings in the study area to enhance the outdoor ventilation at urban scale. The final proposed urban-scale void deck design intervention, in turn, was used to formulate an overall conclusion on the entire research project and the main research question. This can, again, be regarded as research-through-design.

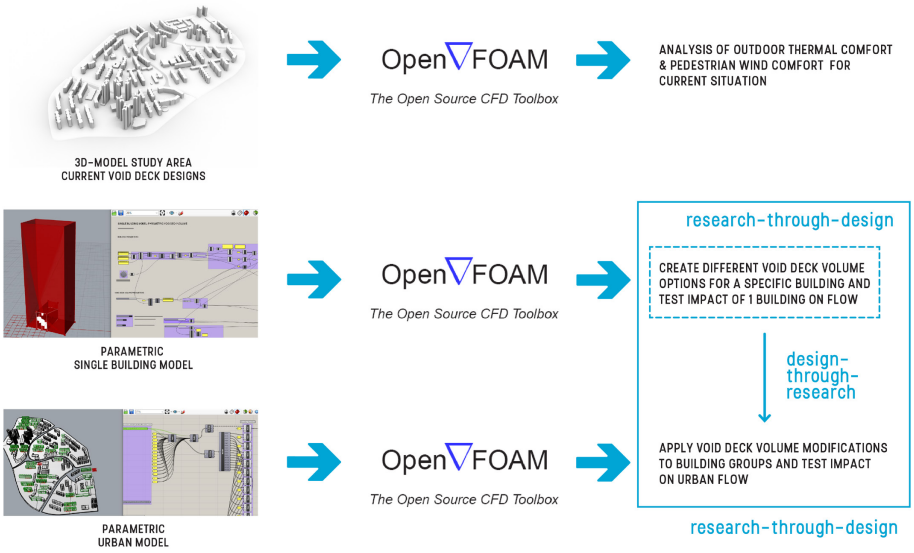

Figure 12.2: research-through-design & design-through-research

Research Process

Although the initial idea was to use a recently developed CityJSON 3D-city model, there were two constraints that impeded this. Firstly, the model only included the public housing blocks, which was insufficient to get an accurate idea of the flows in the entire study area due to the missing buildings. Secondly, the format of the model did not facilitate an easy manipulation of the geometry to model the void decks (which were not included) and make them parametric in Grasshopper. This exposed a workflow bottleneck for designers and urban planners when linking automatically generated 3D-city models with parametric design tools. To solve this, a parameterizable 3D-model of the study area was created using a Grasshopper plugin that allows to import data from OpenStreetMap into Rhino. The base model was generated fairly easy in that way, although the modelling of the void decks themselves was a time-consuming task due to the lack of info (such as dimensions) on the void decks.

The combination of learning an advanced CFD software (OpenFOAM) while getting acquainted with working in a high-performance computing cluster environment and a complex urban case made this a very challenging and time-consuming, yet extremely instructive project. While some of the challenges were related to the urban scale of the project (since it takes e.g. more time to build a parametric 3D model of a whole urban area than of one building and to simulate on a mesh of this extent, but also to figure out small errors in a large collection of input files and parameters within the CFD case folder) and the focus on small elements within this large area (e.g. accurately meshing the void deck features to analyse their effect on the urban-scale flow pattern), others were also related to computational impracticalities, such as transferring files between the computer cluster and local drive, pending jobscripts in the cluster queue and crashing of the visualization software due to the mesh size. However, after getting more acquainted with all the computational tools, a more efficient workflow for some of these steps was found. Having focused a lot on indoor comfort in previous building physics courses, my aim of this thesis was to learn how buildings also affect the outdoor environment. The number of new things learnt during the whole project was tremendous and further fuelled my interest in urban-scale microclimate modelling.

The two main takeaways from this research project are 1) not to overcomplicate a case that is already complicated (since, at the beginning I wanted to do everything as detailed as possible to get the most accurate results, but this later on caused some meshing problems due to the high level of detail of the 3D model, which then had to be simplified) and 2) not to focus only on the desired results but also on the research process as a whole. In fact, many of the things that went wrong during this project can be avoided

when carrying out a similar study in the future. In that sense, it is also good to have at least experienced once which things can go wrong while performing an urban CFD study as more attention will then be drawn to those aspects in subsequent studies.

Societal Impact

According to the World Health Organization (2019), 91% of people worldwide are exposed to excessive ambient air pollution, causing 4.2 million deaths every year. Next to that, cities around the world cope with trapped heat due to urban heat islands. In dense tropical urban environments, these effects are even more apparent. This emphasizes the need for effective urban ventilation strategies in these places. Within this thesis, a commonly applied strategy in Singapore – namely the void decks – to cope with this was explored and typical technical design skills used in the field of Building Technology were applied to optimize the design of these building elements.

Urban ventilation strategies are also relevant in the wider context of the built environment as the indoor and outdoor environment mutually influence one another. For example, natural / hybrid ventilation can only be implemented if the outdoor conditions (air quality and wind speeds) are within an acceptable range. Therefore, wind flows need to be studied at an urban level before natural building ventilation strategies can be formulated and more sustainable and comfortable environments around and within buildings can be achieved.

Scientific Impact

The publication of some recent papers on the effectiveness of void decks for urban ventilation marks the relevance of the topic and the quest of cities for simple methods to improve outdoor comfort and, subsequently, walkability. While previous studies performed wind simulations on generic building shapes with variations in parameters such as the building height and canyon width, this study has aimed to take the research on void decks a step further by performing CFD simulations in a realistic urban setting, namely for the Clementi neighbourhood in Singapore.

Moreover, existing void deck studies mostly focus on the cooling effect of void decks due to wind-speed enhancement. However, the preservation of a good balance between outdoor thermal comfort and pedestrian wind comfort in particular has not been studied before, to the current knowledge of the researcher. Although increased wind speeds are desirable from a thermal comfort point-of-view, void decks should not lead to an increase in wind speed to such extent that it would cause uncomfortable or unsafe conditions for pedestrians.

Lastly, the link between parametric design and computational fluid dynamics in this research is quite unique as CFD is a field that is not often touched upon within design disciplines. Wind studies are, however, very important in the design process of new urban developments as the resulting wind conditions will highly impact how and whether or not outdoor urban spaces will be used. The presented workflow thus aims to bridge this gap, while at the same time exposing the current constraints that complicate the coupling of 3D city models, CFD and parametric design.

APPENDICES

Appendix A: Void Decks Elaboration

A brief summary of void deck characteristics was provided in *section 3.4* of this report. The following sections elaborate on these, focusing on:

- Construction period
- Orientation of opening
- Location within precinct
- Void deck size
- Adjacencies
- Spatial void layout
- Defining elements inside and enclosing void deck
- Amenities

Construction Period

Void decks are a common characteristic of Singapore's public housing buildings, which are managed by the Housing and Development Board (HDB) and accommodate more than 80% of its total population. (Housing and Development Board, 2019) These HDB blocks are organized in 23 – and a 24th one currently in planning phase – residential neighbourhoods, also known as New Towns, spread over the mainland as shown in *figure A1*.

Figure A1: overview of HDB New Towns in Singapore

The HDB building typologies underwent changes as these New Towns developed in different stages. A summary of how the building configurations in the New Towns changed in time is shown in *figure A2*. As can be observed from the figure-ground diagrams, there are also some changes in terms of building orientation. This will be elaborated on in the section Orientation of Opening.

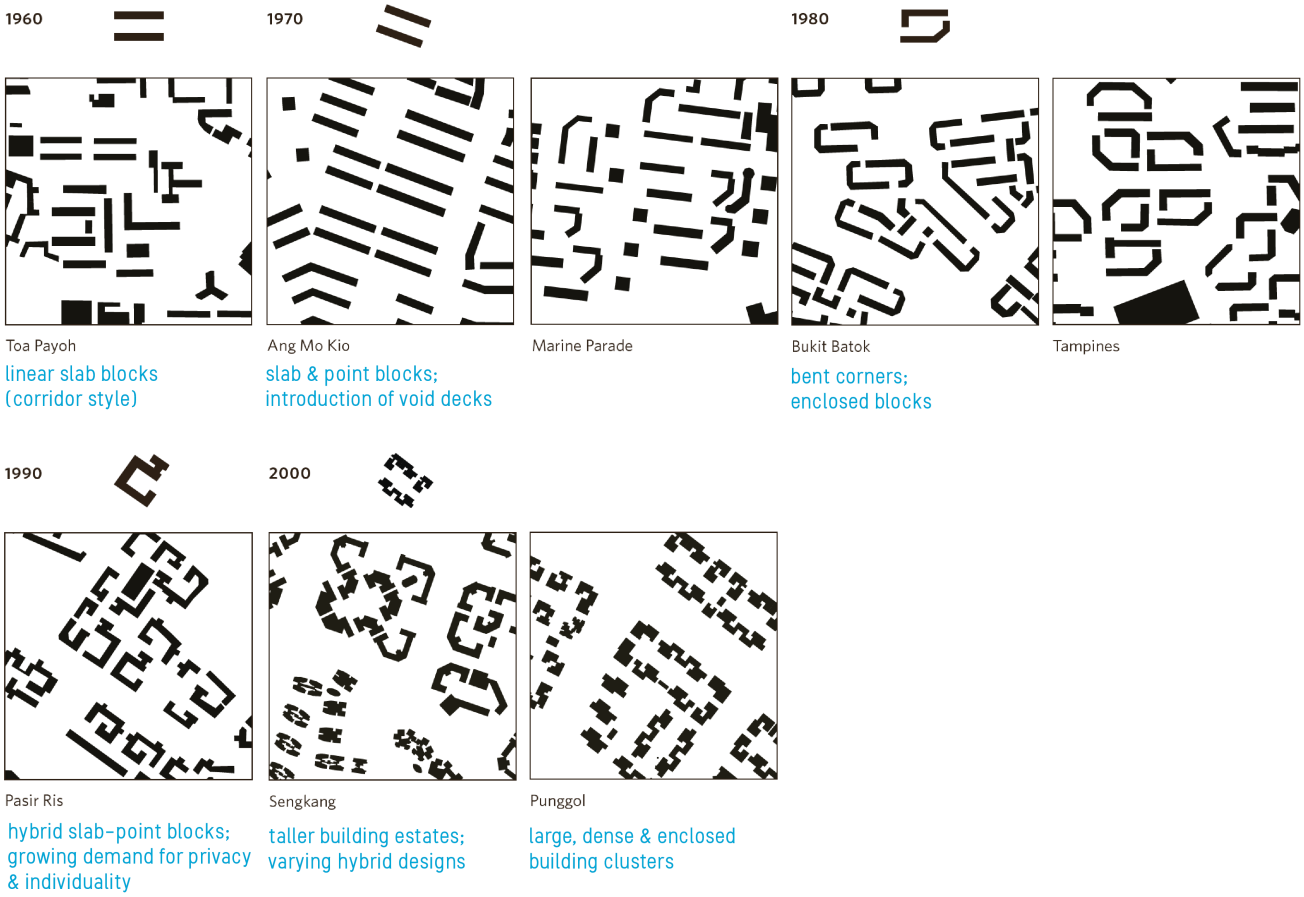

Figure A2: evolution of HDB block configurations. Adapted from "Evolution of New Towns - New domestic landscapes of HDB and popular cultures of natural ventilation" by S. Roesler & A. Vihervaara, Future Cities Laboratory, 2015. (http://e-collection.library.ethz.ch/eserv/eth:49661/eth-49661-01.pdf)

Throughout the past decades, different bio-climatic design strategies have been applied to New Town developments in Singapore, which has resulted in a variety of different block arrangements. (Roesler & Vihervaara, 2015) A first distinction that can be made between void deck in HDB blocks in Singapore thus relates to the period during which the different neighbourhoods were established.

The first HDB estates, dating from the 1960s, did not incorporate open ground floors. (Roesler & Vihervaara, 2015) Housing units and shops mostly filled the ground level of these blocks. Although these ground-floor flats were favoured for their direct access to the outdoor environment, they were criticised for their lack of privacy and proper ventilation as well as the proximity of rubbish chutes. (National Library Board, 2015) An example of this is Toa Payoh, built in the period 1965-1970, which only includes buildings without void decks, as can be seen in *figure A3*.

Figure A3: early HDB block without void decks, Toa Payoh. From: Singapore Press Holdings, 1968.

Figure A4: Tampines Street 45 void deck. From: "HDB Directory" by SRX, 2019. (https://www.srx.com.sg/hdb/tampines/tampines-street-45-hstam0049/524497/hdb-map)

Void decks emerged in the 1970s, the first one supposedly originating from 1963 in Tiong Bahru (Yeo, 2016), and have remained a characteristic of HDB flats in Singapore up until today.

With the elimination of the apartment units at the ground level, a higher sense of privacy and a greater distance from the rubbish chute bins was achieved in these living units. (Housing and Development Board, 1975) Apart from these ground-level voids, Yeh's multidisciplinary study of public housing in Singapore in 1975 noted that more open communal spaces were also being integrated at higher levels at this time. This phenomenon is mostly visible in the latest developments, which often feature elevated void decks and sky gardens, either complementing or substituting ground-floor void decks. An example of the latter are the Clementi Towers, completed in 2011, in which a 4-storey shopping centre and bus interchange replace the common void deck ground floor. Future developments, such as at Northshore Plaza in Punggol, might not include void decks either. (Thinking City, 2018) Moreover, in some newer estates apartment units have been reintroduced on the ground floor to accommodate disabled and elderly people. (Cairns, Jacobs, Ying-ying, Padawangi, Siddique, & Tan, 2014) So, instead of providing void decks underneath each apartment block, it has recently become more common to accommodate the functions of these void decks in a separate communal pavilion, known as precinct pavilions.

These changes, metaphorically described as "a process of "unvoiding" the void deck" by Cairns et al. (2014), have raised questions on the survival of void decks in Singapore's future urban context. Although the reduction or elimination of ground-floor communal spaces can be compensated by the addition of elevated voids and precinct pavilions, it has been observed that these changes also impact urban air flows, and thus the outdoor comfort, around the buildings. Even if the initial introduction of void decks in residential blocks was primarily driven by social aspirations to spark interaction amongst residents and bring a human scale to these high-density living environments, in recent years the use of voids as a strategy to enhance ventilation in and around housing estates has gained increased interest.

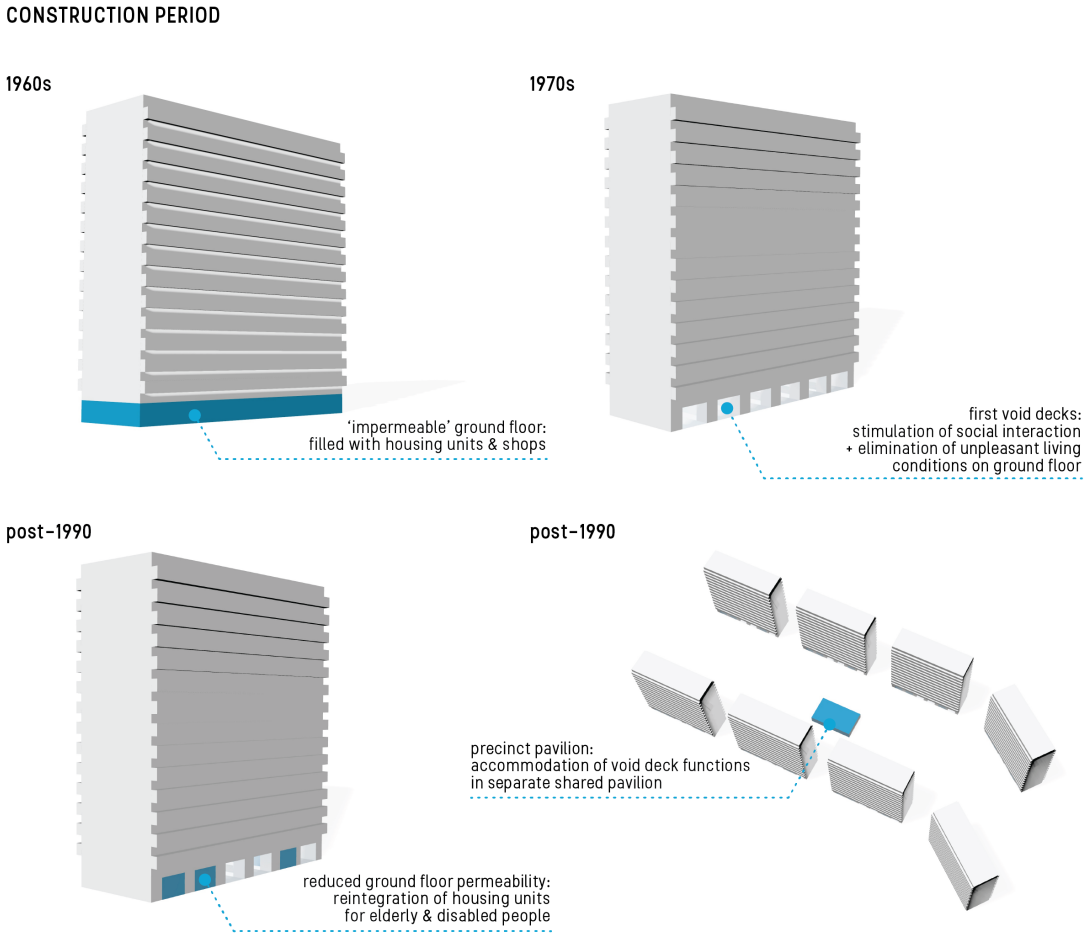

Figure A5: void deck characteristics - construction period

Orientation of Opening

The orientation of the void depends on the orientation of the block it is contained in. The orientation of the earlier HDB blocks was defined according to what would be optimal to prevent excessive solar heat gains on the façade as much as possible. (Roesler & Vihervaara, 2015) As such, most of these buildings are aligned with the East-West axis, in other words with the main façades, and thus also the void decks, facing North and South. This orientation coincides well with the prevailing wind directions in Singapore, being Northerly/North-Easterly and Southerly/South-Easterly (primarily governed by the Northeast and Southwest monsoon), which therefore allows for cross-ventilation in the dwelling units as well as urban ventilation through the building void decks. Although the orientation is thus beneficial in terms of indoor ventilation and ventilation at precinct scale (due to wind flowing through the blocks via the void decks), it should be noted that main façades (almost) perpendicular to the prevailing winds also lead to a significant portion of these wind flows being obstructed at the levels above the ground level, thereby limiting the ventilation at urban scale. This is why Ng (2016, p. 95) emphasized the importance of keeping the street grid length perpendicular to the prevailing wind as limited as possible to achieve a high urban ventilation.

However, more recent projects do not follow this tradition and show more variation in their orientation. One reason for this is the emergence of new building typologies, such as hybrid point-slab blocks, with bent corners and enclosed arrangements in a response to the growing demand for more privacy by residents. These building cluster arrangements involve different block orientations and therefore also different void deck orientations.

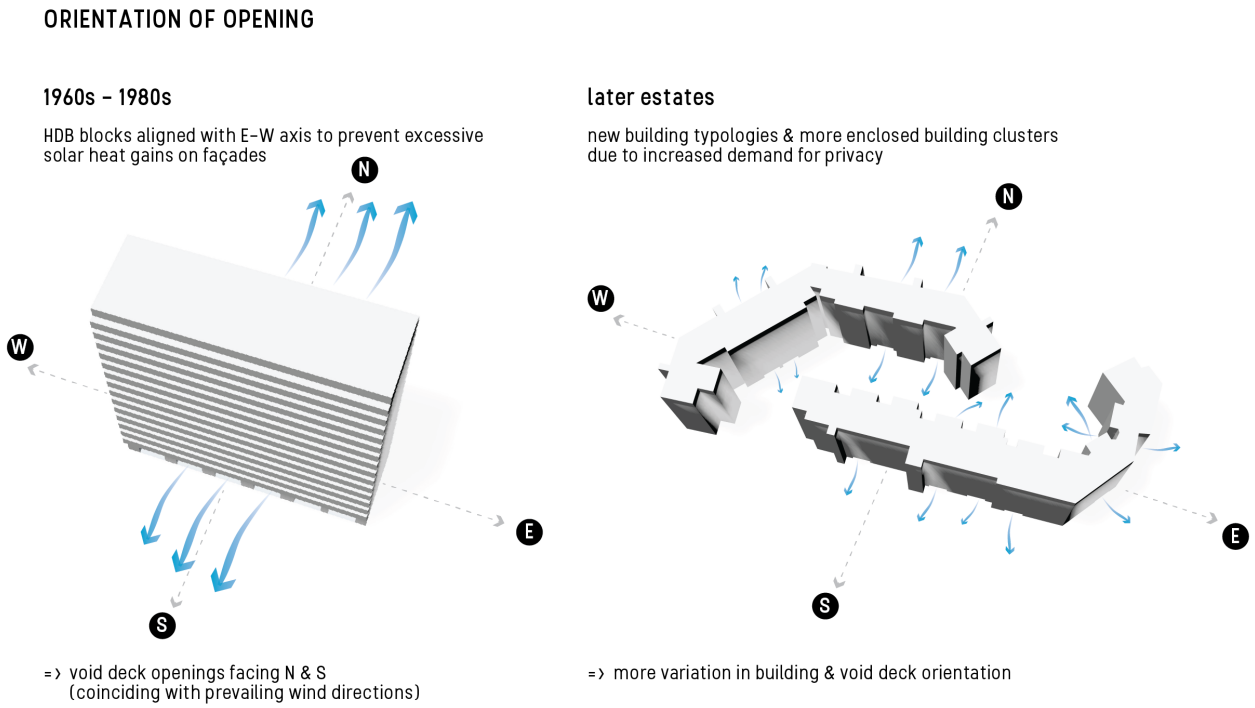

Figure A6: void deck characteristics – orientation of opening

Location within Precinct

The intensity of usage of the void decks depends on several factors. It does not solely depend on the amenities which are provided in the void deck, but also to a great extent on the location of the void deck. For example, a ping-pong table in one void deck may not be used as intensely as a perfectly similar ping-pong table at another nearby void deck. The most-used void decks have been found to be those at the breeziest locations, those which are most visible for passersby, and the ones which are located near

shophouses or simply have a higher probability of encounters with neighbours along the route to e.g. the market. (Giok Ling & Tan, 1992) Similarly, tables and stools located at the end of the block near the road are more likely to be used by parents waiting to pick up their children at the bus stop. (Giok Ling & Tan, 1992) This emphasizes the importance of a strategic location of the void decks in order for them to be successful as places of interaction.

Void Deck Size

Being characterized by slab block configurations, the early void decks contained in HDB apartment blocks can literally be regarded as voids as they constituted a very large portion of the ground floor space. Only a small portion was reserved for essential services (such as mechanical / equipment rooms), circulation (lift lobbies and staircases) and, in some cases, a limited number of flats on the ground floor. The large size of the voids allowed for a flexible community space that could serve a wide variety of uses. (Corporate Planning & Administration Department – Government of Singapore, personal communication, November 27, 2019) Many of the early HDB blocks thus contain one large single void deck at the ground floor. By grouping together different amenities (e.g. ping-pong tables, benches, vending machines etc.) in a single void deck, it was found that a more effective focal point is created compared to several distributed void decks with different amenities which are not visible from all sides. (Giok Ling & Tan, 1992)

While most of these void decks before the 1980s were very spacious and rectangular in shape, there has been more variation in void deck designs recently, with more complex layouts and a reduction in size. (National Heritage Board, 2013) These modified void deck designs are a result of changes in the design of the housing blocks themselves, which, in turn, can be attributed to changes in residents' needs over time. The growing demand for privacy by residents during the 1990s resulted in new apartment block typologies. (Roesler & Vihervaara, 2015) More enclosed blocks emerged and the formerly common slab blocks with their long corridors (and corridor-facing units) were renounced in favour of new hybrid slab-point blocks with better views and increased privacy. As explained by the government's Corporate Development Group (2019), this had consequences for the void deck layouts though, as the reduction in the number of housing units per floor also implied that the ground floor area, and thus the void deck size, would be reduced. Moreover, with buildings growing taller nowadays, this means that the already reduced void deck space would have to be shared by a larger number of residential units.

An interesting exception of the ongoing void shrinking process is Tampines Street 45, which features void decks with a very high ceiling of multiple floor heights, as shown in *figure A4*.

In order to compensate for the overall reduced void deck size, the so-called 'precinct pavilion', an additional shared space, was introduced. Since the ground-floor void decks for social activities underneath the residential units sometimes led to disturbance (noise and privacy issues) to residents, this new shared space is usually located further away from the housing units, thus as a standalone common space. (Corporate Planning & Administration Department – Government of Singapore, personal communication, November 27, 2019)

Besides these precinct pavilions, recent developments also include elevated voids, also referred to as eco-decks or E-decks, and sky gardens to compensate for the reduced communal space on the ground floor. With taller HDB-blocks being built more recently, the formerly common void decks of the ground floor have thus been shifted upwards to provide gathering spaces at different levels. According to a comparative study of HDB precincts with elevated public spaces conducted by the Future Cities Laboratory (2014), the average time spent in the public space by residents increased with increasing elevation. As pointed out based on their observations, a plausible reason for this might be the fact that many of the elevated public spaces include more facilities for active activities, whereas those on the ground floor are more focused on sedentary activities. A side note to be made here is that these elevated spaces generally experience higher wind velocities as a result of the atmospheric boundary layer wind velocity profile, which makes these spaces more suitable for active activities. Further research on wind speed amplification at the pedestrian level through void decks is thus needed to establish the required outdoor comfort levels that would incentivize more people to actively recreate.

Figure A7 (left): void deck covering almost entire ground floor. From: "The Everyday People" by Elephnt, 2019. (http://www.everydaypeople.sg/lifestyle/arts-and-culture/ways-of-seeing-photographer-elephnt-captures-unique-lookout-points-at-hdb-void-decks-in-singapore/)

Figure A8 (right): void deck covering almost entire ground floor, Clementi. By F. Biljecki, 2019.

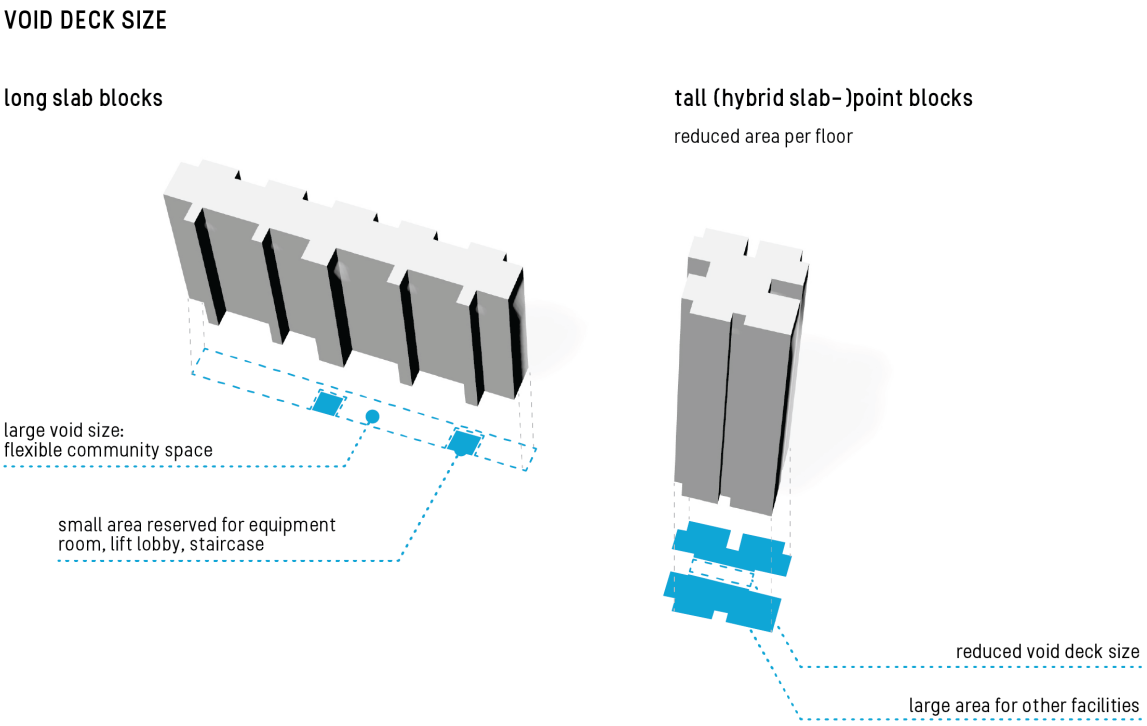

Figure A9: void deck characteristics - void deck size

Adjacencies

Since 1982, void decks and playgrounds have been linked together into precincts, which comprise a cluster of HDB blocks (of each around 500 to 750 apartment units) in a semi-enclosed arrangement, with the playground acting as a focal point. (Giok Ling & Tan, 1992) While some estates feature buildings which are all orientated towards this central open space, others are less enclosed by such a boundary and less fixed in a strictly defined order. (Giok Ling & Tan, 1992) This configuration pattern forms clusters of 2 to 4 ha (e.g. 200m by 200m). According to Cairns et al. (2014), this size was determined based on the distance which people are willing to walk in a tropical climate, namely around 350m. Note that this is much less than in temperate climates. This planning reasoning resulted in the formation of self-sustaining clusters of housing blocks with amenities all within a close, walkable, range.

In the early 1980s, the playgrounds at HDB blocks were reduced in size from 15m by 15m for every 600 to 800 apartment units to 10m by 10m for every 300 to 400 units. (Giok Ling & Tan, 1992) The playgrounds enabled the establishment a community feeling, even in these dense high-rise residential areas. Similar to the addition of recreational elements within the void decks in the 1980s, the playgrounds were also equipped with more facilities, such as benches for adults, in order to encourage a more intensive use of these communal spaces. (Giok Ling & Tan, 1992) Of course, this requires a good outdoor comfort in these areas. For this reason, HDB planted fast-growing trees at 6m-intervals to provide shading on the playgrounds. (Giok Ling & Tan, 1992) Besides, the void decks can play an important role in the outdoor comfort of these areas.

Figure A10: void deck connected to playground at Ang Mo Kio Avenue 5. From: "Void Decks in Singapore: More than a Void" by Ghetto Singapore, 2019. (https://www.ghettosingapore.com/void-decks-in-singapore/)

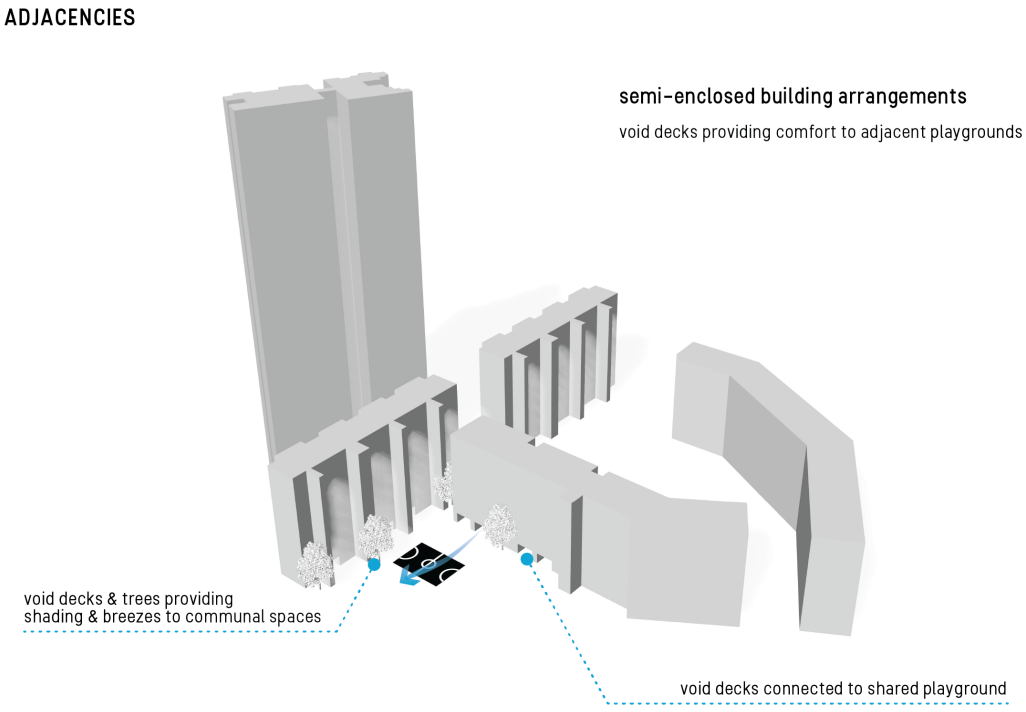

Figure A11: void deck characteristics - adjacencies

Spatial Void Layout

Described as "a kind of slack space in the tightly planned fabric of Singapore's New Towns" by Cairns et al. (2014), void decks are planned – or rather, unplanned – in order to accommodate a large variety of functions and user groups. While most of the void decks before the 1980s were very spacious and rectangular in shape, there has been more variation in void deck designs recently, with more complex layouts and a reduction in size. (National Heritage Board, 2013) Also, refurbishments of older HDB estates, such as Ang Mo Kio, Bedok and Taman, have resulted in extensions and variations of the void deck, as the "voids" in between as well as those around building blocks were upgraded into landscaped or colour patterned tiled walkways, shelters and other structures. (Goh, 2003) As such, we can conclude that the design of the permeable spaces at ground level, both in, between and around buildings, has evolved from bare, unfurnished spaces to more developed designs focused on providing pleasant – both in terms of outdoor comfort and walking experience in general – walking routes through the estates. Goh (2013) refers to this renewal as "second generation void decks". However, he points out that these examples remain limited as the majority of void decks retained their hollow, simplistic layout, contained within a rectangular outline.

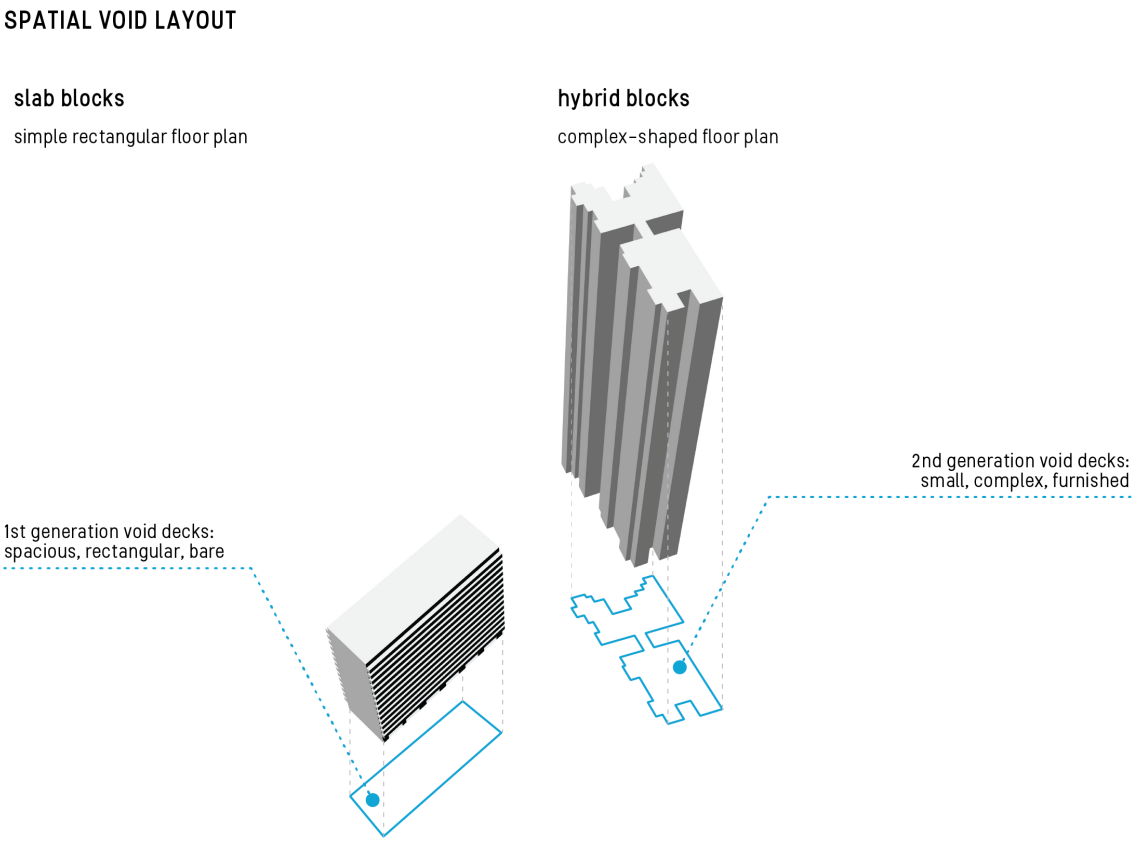

Figure A12: void deck characteristics – spatial void layout

Defining Elements Inside & Enclosing Void Deck

Void decks are commonly known for their openness, which is only obstructed by the load-bearing walls, structural columns, the largely unadorned lift and stairwell core walls and gutters, which facilitates ventilation underneath/through the buildings. (Goh, 2003) The size and spatial configuration of these elements inside the void is, evidently, determined by the structural function they perform. The simplicity of the void decks is also apparent in the finishes of the surfaces, with their unfinished murals, floor tiles and uncovered equipment.

During the 1980s, however, this simplicity was slightly reduced by the addition of recreational elements such as benches and ping-pong tables as well as vending machines. (National Heritage Board, 2013) Some

also include small convenience shops. The objective of these "Community Living Rooms" was to further enhance the social interaction amongst residents. (Corporate Planning & Administration Department – Government of Singapore, personal communication, November 27, 2019)

Furthermore, some void decks include low walls enclosing 'resident's corners'. Since the void decks were conceived as a public space, which thus attracted different types of users (both residents and people who do not live there) and activities, these low walls were introduced in an attempt to give back a sense of territoriality and to stimulate interaction amongst residents. (Giok Ling & Tan, 1992) There are also examples where a part of the void deck has been demarcated by residents, using e.g. benches or flower pots. (Giok Ling & Tan, 1992) However, a study conducted by HDB in 1985 showed that the vast majority of the respondents were in favour of void decks open for public use rather than being exclusively open for residents.

With the aim to turn the void decks into "an extension to the home", they had to evoke the feeling of a main entrance; of a lobby. This is why, around 1985, an imaginary threshold was created at void decks by giving the entrance part of the void a different floor surface and by applying a low parapet wall. (Cairns et al., 2014)

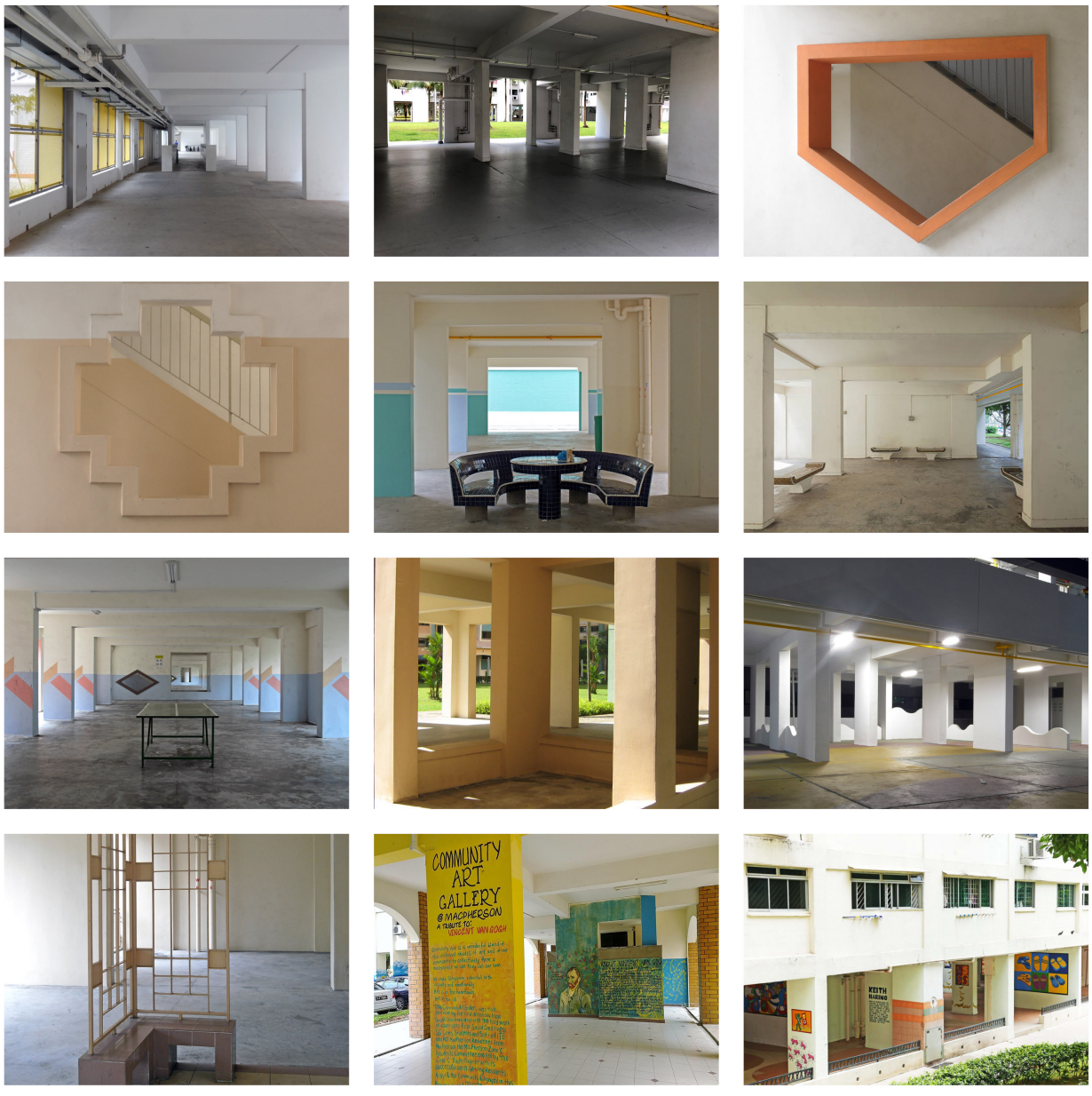

Figure A13: examples of void deck elements (various sources)

The images above (*figure A13*) show some examples of structural and recreational elements, wall openings, resident's corners, tile finishes and low parapet wall entrances of void decks.

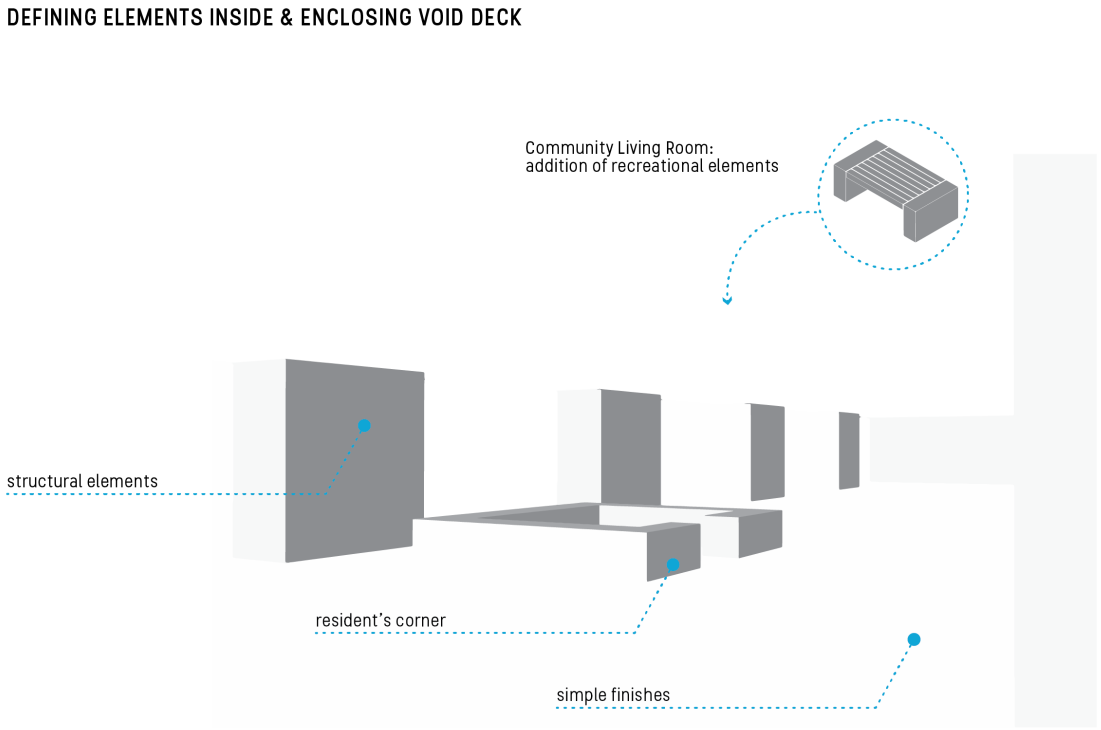

Figure A14: void deck characteristics – defining elements inside and enclosing void deck

Amenities / Functions

As mentioned previously, the simplicity of the void decks allows for a large range of activities and functions. Some examples include:

- Covered play area for children
- Waiting area for school bus
- Kindergarten / childcare centre
- Gathering space of senior citizens' clubs
- Kiosk
- Surveillance (Neighbourhood Police Post)
- Library
- Art gallery
- Gym
- Bicycle storage
- ...

Besides, the void decks can be booked by residents to host specific occasions, such as birthdays, weddings and funeral wakes. Because of this wide variety of activities and user groups, the void decks are used more intensely than the precinct playgrounds. (Giok Ling & Tan, 1992)

As mentioned by the Corporate Planning & Administration Department (Government of Singapore, personal communication, November 27, 2019), some of the community facilities in void decks, such as child, student and elderly day care centres, were included in HDB block plans from the beginning, while others were added progressively. In other words, the void deck amenities can be adapted to meet the changing

needs of the residents. This, again, demonstrates the highly flexible character of void decks in Singapore's social housing blocks.

Apart from the social activities and occasional events, the void decks also serve other functions. For example, they may help in creating a pleasant outdoor environment by allowing breezes and daylight to penetrate "through" buildings, thereby creating a porous urban environment. (Corporate Planning & Administration Department – Government of Singapore, personal communication, November 27, 2019)

Figure A15: void decks as social interaction spaces

AMENITIES / FUNCTIONS

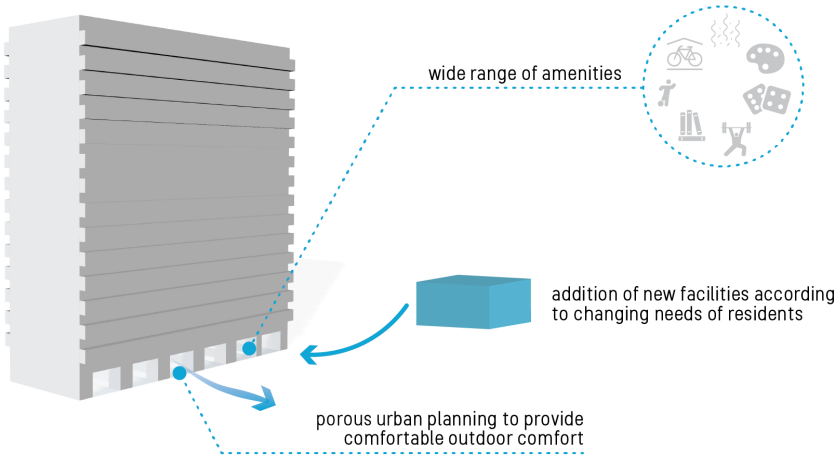

Figure A17: void deck characteristics – amenities / functions

Appendix B: Thermal Indices

A description of other common outdoor thermal comfort indices which were studied but disregarded due to their inapplicability to this Singapore-focused study is given here.

Rational thermal indices

The first available rational thermal index, **Perceived Temperature (PT)**, is an adaptation of the commonly used Predicted Mean Vote (PMV) for indoor comfort assessments to outdoor contexts. (Johansson, 2016) In contrast to the PMV scale, which expresses the thermal sensation ranging from -3 (cold) to +3 (hot) to predict the mean vote of satisfaction with the thermal environment, the PT uses a °C scale. As reported by Johansson (2016), this index has not been applied in many studies in the tropics. The PT model iterates clothing levels between 0.5 clo and 1.75 clo, which is considerably higher than the typical average clothing value in Singapore (0.3 clo, as shown earlier in *table 3.2*), and is therefore not very applicable to this study area.

Another common approach for thermal comfort assessments of outdoor environments is based on the **Physiological Equivalent Temperature (PET)** index. This index was defined by Höppe (1999, p. 71–75, as cited in Alur & Deb, 2010) as "the air temperature at which, in a typical indoor setting (without wind and solar radiation), the heat budget of the human body is balanced with the same [physiological response, i.e.] core and skin temperature as under the complex outdoor conditions to be assessed". As explained by ENVI-met (2019) the logic behind the PET-model is as follows:

1. Define heat gains and losses of human body.
2. Calculate resulting skin and core body temperature.
3. 'Transpose' analysed person to an indoor environment.
4. Reset data that do not apply in indoor environment (e.g. direct solar radiation, forced wind movement)
5. Determine the indoor temperature (= PET) that would result in the same skin and core body temperature as for the particular outdoor environment that is being studied.

A standard clothing value of 0.9 clo and indoor activity level of 80 W are assumed and the typical indoor environment (under absence of solar radiation and wind) – comparable to an office – of step 3 which is used as a base for comparison has the following conditions (Matzarakis & Amelung, 2008):

- mean radiant temperature: MRT = T_a (= air temperature)
- air velocity: v = 0.1 m/s
- vapour pressure: p_v = 12 hPa
- relative humidity: RH = 50 % (corresponds to previous condition)

An important remark regarding the PET index made by Pijpers-van Esch (2015) is that the fixed indoor environmental conditions which are assumed for the room which the outdoor environment is compared to disregard the fact that the outdoor climate varies much more – both temporally and spatially – than the indoor environment. Also, the time it takes for a person to adapt to a climatically different environment is not taken into account.

For tropical climates, the following simplified equation can be used to determine the physiological equivalent temperature (Ng, 2016):

$$PET = 1.2 * T_a - 2.2 * v + 0.55 * (MRT - T_a) \qquad [°C]$$

with

T_a = air temperature [°C]
MRT = mean radiant temperature [°C]
v = air speed [m/s]

The table below (*table B1*) indicates the thermal comfort zone based on PET for some warm and humid climates. While the generally formulated PET thermal comfort zone corresponding to 'no thermal stress' is defined between 18 and 23°C, these reference studies have shown that the comfort zone in warm-humid climates usually lies higher.

Geographical location	Season	Comfort zone (°C)	Percentage of satisfaction	Neutral index temperature (°C)	Preferred index temperature (°C)	Source
Hong Kong	Summer	n/a	n/a	28.1	n/a	Ng and Cheng, 2012
Taichung, Taiwan	Summer and winter	21.3–28.5	90%	25.6	24.5	Lin, 2009
Sun Moon Lake, Taiwan	Summer and winter	24.2–32.8	85%	27.2	n/a	Lin and Matzarakis, 2008
Sydney, Australia	Summer	n/a	n/a	22.9	23.4	Sagnolo and de Dear, 2003
Tel Aviv, Israel	Summer	20–26	80%	23.9	n/a	Cohen *et al.*, 2013

n/a = not available

Table B1: comfort limits, neutral temperatures and preferred temperatures for the PET index from studies in warm-humid and similar climates. From Urban Climate Challenges in the Tropics - Rethinking Planning and Design Opportunities (1st Ed., p. 197), by Emmanuel, R., 2016, UK: Imperial College Press. Copyright 2016 by Imperial College Press.

Table B2 below shows how the PET comfort range of studies in warm humid climates varied depending on the study area. Two studies of Singapore - part of Köppen climate class Af (tropical rainforest climate) - defined the PET comfort range between 24°C - 30°C and 26°C - 31°C respectively.

	City, Country	Source	Acceptable index temperature ranges (°C)			PET (°C)																		
			Winter	Summer	All year	14	15	16	17	18	19	20	21	22	23	24	25	26	27	28	29	30	31	32
A	TROPICAL SAVANNA (Aw)																							
1	Dar es Salaam, Tanzania	Ndetto and Matzarakis,2016	-	23.0–31.0	-																			
2	Guayaquil, Equador	Johansson et al., 2018	Upper 34.3	Upper 25.3	Upper 31.3																			
B	TROPICAL RAINFOREST (Af)																							
1	Singapore	Yang et al., 2013b	-	-	24.0–30.0																			
2	Vitoria, Brazil	da Silva and de Alvarez, 2015	-	-	22.0–30.0																			
3	Singapore	Yang et al., 2013b	-	-	26.3–31.7																			
C	HUMID SUBTROPICAL (Cfa & Cwa)																							
1	Changsha, China	Yang et al., 2013b	-	-	24.0–31.0																			
2	Changsha, China	Liu et al., 2016	-	-	15.0–22.0																			
3	Shanghai, China	Chen et al., 2015	15.0–29.0	-																				
4	Guangzhou, China	Li et al., 2016	18.1–31.1	-																				
5	Sydney, Australia	Spagnolo and de Dear, 2003	21.5–32.4	-																				
6	Hong Kong	Cheng et al., 2012	-	-	19.0–30.0																			
7	Sun Moon Lake, Taiwan	Lin and Matzarakis, 2008	-	-	26.0–30.0																			
8	Taichung, Taiwan	Lin, 2009	-	-	21.3–28.5																			
9	Campo Grande, Brazil	Lucchese et al., 2016	21–27																					
10	Yunlin, Taiwan	Lin et al., 2012			21.3–28.5																			
11	Hong Kong	Ng and Cheng, 2012	14–16	27.0–29.0																				
12	Chiayi, Taiwan	Lin et al., 2012	-	26.1–30.4																				
13	Belo Horizonte, Brazil	Hirashima et al, 2016	-		19.0–27.0																			
14	Chengdu, China	Zeng and Dong, 2015	-	20.0–29.5	-																			
15	Hong, Kong	Huang et al., 2017			16.4–25.2																			
	LEGEND						LOWER LIMIT					UPPER LIMIT							COMFORT ZONE					

Table B2: comparison of acceptable comfortable ranges in sub-climates of warm humid climates based on PET. From Review of studies on outdoor thermal comfort in warm humid climates: challenges of informal urban fabric, by M.M. Baruti, E. Johansson, & J. Åstrand, 2019 (https://doi.org/10.1007/s00484-019-01757-3)

The PET model has been widely used in outdoor thermal comfort analyses, including those of the ongoing Cooling Singapore research project. An extensive review of outdoor thermal comfort studies in warm humid tropical climates by Baruti et al. (2019) shows that the majority of assessments were done based on the PET index. However, since the index takes all of the basic thermal comfort parameters into account, its usage requires a large set of measurement data.

In response to the shortcomings of the PET model, a dynamic thermal comfort model was developed which also takes the acclimatization effect into account. The dynamic aspect implies that the skin temperature, core body temperature, skin wetness etc. are evaluated at different instances. Similar to the PET model, this **Universal Thermal Climate Index (UTCI)** model uses an equivalent temperature, but the reference situation in this case concerns an outdoor environment. (Pijpers-van Esch, 2015) The assumptions of the climatic conditions corresponding to this reference outdoor environment are (Pijpers-van Esch, 2015):

- mean radiant temperature: MRT = T_a (= air temperature)
- air velocity at 10m above ground: v = 0.5 m/s (calm air)
- relative humidity: RH = 50 % (corresponds to previous condition)
- metabolic rate: M = 135 W/m²
- person's walking speed: 1.1 m/s
- ambient temperature-dependent clothing level

The advanced clothing model in this thermal index calculates the resulting clothing insulation as the static clothing insulation modified by the person's walking speed and the relative wind speed using a correction factor. (Blazejczyk, Epstein, Jendritzky, Staiger, & Tinz, 2012)

The universal thermal climate index is universal in the sense that it is applicable to all climate types as well as all seasons. (Johansson, 2016) A major drawback, however, is that the assumed walking speed of 1.1 m/s is rather high for a tropical climate as Singapore (Johansson, 2016), which would result in an overestimation of the UTCI in the study area of this research. Moreover, since the clothing level is determined based on the ambient temperature - while disregarding the influence of e.g. humidity and radiation on one's clothing adaptation behaviour - from observations in Europe, it implies that a similar clothing value will be assumed if a person is in e.g. a hot-humid climate as if (s)he would have been in a hot-dry climate as long as the ambient air temperature is the same. (Johansson, 2016) These observations pose some limitations on the applicability of the UTCI index to this study.

A comparative overview of the rational thermal indices that were discussed is shown below.

PET (°C)	PT(°C)	SET* (°C)	UTCI (°C)	Thermal perception	Thermophysiological stress
			<−40	Frosty	Extreme cold stress
<4	≤−39		−40 to −27	Very cold	Very strong cold stress
4–8	−39 to −26	10.0–14.5	−27 to −13	Cold	Strong cold stress
8–13	−26 to −13	14.5–17.5	−13 to 0	Cool	Moderate cold stress
13–18	−13 to 0	17.5–22.2	0 to 9	Slightly cool	Slight cold stress
18–23	0 to 20	22.2–25.6	9 to 26[a]	Comfortable	No thermal stress
23–29	20 to 26	25.6–30.0		Slightly warm	Slight heat stress
29–35	26 to 32	30.0–34.5	26 to 32	Warm	Moderate heat stress
35–41	32 to 38	34.5–37.5	32 to 38	Hot	Strong heat stress
>41	≥38	>37.5	38 to 46	Very hot	Very strong heat stress
			>46	Sweltering	Extreme heat stress

[a]The thermal comfort zone of UTCI is also referred to as 18–26°C (Bröde *et al.*, 2012a). There is no 'slightly warm' defined for this index.

Table B3: 'original' relationship between thermal perception and the indices PET, PT, SET and UTCI. From* ***Urban Climate Challenges in the Tropics – Rethinking Planning and Design Opportunities*** *(1st Ed., p. 180), by Emmanuel, R., 2016, UK: Imperial College Press. Copyright 2016 by Imperial College Press.*

Lastly, pedestrian thermal acceptability can also be assessed based on skin wettedness (w). This variable depends on the person's metabolic rate M (i.e. their physical activity level), the clothing vapor resistance Re and the atmospheric pressure p_a, and can be calculated with the following formula (Havenith, Holmér, & Parsons, 2002):

$$w = \frac{0.42 * (M - 58) * Re}{5770 - 7.2 * M - p_a}$$

The upper threshold for thermal acceptability is given by $0.0012 * M + 0.15$, which leads to the following thermal criterion (Havenith et al., 2002):

$$w < 0.0012 * M + 0.15$$

A more general threshold value for thermal comfort based on skin wettedness is (Havenith et al., 2002):

$$w < 0.3$$

A comparison to the previous thermal criterion of skin wettedness shows that this simplified version would hold for a metabolic rate M of 125 W/m², which corresponds to a person walking slowly *(see table B4)*. Only in the case of a metabolic rate equal to 125 W/m² the use of the simplified thermal acceptability criterion would be adequate; in all other cases, the simplified thermal comfort threshold would imply an under- (in case of e.g. a running person) or overestimated (in case of e.g. a person standing still) metabolic rate and skin wettedness. The previous thermal acceptability threshold is therefore preferred.

	W/m²	met*
Resting		
Sleeping	40	0.7
Reclining	45	0.8
Seated, quiet	60	1.0
Standing, relaxed	70	1.2
Walking (on level surface)		
3.2 km/h (0.9 m/s)	115	2.0
4.3 km/h (1.2 m/s)	150	2.6
6.4 km/h (1.8 m/s)	220	3.8
Office Activities		
Reading, seated	55	1.0
Writing	60	1.0
Typing	65	1.1
Filing, seated	70	1.2
Filing, standing	80	1.4
Walking about	100	1.7
Lifting/packing	120	2.1
Driving/Flying		
Car	60 to 115	1.0 to 2.0
Aircraft, routine	70	1.2
Aircraft, instrument landing	105	1.8
Aircraft, combat	140	2.4
Heavy vehicle	185	3.2
Miscellaneous Occupational Activities		
Cooking	95 to 115	1.6 to 2.0
Housecleaning	115 to 200	2.0 to 3.4
Seated, heavy limb movement	130	2.2
Machine work		
sawing (table saw)	105	1.8
light (electrical industry)	115 to 140	2.0 to 2.4
heavy	235	4.0
Handling 50 kg bags	235	4.0
Pick and shovel work	235 to 280	4.0 to 4.8
Miscellaneous Leisure Activities		
Dancing, social	140 to 255	2.4 to 4.4
Calisthenics/exercise	175 to 235	3.0 to 4.0
Tennis, singles	210 to 270	3.6 to 4.0
Basketball	290 to 440	5.0 to 7.6
Wrestling, competitive	410 to 505	7.0 to 8.7

*Table B4: typical metabolic heat generation for various activities. From **ASHRAE Fundamentals 2017** (C9 Thermal Comfort, p. 9.6), by American Society of Heating, Refrigerating and Air-Conditioning Engineers, 2017, Atlanta, Georgia: ASHRAE. (https://app.knovel.com/hotlink/toc/id:kpASHRAEQ1/ashrae-handbook-fundamentals/ashrae-handbook-fundamentals)*

Related to this metabolic rate, Emmanuel (2016) suggests to determine the main activity pattern (such as shopping streets, gathering places, evening life, pedestrian paths and nodes) of different locations in a city and to specify the thermal comfort range of each location based on the metabolic rate of these activity levels. Instead of comparing every location in a city to the same thermal comfort threshold value, this approach would result in different comfort ranges for different locations in a single city.

Since rational thermal indices, such as PMV, PT, SET*, PET, UTCI and w take most of the thermal comfort parameters into consideration, they require an extensive meteorological dataset. In case of a lack of data, empirical indices, such as TEP, WBGT and THI, based on multiple regression analyses between measured values and subjective thermal comfort perceptions can be used. (Johansson, 2016) These will be discussed hereafter.

Empirical thermal indices

Temperature of Equivalent Perception (TEP) is an empirical thermal index which, following a large-scale questionnaire conducted in São Paulo, can be calculated for a warm humid environment using the formula below (Monteiro and Alucci, as cited in Johansson, 2016):

$$TEP = -3.777 + 0.4828 * T_a + 0.5172 * MRT + 0.0802 * RH + 2.322 * v \quad [°C]$$

with

T_a = air temperature [°C]
MRT = mean radiant temperature [°C]
RH = relative humidity
v = wind speed [m/s]

Furthermore, the **Wet-Bulb Globe Temperature (WBGT)** is the most commonly used index to express the heat stress experienced by a person in both indoor and outdoor environments. (Johansson, 2016) It can be computed as follows:

$$WBGT = 0.7 * T_{nw} + 0.2 * T_g + 0.1 * T_a \quad [°C]$$

with

T_{nw} = naturally ventilated wet-bulb temperature [°C]
T_g = globe temperature [°C]
T_a = air temperature [°C]

Despite its wide use, this index is not applicable in this research as no on-site measurements of wet-bulb and globe temperature, which require specific measurement equipment, are done.

Appendix C: Local Climate Zones Clementi

The LCZs that apply to the study area, based on the LCZ datasheets of the supplement to the *Local Climate Zones for Urban Temperature Studies* paper by Oke and Stewart (2012), are listed below with their main properties.

6 High-rise towers: open high-rise (LCZ 4)
- Tall buildings to tens of stories
- Mean building height › 25m
- Building surface fraction: 20-40%
- Canyon aspect ratio: H/W › 2 (note: towers are not parallel but under an angle, but both when taking smallest distance W between towers and when taking intermediate distance W, H/W › 2)
- Note: although the towers would classify as compact high-rise according to the canyon aspect ratio, the low building surface fraction clearly corresponds to the open high-rise LCZ. As mentioned by Oke and Stewart (2012), if the area properties do not exactly match with one LCZ, the surface fractions will be the ruling property to determine the appropriate LCZ. This building area therefore classifies as LCZ 4.

Majority of buildings (long slab blocks): open high-rise (LCZ 4)
- Mean building height › 25m
- Canyon aspect ratio: for building height H=34.4m and approximate canyon width W=25m =› aspect ratio H/W ≈ 1.38
- Note: the canyon aspect ratio lies in between the typical values for compact and open high-rise, but looking at the building surface fraction and the zone illustrations, this building area corresponds best to the properties of LCZ 4.

Point blocks: open high-rise (LCZ 4)
- Mean building height › 25m
- Canyon aspect ratio: H/W › 2
- Building surface fraction: 20-40%
- Note, although the towers would classify as compact high-rise according to their canyon aspect ratio, their building surface fraction corresponds to the open high-rise class. Looking at the complete datasheets with the provided zone illustrations, these point blocks better match the characteristics of the open high-rise LCZ than those of the compact LCZ.

Hybrid slab-point blocks (Blk 366 & Blk 367): open high-rise (LCZ 4)
- Mean building height › 25m
- Canyon aspect ratio: H/W › 2
- Note: although the building surface fraction of this sub-area is higher than that of the six towers at Clementi Ridges, this part is also classified as LCZ 4 as the properties and illustrations of this LCZ most closely match the majority of the area's properties.

Supermarket area: large low-rise (LCZ 8)
- Large, low buildings of 1-3 storeys, separated by paved surfaces
- Mean building height: 3-10m
- Building surface fraction: 30-50%
- Pervious surface fraction ‹ 20%
- Surface albedo: 0.15 ‹ α ‹ 0.25 (see table: concrete/paint/asphalt)

School area & community centre: compact mid-rise (LCZ 2)
- Attached or closely spaced buildings 3-9 storeys tall; inner courtyards; heavy construction materials
- Mean building height: 10-25m

Nursing home: open mid-rise (LCZ 5)
- Mean building height: 10–25m
- Building surface fraction: 20–40%

Parking lots: open mid-rise (LCZ 5)
- Mean building height: 10–25m
- Pervious surface fraction: 20–40%

Mosque: open low-rise (LCZ 6)
- Mean building height: 3–10m
- Building surface fraction: 20–40%

Roads land cover: bare rock or paved (LCZ E)
- Impervious ground, predominantly rock, paved or hard-packed
- Function: transportation
- Impervious surface fraction: › 90%
- Surface albedo: 0.15 ‹ α ‹ 0.30 (see table: concrete/paint/asphalt)

Terrain land cover: scattered trees (LCZ B)
- Trees scattered across pervious ground (low plants)
- Urban recreation (lightly wooded parks, green spaces)
- Tree aspect ratio: 0.25–0.75
- Pervious surface fraction: › 90%
- Surface albedo: 0.15 ‹ α ‹ 0.25 (see table: concrete/paint/asphalt)

Appendix D: OpenFOAM Files

The meshing steps in OpenFOAM were as follows:

- Set up initial hexahedral background mesh in the blockMeshDict.
- This background mesh is used as the basis for further iterative grid refinements around the model geometry (attached in STL-format) with snappyHexMesh. The local refinement regions are set up in this dictionary. In this case a higher grid resolution is desired at the void decks, so the refinement level in the lowest part of the domain was increased, similar to the refinement level of the imported building geometry.
- Refine the background mesh in steps, with a refinement factor of √2. This background mesh will anyhow be used as a basis for the castellated mesh refinement step of the snappyHexMesh feature in OpenFOAM. Note that this means that the background mesh is refined by a constant factor √2 each time, but the number of control volumes of the final generated mesh – which is obtained after running snappyHexMesh after blockMesh (background mesh generator) – is thus not refined by a constant refinement factor.

blockMeshDict (wind from S)

```
/*--------------------------------*- C++ -*----------------------------------*\
  =========                 |
  \\      /  F ield         | OpenFOAM: The Open Source CFD Toolbox
   \\    /   O peration     | Website:  https://openfoam.org
    \\  /    A nd           | Version:  7
     \\/     M anipulation  |
\*---------------------------------------------------------------------------*/
FoamFile
{
    version         2.0;
    format          ascii;
    class           dictionary;
    object          blockMeshDict;
}
// * * * * * * * * * * * * * * * * * * * * * * * * * * * * * * * * * * * * * * * * //
convertToMeters 1;   // scale factor (because mesh is always in [m])
vertices   // vertices of computational domain
(

    ( -1253.293  -2681.436    -0.600)    // P0   NOTE: blockMesh set to start at -0.6m instead of 0.0m to solve
issue with ground patch in polyMesh
    (  1170.707  -2681.436    -0.600)    // P1
    (  1170.707   3942.564    -0.600)    // P2
    ( -1253.293   3942.564    -0.600)    // P3
    ( -1253.293  -2681.436   720.000)    // P4
    (  1170.707  -2681.436   720.000)    // P5
    (  1170.707   3942.564   720.000)    // P6
    ( -1253.293   3942.564   720.000)    // P7

);

// number of cells in each direction: open CLEMENTI_current0.foam file (after running blockMesh so that it contains
the computational domain) and check X-,Y-,Z-range in Information tab

xcells  135;   // = X-range/(18m per cell) = 2424m/(18m per cell) = 135 cells (note: round up to ensure the whole
domain fits)
ycells  368;   // = Y-range/(18m per cell) = 6624m/(18m per cell) = 368 cells

zcells   40;   // = Z-range/(18m per cell) =  720m/(18m per cell) =  40 cells

blocks
(
    hex (0 1 2 3 4 5 6 7) ($xcells $ycells $zcells) simpleGrading (1 1 1)  //expansion ratio
);
edges   // curved edges (if not mentioned in this list, the edge is considered straight)
(
);
boundary   // patches: prescribe the patches for the boundary conditions here
(
    outlet
    {
        type patch;
        faces
        (
            (3 7 6 2)
```

```
        );
    }
    side1
    {
        type symmetry;
        faces
        (
            (0 4 7 3)
        );
    }
    side2
    {
         type symmetry;
         faces
         (
             (2 6 5 1)
         );
    }
    inlet
    {
        type patch;
        faces
        (
            (1 5 4 0)
        );
    }
    ground
    {
        type wall;
        faces
        (
            (0 3 2 1)
        );
    }
    top
    {
        type symmetry;
        faces
        (
            (7 4 5 6)
        );
    }
);
mergePatchPairs   // merge disconnected meshed blocks
(
);
// ************************************************************************* //
```

blockMeshDict (wind from N/NNE)

```
/*--------------------------------*- C++ -*----------------------------------*\
  =========                 |
  \\      /  F ield         | OpenFOAM: The Open Source CFD Toolbox
   \\    /   O peration     | Website:  https://openfoam.org
    \\  /    A nd           | Version:  7
     \\/     M anipulation  |
\*---------------------------------------------------------------------------*/
FoamFile
{
    version         2.0;
    format          ascii;
    class           dictionary;
    object          blockMeshDict;
}
// * * * * * * * * * * * * * * * * * * * * * * * * * * * * * * * * * * * * * //
convertToMeters 1;   // scale factor (because mesh is always in [m])
vertices   // vertices of computational domain

(

    ( -2603.798  -4032.100    -0.600)    // P0   NOTE: blockMesh set to start at -0.6m instead of 0.0m to solve
issue with ground patch in polyMesh

    (  2153.386  -4032.100    -0.600)    // P1
    (  2153.386   3016.241    -0.600)    // P2
    ( -2603.798   3016.241    -0.600)    // P3
    ( -2603.798  -4032.100   720.000)    // P4
    (  2153.386  -4032.100   720.000)    // P5
    (  2153.386   3016.241   720.000)    // P6
    ( -2603.798   3016.241   720.000)    // P7

);

// number of cells in each direction: open CLEMENTI_current0.foam file (after running blockMesh so that it contains
the computational domain) and check X-,Y-,Z-range in Information tab (or check in Rhino)

xcells  265;   // = X-range/(18m per cell) = 4757.184m/(18m per cell) = 265 cells (note: round up to ensure the
whole domain fits)
ycells  392;   // = Y-range/(18m per cell) = 7048.341m/(18m per cell) = 392 cells
```

```
zcells   40;   // = Z-range/(18m per cell) =  720m/(18m per cell) =  40 cells
blocks
(
    hex (0 1 2 3 4 5 6 7) ($xcells $ycells $zcells) simpleGrading (1 1 1)  //expansion ratio
);
edges   // curved edges (if not mentioned in this list, the edge is considered straight)
(
);
boundary   // patches: prescribe the patches for the boundary conditions here
(
    outlet
    {
        type patch;
        faces
        (
            (1 5 4 0)
        );
    }
    side1
    {
        type symmetry;
        faces
        (
            (2 6 5 1)
        );
    }
    side2
    {
         type symmetry;
         faces
         (
             (0 4 7 3)
         );
    }
    inlet
    {
        type patch;
        faces
        (
            (3 7 6 2)
        );
    }
    ground
    {
        type wall;
        faces
        (
            (0 3 2 1)
        );
    }
    top
    {
        type symmetry;
        faces
        (
            (7 4 5 6)
        );
    }
);
mergePatchPairs   // merge disconnected meshed blocks
(
);
// ************************************************************************* //
```

snappyHexMeshDict

```
/*--------------------------------*- C++ -*----------------------------------*\
  =========                 |
  \\      /  F ield         | OpenFOAM: The Open Source CFD Toolbox
   \\    /   O peration     | Website:  https://openfoam.org
    \\  /    A nd           | Version:  7
     \\/     M anipulation  |
\*---------------------------------------------------------------------------*/
FoamFile
{
    version     2.0;
    format      ascii;
    class       dictionary;
    object      snappyHexMeshDict;
}

// * * * * * * * * * * * * * * * * * * * * * * * * * * * * * * * * * * * * * //

// terrain + buildings outline coordinates
x_min -547;
y_min -554;
z_min    0;
x_max  430;
```

```
y_max  634;
z_max  120;  // = H = H_terrain + H_maxbuilding = 2m + 118m

// CD vertices (copy from blockMeshDict)
CD_x_min -1253.293;
CD_x_max  1170.707;
CD_y_min -2681.436;
CD_y_max  3942.564;
CD_z_min     0.000;
CD_z_max   720.000;  // (terrain+Hmax)*6=(2m+118m)*6=720m


// VERTICES OF REFINEMENT BOXES   (define variables here to be used later in refinement box definition)
// 3 refinement boxes within CD (CD is set in blockMeshDict)

// box 1: refinement box for 6 hybrid (complex-shaped) buildings
x1_min -503.963;
x1_max -240.214;
y1_min 196.067;
y1_max 376.791;
z1_min 2.000;    // the bld. are on top of the terrain (2m), so the ref.box can start at that height
z1_max 121.000;



// box 2: box at start of terrain  NOTE: for this refinement box, you can just take the coordinates of the terrain
outline (see above)
x2_min $x_min;
x2_max $x_max;
y2_min $y_min;
y2_max $y_max;
z2_min 0.000;
z2_max 73.000;

// box 3: void decks box at bottom covering whole CD
x3_min $CD_x_min;
x3_max $CD_x_max;
y3_min $CD_y_min;
y3_max $CD_y_max;

z3_min $CD_z_min;

z3_max 5.7;       // top of terrain is at +2m and GF (where void decks are located) is 3.6m high => so take 2m +
3.7m


//_____________________________________________

// Which of the mesh refinement steps to run
castellatedMesh true;
snap            true;
addLayers       false;

//_____________________________________________


// Geometry. Definition of all surfaces. All surfaces are of class
// searchableSurface.
// Surfaces are used
// - to specify refinement for any mesh cell intersecting it
// - to specify refinement for any mesh cell inside/outside/near
// - to 'snap' the mesh boundary to the surface


// REFINEMENT BOXES INSIDE COMPUTATIONAL DOMAIN
//_____________________________________________

geometry   // specify refinement boxes & roughness patches here
{
    box1
    {
        type searchableBox;
        min ($x1_min $y1_min $z1_min);
        max ($x1_max $y1_max $z1_max);
    }

    box2
    {
        type searchableBox;
        min ($x2_min $y2_min $z2_min);
        max ($x2_max $y2_max $z2_max);
    }

    box3
    {
        type searchableBox;
        min ($x3_min $y3_min $z3_min);
        max ($x3_max $y3_max $z3_max);
    }

    Buildings
    {
```

```
        type triSurfaceMesh;
        file "Buildings_closedpolysrf.stl";
    }

    terrainislands
    {
        type triSurfaceMesh;
        file «terrainislandsNew3.stl»;
    }

    terrainfront
    {
        type triSurfaceMesh;
        file «terrainfrontNew.stl»;
    }

    terrainback
    {
        type triSurfaceMesh;
        file «terrainbackNew.stl»;
    }

    terrainsides
    {
        type triSurfaceMesh;
        file «terrainsidesNew3.stl»;
    }

    mosque
    {
        type triSurfaceMesh;
        file «mosque_closedpolysrf.stl»;
    }

    nursinghome
    {
        type triSurfaceMesh;
        file "nursinghome_closedpolysrf.stl";
    }

    parking
    {
        type triSurfaceMesh;
        file "parking_closedpolysrf_simplified.stl";
    }

    schoolcommunitycentre
    {
        type triSurfaceMesh;
        file "schoolcommunitycentre_closedpolysrf.stl";
    }

    supermarket
    {
        type triSurfaceMesh;
        file "supermarket_closedpolysrf.stl";
    }

};

//____________________________________________

// CASTELLATED MESH SETTINGS
//____________________________________________


// Settings for the castellatedMesh generation.
castellatedMeshControls
{

    maxLocalCells 1000000;
    maxGlobalCells 29000000;
    minRefinementCells 0;
    maxLoadUnbalance 0.10;
    nCellsBetweenLevels 3;

    features
    (
        {
            file "Buildings_closedpolysrf.eMesh";
            level 5;
        }

        {
            file "mosque_closedpolysrf.eMesh";
            level 5;
        }

        {
            file "nursinghome_closedpolysrf.eMesh";
            level 5;
        }
```

```
        {
            file "parking_closedpolysrf_simplified.eMesh";
            level 5;
        }

        {
           file "schoolcommunitycentre_closedpolysrf.eMesh";
            level 5;
        }

        {
            file "supermarket_closedpolysrf.eMesh";
            level 5;
        }

        {
            file "terrainislandsNew3.eMesh";
            level 5;
        }

);

refinementSurfaces   // SURFACE-BASED REFINEMENTS
{
    Buildings
    {
        // Surface-wise min and max refinement level
        level (5 5);

        //- Optional angle to detect small-large cell situation
        //  perpendicular to the surface. Is the angle of face w.r.t.
        //  the local surface normal. Use on flat(ish) surfaces only.
        //  Otherwise leave out or set to negative number.
        // perpendicularAngle 10;


        //- Optional faceZone and (for closed surface) cellZone with
        //  how to select the cells that are in the cellZone
        //  (inside / outside / specified insidePoint)
        // faceZone sphere;
        // cellZone sphere;
        // cellZoneInside inside;  // outside/insidePoint
    }

    mosque
    {
        level (5 5);
    }

    nursinghome
    {
        level (5 5);
    }

    parking
    {
        level (5 5);
    }

    schoolcommunitycentre
    {
        level (5 5);
    }

    supermarket
    {
        level (5 5);
    }

    terrainislands
    {
        level (5 5);
    }

    terrainfront
    {
        level (5 5);
    }

    terrainback
    {
        level (5 5);
    }

    terrainsides
    {
        level (5 5);
    }

}
```

```
    resolveFeatureAngle 10;   // angle refinement (refined cells at curved surfaces)

    refinementRegions   // VOLUME REFINEMENTS
    {
        box1
        {
            mode inside;
            levels ((1E15 4));
        }

        box2
        {
            mode inside;
            levels ((1E15 3));
        }

        box3
        {
            mode inside;
            levels ((1E15 5));
        }

    }


    locationInMesh (-1250.2 -2680.3 700.3);   // specify one random point in the mesh (comma, to be sure it is in-
side a cell and not at edge)
    allowFreeStandingZoneFaces true;
}

//____________________________________________

// SNAP SETTINGS
//____________________________________________


// Settings for the snapping.
snapControls
{
    nSmoothPatch 2;
    tolerance 4.0;
    nSolveIter 50;
    nRelaxIter 5;
    // Feature snapping

    //- Number of feature edge snapping iterations.
    //  Leave out altogether to disable.
    nFeatureSnapIter 10;

    //- Detect (geometric only) features by sampling the surface
    //  (default=false).
    implicitFeatureSnap false;

    //- Use castellatedMeshControls::features (default = true)
    explicitFeatureSnap true;

    //- Detect points on multiple surfaces (only for explicitFeatureSnap)
    multiRegionFeatureSnap false;
}


// Generic mesh quality settings. At any undoable phase these determine
// where to undo.
meshQualityControls
{
    maxNonOrtho 65;                 // face orthogonality check
    maxBoundarySkewness 20;         // face skewness check
    maxInternalSkewness 4;
    maxConcave 80;                  // internal angles of face check
    minVol 1e-13;
    minTetQuality 1e-30;     // tetrahedra quality check
    minArea -1;                     // min. face area check
    minTwist 0.05;
    minDeterminant 0.001;
    minFaceWeight 0.05;
    minVolRatio 0.01;
    minTriangleTwist -1;
    // minVolCollapseRatio 0.5;
    nSmoothScale 4;
    errorReduction 0.75;
    relaxed
    {
        maxNonOrtho 75;
    }
}


// Advanced
mergeTolerance 1e-6;

// ************************************************************************* //
```

initialConditions (wind from S)

```
/*--------------------------------*- C++ -*----------------------------------*\
  =========                 |
  \\      /  F ield         | OpenFOAM: The Open Source CFD Toolbox
   \\    /   O peration     | Website:  https://openfoam.org
    \\  /    A nd           | Version:  7
     \\/     M anipulation  |
\*---------------------------------------------------------------------------*/
flowVelocity         (0 2.2 0);
pressure             0;
turbulentKE          0.044;
turbulentEpsilon     0.00037;
airTemperature       300.7;
// ************************************************************************* //
```

initialConditions (wind from N/NNE)

```
/*--------------------------------*- C++ -*----------------------------------*\
  =========                 |
  \\      /  F ield         | OpenFOAM: The Open Source CFD Toolbox
   \\    /   O peration     | Website:  https://openfoam.org
    \\  /    A nd           | Version:  7
     \\/     M anipulation  |
\*---------------------------------------------------------------------------*/
flowVelocity         (0 -2.6 0);
pressure             0;
turbulentKE          0.409;
turbulentEpsilon     0.00997;
airTemperature       300.7;
// ************************************************************************* //
```

ABLConditions (wind from S)

```
/*--------------------------------*- C++ -*----------------------------------*\
  =========                 |
  \\      /  F ield         | OpenFOAM: The Open Source CFD Toolbox
   \\    /   O peration     | Website:  https://openfoam.org
    \\  /    A nd           | Version:  7
     \\/     M anipulation  |
\*---------------------------------------------------------------------------*/
Uref                 2.2;
Zref                 10;
zDir                 (0 0 1);
flowDir              (0 1 0);
z0                   uniform 0.0040;  // aerodynamic roughness length of roughness area 1 (upstream of CD)
z0_terrainfront       uniform 1.0;     // aerodynamic roughness length of roughness area 2
z0_terrainsides       uniform 1.0;     // aerodynamic roughness length of roughness area 3
z0_terrainback        uniform 0.5;     // aerodynamic roughness length of roughness area 5
z0_grass      uniform 0.06;    // z0-value for elevated terrainislands (grass & trees)
zGround              uniform 0.0;     // minimum z-coordinate [m] (uniform because flat)
// ************************************************************************* //
```

ABLConditions (wind from N/NNE)

```
/*--------------------------------*- C++ -*----------------------------------*\
  =========                 |
  \\      /  F ield         | OpenFOAM: The Open Source CFD Toolbox
   \\    /   O peration     | Website:  https://openfoam.org
    \\  /    A nd           | Version:  7
     \\/     M anipulation  |
\*---------------------------------------------------------------------------*/
Uref                 2.6;
Zref                 10;
zDir                 (0 0 1);
flowDir              (0 -1 0);        // NOTE: for wind from N, wind is in the -y direction so -2.6 in y!
z0                   uniform 0.50;  // aerodynamic roughness length of roughness area 1 (upstream of CD)
z0_terrainfront       uniform 0.50;     // aerodynamic roughness length of roughness area 2
z0_terrainsides       uniform 1.0;     // aerodynamic roughness length of roughness area 3
z0_terrainback        uniform 1.0;     // aerodynamic roughness length of roughness area 5
z0_grass      uniform 0.06;    // z0-value for elevated terrainislands (grass & trees)
zGround              uniform 0.0;     // minimum z-coordinate [m] (uniform because flat)
// ************************************************************************* //
```

0-folder › U

```
/*--------------------------------*- C++ -*----------------------------------*\
  =========                 |
  \\      /  F ield         | OpenFOAM: The Open Source CFD Toolbox
   \\    /   O peration     | Website:  https://openfoam.org
    \\  /    A nd           | Version:  7
     \\/     M anipulation  |
\*---------------------------------------------------------------------------*/
FoamFile
{
    version     2.0;
    format      ascii;
    class       volVectorField;
    location    "0";
    object      U;
}
// * * * * * * * * * * * * * * * * * * * * * * * * * * * * * * * * * * * * * //
#include        "include/initialConditions"
dimensions      [0 1 -1 0 0 0 0];
internalField   uniform $flowVelocity;
boundaryField
{
    top
    {
        type             symmetry;
    }
    outlet
    {
        type            inletOutlet;
        inletValue      uniform (0 0 0);
        value           $internalField;
    }
    inlet
    {
        type            atmBoundaryLayerInletVelocity;
        #include        "include/ABLConditions"
    }
    terrainislands
    {
        type             noSlip;
    }
    terrainfront
    {
        type             noSlip;
    }
    terrainback
    {
        type             noSlip;
    }
    terrainsides
    {
        type             noSlip;
    }
    Buildings
    {
        type             noSlip;
    }
    mosque
    {
        type             noSlip;
    }
    nursinghome
    {
        type             noSlip;
    }
    parking
    {
        type             noSlip;
    }
    schoolcommunitycentre
    {
        type             noSlip;
    }
    supermarket
    {
        type             noSlip;
    }
    side1
    {
        type            symmetry;
    }
    side2
    {
        type             symmetry;
    }
}
// ************************************************************************* //
```

0-folder › p

```
/*--------------------------------*- C++ -*----------------------------------*\
  =========                 |
  \\      /  F ield         | OpenFOAM: The Open Source CFD Toolbox
   \\    /   O peration     | Website:  https://openfoam.org
    \\  /    A nd           | Version:  7
     \\/     M anipulation  |
\*---------------------------------------------------------------------------*/
FoamFile
{
    version     2.0;
    format      ascii;
    class       volScalarField;
    object      p;
}
// * * * * * * * * * * * * * * * * * * * * * * * * * * * * * * * * * * * * * * * //
#include        "include/initialConditions"
dimensions      [0 2 -2 0 0 0 0];
internalField   uniform $pressure;
boundaryField
{
    outlet
    {
        type            uniformFixedValue;
        uniformValue     constant $pressure;
    }
    inlet
    {
        type            zeroGradient;
    }
    top
    {
        type             symmetry;
    }
    Buildings
    {
        type            zeroGradient;
    }
    mosque
    {
        type             zeroGradient;
    }
    nursinghome
    {
        type             zeroGradient;
    }
    parking
    {
        type             zeroGradient;
    }
    schoolcommunitycentre
    {
        type             zeroGradient;
    }
    supermarket
    {
        type             zeroGradient;
    }
    terrainislands
    {
        type             zeroGradient;
    }
    terrainfront
    {
        type            zeroGradient;
    }
    terrainback
    {
        type            zeroGradient;
    }
    terrainsides
    {
        type            zeroGradient;
    }
    side1
    {
        type            symmetry;
    }

    side2
    {
        type            symmetry;
    }
}

// ************************************************************************* //
```

0-folder › T

```
/*--------------------------------*- C++ -*----------------------------------*\
  =========                 |
  \\      /  F ield         | OpenFOAM: The Open Source CFD Toolbox
   \\    /   O peration     | Website:  https://openfoam.org
    \\  /    A nd           | Version:  7
     \\/     M anipulation  |
\*---------------------------------------------------------------------------*/
FoamFile
{
    version     2.0;
    format      ascii;
    class       volScalarField;
    object      T;
}
// * * * * * * * * * * * * * * * * * * * * * * * * * * * * * * * * * * * * * //
#include        "include/initialConditions"
dimensions      [0 0 0 1 0 0 0];
internalField   uniform 300.7;
boundaryField
{
    outlet
    {
        type            inletOutlet;
        inletValue      uniform 300.7;
        value           uniform 300.7;
    }
    inlet
    {
        type            fixedValue;
        value           uniform 300.7;
    }
    top
    {
        type            symmetry;
    }
    Buildings
    {
        type            fixedValue;
        value           uniform 315.9;
    }
    mosque
    {
        type            fixedValue;
        value           uniform 316.6;
    }
    nursinghome
    {
        type            fixedValue;
        value           uniform 317.7;
    }
    parking
    {
        type            fixedValue;
        value           uniform 317.7;
    }
    schoolcommunitycentre
    {
        type            fixedValue;
        value           uniform 317.8;
    }
    supermarket
    {
        type            fixedValue;
        value           uniform 320.6;
    }
    terrainislands
    {
        type            fixedValue;
        value           uniform 312.8;
    }
    terrainfront
    {
        type            fixedValue;
        value           uniform 315.9;
    }
    terrainback
    {
        type            fixedValue;
        value           uniform 316.6;
    }
    terrainsides
    {
        type            fixedValue;
        value           uniform 316.2;
    }
    side1
    {
        type            symmetry;
```

```
    }

    side2
    {
        type            symmetry;
    }
}
// ************************************************************************* //
```

0-folder › k

```
/*--------------------------------*- C++ -*----------------------------------*\
  =========                 |
  \\      /  F ield         | OpenFOAM: The Open Source CFD Toolbox
   \\    /   O peration     | Website:  https://openfoam.org
    \\  /    A nd           | Version:  7
     \\/     M anipulation  |
\*---------------------------------------------------------------------------*/
FoamFile
{
    version     2.0;
    format      ascii;
    class       volScalarField;
    object      k;
}
// * * * * * * * * * * * * * * * * * * * * * * * * * * * * * * * * * * * * * //
#include        "include/initialConditions"
dimensions      [0 2 -2 0 0 0 0];
internalField   uniform $turbulentKE;
boundaryField
{
    top
    {
        type            symmetry;
    }
    Buildings
    {
        type            kqRWallFunction;
        value           $internalField;
    }
    mosque
    {
        type            kqRWallFunction;
        value           $internalField;
    }
    nursinghome
    {
        type            kqRWallFunction;
        value           $internalField;
    }
    parking
    {
        type            kqRWallFunction;
        value           $internalField;
    }
    schoolcommunitycentre
    {
        type            kqRWallFunction;
        value           $internalField;
    }
    supermarket
    {
        type            kqRWallFunction;
        value           $internalField;
    }
    terrainislands
    {
        type            kqRWallFunction;
        value           $internalField;
    }
    terrainfront
    {
        type            kqRWallFunction;
        value           $internalField;
    }
    terrainback
    {
        type            kqRWallFunction;
        value           $internalField;
    }
    terrainsides
    {
        type            kqRWallFunction;
        value           $internalField;
    }

    side1
    {
        type            symmetry;
```

```
    }

    side2
    {
        type            symmetry;
    }
    outlet
    {
        type            inletOutlet;
        inletValue      uniform $turbulentKE;
        value           $internalField;
    }
    inlet
    {
        type            atmBoundaryLayerInletK;
        #include        "include/ABLConditions"
    }
}
// ************************************************************************* //
```

0-folder › epsilon

```
/*--------------------------------*- C++ -*----------------------------------*\
  =========                 |
  \\      /  F ield         | OpenFOAM: The Open Source CFD Toolbox
   \\    /   O peration     | Website:  https://openfoam.org
    \\  /    A nd           | Version:  7
     \\/     M anipulation  |
\*---------------------------------------------------------------------------*/
FoamFile
{
    version     2.0;
    format      ascii;
    class       volScalarField;
    location    "0";
    object      epsilon;
}
// * * * * * * * * * * * * * * * * * * * * * * * * * * * * * * * * * * * * * //
dimensions      [0 2 -3 0 0 0 0];
#include        "include/initialConditions"
internalField   uniform $turbulentEpsilon;
boundaryField
{
    #include        "include/ABLConditions"
    Buildings
    {
        type            epsilonWallFunction;
        value           $internalField;
    }
    mosque
    {
        type            epsilonWallFunction;
        value           $internalField;
    }
    nursinghome
    {
        type            epsilonWallFunction;
        value           $internalField;
    }
    parking
    {
        type            epsilonWallFunction;
        value           $internalField;
    }
    schoolcommunitycentre
    {
        type            epsilonWallFunction;
        value           $internalField;
    }
    supermarket
    {
        type            epsilonWallFunction;
        value           $internalField;
    }
    terrainislands
    {
        type            epsilonz0WallFunction;
        z0              $z0_grass;
        value           $internalField;
    }
    terrainfront
    {
        type            epsilonz0WallFunction;
        z0              $z0_terrainfront;
        value           $internalField;
    }
    terrainback
    {
        type            epsilonz0WallFunction;
```

```
        z0                $z0_terrainback;
        value           $internalField;
    }
    terrainsides
    {
        type            epsilonz0WallFunction;
        z0                $z0_terrainsides;
        value           $internalField;
    }
    outlet
    {
        type            inletOutlet;
         inletValue       uniform $turbulentEpsilon;
         value            $internalField;
    }
    inlet
    {
        type            atmBoundaryLayerInletEpsilon;
        #include        "include/ABLConditions"
    }
    side1
    {
        type            symmetry;
    }
    side2
    {
         type             symmetry;
    }
    top
    {
         type             symmetry;
    }
}
// ************************************************************************* //
```

0-folder › nut

```
/*--------------------------------*- C++ -*----------------------------------*\
  =========                 |
  \\      /  F ield         | OpenFOAM: The Open Source CFD Toolbox
   \\    /   O peration     | Website:  https://openfoam.org
    \\  /    A nd           | Version:  7
     \\/     M anipulation  |
\*---------------------------------------------------------------------------*/
FoamFile
{
    version     2.0;
    format      ascii;
    class       volScalarField;
    location    "0";
    object      nut;
}
// * * * * * * * * * * * * * * * * * * * * * * * * * * * * * * * * * * * * * //
dimensions      [0 2 -1 0 0 0 0];
internalField   uniform 0;
boundaryField
{
    #include "include/ABLConditions"
    inlet
    {
        type            calculated;
        value           uniform 0;
    }
    outlet
    {
        type            calculated;
        value           uniform 0;
    }
    top
    {
         type             symmetry;
    }
    side1
    {
         type             symmetry;
    }
    side2
    {
         type             symmetry;
    }
    terrainislands
    {
         type             nutkAtmRoughWallFunction;
         z0               $z0_grass;
         value            uniform 0.0;
    }
    terrainfront
    {
```

```
        type            nutkAtmRoughWallFunction;
        z0              $z0_terrainfront;
        value           uniform 0.0;
    }
    terrainback
    {
        type            nutkAtmRoughWallFunction;
        z0              $z0_terrainback;
        value           uniform 0.0;
    }
    terrainsides
    {
        type            nutkAtmRoughWallFunction;
        z0              $z0_terrainsides;
        value           uniform 0.0;
    }

    Buildings
    {
        type            nutkWallFunction;
        value           uniform 0.0;
    }
    mosque
    {
        type            nutkWallFunction;
        value           uniform 0.0;
    }
    nursinghome
    {
        type            nutkWallFunction;
        value           uniform 0.0;
    }
    parking
    {
        type            nutkWallFunction;
        value           uniform 0.0;
    }
    schoolcommunitycentre
    {
        type            nutkWallFunction;
        value           uniform 0.0;
    }
    supermarket
    {
        type            nutkWallFunction;
        value           uniform 0.0;
    }
}
// NOTE: z0 aerodynamic roughness lengths for the roughness areas are specified in folder 0 > include > ABLCondi-
tionsT
// ************************************************************************* //
```

transportProperties

```
/*--------------------------------*- C++ -*----------------------------------*\
  =========                 |
  \\      /  F ield         | OpenFOAM: The Open Source CFD Toolbox
   \\    /   O peration     | Website:  https://openfoam.org
    \\  /    A nd           | Version:  7
     \\/     M anipulation  |
\*---------------------------------------------------------------------------*/
FoamFile
{
    version     2.0;
    format      ascii;
    class       dictionary;
    object      transportProperties;
}
// * * * * * * * * * * * * * * * * * * * * * * * * * * * * * * * * * * * * * //
transportModel  Newtonian;                  // assumes viscosity=cte
// values for T_air = 300K:
nu              [0 2 -1 0 0 0 0] 1.568e-05;  // kinematic viscosity of air [m2/s]
Pr              Pr [0 0 0 0 0 0 0] 0.707;
Prt             Prt [0 0 0 0 0 0 0] 0.85;   // turbulent Prandtl number (conventional fluid; standard wall function)
// ************************************************************************* //
```

fvSchemes

```
/*--------------------------------*- C++ -*----------------------------------*\
  =========                 |
  \\      /  F ield         | OpenFOAM: The Open Source CFD Toolbox
   \\    /   O peration     | Website:  https://openfoam.org
    \\  /    A nd           | Version:  7
     \\/     M anipulation  |
\*---------------------------------------------------------------------------*/
FoamFile
{
    version     2.0;
    format      ascii;
    class       dictionary;
    object      fvSchemes;
}
// * * * * * * * * * * * * * * * * * * * * * * * * * * * * * * * * * * * * * //
ddtSchemes
{
    default             steadyState;
}
gradSchemes
{
    default             Gauss linear;
}
divSchemes
{
    default             none;
    div(phi,U)          bounded Gauss upwind;
    div(phi,epsilon)    bounded Gauss upwind;
    div(phi,k)          bounded Gauss upwind;
    div(phi,T)          bounded Gauss upwind;
    div((nuEff*dev2(T(grad(U)))))    Gauss linear;
}
laplacianSchemes
{
    default             Gauss linear limited corrected 0.33;
}
interpolationSchemes
{
    default             linear;
}
snGradSchemes
{
    default             limited corrected 0.33;
}
// ************************************************************************* //
```

fvSolution

```
/*--------------------------------*- C++ -*----------------------------------*\
  =========                 |
  \\      /  F ield         | OpenFOAM: The Open Source CFD Toolbox
   \\    /   O peration     | Website:  https://openfoam.org
    \\  /    A nd           | Version:  7
     \\/     M anipulation  |
\*---------------------------------------------------------------------------*/
FoamFile
{
    version     2.0;
    format      ascii;
    class       dictionary;
    object      fvSolution;
}
// * * * * * * * * * * * * * * * * * * * * * * * * * * * * * * * * * * * * * //
solvers
{
    p
    {
        solver           GAMG;
        tolerance        1e-7;
        relTol           0.1;
        smoother         GaussSeidel;
    }
    U
    {
        solver           smoothSolver;
        smoother         GaussSeidel;
        tolerance        1e-8;
        relTol           0.1;
        nSweeps          1;
    }
    k
    {
        solver           smoothSolver;
        smoother         GaussSeidel;
        tolerance        1e-8;
        relTol           0.1;
        nSweeps          1;
```

```
    }
    epsilon
    {
        solver          smoothSolver;
        smoother        GaussSeidel;
        tolerance       1e-8;
        relTol          0.1;
        nSweeps         1;
    }
    T
    {
         solver          smoothSolver;
        smoother GaussSeidel;
        tolerance        1e-8;
        relTol           0.1;
        nSweeps         1;
    }
}
SIMPLE
{
    nNonOrthogonalCorrectors 0;
    residualControl
    {
        p               1e-3;
        U               1e-4;
        "(k|epsilon|T)"   1e-4;
    }
}
relaxationFactors
{
    fields
    {
        p               0.3;
    }
    equations
    {
        U               0.5;
        k               0.5;
        epsilon         0.5;
         T                0.5;
    }
}
cache
{
    grad(U);
}

// ************************************************************************* //
```

Computational times and CPU usage

	SINGLE BUILDING CASES	URBAN CASE (CURRENT)		URBAN CASE (INTERVENTION)
	simpleFoam without temperature	computational domain for wind from S - simpleFoam with temperature as passive scalar	computational domain for wind from N/NNE - simpleFoam with temperature as passive scalar	computational domain for wind from N/NNE - simpleFoam with temperature as passive scalar
mesh size	≈ 3 * 10^6 cells	≈ 32 * 10^6 cells	≈ 44 * 10^6 cells	≈ 44 * 10^6 cells
meshing processors	6	48	48	48
meshing time	≈ 5 min	≈ 1 h	≈ 1 h	≈ 45 min
simulation processors	6	48	48	48
simulation time	≈ 1 h 45 min	≈ 5 h	≈ 9 h 45 min	≈ 10 h 30 min

Table D1: computational times and CPU usage

REFERENCE LIST

Acero, J.A., & Ruefenacht, L.A. (2017). *Strategies for cooling Singapore. A catalogue of 80+ measures to mitigate urban heat island and improve outdoor thermal comfort* (Cooling Singapore 2017). Retrieved from Cooling Singapore website: https://www.coolingsingapore.sg/catalogue-of-strategies

Axhausen, K., Erath, A., Ordóñez, S., & van Eggermond, M., Future Cities Laboratory (2015). Modelling for Walkability: Understanding pedestrians' preferences in Singapore. *14th International Conference on travel behavior research, 2015*. https://doi.org/10.3929/ethz-b-000106077

Baruti, M., Johansson, E., & Åstrand, J. (2019). Review of studies on outdoor thermal comfort in warm humid climates: Challenges of informal urban fabric. *International Journal of Biometeorology*, 63(10), 1449-1462. doi:10.1007/s00484-019-01757-3

Biljecki, F., Ledoux, H., & Stoter, J.E. (2017). Generating 3D city models without elevation data. *Computers, Environment and Urban Systems*, 64(2017), 1-18.
https://doi.org/10.1016/j.compenvurbsys.2017.01.001

Blocken, B. (2015). Computational Fluid Dynamics for Urban Physics: Importance, scales, possibilities, limitations and ten tips and tricks towards accurate and reliable simulations. *Building and Environment, 2015*(2015 01 02). doi: 10.1016/j.buildenv.2015.02.015

Blocken, B., & Carmeliet, J. (2004). Pedestrian wind environment around buildings: Literature review and practical examples. *Journal of Thermal Envelope and Building Science*, 28(2), 107-159.

Blocken, B., Stathopoulos, T., & Van Beeck, J. (2016). Pedestrian-level wind conditions around buildings: Review of wind-tunnel and cfd techniques and their accuracy for wind comfort assessment. *Building and Environment*, 100, 50-81.

Building and Construction Authority (2010). *Building planning and massing*. Retrieved from BCA website: https://www.bca.gov.sg/GreenMark/others/bldgplanningmassing.pdf

Building and Construction Authority (2017). *3rd Green Building Masterplan* (BCA Green Mark 3rd Green Building Masterplan). Retrieved from Building and Construction Authority website: https://www.bca.gov.sg/GreenMark/others/3rd_Green_Building_Masterplan.pdf

Cairns, S., Jacobs, J.M., Yingying, J., Padawangi, R., Siddique, S., & Tan, E. (2014). Singapore's Void Decks. *World Scientific*, Public Space in Urban Asia, 80-89.
https://doi.org/10.1142/9789814578332_0005

Cao, C., & Chitty, R. (2014). *Computational fluid dynamics in building design*. Watford, Herts: IHS BRE Press

Chew, L.W., & Norfort, L.K. (2019). Pedestrian-level wind speed enhancement with void decks in three-dimensional urban street canyons. *Building and Environment*, 155(2019), 399-407. doi: 10.1016/j.buildenv.2019.03.058

City of London Corporation (2019). *Wind microclimate guidelines for developments in the city of London*. Retrieved from: https://www.cityoflondon.gov.uk/services/environment-and-planning/planning/design/Documents/city-of-london-wind-microclimate-guidelines.pdf

COST Office – Carissimo, B., Franke, H., Hellsten, A., & Schlünzen, H. (2007). *Best practice guideline for the CFD simulation of flows in the urban environment*. Retrieved from: http://theairshed.com/pdf/COST%20732%20Best%20Practice%20Guideline%20May%202007.pdf

De Dear, R. (2011). Revisiting an old hypothesis of human thermal perception: Alliesthesia. *Building Research & Information*, 39(2), 108-117. doi:10.1080/09613218.2011.552269

Emmanuel, R. (2005). Thermal comfort implications of urbanization in a warm-humid city: The colombo metropolitan region (cmr), sri lanka. *Building and Environment, 40*(12), 1591-1601. doi:10.1016/j.buildenv.2004.12.004

Ferziger, J.H., Perić, M., & Street, R.L. (2020). *Computational Methods for Fluid Mechanics*. Switzerland: Springer Nature Switzerland.

García-Sánchez, C., Gorlé, C., & Philips, D.A. (2014). Quantifying inflow uncertainties for CFD simulations of the flow in downtown Oklahoma City. *Building and Environment*, 78(2014), 118-129. doi: 10.1016/j.buildenv.2014.04.013

Giok Ling, O., & Tan, T. T.W. (1992). The Social Significance of Public Spaces in Public Housing Estates. In N. Edwards. & C. Beng Huat (Ed.), *Public Space – Design, use and management* (pp.69-81). Singapore: Singapore University Press.

Green Mark Department, Building and Construction Authority (2017). *Green Mark for Residential Buildings: 2016 Criteria, 2017*. Retrieved from BCA website: https://www.bca.gov.sg/GreenMark/others/GM_RB_2016_criteria_final.pdf

Heng, S., & Chow, W. (2019). How 'hot' is too hot? evaluating acceptable outdoor thermal comfort ranges in an equatorial urban park. *International Journal of Biometeorology, 63*(6), 801-816. doi:10.1007/s00484-019-01694-1

Hicks, R. (2018, September 28). Air-con addicted Singapore seeks new ways to escape urban heat trap. *Eco-Business*. Retrieved from https://www.eco-business.com/news/air-con-addicted-singapore-seeks-new-ways-to-escape-urban-heat-trap/

Housing and Development Board (2014). *Precast pictorial guide*. Retrieved from BCA website: https://www.bca.gov.sg/Publications/BuildabilitySeries/others/HDB_Precast_pictorial_guide_BCA.pdfHousing and Development Board. (1975). *Public Housing in Singapore: A Multi-Disciplinary Study*. Singapore: Yeh.

Housing and Development Board. (2019). Public Housing – A Singapore Icon. Retrieved December 20, 2019, from https://www.hdb.gov.sg/cs/infoweb/about-us/our-role/public-housing--a-singapore-icon

Janssen, W., Blocken, B., & Van Hooff, T. (2013). Pedestrian wind comfort around buildings: Comparison of wind comfort criteria based on whole-flow field data for a complex case study. *Building and Environment*, 59, 547-562. doi:10.1016/j.buildenv.2012.10.012

Johansson, E. (2016). Urban thermal comfort in the tropics. In R. Emmanuel (Ed.), Urban climate challenges in the tropics. Rethinking Planning and Design Opportunities (pp.163-204). London: Imperial College Press.

Ladybug Tools. (2019). EPWMap. Retrieved November 1, 2019, from https://www.ladybug.tools/epwmap/

Lin, Y., Wong, N.H., & Yang, W. (2015). Thermal Comfort in High-rise Urban Environments in Singapore. *Procedia Engineering*, 121 (2015), 2125-2131. doi: 10.1016/j.proeng.2015.09.083

Logan, T. (2016). Elk (Elk 2.2.2) [Grasshopper plugin]. Retrieved from https://www.food4rhino.com/app/elk

Meteorological Service Singapore. (2019). Climate of Singapore. Retrieved October 30, 2019, from http://www.weather.gov.sg/climate-climate-of-singapore/

Meteorological Service Singapore. (2017). *Annual Climatological Report 2017*. Retrieved from Meteorological Service Singapore website: http://www.weather.gov.sg/climate-annual-climate-reports/

National Technology & Engineering Solutions of Sandia, LLC (NTESS), Kitware Inc. (2005-2017). ParaView (5.8.0-RC3) [data analysis and visualization application]. Retrieved from https://www.paraview.org/

NEN. Wind comfort and wind danger in the built environment. NEN 8100 (in Dutch) Dutch standard; 2006.

Ng, E. (2016). Urban air ventilation in high-density cities in the tropics. In R. Emmanuel (Ed.), *Urban Climate Challenges in the Tropics – Rethinking Planning and Design Opportunities* (pp.79-110). London: Imperial College Press.

Nicol, F., Humphreys, M., & Roaf, S. (2012). Adaptive thermal comfort: principles and practice. doi: 10.4324/9780203123010

OpenCFD Ltd. (2019). OpenFOAM (v1912) [open source CFD toolbox]. Retrieved from https://www.openfoam.com/download/install-windows-10.php

OpenStreetMap contributors. (2020). [OpenStreetMap location of Clementi, Singapore]. Retrieved from https://www.openstreetmap.org/search?query=clementi%20singapore#map=16/1.3151/103.7652

Parkinson, T., & De Dear, R. (2015). Thermal pleasure in built environments: Physiology of alliesthesia. *Building Research & Information*, 43(3), 288-301. doi:10.1080/09613218.2015.989662

Pijpers-van Esch, M. (2015). *Designing the Urban Microclimate: A framework for a design-decision support tool for the dissemination of knowledge on the urban microclimate to the urban design process* (PhD thesis). Retrieved from https://books.bk.tudelft.nl/index.php/press/catalog/book/isbn.9789461865014

Roesler, S., & Vihervaara, A. (2015). Evolution of New Towns. *FCL Magazine*, 2015 special issue Natural Ventilation, Revisited, 84-110. https://doi.org/10.3929/ethz-a-010709200

Roudsari, M.S. (2017-2020). Ladybug Tools (Ladybug 2020.01.0.0.0.68) [Grasshopper plugin]. Retrieved from https://www.food4rhino.com/app/ladybug-tools

Stull, R.B. (1988). An Introduction to Boundary Layer Meteorology. Dordrecht, The Netherlands: Kluwer Academic Publishers.

The PyVista Developers (2017-2020). PyVista (conda-forge v0.25.3) [Python module]. Retrieved from https://docs.pyvista.org/index.html

Tominaga, Y., Mochida, A., Yoshie, R., Kataoka, H., Nozu, T., Yoshikawa, M., Shirasawa, T. AIJ guidelines for practical applications of CFD to pedestrian wind environment around buildings. J Wind Eng Ind Aerodyn 2008;96(10-11):1749-1761.

Yang, W., Wong, N., & Jusuf, S. (2013). Thermal comfort in outdoor urban spaces in Singapore. *Building and Environment*, 59, 426-435. doi:10.1016/j.buildenv.2012.09.008

Yeo, A. (2016, March 17). Voiding the kampung spirit? *The Straits Times*. Retrieved from https://www.straitstimes.com/opinion/st-editorial/voiding-the-kampung-spirit

BIBLIOGRAPHY

Alur, R., & Deb, C. (2010). The significance of Physiological Equivalent Temperature (PET) in outdoor thermal comfort studies. *International Journal of Engineering Science and Technology*, Vol. 2(7), 2825-2828. https://www.researchgate.net/publication/50315274_The_significance_of_Physiological_Equivalent_Temperature_PET_in_outdoor_thermal_comfort_studies

American Society of Heating, Refrigerating and Air-Conditioning Engineers (2010). *ANSI/ASHRAE Standard 55-2010 Thermal Environmental Conditions for Human Occupancy*. Atlanta, GA: ASHRAE.

Blazejczyk, K., Epstein, Y., Jendritzky, G., Staiger, H., & Tinz, B. (2012). Comparison of UTCI to selected thermal indices. *International Journal of Biometeorology*, 56(3), 515-535. https://doi-org.tudelft.idm.oclc.org/10.1007/s00484-011-0453-2

ENVI-met. (2019). PET. Retrieved December 9, 2019, from http://www.envi-met.info/doku.php?id=apps:biomet_pet

Goh, R. B.H. (2003). Things to a Void: Utopian Discourse, Communality and Constructed Interstices in Singapore Public Housing. In *Theorizing the Southeast Asian City as Text* (pp. 51-71). Retrieved from https://books.google.nl/books?hl=en&lr=&id=CVbxKuuXBJQC&oi=fnd&pg=PA51&dq=hdb+void+deck&ots=LnzfzvdYdZ&sig=YMvRuyWdlzw6dDVdIanmNfH2S8E&redir_esc=y#v=onepage&q=hdb%20void%20deck&f=false

Havenith, G., Fiala, D., Błazejczyk, K., Richards, M., Bröde, P., Holmér, I., Rintamaki, H., Benshabat, Y., & Jendritzky, G. (2012). The UTCI-clothing model. *International Journal of Biometeorology*, 56(3), 461-470. doi: 10.1007/s00484-011-0451-4

Havenith, G., Holmér, I., & Parsons, K. (2002). Personal factors in thermal comfort assessment: Clothing properties and metabolic heat production. *Energy & Buildings*, 34(6), 581-591. doi:10.1016/S0378-7788(02)00008-7

Matzarakis, A., & Amelung, B. (2008). Physiological Equivalent Temperature as Indicator for Impacts of Climate Change on Thermal Comfort of Humans. In M.C. Thomson, R. García-Herrera & M. Beniston (Ed.), *Seasonal Forecasts, Climatic Change and Human Health*.(pp. 161-172). Dordrecht, The Netherlands: Springer. doi: https://doi-org.tudelft.idm.oclc.org/10.1007/978-1-4020-6877-5

National Heritage Board (2013). *Community Heritage Series III: Void Decks*. Retrieved from https://www.nhb.gov.sg/~/media/nhb/files/resources/publications/ebooks/nhb_ebook_void_decks.pdf

National Library Board. (2015). *Void deck.* In Singapore Infopedia. Retrieved October 10, 2019, from https://eresources.nlb.gov.sg/infopedia/articles/SIP_2015-01-27_191959.html

Thinking City. (2018, November 21). The void deck: Singapore's secret community infrastructure [Web log post]. Retrieved from https://thinkingcity.org/2018/11/21/the-void-deck-singapores-secret-community-infrastructure/

Zhang, M. H. (2015). Wind Statistics. In *Wind Resource Assessment And Micro-Siting. Science and Engineering* (pp. 132-164). Singapore: John Wiley & Sons Singapore Pte. Ltd.

TU Delft